Republic of Iraq
Ministry of Higher Education
And Scientific Research
University of Baghdad
College of Education for pure science Ibn Al-Haitham
Department of Chemistry

Synthesis, characterization and biological activity of azo dyes complexes with some metal ions

A Dissertation

Submitted to the College of Education For Pure Science / Ibn Al-Haitham at the University of Baghdad as a Partial Fulfillment of the Requirements for the degree of Philosophy doctorate in Chemistry

By

Jinan Mohammed Mahmood

(B.Sc. In Chemistry 1999 Baghdad University)
(M.Sc. In Chemistry 2002 Baghdad University)

Supervised

Prof. Dr. Amer J. Jarad

1440AH **2019A.D.**

بِسْمِ اللَّهِ الرَّحْمَٰنِ الرَّحِيمِ

﴿ يَرْفَعِ اللَّهُ الَّذِينَ آمَنُوا مِنكُمْ

وَالَّذِينَ أُوتُوا الْعِلْمَ دَرَجَاتٍ ۚ

وَاللَّهُ بِمَا تَعْمَلُونَ خَبِيرٌ ﴾

صدق اللَّهُ العظيم

(سورة المجادلة/ الآية 11)

Supervisor Certification

We certify that, this dissertation was prepared under my supervision at Department of Chemistry, College of Education For Pure Science/ Ibn-Al-Haitham- University of Baghdad in partial requirements for the Degree of Doctorate of Philosophy in Inorganic Chemistry, and this work has never submitted or published anywhere else.

Signature:

Supervisor

Name: **Dr. Amer J. Jarad**
Title: Prof.
Address: Department of Chemistry/ College of Education For Pure Science/ Ibn-Al-Haitham- University of Baghdad
Date: 21 / 5 / 2019

In the view of the available recommendation, I forward this dissertation for debate by the Examination Committee.

Signature

Name: Dr. Mohamad Jaber Al-Jeboori

Title: Prof.

Address: Head of Chemistry Department / College of Education For Pure Science / Ibn-Al-Haitham- University of Baghdad

Date: 21 / 5 / 2019

Examination committee certificate

We chairman and members of the examination committee, certify that we have studies this thesis presented by the student **Jinan Mohammed Mahmood** and examined her in its contents and that, we have found its worthy to be accepted for the degree of the doctor of Philosophy in chemistry with (**excellent**).

Signature:
Name: **Dr. Sajid Mahmood Lateef**
Title: **Professor**
Date: 18/7/2019
(Chairman)

Signature:
Name: **Dr.Abbas Ali Salih Al- Hamdani**
Title: .**Prof.**
Date: 18/7/2019
(Member)

Signature:
Name: **Dr.Hayder Hamied Mihsen**
Title: .**Prof.**
Date: 18/7/2019
(Member)

Signature:
Name: **Dr.Tariq Hussein Mgheer**
Title: **Asst.Prof.**
Date: 18/7/2019
(Member)

Signature:
Name: **Dr.Lekaa Khalid Abdul Karem**
Title: **Asst.Prof.**
Date: 18/7/2019
(Member)

Signature:
Name: **Dr .Amer Jabbar Jarad**
Title: **Professor**
Date: 18/7/2019
Member (Supervisor)

I have certified upon the discussion of the examination committee

Signature:
Prof. **Dr. Hasan Ahmed Hasan**
The Dean of collage of Education For Pure Sciences / Ibn al Haitham

Date: 21/7/2019

Dedication

I would like to dedicate this humble effort to:

My great parent….

The symbol of love and giving

My dearest husband…. with my love for his

Outstanding encouragement

My beloved sisters and my brothers ….

The candles of my life

My beloved kids ….

The butterflies that beaulify my days

Jinan

Acknowledgment

Praise be to Allah, and Allah's blessing and peace be apon our prophet Mohammed who rescued mankind from darkness to light.

The words betray me in describing these mixed moments with joy and tears I praise Allah almighty very much for granting me success to complete this thesis. I would like to express my sincere thanks and appreciation to my supervisor Prof. Dr. Amer J. Jarad. I extend my grateful thanks to Prof. Dr. Taqi al-Din A. Hamdan an Assistant Prof. Dr. Zainab A. Al- Mousway during my study. Who have encouraged and supported me during my stud.

Also, I extend my deep gratitude for the deanery of the College of Education for pure sciences (Ibn-Al-Haitham) and to all my virtuous professors in the department of chemistry,I am grateful to; the Central Laboratory in College of Education for Pure Science (Ibn Al-Haitham) for performing some measurements carried out in this work, to all the higher studies students who gave me help and sincere cooperation.

The researcher Jinan

Summary

New azo ligands (L_1-L_4) have been produced all rest on the 4-aminoantipyrine and 2-aminebenzothiazole as a back-bone of the prepared ligands having the following structures.

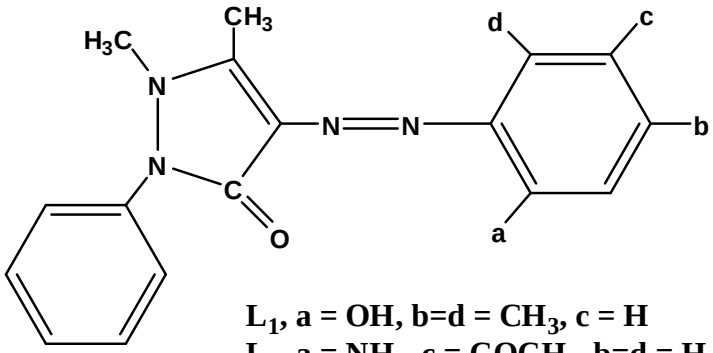

L_1, a = OH, b=d = CH_3, c = H
L_2, a = NH_2, c = $COCH_3$, b=d = H

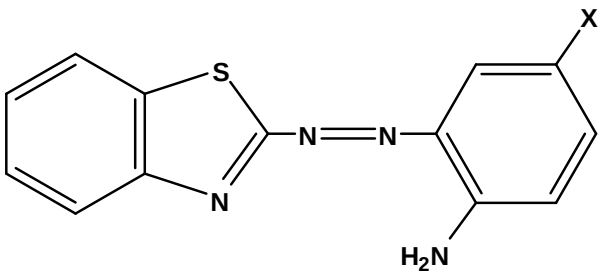

L_3 , X = $COCH_3$, L_4 , X = NO_2

Produced azo ligands have been characterized by (FT–IR, ^{1}H, ^{13}C—NMR, UV-Vis and Lc—Mass) spectroscopic methods , microelemental analysis (C.H.N.S.O) and thermogravimetric analysis (TGA) .

The other part of this project refer to the synthesis of metal chelates Co^{II}, Ni^{II}, Cu^{II} and Zn^{II} with all prepared azo ligands.

All production was performed after fixing the ideal pH and molar concentration that obeyed Lambert- Beer's law in the studies pH rates.

According to the molar ratio and Job methods, the structure of these metal chelates was deduced depending on the spectroscopic studies of the complex solution of the above ions. However, ration of 1:2 M:L for all ions were obtained. The mole ratio of mixed ligand complexes was 1:1:1(M:L:L).

FT–IR, UV-Vis spectra, conductivity, magnetic susceptibility and melting points measurements using to characterize of prepared complexes.

Flameless atomic absorption technique has been measured to calculate the percentage of the metals in the complexes. (C.H.N.S.O) analysis were also found, the results are in agreement with the calculated values. All the complexes are quite stable and could be stored for months without any appreciable change.

Depending to the results obtained by elemental and spectral analysis, an octahedral structure suggested for all produced complexes.

In addition the dyeing performance of the produced compound have been assessed on cotton fabric, the dyes were tested for light and detergent fastness.

Finally azo ligand and newly metal chelats were screened in vitro for their antibacterial and antifungal activity against: *Staphylococcus aureus*, *Esherichia Coli*, *Candida albicans* and *Candida tropicalis*

List of Contents

Subject		Page
	Summary	A-B
	List of contents	I-IV
	List of tables	V-VI
	List of figures	VII-XIII
	List of schemes	XIV
	Abbreviation	XV
Chapter One: Introduction		
1.1.	Introduction	1
1.2.	Azo dyes	1
1.3.	Synthesis of azo dyes	3
1.3.1.	Diazotization	3
1.3.2.	Azo coupling reaction	4
1.4.	Isomerism in azo compounds	4
1.4.1.	Geometrical isomerism	4
1.4.2.	Toutomerisim	5
1.5.	Alkyl and aryl azo compounds	6
1.5.1.	Aliphatic azo compounds	6
1.5.2.	Aromatic azo compounds	6
1.5.2.1.	Homocyclic azo compounds	7
1.5.2.2.	Heterocyclic azo compounds	13
1.5.2.2.1.	Pyridyl azo compounds	14
1.5.2.2.2.	Thiazolyl azo compounds	16
1.5.2.2.3.	Imidazol and Pyrimidyl azo compounds	21
1.5.2.2.4.	Pyrazolone azo compounds	26
1.6.	Mixed ligand complexes	33
1.7.	Aim of the work	38

	Subject	Page
	Chapter Two: Experimental part	
2.1.	Chemicals	39
2.2.	Instruments	40
2.3.	Synthesis of azo ligands	41
2.3.1.	Synthesis for ligand (L_1, L_2)	41
2.3.1.	Synthesis for ligand (L_3,L_4)	42
2.4.	Buffer solution	43
2.5.	Standard solution	43
2.6.	Preparation of solutions for spectral studies	43
2.6.1.	Mole ratio	43
2.6.2.	Job method	43
2.7.	Synthesis of metal chelates	44
2.7.1.	Synthesis of metal chelates for azo ligands (L_1-L_4)	44
2.7.2.	Synthesis of metal chelates for mixed ligands (L_1,L_2)	44
2.7.3.	Synthesis of metal chelates for mixed ligands (L_3,L_4)	44
2.8.	Biological activity	47
2.9.	Dyeing method	48
	Chapter Three: Results and Discussion	
3.1.	Synthesis of azo dyes ligands	49
3.2.	Mass spectra of azo dyes ligands	51
3.2.1.	Mass spectrum of the ligand (L_1)	51
3.2.2.	Mass spectrum of the ligand (L_2)	54
3.2.3.	Mass spectrum of the ligand (L_3)	56
3.2.4.	Mass spectrum of the ligand (L_4)	57
3.3.	Thermal analysis	59
3.4.	^{1}HNMR spectra of azo dyes ligands	63
3.4.1.	^{1}HNMR spectrum of the ligand (L_1)	63

	Subject	Page
3.4.2.	^{1}HNMR spectrum of the ligand (L_2)	64
3.4.3.	^{1}HNMR spectrum of the ligand (L_3)	64
3.4.4.	^{1}HNMR spectrum of the ligand (L_4)	65
3.5.	^{13}CNMR spectra of azo dyes ligands	66
3.5.1.	^{13}CNMR spectrum of the ligand (L_1)	66
3.5.2.	^{13}CNMR spectrum of the ligand (L_2)	67
3.5.3.	^{13}CNMR spectrum of the ligand (L_3)	68
3.5.4.	^{13}CNMR spectrum of the ligand (L_4)	69
3.6.	FTIR spectra of azo dyes ligands	70
3.6.1.	FTIR spectrum of the ligand (L_1)	70
3.6.2.	FTIR spectrum of the ligand (L_2)	72
3.6.3.	FTIR spectrum of the ligand (L_3)	74
3.6.4.	FTIR spectrum of the ligand (L_4)	75
3.7.	UV-Vis spectra of azo dyes ligands	77
3.7.1.	UV-Vis spectrum of the ligand (L_1)	77
3.7.2.	UV-Vis spectrum of the ligand (L_2)	77
3.7.3.	UV-Vis spectrum of the ligand (L_3)	78
3.7.4.	UV-Vis spectrum of the ligand (L_4)	79
3.8.	UV-Vis spectral studies	80
3.8.1.	Effect of pH and concentration	82
3.8.2.	Complexes nature	89
3.8.3.	Effect of time on absorbance	98
3.8.4.	Stability constant	103
3.9.	Synthesis of solid complexes and characterization techniques	104
3.9.1.	Thermal analysis	107
3.9.2.	Mass spectra of metal chelates	112

	Subject	Page
3.9.3.	Solubility	121
3.9.4.	Molar conductivity	122
3.9.5.	Magnetic properties	124
3.9.6.	FT-IR spectra of complexes	126
3.9.6.1.	FT-IR spectra of azo ligand(L_1) metal chelates	126
3.9.6.2.	FT-IR spectra of azo ligand(L_2) metal chelates	130
3.9.6.3.	FT-IR spectra of azo ligand (L_3) metal chelates.	134
3.9.6.4.	FT-IR spectra of azo ligand(L_4) metal chelates	138
3.9.6.5.	FT-IR spectra of mixed ligand(L_1,L_2) metal chelates	142
3.9.6.6.	FT-IR spectra of mixed ligand(L_3,L_4) metal chelates	146
3.9.7.	UV-Vis spectra of complexes	150
3.9.7.1.	UV-Vis spectra of azo ligand(L_1) metal chelates	150
3.9.7.2.	UV-Vis spectra of azo ligand(L_2) metal chelates	155
3.9.7.3.	UV-Vis spectra of azo ligand(L_3) metal chelates	159
3.9.7.4.	UV-Vis spectra of azo ligand (L_4) metal chelates	164
3.9.7.5.	UV-Vis spectra of mixed azo ligand (L_1,L_2) metal chelates	169
3.9.7.6.	UV-Vis spectra of mixed azo ligand (L_3,L_4) metal chelates	173
3.10.	The Proposed molecular structures	177
3.11.	Biological activity	180
3.12.	Dyeing	186
	Conclusions	195
	Prospective studies	195
	References	196
	الخلاصة باللغة العربية	أ

List of tables

	Tables	*Page*
(2–1)	Chemicals used in this work and its suppliers.	39
(2–2)	Nomenclature and some physical properties for azo ligands (L_1-L_4).	42
(2–3)	Nomenclature and some physical properties for metal chelates with azo ligands (L_1-L_4).	45
(3–1)	Solubility of azo ligands in different solvents.	50
(3–2)	Microanalysis results of the azo ligands (L_1-L_4).	51
(3–3)	Characterization parameters of thermal decomposition (10°C min^{-1}) ligands.	62
(3–4)	Absorbance at λ_{max} for molar concentration of mixed solutions of metal ions with azo ligasnds.	83
(3–5)	Absorbance at different pH and perfect concentration of mixed solutions of metal ions with azo ligasnds.	86
(3–6)	UV-Vis spectral data at (λ_{max}) for mole ratio method at perfect pH and concentration of mixed solutions of metal ions with azo ligasnds	90
(3–7)	UV-Vis spectra data at (λ_{max}) for job method at perfect pH and L_1concentration of mixed solutions of metal ions with azo ligasnds	94
(3–8)	Absorbance for mixed solutions of metal ions with azo ligands at the change of time.	98
(3–9)	Stability constant and Gibbs free energy of the prepared complexes with azo dyes ligands (L_1-L_4)	104
(3–10)	Metal content and (C.H.N.S.O) analysis data for prepared compounds	105
(3–11)	Characterization parameters of thermal decomposition (10°C min^{-1}) metal complexes.	107

	Tables	Page
(3–12)	Solubility for complexes in different solvents.	121
(3-13)	Molar conductance data at different solvents.	122
(3–14)	Molar conductance for metal chelates in dimethylsulphoxide (DMSO) (10^{-3} mole/L).	123
(3–15)	Magnetic moments data for the prepared metal chelates at 23°C.	125
(3–16)	Infrared spectral data for the azo ligand (L_1) and their metal chelates (cm^{-1}).	127
(3–17)	Infrared spectral data for the azo ligand (L_2) and their metal chelates (cm^{-1}).	131
(3–18)	Infrared spectral data for the azo ligand (L_3) and their metal chelates (cm^{-1}).	135
(3–19)	Infrared spectral data for the azo ligand (L_4) and their metal chelates (cm^{-1}).	139
(3–20)	Infrared spectral data for mixed ligand (L_1,L_2) metal chelates (cm^{-1}).	143
(3–21)	Infrared spectral data for mixed ligand(L_3,L_4) metal chelates (cm^{-1}).	147
(3–22)	UV-Vis spectral data for azo ligand (L_1) metal chelates.	152
(3–23)	UV-Vis spectral data for azo ligand (L_2) metal chelates.	156
(3–24)	UV-Vis spectral data for azo ligand (L_3) metal chelates.	161
(3–25)	UV-Vis spectral data for azo ligand (L_4) metal chelates.	166
(3–26)	UV-Vis spectral data for mixed azo ligand (L_1, L_2) metal chelates.	170
(3–27)	UV-Vis spectral data for mixed azo ligand (L_3, L_4) metal chelates.	174
(3–28)	Diameters (mm) at suppression for microbial activity to the azo ligands and compounds.	181

List of Figures

Figures		Page
(1–1)	Azo dye structure.	2
(1–2)	General formula of azo dyes	3
(1–3)	Chemical structure of (AIBN).	6
(1–4)	The structure of Cu^{2+} and Fe^{2+} complexes.	8
(1–5)	Proposed structure of Cu^{II} and Co^{III} complexes.	9
(1–6)	Proposed structure of Cr^{III} complexes.	9
(1–7)	Proposed structure of Co^{II}, Ni^{II} and Cu^{II} metal chelates.	9
(1–8)	Structure of Ni^{II} and Cu^{II} metal chelates.	10
(1–9)	Structure of Ni^{II} and Cu^{II} with azo dyes ligands.	11
(1–10)	Chemical structure of Ni^{II} complex.	12
(1–11)	Structure of azo complexes.	13
(1–12)	Structure of PAN and PAR azo dyes.	14
(1–13)	Proposed structure of metal complexes for 4-(2-pyridyl azo)-resorcinol.	15
(1–14)	The Proposed structure of the azo dye complexes.	16
(1–15)	Structure of (TAR) and (TAN).	16
(1–16)	Proposed structure of azo dyes ligands.	17
(1–17)	Structure of Cu^{II} complex with (NO_2BTAHBA).	18
(1–18)	Structure of metal chelates of azo ligand.	19
(1–19)	Suggested structure for [Cr^{III}, Mn^{II}, Fe^{III}, Co^{II}, Ni^{II}, Cu^{II} and Zn^{II}] complexes.	20
(1–20)	Proposed structure of metal complexes for 2-(2-benzathiazolyl azo)-3,5-dimethylphenol.	21
(1–21)	Suggested structure of metal complexes with 2-[2-(6-nitro benzothiazolyl)azo]-imidazole	22

	Figures	Page
(1–22)	Structure of Ag^{I} complex.	23
(1–23)	Structure of Co^{II} and Cu^{II} complexes with bis azo dye ligand.	24
(1–24)	Proposed structure of metal complexes for pyrimidyl azo dye.	25
(1–25)	Chemical structure of Pt^{IV} complex	26
(1–26)	Structure of metal complexes for (E)-4-((4-hydroxy-6-methyl-2-oxo-2H-pyran-3-yl)diazenyl)-1,5-dimethyl-2-phenyl-1H-pyrazol-3(2H)-one.	28
(1–27)	Proposed structure of metal chelate for pyrazolyl azo dye.	29
(1–28)	Structure of Y^{III} and La^{III} metal chelates.	30
(1–29)	Proposed structure of metal chelates for sulfonyl azo dyes.	31
(1–30)	Structure of metal complexes [Co^{II}, Ni^{II}, Cu^{II} and Zn^{II}].	31
(1–31)	Proposed structure of metal chelate for(E)-4-(((4,5-bis(4-methoxyphenyl)-4,5-dihydro-1H-imidazol-2-yl)-diazenyl)-1,5-dimethyl-2-phenyl-1H-pyrazol-3(2H)-one.	32
(1–32)	Chemical structure of the mixed-ligand Cu^{II} complexes	34
(1–33)	Chemical structure of the mixed-ligand Pr^{III} complex.	35
(1–34)	Structure of Cu^{II} and Ni^{II} mixed-ligand complexes.	36
(1–35)	Proposed structure of Zr^{IV} complex.	36
(1–36)	Structure of mixed-ligand (Mn^{II}, Ni^{II} and Cu^{II}) complexes.	37
(3–1)	Mass spectrum of the ligand (L_1).	52
(3–2)	Mass spectrum of the ligand (L_2).	54

	Figures	Page
(3–3)	Mass spectrum of the ligand (L_3).	56
(3–4)	Mass spectrum of the ligand (L_4).	58
(3–5)	TG/DSC Thermogram of the ligand (L_1).	59
(3–6)	TG/DSC Thermogram of the ligand (L_2).	59
(3–7)	TG/DSC Thermogram of the ligand (L_3).	60
(3–8)	TG/DSC Thermogram of the ligand (L_4).	60
(3–9)	^{1}HNMR spectrum of the ligand (L_1).	63
(3–10)	^{1}HNMR spectrum of the ligand (L_2).	64
(3–11)	^{1}HNMR spectrum of the ligand (L_3).	65
(3–12)	^{1}HNMR spectrum of the ligand (L_4).	66
(3–13)	^{13}CNMR spectrum of the ligand (L_1).	67
(3–14)	^{13}CNMR spectrum of the ligand (L_2).	68
(3–15)	^{13}CNMR spectrum of the ligand (L_3).	69
(3–16)	^{13}CNMR spectrum of the ligand (L_4).	70
(3–17)	FTIR spectrum of 4-aminoantipyrine.	71
(3–18)	FTIR spectrum of 3,5-dimethyphenol.	71
(3–19)	FTIR spectrum of the ligand (L_1).	72
(3–20)	FTIR spectrum of 4-aminoacetophenone.	73
(3–21)	FTIR spectrum of the ligand (L_2).	73
(3–22)	FTIR spectrum of 2-aminobenzothiazole	74
(3–23)	FTIR spectrum of the ligand (L_3).	75
(3–24)	FTIR spectrum of 4-nitroaniline.	76
(3–25)	FTIR spectrum of the ligand (L_4).	76
(3–26)	UV-Vis spectrum of the ligand (L_1).	77
(3–27)	UV-Vis spectrum of the ligand (L_2).	78
(3–28)	UV-Vis spectrum of the ligand (L_3).	79

	Figures	Page
(3–29)	UV-Vis spectrum of the ligand (L_4).	80
(3–30)	UV-Vis spectra: a) Free ligand (L_2) solution, b) Cu-L_2 mixed solution. b) Free ligand (L_4) solution, d) Co-L_4 mixed solution	81
(3–31)	Linear correlation between molar concentration and absorbance for mixed solutions of metal ions with azo ligasnds.	84
(3–32)	Effect of pH on absorbance at λ_{max} of mixed solutions of metal ions with azo ligasnds at perfect concentrations.	87
(3–33)	Mole ratio plot for (M:L) ratio at perfect pH and concentration of mixed solutions of metal ions with azo ligasnds.	92
(3–34)	Job method plot for (M:L) ratio at perfect pH and concentration of mixed solutions of metal ions with azo ligasnds.	96
(3–35)	Time effect for mixed solutions of metal ions with azo ligands (L_1-L_4).	101
(3–36)	TG/DSC Thermogram of $[Ni(L_1)_2]$ complex.	108
(3–37)	TG/DSC Thermogram of $[Ni(L_2)_2].H_2O$ complex.	109
(3–38)	TG/DSC Thermogram of $[Zn(L_3)_2]$ complex.	110
(3–39)	TG/DSC Thermogram of $[Cu(L_4)_2]$ complex.	111
(3–40)	Mass spectrum for $[Co(L_1)_2]$ complex.	113
(3–41)	Mass spectrum for $[Ni(L_2)_2].H_2O$ complex.	113
(3–42)	Mass spectrum for $[Cu(L_3)_2]$ complex.	116
(3–43)	Mass spectrum for $[Zn(L_4)_2]$ complex.	116
(3–44)	Mass spectrum for $[Ni(L_1)(L_2)]$ complex.	119

Figures		Page
(3–45)	Mass spectrum for $[Cu(L_3)(L_4)]$ complex.	119
(3–46)	FTIR spectrum of the $[Co(L_1)_2]$ complex.	128
(3–47)	FTIR spectrum of the $[Ni(L_1)_2]$ complex.	128
(3–48)	FTIR spectrum of the $[Cu(L_1)_2]$ complex.	129
(3–49)	FTIR spectrum of the $[Zn(L_1)_2]$ complex.	129
(3–50)	FTIR spectrum of the $[Co(L_2)_2].H_2O$ complex.	132
(3–51)	FTIR spectrum of the $[Ni(L_2)_2].H_2O$ complex.	132
(3–52)	FTIR spectrum of the $[Cu(L_2)_2].H_2O$ complex.	133
(3–53)	FTIR spectrum of the $[Zn(L_2)_2].H_2O$ complex.	133
(3–54)	FTIR spectrum of the $[Co(L_3)_2]$ complex.	136
(3–55)	FTIR spectrum of the $[Ni(L_3)_2]$ complex.	136
(3–56)	FTIR spectrum of the $[Cu(L_3)_2]$ complex.	137
(3–57)	FTIR spectrum of the $[Zn(L_3)_2]$ complex.	137
(3–58)	FTIR spectrum of the $[Co(L_4)_2]$ complex.	140
(3–59)	FTIR spectrum of the $[Ni(L_4)_2]$ complex.	140
(3–60)	FTIR spectrum of the $[Cu(L_4)_2]$ complex.	141
(3–61)	FTIR spectrum of the $[Zn(L_4)_2]$ complex.	141
(3–62)	FTIR spectrum of the $[Co(L_1)(L_2)]$ complex.	144
(3–63)	FTIR spectrum of the $[Ni(L_1)(L_2)]$ complex.	144
(3–64)	FTIR spectrum of the $[Cu(L_1)(L_2)]$ complex.	145
(3–65)	FTIR spectrum of the $[Zn(L_1)(L_2)]$ complex.	145
(3–66)	FTIR spectrum of the $[Co(L_3)(L_4)]$ complex.	148
(3–67)	FTIR spectrum of the $[Ni(L_3)(L_4)]$ complex.	148
(3–68)	FTIR spectrum of the $[Cu(L_3)(L_4)]$ complex.	149
(3–69)	FTIR spectrum of the $[Zn(L_3)(L_4)]$ complex.	149
(3–70)	UV-Vis spectrum for $[Co(L_1)_2]$ complex.	153

Figures		Page
(3–71)	UV-Vis spectrum for $[Ni(L_1)_2]$ complex.	153
(3–72)	UV-Vis spectrum for $[Cu(L_1)_2]$ complex.	154
(3–73)	UV-Vis spectrum for $[Zn(L_1)_2]$ complex.	154
(3–74)	UV-Vis spectrum for $[Co(L_2)_2].H_2O$ complex.	157
(3–75)	UV-Vis spectrum for $[Ni(L_2)_2].H_2O$ complex.	157
(3–76)	UV-Vis spectrum for $[Cu(L_2)_2].H_2O$ complex.	158
(3–77)	UV-Vis spectrum for $[Zn(L_2)_2].H_2O$ complex.	158
(3–78)	UV-Vis spectrum for $[Co(L_3)_2]$ complex.	162
(3–79)	UV-Vis spectrum for $[Ni(L_3)_2]$ complex.	162
(3–80)	UV-Vis spectrum for $[Cu(L_3)_2]$ complex	163
(3–81)	UV-Vis spectrum for $[Zn(L_3)_2]$ complex.	163
(3–82)	UV-Vis spectrum for $[Co(L_4)_2]$ complex.	167
(3–83)	UV-Vis spectrum for $[Ni(L_4)_2]$ complex.	167
(3–84)	UV-Vis spectrum for $[Cu(L_4)_2]$ complex.	168
(3–85)	UV-Vis spectrum for $[Zn(L_4)_2]$ complex.	168
(3–86)	UV-Vis spectrum for $[Co(L_1)(L_2)]$ complex.	171
(3–87)	UV-Vis spectrum for $[Ni(L_1)(L_2)]$ complex.	171
(3–88)	UV-Vis spectrum for $[Cu(L_1)(L_2)]$ complex.	172
(3–89)	UV-Vis spectrum for $[Zn(L_1)(L_2)]$ complex.	172
(3–90)	UV-Vis spectrum for $[Co(L_3)(L_4)]$ complex.	175
(3–91)	UV-Vis spectrum for $[Ni(L_3)(L_4)]$ complex.	175
(3–92)	UV-Vis spectrum for $[Cu(L_3)(L_4)]$ complex.	176
(3–93)	UV-Vis spectrum for $[Zn(L_3)(L_4)]$ complex.	176
(3–94)	Suggested geometry for metal chelates of ligand (L_1).	177
(3–95)	Suggested geometry for metal chelates of ligand (L_2).	177
(3–96)	Suggested geometry for metal chelates of ligand (L_3).	178

	Figures	Page
(3–97)	Suggested geometry for metal chelates of ligand (L_4).	178
(3–98)	Suggested geometry for mixed azo ligand(L_1,L_2) metal chelates.	179
(3–99)	Suggested geometry for mixed azo ligand(L_3,L_4) metal chelates.	179
(3–100)	Bacterial activity for azo ligands and their metal chelates against *Staphylococcus aureus*.	182
(3–101)	Bacterial activity for azo ligands and their metal chelates against *Esherichia coli*.	183
(3–102)	Antifungal activity for azo ligands and their metal chelates against *Candida albicans*.	184
(3–103)	Antifungal activity for azo ligands and their metal chelates against *Candida tropicalis.*	185
(3–104)	Ni^{II} and Cu^{II}-azo dye complexes.	186
(3–105)	Co^{II}, Ni^{II} and Cu^{II}-azo dye complexes.	187
(3–106)	Textiles dyeing by azo ligand (L_1) and their metal chelates.	189
(3–107)	Textiles dyeing by azo ligand (L_2) and their metal chelates.	190
(3–108)	Textiles dyeing by azo ligand (L_3) and their metal chelates.	191
(3–109)	Textiles dyeing by azo ligand (L_4) and their metal chelates.	192
(3–110)	Textiles dyeing by mixed azo ligand (L_1,L_2) metal chelates.	193
(3–111)	Textiles dyeing by mixed azo ligand (L_3,L_4) metal chelates.	194

List of Schemes

	Schemes	*Page*
(1–1)	Mechanism of diazotization of aromatic amine.	4
(1–2)	Azo coupling reaction.	4
(1–3)	Geometrical isomerism of azo benzene.	5
(1–4)	Toutomerisim of azo dyes.	5
(1–5)	Synthesis of azo pyrazole derivatives.	27
(3–1)	synthesis of azo dyes ligands (L_1 and L_2).	49
(3–2)	synthesis of azo dyes ligands (L_3 and L_4).	50
(3-3)	Fragmentation pattern of the ligand (L_1).	53
(3-4)	Fragmentation pattern of the ligand (L_2).	55
(3-5)	Fragmentation pattern of the ligand (L_3).	57
(3-6)	Fragmentation pattern of the ligand (L_4).	58
(3-7)	Tentative decomposition reaction of ligands (L_1-L_4).	61
(3-8)	The tentative decomposition reaction of $[Ni(L_1)_2]$ complex.	108
(3-9)	The tentative decomposition reaction of $[Ni(L_2)_2].H_2O$ complex.	109
(3-10)	The tentative decomposition reaction of $[Zn(L_3)_2]$ complex.	110
(3-11)	The tentative decomposition reaction of $[Cu(L_4)_2]$ complex.	111
(3-12)	Fragmentation pattern for $[Co(L_1)_2]$ complex.	112
(3-13)	Fragmentation pattern for $[Ni(L_2)_2].H_2O$ complex.	114
(3-14)	Fragmentation pattern for $[Cu(L_3)_2]$ complex.	115
(3-15)	Fragmentation pattern for $[Zn(L_4)_2]$ complex.	117
(3-16)	Fragmentation pattern for $[Ni(L_1)(L_2)]$ complex.	118
(3-17)	Fragmentation pattern for $[Cu(L_3)(L_4)]$ complex.	120

List of Abbreviations

FT-IR	Fourier Transform Infrared
UV-Vis	Ultraviolet-Visible Spectrophotometry
1HNMR	Proton Nuclear Magnetic Resonance
13CNMR	Carbon (13) Nuclear Magnetic Resonance
M.Wt	Molecular Weight
m.p	Melting point
DMSO	Dimethyl sulfoxide
DMF	*N*,*N*-Dimethylformamide
Ppm	Part per million
ε_{max}	Molar Absorptivity
B.M	Bohr Magneton
DMSO-d_6	Deuteriodimethylsulphoxide
nm	Manometer
λ_{max}	Wave length
LC–MS	Liquid Chromatography _ Mass Spectrometry
TGA/DSC	Thermogravimetric Analysis/ Differential Scanning Calorimetry
DNA	Deoxyribonucleic acid
RNA	Ribonucleic acid
$0^{\circ}C$	Zero Celsius

Chapter One

Introduction

1.1. Introduction

Coordination chemistry of transition metal complexes with azo ligands are of current attraction due to the interesting physical, chemical, photophysical and photochemical, catalytic and different material properties. The coordination compounds involving azo ligands are significant importance and play a vital role in industry technology and life processes[1,2]. Azo group is characterized by alone pair of orbital's containing two electrons on nitrogen atom, if linked to an aromatic ring carrying an additional donor sites is best suitable for chelation[3], this type of molecule has several advantages. To cite a few the azo group is photochromic, redox responsive, pH-sensitive, they are highly colored and have been used as dyes and pigments in textile fibers, they have been studied widely because of their excellent thermal and optical properties[4]. Also they are including a number of biomedical studies such inhibition of DNA, RNA and protein synthesis, carcinogenesis. Furthermore, they were proved to have biological activity against bacteria and fungi[5].

Advanced application in organic synthesis and high technology areas such as Laser, liquid crystalline displays, electro-optical devices and ink-jet printers[6,7].

Recently many researchers developed a sensitive method for the Determination of metal ions with azo compound as complexmetric agents by spectroscopic studies[8-10].

1.2. Azo dyes

The history of dyeing can be classified into two great periods, the pre Aniline extending to 1856 and the post-aniline period. The former was characterized by a rather limited range of colors that were based on

dye-producing animals and plants[11], the interest towards these dyes increased due to their thermal properties, mixed donor characters (soft-hard), properties that include them as candidates for metal complexes[12].

These compounds have played a powerful role in organic colorants because of at least a conjugated chromophore azo (-N=N-) group which is connected to benzene and naphthalene rings, but can also be attached to aromatic heterocyclic or analyzable aliphatic groups. These side groups are necessary for imparting the color of the dye, with many different shades and intensities being possible, a common example of an azo dye is shown in Figure (1-1),[13].

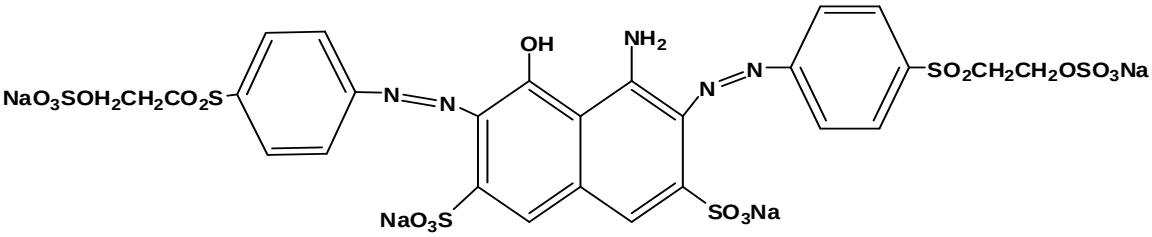

Figure (1-1): Azo dye structure.

This chromophoric system is attached with two or more aromatic or heterocyclic rings. The color properties of organic dye depend on both the presence of chromophores (aromatic) functional groups that absorb light, the most common of these are azo, nitro and carbonyl groups (-N=N-, NO_2, C=O) and nucleophiles are referred to as auxochromes functional groups that increase the intensity of the color, the most common of these auxochromic groups are hydroxyl, amino, sulfanate, carboxylate groups (-OH,-NH_2,-SO_3H,-COOH,) together, the dye molecule is often described as a chromogen[14,15].

Azo dyes can be classified according to the number of azo groups that are present in the dye molecules: monoazo for one, diazo for two, triazo for three or more azo groups. They can also be classified according

to the auxochromic group that is found in it, for example, acidic azo dyes (that have acidic groups such as $-SO_3H$,-COOH.) and basic dyes (that have basic groups such as dialylamino, alkylamino and amino)[16], the general structure of azo dye as shown in Figure (1-2).

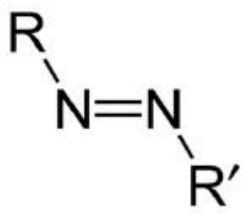

Figure (1-2): General formula of azo dyes.

1.3. Synthesis of azo dyes

Azo compounds have been characterized by the presence of azo group (-N=N-) which links to sp^2-hybridized carbon atoms the azo groups are usually linked to substituted aromatic or hetero aromatic cyclic groups, the general synthetic route of azo compounds includes two steps: diazotization of an aromatic amine and azo coupling[17].

1.3.1. Diazotization

A diazotization is the conversion of an aromatic or hetero aromatic primary amine to diazonium ion then followed by coupling the product to an electron-rich nucleophile Scheme (1-1) at low temperature and in acidic aqueous solution containing nitrous acid (HNO_2) at (0- 5C°). Usually added as sodium nitrite ($NaNO_2$) with, an aqueous mineral acid such as hydrochloric acid, the diazonium ion is very unstable because of presence of the benzene ring with its high electron density stabilizes the ±N≡N group[18].

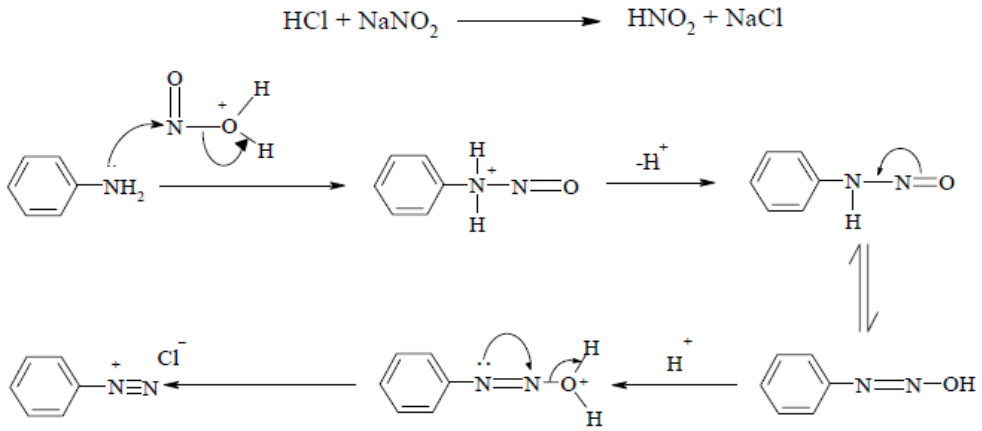

Scheme (1-1): Mechanism of diazotization of aromatic amine.

1.3.2. Azo coupling reaction

The coupling reaction is performed by treating the unstable diazonium salt in cold aqueous solution with a coupling component such as phenols or aromatic amines Scheme (1-2) is this way as table azo dye is formalized[19].

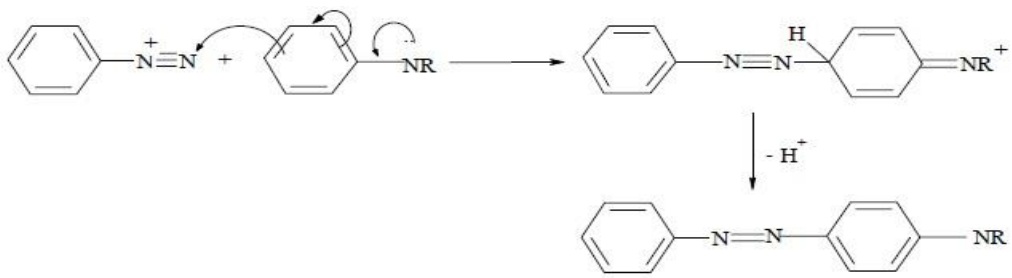

Scheme (1-2): Azo coupling reaction.

1.4. Isomerism in azo compounds

1.4.1. Geometrical isomerism

The planar (-N=N-) bond is usually exists to geometrical isomers. Azo benzene is a typically photochromic molecule can exist in two configurations, the E (trans) and Z(cis) forms, that can be interconverted either photochemically or thermally. Upon irradiation a change from the stable E-azo benzene (E-AB) to the meta stable Z-azo benzene (Z-AB) is

induced Scheme (1-3) where a reversible color change of the dye. Interestingly, this effect was considered to be an inconvenience and was prevented by carful development of more stable azo dyes[20].

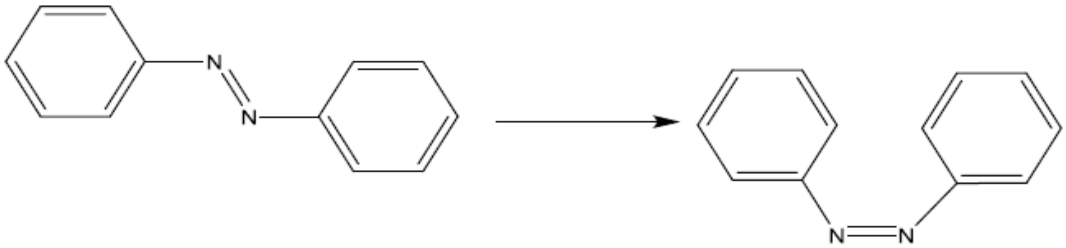

E-azo benzene **Z-azo benzene**

Scheme (1-3): Geometrical isomerism of azo benzene.

1.4.2. Toutomerisim

When a hydrogen atom in a molecule is trans ported removed from one part to another, this is called toutomerisim. This is happened in azo dyes when an (-OH) group is present in the para or ortho position explained in Scheme (1-4).

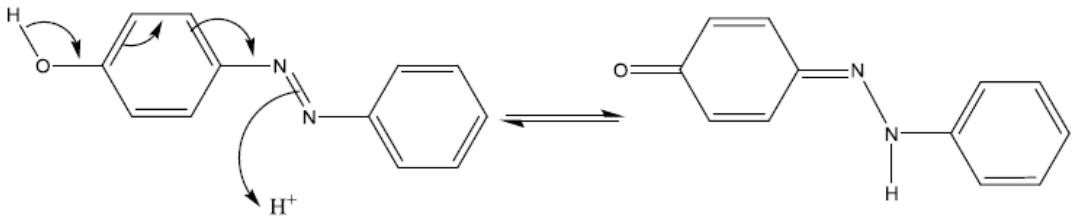

Scheme (1-4): Toutomerisim of azo dyes.

Toutomeric forms can be identified spectroscopically. The keto hydrazones absorb at higher wavelengths than their hydroxyl azo forms. keto hydrazones also have larger molar absorptivites. However, not all azo compounds show tautomerisim and some tautomeric forms are more stable than others[21].

1.5. Alkyl and aryl azo compounds

The literature survey reveals that large number of azo dyes have been investigated by many workers, as chelating agent and their metal chelates. Azo dyes are compounds bearing the functional group (R–N=N–R^*) In which R and R^* can be either alkyl or aryl groups[22].

1.5.1. Aliphatic azo compounds

The dyes are called aliphatic azo dyes when both substituents are aliphatic (alkyl group), these are less common as dyes because of they have low absorptivity in the visible range and are not stable. In certain alkyl azo compounds breaks into two radicals and to nitrogen gas therefore, they can be used as radical initiators. Commercially important initiator is azo bisbutyronitrile (AIBN), as shown below[23], Figure (1-3).

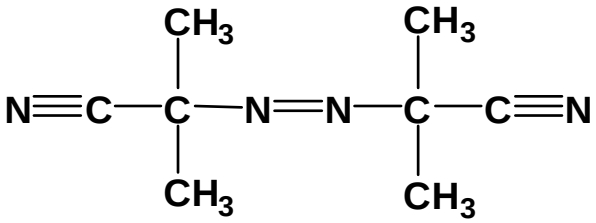

Figure (1-3): Chemical structure of (AIBN).

1.5.2. Aromatic azo compounds

In aromatic azo compounds the (R) groups are aryl rings the structures of these compounds are generally more stable and tend to be crystalline such as azo benzene than if the (R) groups are alkyl groups because of (i) the (-N=N-) group becomes part of an extended delocalized system involving the aryl groups. (ii) the aromatic azo groups are highly colored and are often used as dyes they are usually strongly colored compounds which can be intensity colorless→ yellow→ orange→ red→ green→ blue, the colors differences are caused by different substituent's on aromatic rings which lead to differences in the extent of conjugation of

the π-system in the azo compound. Usually least than extensive the conjugated π-system of a molecule. There are two kinds of aromatic azo compound were recognized the homo and the heterocyclic azo compounds[24,25].

1.5.2.1. Homocyclic azo compounds

Homocyclic azo compound from typical octahedral complexes transition metals by way of coordination through N atom of the azo group and a strongly electron donating in the ortho position next to the azo group[26]. These azo compounds considered as important reagents in analytical chemistry as it used as indicators or spectra-reagents.

When one or both of the homocyclic rings may be contain different acidic or basic substitutes that increase the ligands selectivity to be used us an organic reagents[27].

Modhavadiya [28], synthesis of Fe^{II} and Cu^{II} complexes with sulfa drugs azo dye ligand derived from sulfadimidine and 2-ethyl-4-methyl phenol. Metal complexes were characterized from spectroscopic and analytical data (FT-IR and UV-Vis spectra) elemental analysis, metal contents, magnetic properties and molar conductance. A square planner geometry around Cu^{II} complex was proposed and an octahedral geometry about Fe^{II} complex was proposed, Figure (1-4). Biological activity measurements revealed that ligand has lower antimicrobial activity than their metal complexes.

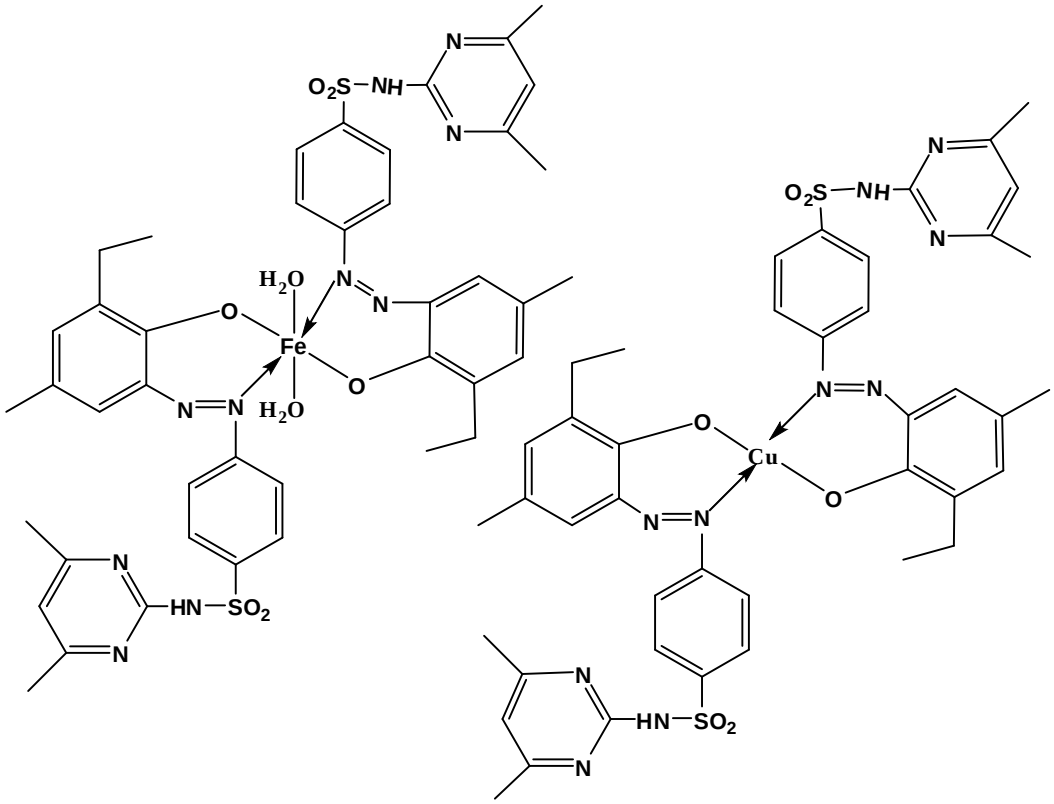

Figure (1-4): The structure of Cu^{2+} and Fe^{2+} complexes.

In 2012 Turcas and Sebe [29], reported the synthesis of copper, cobalt and chromium complexes with four new azo dyes, these complexes were prepared from 1-diazo-2-naphthol-4-sulphonic and 6-nitro-1-diazo-2-naphthol-4-sulphonic acids by coupling with β-naphthol, or N,N-diethyl-m-amino-naphthol. Complexes have been characterized using elemental analysis, UV–Vis and FT-IR spectral methods. On the basis of analytical and spectral studies, the Cu^{II} and Co^{III} complexes are assigned to be tetrahedral, Figure (1-5). While the Cr^{III} complexes have been octahedral, Figure (1-6). The dyeing resistances were determined on wool and polyamide.

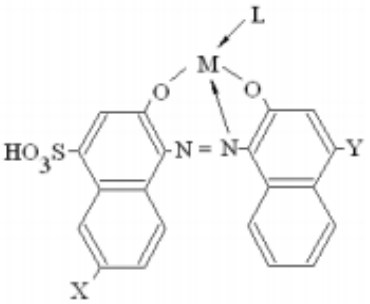

Complex I	X	Y	L (ligand)	M(metal)
Cu1	NO_2	H	CH_3OH	Cu
Cu2	H	H	CH_3OH	Cu
Cu3	NO_2	NEt_2	H_2O	Cu
Cu4	H	NEt_2	H_2O	Cu
Co1	NO_2	H	CH_3OH	Co
Co2	H	H	CH_3OH	Co
Co3	NO_2	NEt_2	CH_3OH	Co
Co4	H	NEt_2	CH_3OH	Co

Figure (1-5): Proposed structure of Cu^{II} and Co^{III} complexes.

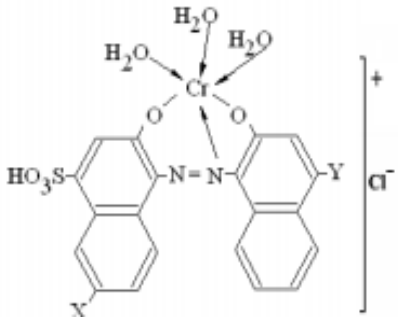

Complex II	X	Y	L (ligand)	M(metal)
Cr1	NO_2	H	$3H_2O$	Cr
Cr2	H	H	$3H_2O$	Cr
Cr3	NO_2	NEt_2	$3H_2O$	Cr
Cr4	H	NEt_2	$3H_2O$	Cr

Figure (1-6): Proposed structure of Cr^{III} complexes.

In 2014 Canakci, *et.al* [30], have been synthesized a new metal chelates by reaction azo dye [1-(2-nitrophenl azo)-2,7-dihydroxy naphthalene] with metal salts (Co^{II}, Ni^{II} and Cu^{II}) in alcoholic medium were mixed in 1:2 (metal: ligand) ratio. Compounds were characterized by various spectroscopic studies (FT-IR, UV-Vis and ^{1}HNMR) elemental analysis, magnetic measurements. According of the analytical and spectral studies, an octahedral geometry have been assigned for these complexes, Figure (1-7).

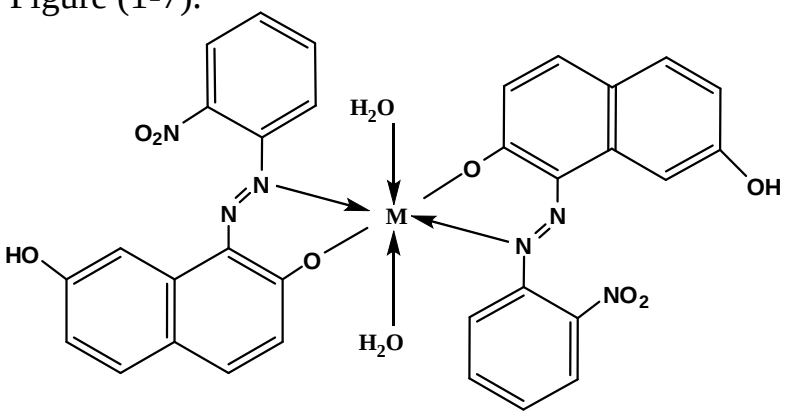

M = Co^{II},Ni^{II} and Cu^{II}

Figure (1-7): Proposed structure of Co^{II}, Ni^{II} and Cu^{II} metal chelates.

In 2015 Anitha ,*et.al* [31], prepared a series of (Cu^{II} and Ni^{II}) complexes with novel bisazo dye 2,2[benzene-1,3-diyl di (E)diazene-2,1-diyl] dianiline derived from m-phenylenediamie and aniline. Stoichiometric ratio of the complexes has been found to be 1:1 (M:L). Depending on physico-chemical analysis square planar geometry were proposed for the azo complexes, Figure (1-8).

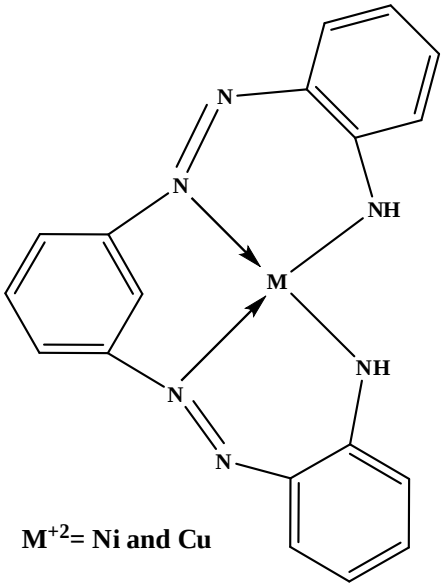

Figure (1-8): Structure of Ni^{II} and Cu^{II} metal chelates.

In the same year Kadhim [32], have produced chelates of the azo dyes ligands derived from 2,4-dimethylphenol and 3 or 4-aminobenzoicacid with (Ni^{II} and Cu^{II}) in (1:2,M:L) ratio. Complexes have been characterized by elemental analysis, spectroscopic techniques (FT-IR, UV-Vis and ^{1}H- NMR), conductivity and magnetic susceptibility measurements .The spectral and chemical analysis assigned tetrahedral geometry for the azo complexes, Figure (1-9).

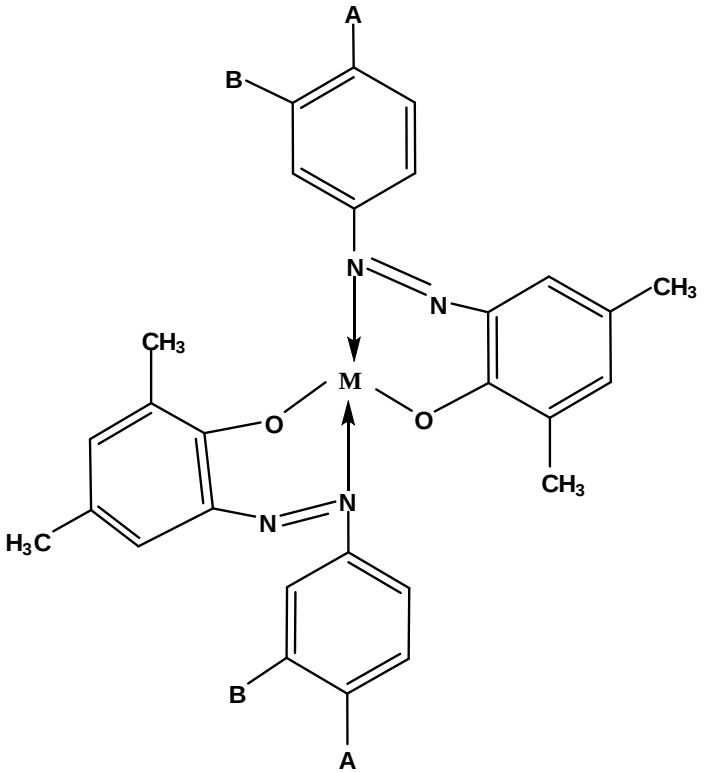

L_1, (A = H, B = COOH) **L_2, (A = COOH, B = H**

M = Ni(II) and Cu(II)

Figure (1-9): Structure of Ni^{II} and Cu^{II} with azo dyes ligands.

In 2016 EL-Ansary, *et.al* [33], synthesized of Ni^{II} macromolecular complex with azo dye derived from sulfadimidine and 3-hydroxy-2-naphthoic acid. Ni^{II} complexes has been characterized by elemental analyses, magnetic moment, conductance measurements and spectral techniques (FT-IR, UV-Vis, ESR, ^{1}H-NMR). Depending on the spectral and chemical analyses, the suggested geometry was octahedral for Ni^{II} complex, Figure (1-10).

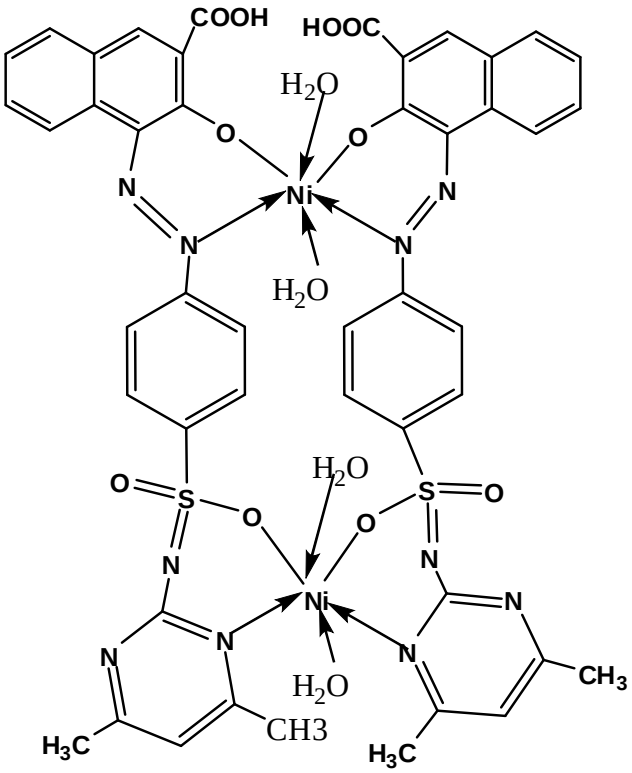

Figure (1-10): Chemical structure of Ni^{II} complex.

Jarad, *et.al* [34], synthesized a complexes of (Ni^{II} and Cu^{II}) with azo dyes ligands were obtained by coupling the diazonium salts of amines with 3-hydroxyacetophenone. Compounds were identified by (FT-IR, UV-Vis, ^{1}H and ^{13}C- NMR) spectroscopic methods, elemental analysis, atomic absorption, conductivity and magnetic quantification. The results suggested that the complexes have a 1:2 (M:L) molar ratio, these studies confirmed the tetrahedral structure for complexes, Figure (1-11).

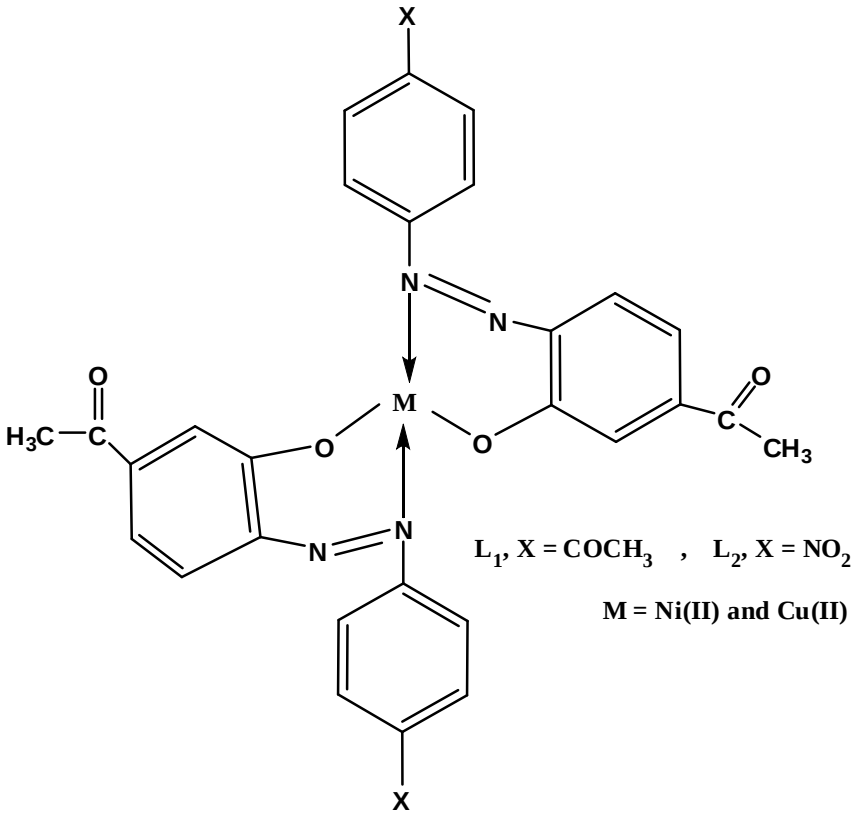

Figure (1-11): Structure of azo complexes.

1.5.2.2. Heterocyclic azo compounds

Heterocyclic azo compound are a class of molecules that contain hetero atom in *ortho*-position of azo (-N=N-) group[35]. Heterocyclic azo dyes are well known for their outstanding photometric sensitivities constitute an important class amongst the various organic reagents used in the determination of metal ions[36]. At present, the numbers of heterocyclic azo compounds are used in analytical chemistry substantially.

The application of these azo dyes in spectrophotometery is based on the color resulting from reaction with most of the metals especially with some transition metals usually stable chelates are produced. The reagents and their metal complexes have rather limited solubility in

aqueous solutions but much greater solubility in organic systems thus they are employed as indicators[37].

1.5.2.2.1. Pyridyl azo compounds

Heterocyclic azo dyes of pyridyl type are an important class of organic reagents with good complexing capacity, the most important compounds of this class are 1-(2-pyridyl azo)-2-naphthol (PAN) and 4-(2-pyridyl azo)-resorcinol (PAR), these azo dyes have been used for the spectrophotometic determination of more than fifty elements because of these ligand intensely colored complexes and act as tridentate ligands[38,39], Figure (1-12).

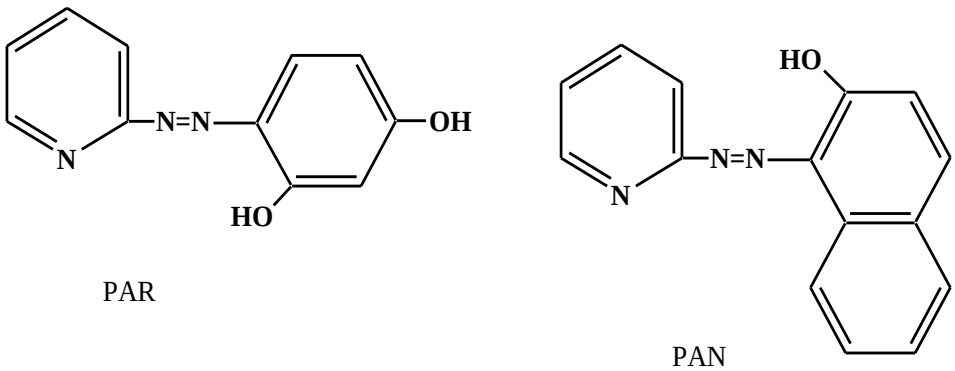

Figure (1-12): Structure of PAN and PAR azo dyes.

Karipcin and kabalcilar [40], reported the preparation of (Mn^{II}, Fe^{II}, Co^{II}, Ni^{II}, Cu^{II}, Zn^{II} and Cd^{II}) complexes with 4-(2-pyridyl azo)-resorcinol in 1:2 (M:L) ratio. Solid complexes were characterized by elemental and thermal analyses, (FT-IR, UV-Vis spectra), molar conductance and magnetic measurements. Depending on the spectral and analytical studies an octahedral geometry have been suggested for these metal chelates, Figure (1-13).

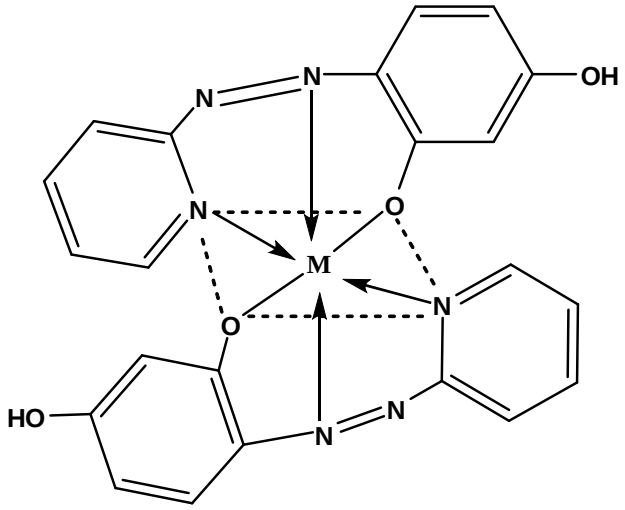

M = Mn^{II},Fe^{II}, Co,$^{II}Ni^{II}$, Cu^{II}, Zn^{II} and Cd^{II}

Figure (1-13): Proposed structure of metal complexes for 4-(2-pyridyl azo)-resorcinol.

In 2016 Mahmoud, *et.al* [41], synthesized chelates of new N_3O_2 donor pentadentate azo dye ligand was obtained by reaction of 2,6-diamino pyridine and p-methoxybenzaldehyde with transition metal ions (Cr^{III}, Mn^{II}, Fe^{II}, Co^{II}, Ni^{II}, Cu^{II}, Zn^{II} and Cd^{II}). Metal complexes were characterized by elemental analysis, molar conductance, FT-IR, UV-Vis, ^{1}HNMR, ESR spectral studies, magnetic susceptibility measurements, thermo gravimetric analyses (TG) and X-ray diffraction (XRD), these studies confirmed an octahedral structures for all complexes, Figure (1-14). Biological activity measurements revealed that all complexes have higher antimicrobial activity than the free azo ligand except Mn^{II} and Fe^{II} complexes which have no antimicrobial activity.

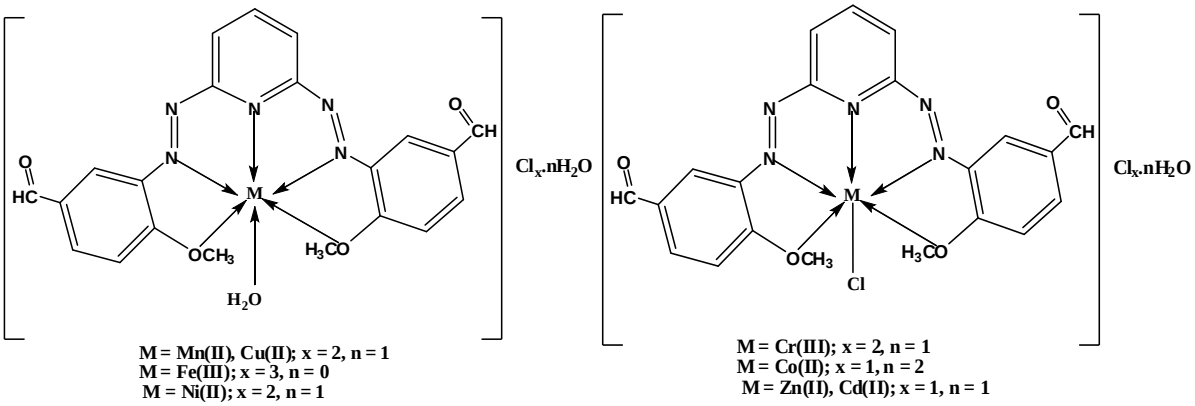

Figure (1-14): The Proposed structure of the azo dye complexes.

1.5.2.2.2. Thiazolyl azo compounds

Thiazol and Benzothiazolyl azo dyes as spectrophotometric reagents, these compounds are easily prepared from a wide range of phenols, naphthols and the other non-phenolic substances by coupling reaction with diazonuium salt of 2-amino thiazole and 2-amino benzothiazole, this azo compounds have important role in spectral determination field to determine the trace amount of elements especially transition metal ions because of high sensitivity and selectivity[42,43].

A number of these dyes were synthesized and their abilities as chelating ligands[44]. The common reagent of these compounds is (TAR) and (TAN), Figure (1-15).

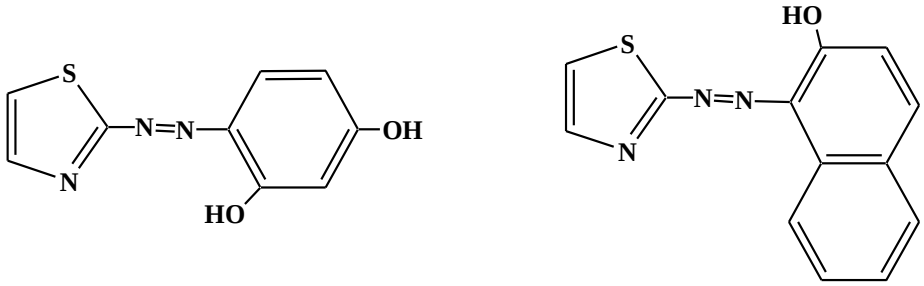

4-(2-Thiazolyl azo)-resorcinol (TAR) **1-(2-Thiazolyl azo)-2-naphthol (TAN)**

Figure (1-15): Structure of (TAR) and (TAN).

Keshavayya, *et.al* [45], synthesized a three heterocyclic azo dyes using 6-methoxy-2-aminobenzothiazol (IA), 4-(4-nitrophenyl)-2-aminothiazole (IB) and 6-methyl-2-aminobenzothiazol (IC) as diazo components which were diazotized and coupled with barbituric acid in basic media (pH=9-10). The structures of these azo dyes were characterized by (FT-IR, UV-Vis, ^{1}HNMR and Mass) spectroscopic techniques, the electrochemical properties of these azo dyes have been studied by using cyclic voltammetric (CV) technique, Figure (1-16).

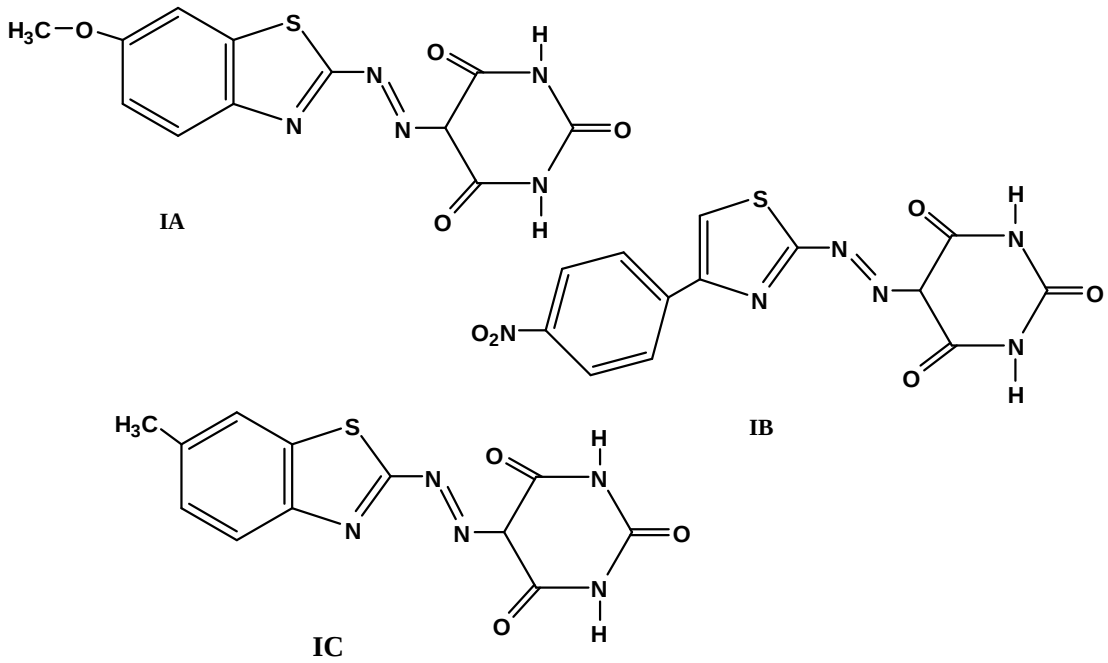

Figure (1-16): Proposed structure of azo dyes ligands.

In 2015 Jreo [46], described the synthesis of new 2-(6-nitro-2-benzothiazolyl azo)-4-hydroxybenzoic acid (NO_2BTAHBA) organic reagent with Cu^{II} at (M:L) ratio (1:2). Cu^{II} (NO_2BTAHBA) complex was characterized by spectral and analytical studies. Depending results confirmed the octahedral arrangement about metal centre, Figure (1-17).

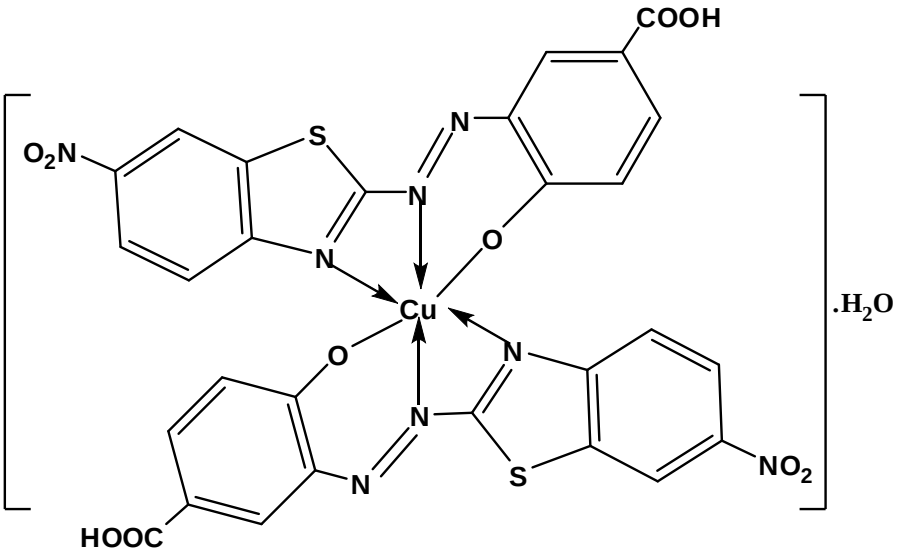

Figure (1-17): Structure of Cu^{II} complex with (NO_2BTAHBA).

The formation of some new metal-azo chelates of metal ions (Ni^{II}, Cu^{II} and Zn^{II}) with a mono negative tridentate azo ligand 1-(6-methyl-2-benzothiazolyl azo)-2-naphthol-4-sulfonic acid (BANS) at (1:2) metal to ligand[47], metal chelates have been identified by elemental analysis, ^{1}HNMR, FT-IR and UV-Vis, magnetic moment measurements and molar conductance. The Analytical analyses suggested that metal-azo chelates have octahedral geometry, Figure (1-18). Biological activity measurements showed that complexes have higher antimicrobial activity than the free ligand.

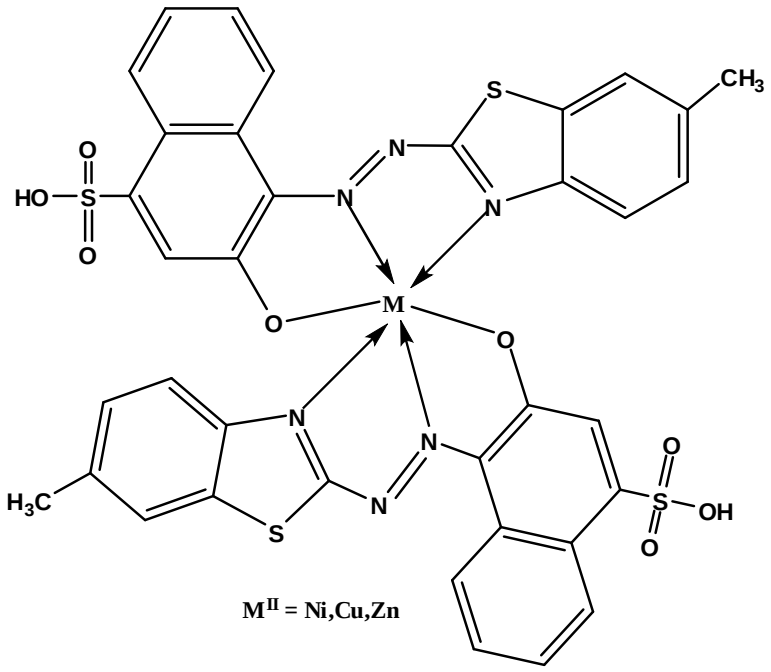

Figure (1-18): Structure of metal chelates of azo ligand.

In 2017 AL-Adilee, *et.al* [48], reported the synthesis of a novel heterocyclic mono azo dye bidentate ligand which obtained from coupling reaction between 5-nitro-thiazole diazonium chloride and 2-amino-4-methylpyridine in alkaline alcoholic solution. A series of some transition metal complexes were prepared by reaction of ligand with salt of [Cr^{III}, Mn^{II}, Fe^{III}, Co^{II}, Ni^{II}, Cu^{II} and Zn^{II}], these compound were characterized by [^{1}H, ^{13}CNMR, FT-IR, V-Vis and Mass] spectroscopy, (C.H.N) analysis, magnetic susceptibility, atomic absorption and molar conductivity. The analytical data is found to be 1:2 [M:L] in all complexes, the geometry proposed for all metal complexes were octahedral stereochemistry, Figure (1-19).

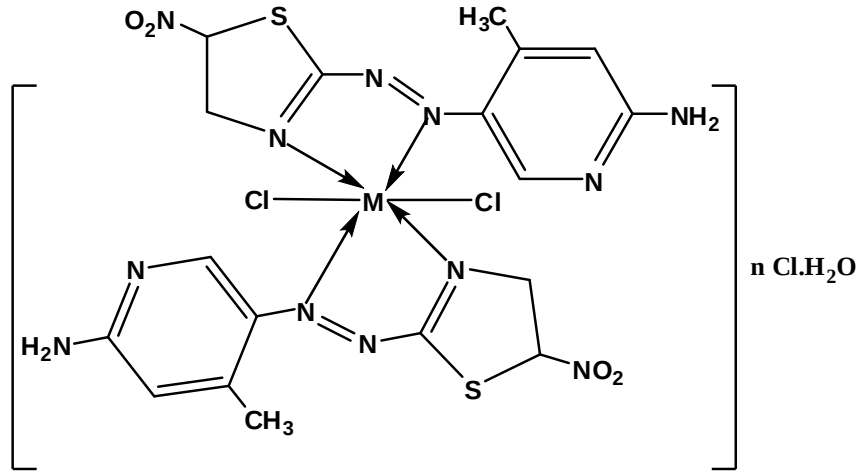

M^{III} = Cr and Fe ; n = 1, M^{II} = Mn, Co, Ni, Cu and Zn ; n = 0

Figure (1-19): Suggested structure for [Cr^{III}, Mn^{II}, Fe^{III}, Co^{II}, Ni^{II}, Cu^{II} and Zn^{II}] complexes.

Jarad, *et.al* [49], formtion of 2-(2-benzathiazolyl azo)-3,5-dimethylphenol was formed by grouping the 2-benzothiazole diazonium chloride with 3,5-dimethylphenol. Complexation of tridentate azo dye with (Co^{II}, Ni^{II}, Cu^{II} and Zn^{II}) in aqueous of ethyl alcohol with a 1:2 metal:ligand and at ideal pH. The formation of metal chelates are assigned using flame atomic absorption, FTIR and UV-Vis spectral analysis, other than conductivity and magnetic estates, these studies confirmed an octahedral structure for metal chelates, Figure (1-20).

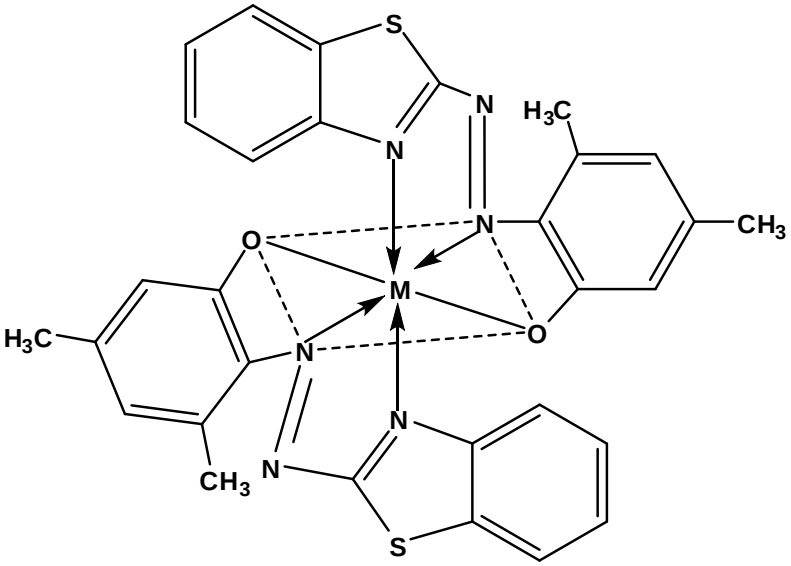

M^{2+}= Co,Ni,Cu and Zn

Figure (1-20): Proposed structure of metal complexes for 2-(2-benzathiazolyl azo)-3,5-dimethylphenol.

1.5.2.2.3. Imidazol and Pyrimidyl azo compounds

Imidazoles are well known a five-membered hetero-aromatic compounds containing active π-acidimine (-C=N-) group and efficient reagent to stabilize low valent metal oxidation states. They possess both acidic and basic characteristics, the NH group present in imidazole is relatively strongly acidic and also weakly basic. Another characteristic of imidazole is that they have the capacity to form salts. The imidazole azo compounds usually react with transition and non transition metal ions as bidentate or as tridentate ligand in the field of coordination chemistry. Imidazole derivatives have an important pharmacological properties and play a significant role in many biochemical processes such as inhibitors fungicides and therapeutic agents, these compounds were widely studied in analytical separation and spectrophotometric determination of some metal cations[50-52].

The synthesis of a new series of (Co^{II}, Ni^{II}, Cu^{II}, Zn^{II}, Cd^{II} and Hg^{II}) complexes with bidentate chelating azo dye ligand 2-[2-(6-nitro benzothiazolyl)azo]-imidazole (NBTAI) have been prepared and characterized by elemental analysis, molar conductance measurements, magnetic moment measurements and (FT-IR, UV-Vis) spectra, the analytical data was showed that the metal to ligand ratio (1:2). The geometry proposed for all complexes octahedral stereochemistry[53], Figure (1-21).

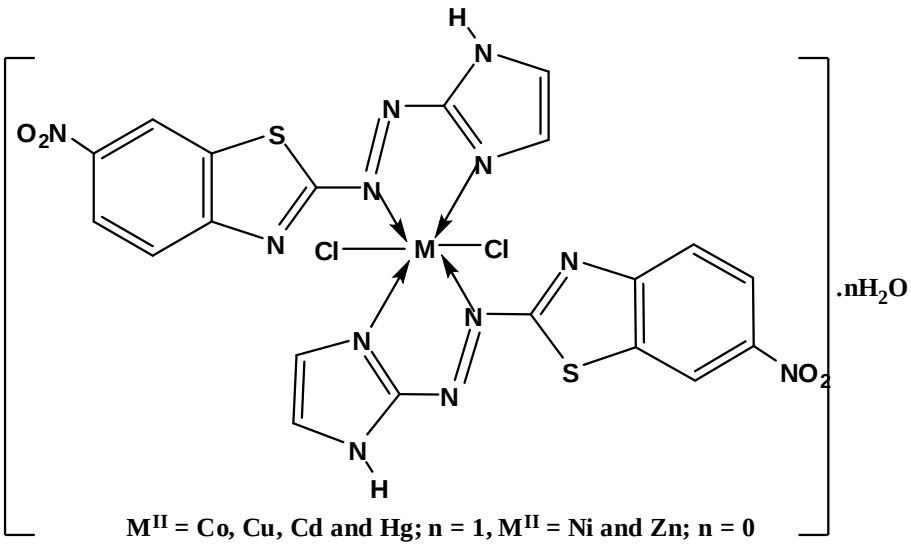

Figure (1-21): Suggested structure of metal complexes with 2-[2-(6-nitro benzothiazolyl)azo]-imidazole

Formation of Ag(I) complex with 4-(2-benzimidazolyl azo)-proline ligand has been reported and identified by elemental analysis, (FT-IR, UV-Vis and ^{1}HNMR) spectroscopy and molar conductivity, the stoichiometry measurement investigated that the molar ratio (1:2). A tetrahedral arrangement was suggested for Ag(I) complex[54], Figure (1-22).

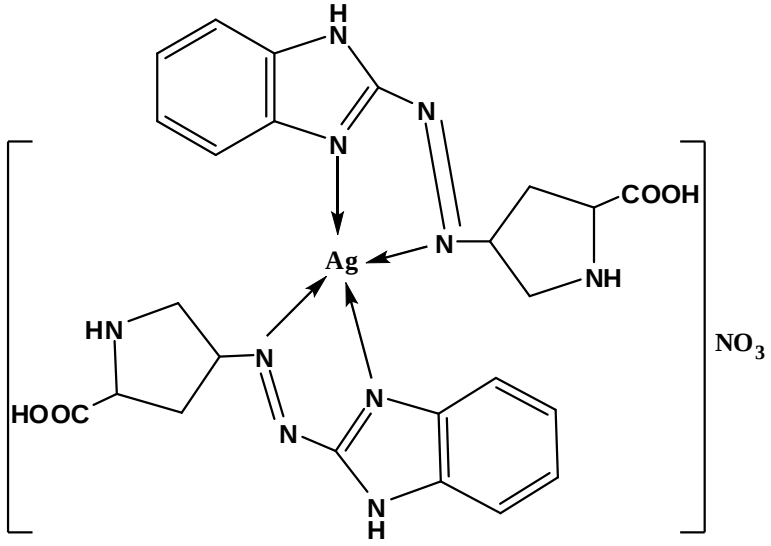

Figure (1-22): Structure of Ag^{I} complex.

Farhan [55], described the preparation of a new bis azo dye 2-(4-methoxy-2-(4-methoxy phenyl)diazenyl)-phenyl-diazenyl-4,5-diphenyl-Imidazole with transition metal complexes of Co^{II} and Cu^{II}. Structural characterization of these complexes were carried out using elemental analysis, (FT-IR, UV-Vis, ^{1}H,^{13}C-NMR) spectroscopy and molar conductivity measurements, The results suggested that the bis azo ligand was chelated to the metal ion as tridentate ligand with (1:2) (M:L) stoichiometry, these studies confirmed the octahedral structure for the complexes, Figure (1-23).

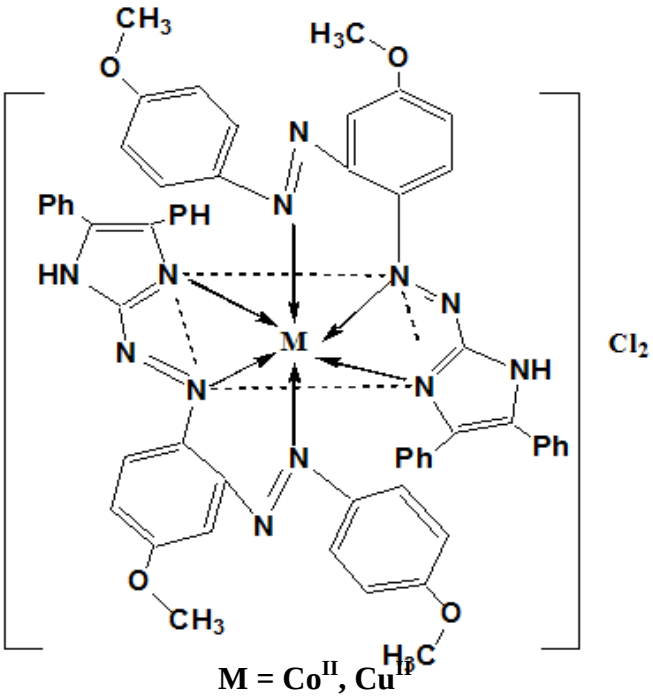

Figure (1.23): Structure of Co^{II} and Cu^{II} complexes with bis azo dye ligand

Pyrimidines are a six-membered heterocyclic aromatic organic compounds, the basic skeleton of a pyrimidine ring is composed of two elements carbon and nitrogen and are also named as diazines having two nitrogen atoms at position 1 and 3.

The significant position of pyrimidine and its derivatives in organic chemistry is constitute nucleic acids which is the base of life. Three nucleobases (cytosine, thymine and uracil) are pyrimidine derivatives[56].

Pyrimidine azo coupling reactions are well known compounds synthesized as a result of these reaction are colored so they play an important role in analytical chemistry as metal chromogenic agents[57]. Furthermore transition metal complexes of these compounds can also be synthesized with therapeutic potencies bioactivity of pyrimidine azo

compounds is very large including anti-inflammatory, antibacterial and antifungal activities[58].

In 2012 Dhahir, *et.al* [59], have been synthesized metal chelates of [Fe^{II}, Co^{II}, Ni^{II}, Cd^{II} and Cu^{II}] with 2-[2-amino-5-(3,4,5-trimethoxy-benzyl)-pyrimidyl-4-azo]-4-bromophenol, these complexes were characterized by FT-IR and UV-Vis spectroscopic methods, conductivity, metal analyses and magnetic moment measurements. These studies indicated the preparation of complexes with octahedral arrangement around metal centers, Figure (1-24). Antibacterial activities data revealed that complexes how more toxicity against the bacterial species of the free ligand.

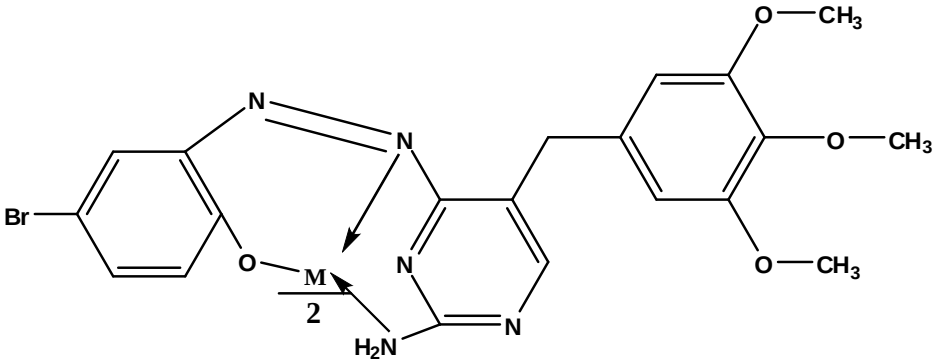

M^{II} = Fe, Co, Ni, Cu and Cd

Figure (1-24): Proposed structure of metal complexes for pyrimidyl azo dye.

The formation of Pd^{II} azo complex with a novel azo pyrimidin ligand N-(1-(4-aminophenyl)ethyidine)-4-(2-amino-3-(4-methoxy-phenyl)diazenyl)[1,5-a] pyrimidin-7-yl) benzene amine was reported[60]. The stereochemistry and the mode of bonding of complex was confirmed depending on elemental analysis, conductance measurements and (IR, UV-Vis, ^{1}HNMR, ESR and Mass) spectroscopy and thermo-gravimetric

analysis (TGA). Square planer arrangement was proposed for Pd^{II} complex, Figure (1-25).

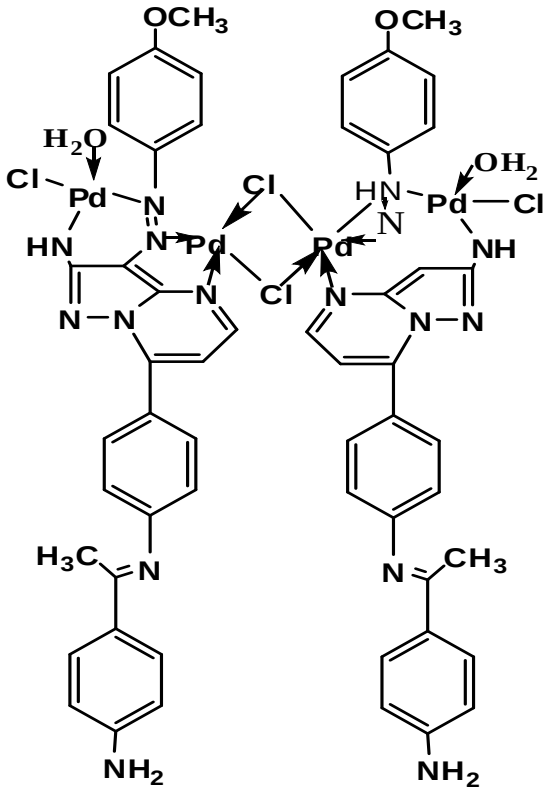

Figure (1-25): Chemical structure of Pd^{II} complex.

1.5.2.2.4. Pyrazolone azo compounds

Pyrazolone is a Five-membered lactam ring heterocyclic compound containing two nitrogen atoms and ketone in the same molecule. Pyrazolone is an active moiety as a pharmaceutical ingredient especially in the class of nonsteroidal anti-flamematory agent and intermediates in dye industry and exhibited a wide variety of biological and pharmaceutical activities therefore they play an important role in medicinal chemistry[61]. Azo pyrozole derivatives containing (O,N) donor atoms act as superior chelating agents for the transition and non-transition metal ions, these azo compounds give bright, high intensity colors, therefore they are used in preparing dyes and Pigments[62,63].

Antipyrine (2,3-Dimethyl-1-Phenyl-5-Pyrazolone) and their metal complexes have a variety of applications in biological, clinical, analytical and pharma-cological area[64,65].

Rizk, *et.al* [66], synthesized a series of novel pyrazole derivatives heterocyclic azo dyes using 3-substituted-5-aminopyrazales as diazo compounds which were diazotized and coupled with different phenols. These dyes were confirmed by (FT-IR, UV-Vis, ^{1}H-NMR) spectroscopy and elemental analysis. all of the dyes were investigated for their dying characteristics on different types of fibers (wool, Polyester and wool/ polyester blend and the fastness properties were evaluated for the dyes fabrics, Scheme (1-5).

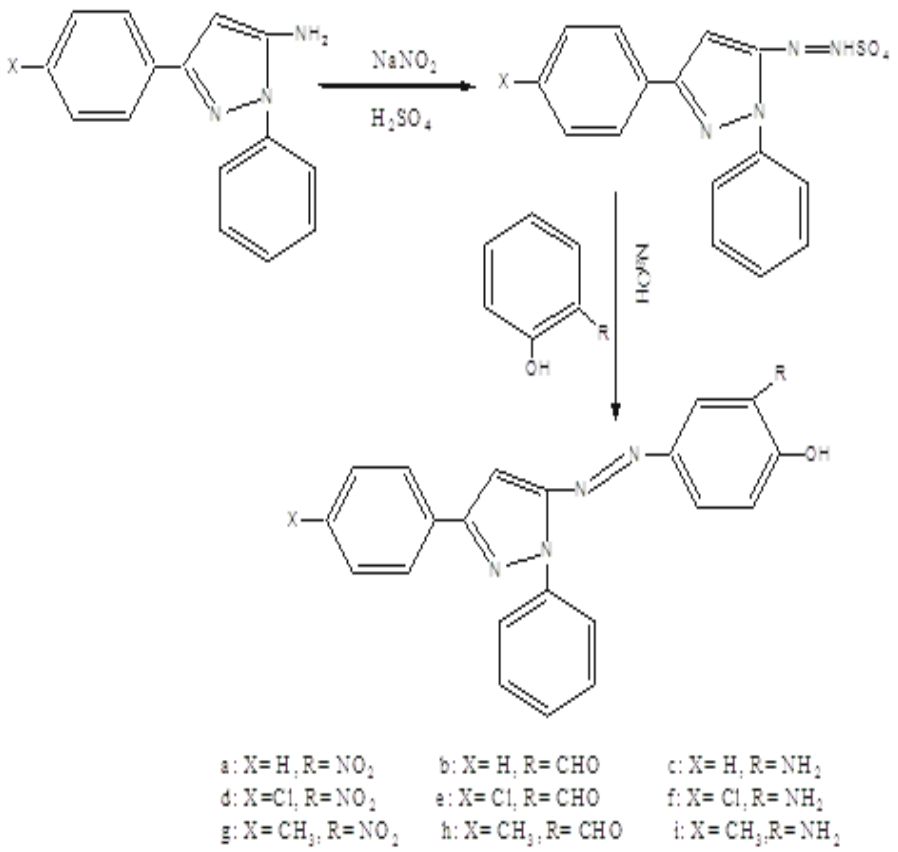

Scheme (1-5): Synthesis of azo pyrazole derivatives.

The formation a series of novel metal ions [Cr^{III}, Fe^{III}, Mn^{II}, Co^{II}, Ni^{II} and Cu^{II}] complexes with the new tridentate azo dye (E)-4-((4-hydroxy-6-methyl-2-oxo-2H-pyran-3-yl)diazenyl)-1,5-dimethyl-2-phenyl-1H-pyrazol-3(2H)-one were reported [67]. Metal chelates have been characterized by elemental analysis, molar conductivity measurements, magnetic susceptibility data and (^{1}H, ^{13}C-NMR, FT-IR, UV-Vis) spectroscopic results, these studies indicated that an octahedral geometry for all metal(II) complexes, Figure (1-26).

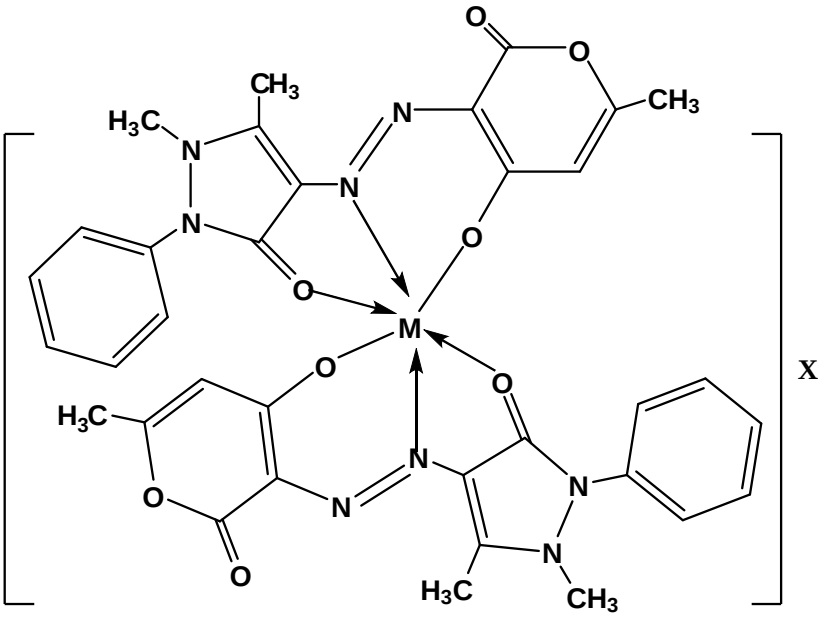

M = Cr^{III} and Fe^{III}; X = Cl, M = Mn^{II},Co^{II},Ni^{II} and Cu^{II} ; X = 0

Figure (1-26): Structure of metal complexes for (E)-4-((4-hydroxy-6-methyl-2-oxo-2H-pyran-3-yl)diazenyl)-1,5-dimethyl-2-phenyl-1H-pyrazol-3(2H)-one.

Chaulia [68], synthesized a series of dinuclear complexes of [Co^{II}, Ni^{II}, Cu^{II} and Zn^{II}] with new tetradentate azo dye ligand derived from 4-aminoantipyrine and 2,4-dihydroxybenzoic acid. Compounds were characterized by molar conductance, magnetic susceptibility measurement, spectroscopic methods (FT-IR, UV-Vis, ^{1}H-NMR, Mass,

ESR, XRD powder pattern) and thermogravimetric analysis, an octahedral geometry a bout Co^{II}, Ni^{II}, Cu^{II} were proposed. Biological measurement indicates the antibacterial properties and DNA binding activity of the investigating compounds, Figure (1-27).

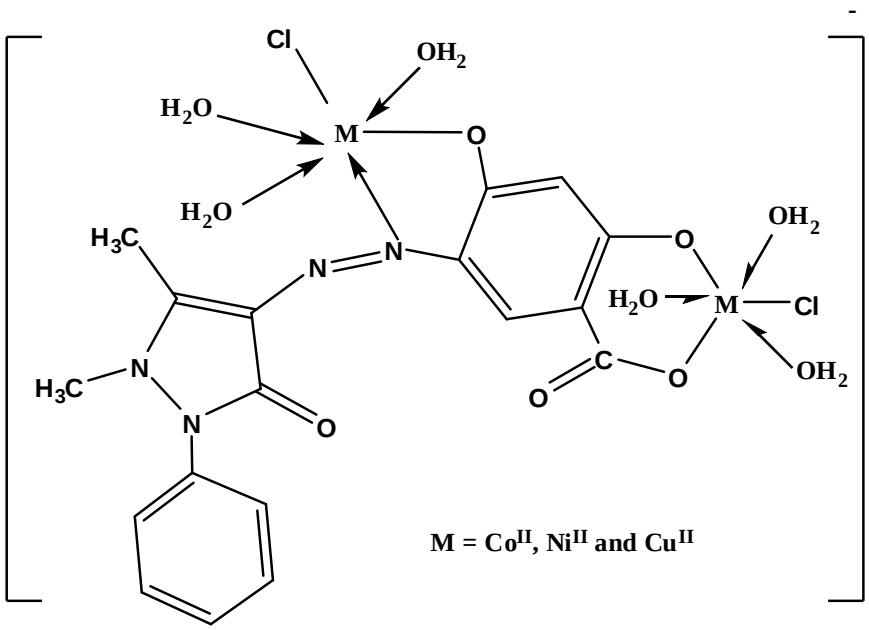

Figure (1.27): Proposed structure of metal chelate for pyrazolyl azo dye.

In 2016 Jarad [69], studied the synthesis of 4-(2-Amino-5-nitro-phenyl azo)-1,5-dimethyl-2-phenyl-1,2-dihydro-pyrazole-3-one tridentate azo dye ligand which derived from 4-aminoantipyrine and 4-nitroaniline. Complexes were prepared from reaction of azo dye with metal salts ($M=Y^{III}$ and La^{III}) with a 1:2 M:L ratio at optimum PH, produced compounds have been identified by analytical and spectral studies, an octahedral geometry suggested for complexes, Figure (1-28). All prepared compounds revealed good antibacterial activity, the ligand and their complexes were application to cotton fabric and study of detergent fastness.

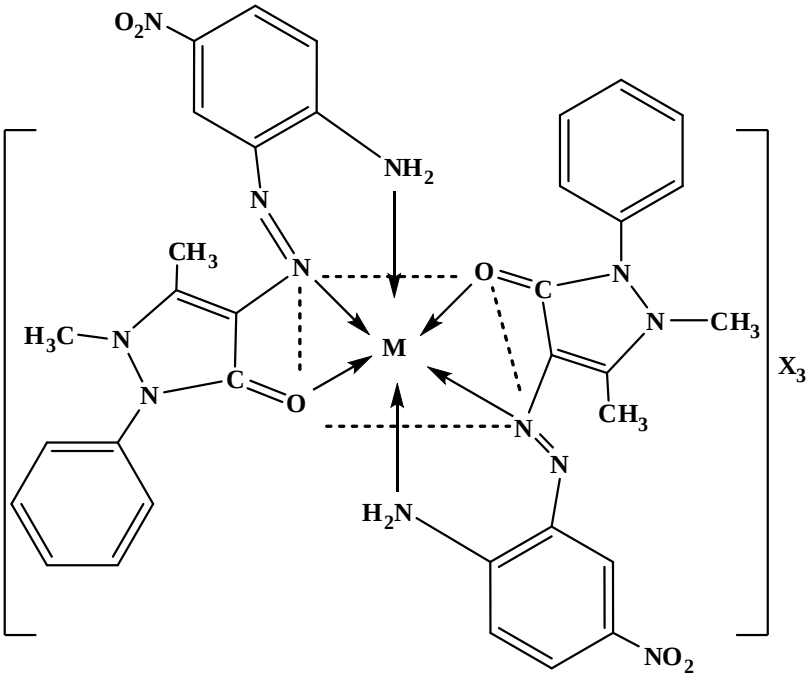

M = Y(III) when x = NO_3, La(III) when x = Cl

Figure (1-28): Structure of Y^{III} and La^{III} metal chelates.

In 2017 Hussain, *et. al*[70], described the synthesis new complexes of [Fe^{II} and Cu^{II}] with a series of new acid dyes ligands, derived from the reaction of 4-amino-1-(4-sulfophenyl)-3-methyl-5-pyrazolone with alkaline solution of phenol derivatives which include 4-chlorophenol, 4-nitrophenol, 4-hydroxybenzene sulfonic acid, 2-nitrophenol-4-sulfonic acid, resorcinol and bis phenol. The structures of these dyes and their complexes confirmed by FT-IR, UV-Vis and ^{1}H, ^{13}C-NMR spectroscopy. The spectral and chemical analyses suggested that Fe^{II} and Cu^{II} complexes have octahedral geometry, Figure (1-29). Metal complex dyes have better application properties on leather as compared to ligand dyes.

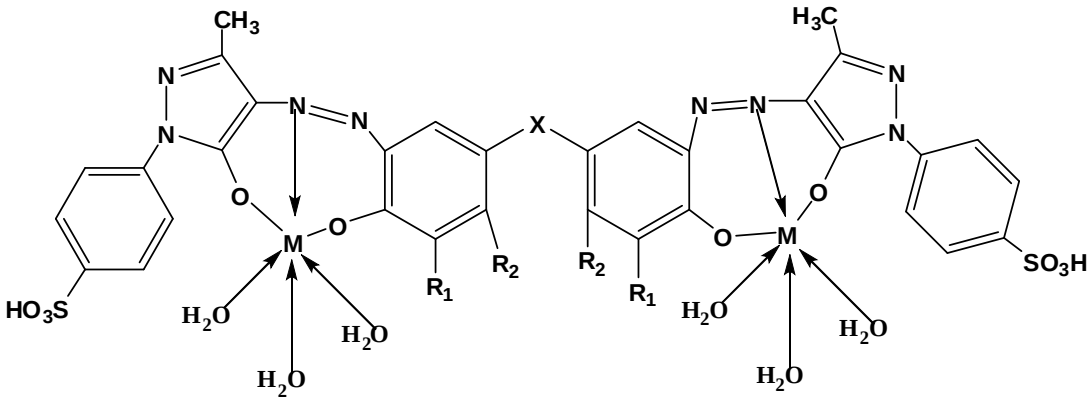

$R_1 = R_2 = H$; X = SO_2, $C(CH3)_2$; M = Fe^{II} and Cu^{II}

Figure (1-29): Proposed structure of metal chelates for sulfonyl azo dyes.

A series of new [Co^{II},Ni^{II},Cu^{II} and Zn^{II}] complexes with azo dye 5-methyl-2-phenyl-4-[(E)-1,3-thiazol-2-yl-diazenyl]-2,4-dihydro-3H-pyrazol-3-one was obtained from diazo coupling reaction of 5-methyl-2-phenyl-2,4-dihydro-3H-pyrazol-3-one with 2-aminothiazole have been reported [71]. The structure around metal centers was characterized from spectroscopic (FT-IR, UV-Vis, ^{1}H-NMR) and analytical data, octahedral geometry was proposed for metal complexes. Figure (1-30). The uncoordinated ligand and their complexes were revealed good viability cytotoxicity (anti-cancer) and antimicrobial activities.

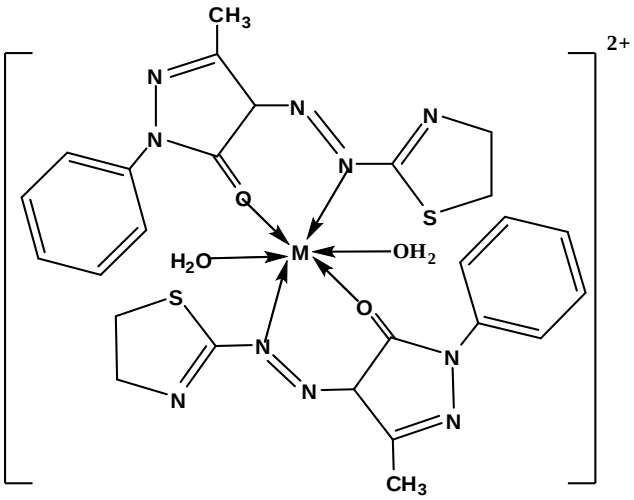

M = Co^{II},Ni^{II},Cu^{II} and Zn^{II}

Figure (1-30): Structure of metal complexes [Co^{II}, Ni^{II}, Cu^{II} and Zn^{II}].

In 2018 Al-Khafagy [72], reported the formation of new heterocyclic tridentate azo dye ligand (E)-4-(((4,5-bis(4-methoxyphenyl)-4,5-dihydro-1H-imidazol-2-yl)-diazenyl)-1,5-dimethyl-2-phenyl-1H-pyrazol-3(2H)-one which has been achieved from coupling reaction of 4-aminoantipyrine with 4,5-bis(4-methoxyphenyl) imidazole. Complexes were prepared from reaction of azo dye ligand with some metal salts (M=Co^{II}, Ni^{II}, Cu^{II}, Zn^{II}, Cd^{II} and Hg^{II} ions) with a 1:2 M:L ratio. Characterization of these compounds were carried out by (FT-IR, UV-Vis, ^{1}H-NMR and Mass) spectroscopic techniques, microelemental analysis, molar conductance measurements and magnetic susceptibility, the studies proposed that the octahedral geometry for all complexes, Figure (1-31).

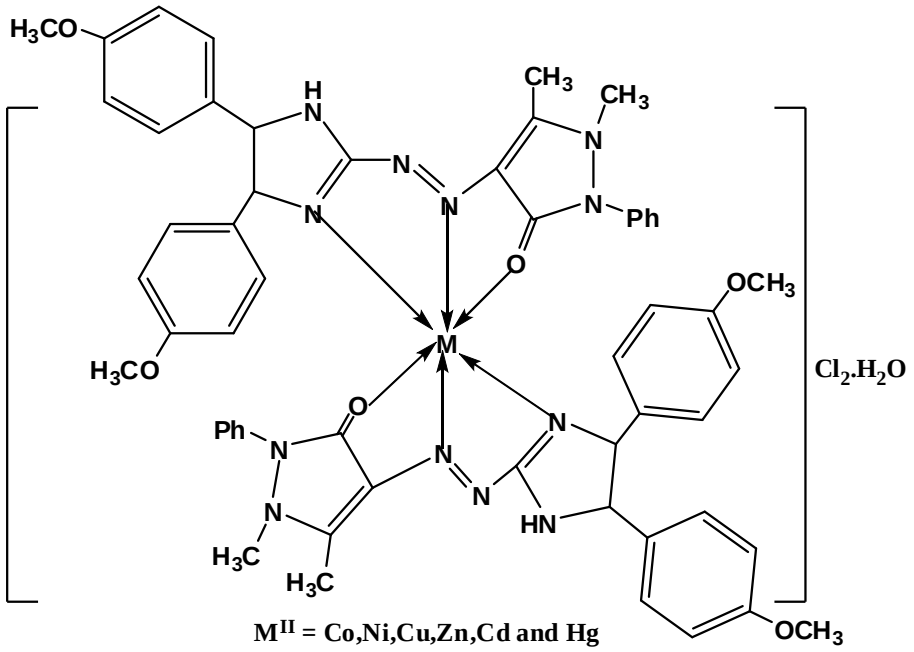

Figure (1-31): Proposed structure of metal chelate for(E)-4-(((4,5-bis(4-methoxyphenyl)-4,5-dihydro-1H-imidazol-2-yl)-diazenyl)-1,5-dimethyl-2-phenyl-1H-pyrazol-3(2H)-one.

1.6. Mixed ligand complexes

Mixed ligand are bi- or polydentate ligands that contain at least two different types of chemical functionality capable of binding to metal centers. The synthesis of ligands which containing both hard and soft donors that different and contrasting reactivity associated within the same molecule would lead to novel and unprecedented properties for the resulting metal complexes, chelating ligands containing (O, S and N) donor atoms show broad biological activity because of the variety of ways in which they are coordinated metal ions[73,74].

Mixed ligand complexes differ from classical complexes which include one type of ligand molecules attached to the metal in the sence that they are having more than one type of ligands attached to the same metal atom in a complex[75]. In recent years mixed ligand complexes have been extensively studied in solution as well as in the solid state, ternary complexes are found to be more stable than binary complexes[76], steric effect and back donation have also been invoked to account for the preferred formation of mix-ligand complexes[77]. The study of mixed ligand complexes formation is relevant in the field of analytical chemistry, the use of mixed ligand complexes allows. The development of methods with increased selectivity, sensitivity and has also great importance in the field of biological and environmental chemistry[78].

Kirkan, *at.el* [79], reported the synthesis of Cu^{II} dinuclear complexes that derived from the bidentate ligand 1,10-phenanthroline and four new azo dyes L^1,L^2,L^3 and L^4 have been prepared from diazo-coupling reaction of benzaldehyde-4-aminobenzoyl hydrazone and 4-hydroxybenzaldehyd-4-aminobenzoyl hydrazone with barbituric acid and 1,3-dimethylbarbituric acid. The structures of Cu^{II} complexes were

characterized by elemental analyses, magnetic measurements and spectral techniques (FT-IR, UV-Vis, Mass and ^{1}H-NMR), the studies showed tetrahedral geometry, Figure (1-32).

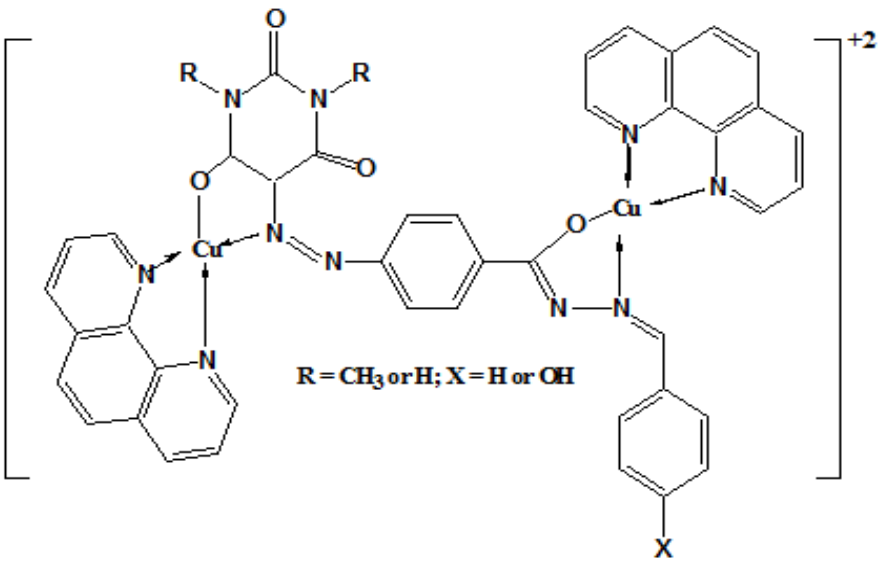

Figure (1-32): Chemical structure of the mixed-ligand Cu^{II} complexes

The formation of new Pr^{III} complex with new tridentate amino acid-based (leucine) azo dye (L_1) and 1,10 phenanthroline (L_2) was described [80]. Azo dye was prepared from diazo-coupling reaction of leucine with N,N-dimethyl aniline. Reaction of Pr^{III} ion with L_1 and L_2 at (1:2:1) ratio with general formula $[Pr(L_1)_2(L_2)(H_2O)_2]$, the structure around metal centre was predicted from spectroscopic and analytical data, Figure (1-33).

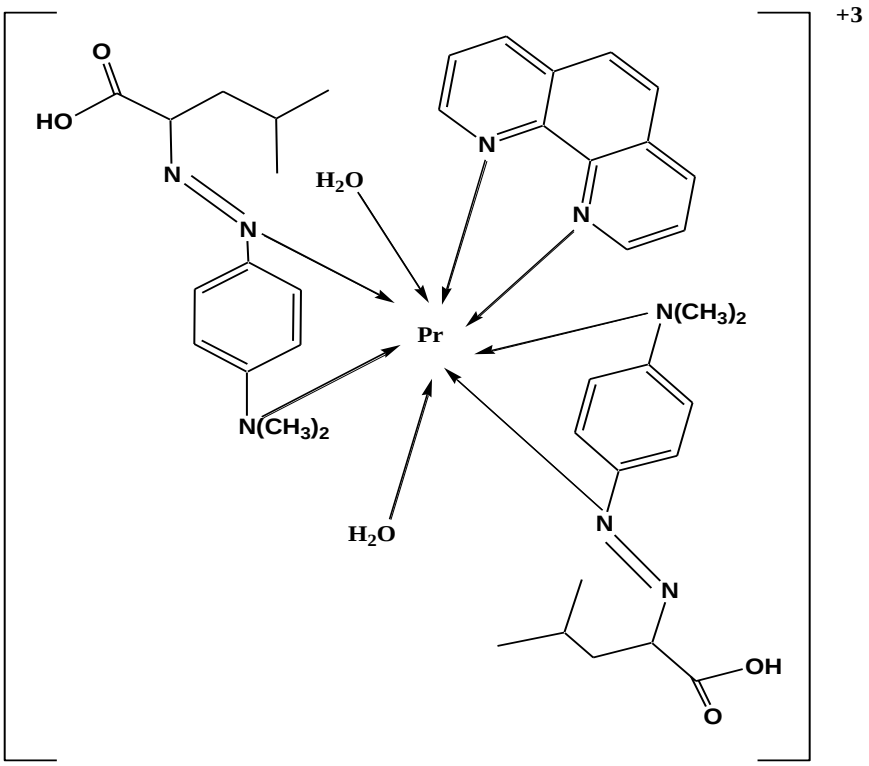

Figure (1-33): Chemical structure of the mixed-ligand Pr^{III} complex.

Rajavel, *et.al* [81], reported mixed ligand complexes of [Ni^{II} and Cu^{II}] with 1-(4-chlorophenyl azo)-naphthalene-2-ol and 2-(1-(4-chlorophenyl imino)-ethyl)-phenol. Metal chelates have been characterized by elemental analysis, molar conductance measurements, magnetic studies, (FT-IR, UV-Vis and ESR) spectroscopy and molecular modelling, these studies suggested that Cu^{II} and Ni^{II} complexes have square planer structure, Figure (1-34).

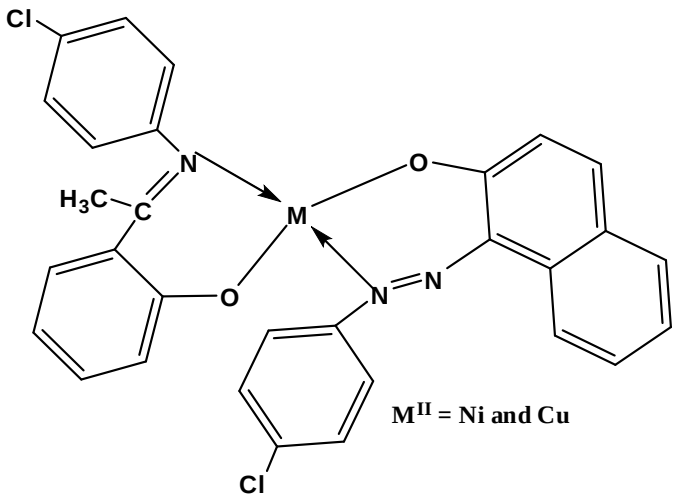

Figure (1-34): Structure of Cu^{II} and Ni^{II} mixed-ligand complexes.

In 2017 Moustafa, *et.al* [82], studied the synthesis of novel Zr^{IV} mixed ligand-drug complex with thiamine hydrochloride as a primary ligand and azo compound as secondary ligands. Zr^{IV} complex was characterized by elemental analysis, thermogravimetric analysis, molar conductivity, magnetic susceptibility and (FT-IR, UV-Vis) spectroscopy. Depending on the analytical and spectral data the complexes were formulated as [Azo-M-Thiamine $(H_2O)_n]^+Cl^-$, the suggested geometry was octahedral for Zr^{IV}, Figure (1-35).

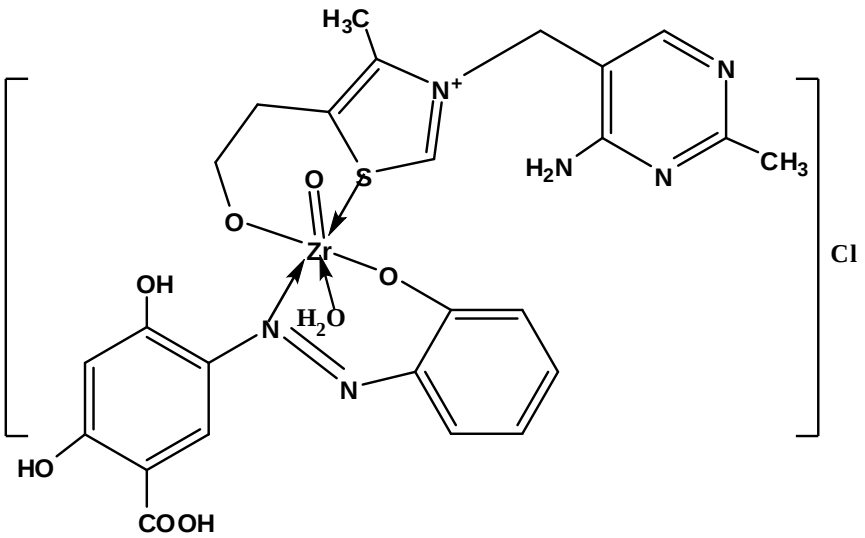

Figure (1-35): Proposed structure of Zr^{IV} complex.

The synthesis of a series new mixed-ligand saccharin complexes of [Mn^{II}, Co^{II} and Cd^{II}] with azo dye ligand [5-methyl-4-(4-methylphenyl azo)-2H-pyrazole-3-ylamine] were reported by Adiguzel, *et.al* [83], structures of the complexes were characterized by elemental analysis, magnetic susceptibility, (FT-IR, Mass, UV-Vis) spectroscopic methods and thermal analysis. These studies suggested that the mononuclear and monomeric structure in octahedral geometry for mixed ligand-metal complexes, Figure (1-36), the biological activity measurements showed that mixed ligand-metal complexes have better antibacterial and anti candidal activities.

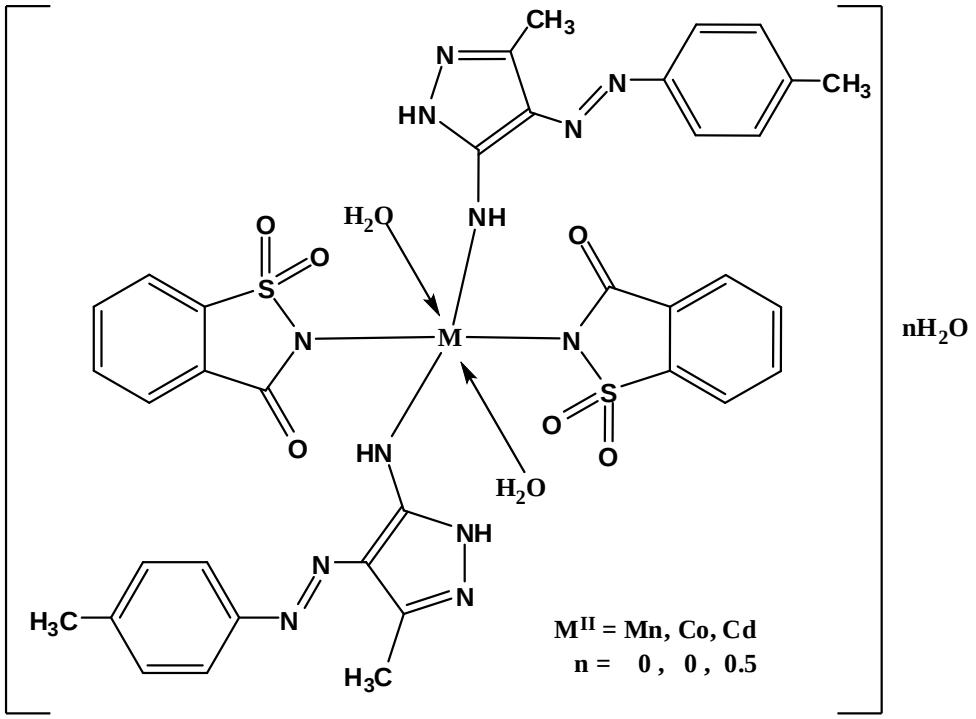

Figure (1-36): Structure of mixed-ligand (Mn^{II}, Co^{II} and Cd^{II}) complexes.

1.7. Aim of the work

Given the widespread use of organic azo compounds and the extension of previous research conducted in our laboratory, our objectives have also expanded to include.

- Preparation and characterization of a number of organic ligands in the available methods.
- Spectroscopic study of [Co^{II}, Ni^{II}, Cu^{II} and Zn^{II}] mixtures with the prepared ligand solution. The optimum conditions of concentration, pH and metal content are determined: Ligand:Metal for the preparation of the solid complexes metal ions of the above.
- Characterization of complexes in spectral and analytical techniques and study the constants of their stability.
- Studying the biological activity for the prepared ligands and their metal complexes.
- Finally, studying the ability of the prepared ligands and their complexes to dye the tissue and the amount of stability of these pigments towards light, washing and detergents.

Chapter Two

Experimental Part

2.1. Chemicals

All the chemicals used in this work and its suppliers are obtained in Table (2-1), all these chemicals have been used without further purification.

Table (2-1): Chemicals used in this work and its suppliers.

Substance	Formula	Company	Purity%
Ammonium acetate	$CH_3CO_2NH_4$	Fluka	99
Ammonia solution	NH_4OH	B.D.H	25
Acetic acid glacial	CH_3COOH	B.D.H	99.5
2-Aminobenzothiazole	$C_7H_6N_2S$	B.D.H	98
Cobalt(II) chloride hexahydrate	$CuCl_2.6H_2O$	Merck	98
Copper(II) chloride dihydrate	$CuCl_2.2H_2O$	Merck	98
Dimethyl sulphoxide	$(CH_3)_2SO$	BDH	99
Dimethyl foramide	C_3H_7NO	Merck	99.5
Dichloromethane	CH_2Cl_2	Fluka	98
3,5-Dimethylphenol	$C_8H_{10}O$	B.D.H	98
Ethanol	C_2H_5OH	B.D.H	99
Metanol	CH_3OH	B.D.H	99
Nickel(II) chloride hexahydrate	$NiCl_2.6H_2O$	Merck	99
P-nitro aniline	$C_6H_6N_2O_2$	Fluka	98
Sodium nitrite	$NaNO_2$	Merck	99
Sodium hydroxide	NaOH	Fluka	98
Zinc Chloride	$ZnCl_2$	Merck	98
4– Aminoantipyrine	$C_{11}H_{13}N_3O$	Fluka	99
4– Aminoacetophenone	C_8H_9NO	Fluka	99
Hydrochloric acid	HCl(12N)	BDH	Analar grade

2.2. Instruments

2.2.1. Electronic spectra

The electronic (UV-Vis) spectra were measured for (10^{-3} m/L) in ethyl alcohol at department of Chemistry, College of Education for Pure Science/Ibn-Al-Haitham using (Shimadzu UV-160A) Ultra Violet-Visible Spectrophotometer).

2.2.2. Infrared spectra (FTIR)

Infrared spectra were obtained as (KBr disc) by using (Shimadzu, FT.IR- 8400S Fourier Transform Infrared Spectrophotometer) at Ibn Sina Company, Ministry of Industry.

2.2.3. Metal analysis

Meta content of the metal chelats were determined by flame atomic absorption using (Shimadzu A.A-160) Atomic Absorption/ Flame Emission Spectrophotometer) at Ibn Sina Company, Ministry of Industry.

2.2.4. ^{1}H, ^{13}CNMR spectra

Spectra were noted at (Brucker-300 MHz Ultra Shield Spectrometer) in Al-al-Bayt University utilizing DMSO as solvent and tetramethylsilane (TMS) as reference.

2.2.5. Mass spectra

Mass spectra were measured on LC-MS QP5OA: Shimadzu (E170 EV) Spectrometer, at Damascus University, Syria.

2.2.6. Microelemental analysis

Microelemental analysis (C.H.N.S.O) have been done in Damascus University, Syria, employing Euro vector EA 3000, single V.3.Osingle.

2.2.7. Molar conductivity

Conductivity for the compounds resolved at dimethylsulphoxide (10^{-3} m/L) was recorded at room temperature utilizing Philips PW-

Digital Conductimeter, at department of Chemistry, College of Education for Pure Science/ Ibn-Al-Haitham.

2.2.8. Magnetic susceptibility

Magnetic properties have been obtained at (296 °K) by using (Auto Magnetic Susceptibility Balance Sherwood Scientific) at College of science/ Al-Mustansiriyah University.

2.2.9. Thermal analysis

Thermal analyses have been measured under atmosphere of argon gas on heating at 10 °C/min, by using a STA PT-1000 Linseis company/ Germany, at Central Service Laboratory/ College of Education for Pure Science/ Ibn-Al-Haitham.

2.2.10. Melting points

Melting point for the azo ligand and their metal chelates have been determined using (Stuart MSRS Digital Melting Point Apparatus).

2.3. Synthesis of azo ligands

2.3.1. Synthesis for ligand (L_1, L_2)

4-aminoantipyrine (0.503gm, 1mmole), dissolved in mixture (10ml ethyl alcohol, 2ml conc. HCl), and diazotized at 5°C with 10% solution of $NaNO_2$. Diazotized solution has been added collyrium wise for stirring separately into a cooled ethyl alcohol solution (1 mmole) at (0.305 gm, 3,5-dimethylphenol or 0.337 gm, 4-aminoacetophenone) then 25 ml at 1M NaOH solution has been followed into dusky colored mix and precipitation for azo ligand has been noticed. This deposit have been filtrated, washed number ounces for (1:1) C_2H_5OH: H_2O, mixture subsequently left into dry[84] Table (2-2) consist name of ligands, M.wt and melting points.

2.3.2. Synthesis for ligand (L_3, L_4)

2-aminobenzothiazole (0.375 gm, 1 mmole), dissolved in mixture (10ml ethyl alcohol, 2ml conc. HCl), and diazotized at 5°C with 10% solution of $NaNO_2$. Diazotized solution has been added collyrium wise for stirring separately into a cooled ethyl alcohol solution (1 mmole) at (0.337 gm,4-aminoacetophenone or 0.345 gm, 4-nitroaniline) then 25ml at 1M NaOH solution has been followed into dusky colored mix and precipitation for azo ligand has been noticed. This deposit have been filtrated, washed number ounces for (1:1) C_2H_5OH: H_2O, mixture subsequently left into dry[85]. Table (2-2) consist name of ligands, M.wt and melting points.

Table (2-2): Nomenclature and some physical properties for azo ligands (L_1- L_4).

Name	Color	Yield	M.wt	M.P$^\circ$C	Ligand
4-[(2-hydroxy-4,6-dimethylphenyl)-diazenyl]-1,5-dimethyl-2-phenyl-1H-pyrazol-3(2H)-one	Reddish orange	80	336	216-218	L_1
4-[(5-acetyl-2-aminophenyl)-diazenyl]-1,5-dimethyl-2-phenyl-1H-pyrazol-3(2H)-one	Brown	83	349	> 300	L_2
1-(4-amino-3-(benzo[d]thiazol-2-yldiazenyl)phenyl)ethanone	Reddish brown	83	296	196-198	L_3
2-(benzo[d]thiazol-2-yldiazenyl)-4-nitroaniline	Brown	81	299	201-203	L_4

2.4. Buffer solution

(0.01 M, 0.771 gm) for CH_3COONH_4 has been resolved at one liter for doubly deionized water. Only the pH scope (5-9) was using CH_3COOH or NH_3 solution.

2.5. Standard solution

A group from standard solutions for metal salts have been made at varying condensation (10^{-5}-10^{-3} M) in pH rate (5-9). In the same time a group from ethyl alcohol solutions to the ligand during the extent for condensation (10^{-5}-10^{-3} M) has been as well produced.

2.6. Preparation of solutions for spectral studies

Solution have been produced by mixed same concentration of ligand and metal salt at perfect concentration and pH, to find M:L ratio using the following states.

2.6.1. Mole ratio

Absorption spectra have been obtained for several mixed solutions containing (1ml) of metal ion salt, and various volumes of ligand solution at ideal pH and concentration. Ratio has been obtained by plotting the relationship between the mole ratio in X-axis and absorption at Y-axis, the intercept for two straight lines due to M:L ratio.

2.6.2. Job method

In this state various volumes of solutions containing equal concentration for ligand and metal salt, the total volume has been kept constant. Absorption spectra have been measured by plotting the relationship between the (V_m/V_m+V_L) in X-axis (V_m=volume of the metal, V_L=volume of ligand) and absorption at Y-axis, the intercept for two straight lines due to M:L ratio.

2.7. Synthesis of metal chelates

2.7.1. Synthesis of metal chelates for azo ligands (L_1-L_4)

Ethyl alcohol solution to the ligands (0.336, 0.349, 0.296 and 0.299 gm, 2 mmole) have been added sequence during stirring of the (0.118, 0.118, 0.085 and 0.064 gm/1mmole) of the metal salts of Cobalt chloride hexahydrate, Nickel chloride hexahydrate, Copper chloride dihydrate and Zinc chloride dissolved at pH solution for perfect pH. The mixture has been cooled until dark color precipitate has been contained, filtered, as well washed number ounces for 1:1 H_2O: C_2H_5OH mixture, Table (2-3) consist name of metal chelates, M.wt, perfect pH solution and melting points.

2.7.2. Synthesis of metal chelates for mixed ligands (L_1,L_2)

Ethyl alcohol solution to the ligand (L_1) (0.336 gm, 1 mmole) and alcoholic solution (0.349 gm, 1 mmole) for azo (L_2) have been added sequence during stirring of the 0.118, 0.118, 0.085 and 0.064 gm of the metal salts of Cobalt chloride hexahydrate, Nickel chloride hexahydrate, Copper chloride dihydrate and Zinc chloride dissolved at aqueous solution. The mixture has been cooled until dark color precipitate has been contained, filtered, as well washed number ounces for 1:1 H_2O: C_2H_5OH mixture, see Table (2-3).

2.7.3. Synthesis of metal chelates for mixed ligands (L_3, L_4)

Ethyl alcohol solution to the ligand (L_3) (0.296 gm, 1mmole) and alcoholic solution (0.299 gm, 1 mmole) for azo (L_4) have been added sequence during stirring of the 0.118, 0.118, 0.085 and 0.064 gm of the metal salts of Cobalt chloride hexahydrate, Nickel chloride hexahydrate, Copper chloride dihydrate and Zinc chloride dissolved at aqueous solution. The mixture has been cooled until dark color precipitate has

been contained, filtered, as well washed number ounces for 1:1 H_2O: C_2H_5OH mixture, see Table (2-3).

Table (2-3): Nomenclature and some physical properties for metal chelates with azo ligands (L_1-L_4).

Complexes	pH	M.P°C	M.wt	Yield%	Color	Name
$[Co(L_1)_2]$	7	251-253	729	84	Brown	Bis[4-[(hydroxy-4,6-dimethylphenyl)diazenyl]-1,5-dimethyl-2-phenyl-1H-pyrazol-3(2H)-one]cobalt(II)
$[Ni(L_1)_2]$	7	241-243	728	87	Orange	Bis[4-[(2-hydroxy-4,6-dimethylphenyl)diazenyl]-1,5-dimethyl-2-phenyl-1H-pyrazol-3(2H)-one]nickel(II)
$[Cu(L_1)_2]$	7	226-228	734	85	Deep brown	Bis[4-[(2-hydroxy-4,6-dimethylphenyl)diazenyl]-1,5-dimethyl-2-phenyl-1H-pyrazol-3(2H)-one]copper(II)
$[Zn(L_1)_2]$	7	243-245	735	83	Yellowish orange	Bis[4-[(2-hydroxy-4,6-dimethylphenyl)diazenyl]-1,5-dimethyl-2-phenyl-1H-pyrazol-3(2H)-one]zinc(II)
$[Co(L_2)_2].H_2O$	9	203-205	773	80	Dark brown	Bis[4-[(5-acetyl-2-aminophenyl)diazenyl]-1,5-dimethyl-2-phenyl-1H-pyrazol-3(2H)-one]cobalt(II).hydrate
$[Ni(L_2)_2].H_2O$	9	227-229	772	85	Deep brown	Bis[4-[(5-acetyl-2-aminophenyl)diazenyl]-1,5-dimethyl-2-phenyl-1H-pyrazol-3(2H)-one]nickel(II).hydrate
$[Cu(L_2)_2].H_2O$	9	168-170	778	82	Dark brown	Bis[4-[(5-acetyl-2-aminophenyl)diazenyl]-1,5-dimethyl-2-phenyl-1H-pyrazol-3(2H)-one]copper(II).hydrate
$[Zn(L_2)_2].H_2O$	9	234-236	779	87	Dark brown	Bis[4-[(5-acetyl-2-aminophenyl)diazenyl]-1,5-dimethyl-2-phenyl-1H-pyrazol-3(2H)-one]zinc(II).hydrate

$[Co(L_3)_2]$	9	260 D	649	80	Orange	Bis[1-(4-amino-3-(benzo[d]thiazol-2-yldiazenyl)phenyl)ethanone]cobalt(II)
$[Ni(L_3)_2]$	9	295 D	648	81	Yellowish orange	Bis[1-(4-amino-3-(benzo[d]thiazol-2-yldiazenyl)phenyl)ethanone]nickel(II)
$[Cu(L_3)_2]$	9	>300	654	84	Brown	Bis[1-(4-amino-3-(benzo[d]thiazol-2-yldiazenyl)phenyl)ethanone]copper(II)
$[Zn(L_3)_2]$	9	176-178	655	83	Yellow	Bis[1-(4-amino-3-(benzo[d]thiazol-2-yldiazenyl)phenyl)ethanone]zinc(II)
$[Co(L_4)_2]$	9	234-236	655	87	Reddish brown	Bis[2-(benzo[d]thiazol-2-yldiazenyl)-4-nitroaniline]cobalt(II)
$[Ni(L_4)_2]$	9	268-270	654	81	Pal brown	Bis[2-(benzo[d]thiazol-2-yldiazenyl)-4-nitroaniline]nickel(II)
$[Cu(L_4)_2]$	9	168-170	660	80	Deep brown	Bis[2-(benzo[d]thiazol-2-yldiazenyl)-4-nitroaniline]copper(II)
$[Zn(L_4)_2]$	9	133-135	661	88	Deep brown	Bis[2-(benzo[d]thiazol-2-yldiazenyl)-4-nitroaniline]zinc(II)
$[Co(L_1)(L_2)]$	-	218-220	742		Deep green	4-[(hydroxy-4,6-dimethylphenyl)diazenyl]-1,5-dimethyl-2-phenyl-1H-pyrazol-3(2H)-one 4-[(5-acetyl-2-aminophenyl)diazenyl]-1,5-dimethyl-2-phenyl-1H-pyrazol-3(2H)-one cobalt(II)
$[Ni(L_1)(L_2)]$	-	194-196	741	82	Reddish brown	4-[(hydroxy-4,6-dimethylphenyl)diazenyl]-1,5-dimethyl-2-phenyl-1H-pyrazol-3(2H)-one 4-[(5-acetyl-2-aminophenyl)diazenyl]-1,5-dimethyl-2-phenyl-1H-pyrazol-3(2H)-one nickel(II)
$[Cu(L_1)(L_2)]$	-	151-153	747	88	Brown	4-[(hydroxy-4,6-dimethylphenyl)diazenyl]-1,5-dimethyl-2-phenyl-1H-pyrazol-3(2H)-one 4-[(5-acetyl-2-aminophenyl)-diazenyl]-1,5-dimethyl-2-phenyl-1H-pyrazol-3(2H)-one copper(II)

$[Zn(L_1)(L_2)]$	-	210-212	748	85	Deep gray	4-[(hydroxy-4,6-dimethyl-phenyl)diazenyl]-1,5-dimethyl-2-phenyl-1H-pyrazol-3(2H)-one 4-[(5-acetyl-2-aminophenyl)diazenyl]-1,5-dimethyl-2-phenyl-1H-pyrazol-3(2H)-one zinc(II)
$[Co(L_3)(L_4)]$	-	163-165	652	81	Reddish brown	1-(4-amino-3-(benzo[d]thiazol-2-yldiazenyl)phenyl)ethanone2-(benzo-[d]thiazol-2-yldiazenyl)-4-nitroanilinecobalt(II)
$[Ni(L_3)(L_4)]$	-	250 D	651	83	Deep brown	1-(4-amino-3-(benzo[d]thiazol-2-yldiazenyl)phenyl)ethanone2-(benzo[d]thiazol-2-yldiazenyl)-4-nitroanilinenickel(II)
$[Cu(L_3)(L_4)]$	-	191-193	657	84	Pal brown	1-(4-amino-3-(benzo[d]thiazol-2-yldiazenyl)phenyl)ethanone2-(benzo[d]thiazol-2-yldiazenyl)-4-nitroanilinecopper(II)
$[Zn(L_3)(L_4)]$	-	165-167	658	84	Brown	1-(4-amino-3-(benzo[d]thiazol-2-yldiazenyl)phenyl)ethanone2-(benzo[d]thiazol-2-yldiazenyl)-4-nitroanilinezinc(II)

2.8. Biological activity

Azo dyes ligands and their metal chelates have been screened at vitro with their antibacterial and antifungal efficiency contra: *Staphylococcus aureus*, *Esherichia Coli*, *Candida albicans* as well *Candida tropicalis* employing the paper disc method.

2.9. Dyeing method

Dyeing properties for produced ligands and their metal chelates were applied on cotton fabric as (1% shade) using the Azoic Dyes Method, the laboratory model glycerin-bath higher temperature flask-dyeing machine has been used. Finally powdered dye (2.5 gm) has been mixed with (0.1 gm) for azotic dyes agent, then mixture dispersed in a ultrasonic vibrator for (30 min) at 25°C. The dyeing of the fabric was done at (15- 20°C) for (1 hr), and at pH (10) by adding NaOH.

Chapter Three

Results & Discussion

3.1. Synthesis of azo dyes ligands

The reaction scheme of azo ligands (L_1 and L_2) from 4-amino-antipyrine is shown in Scheme (3-1). First step in this mechanism containing of antipyrine diazonium salt, than coupling with the ethyl alcohol solution of the selected agents.

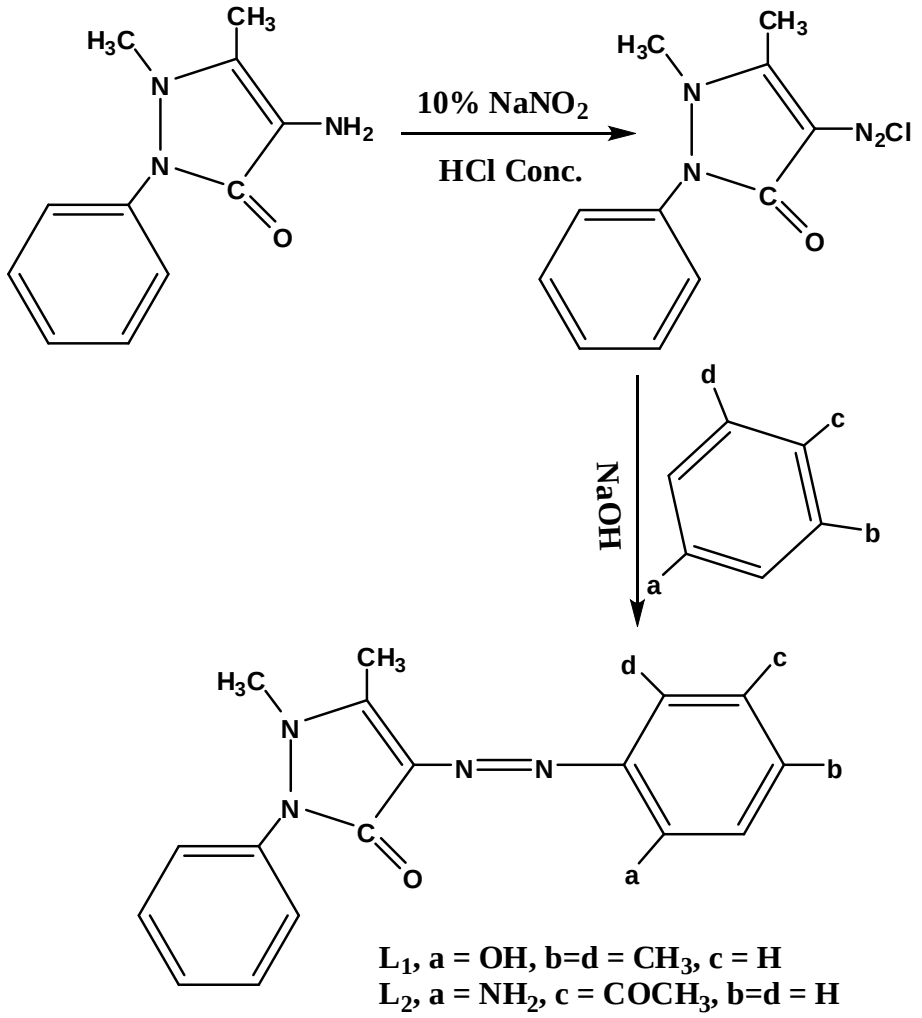

Scheme (3-1): synthesis of azo dyes ligands (L_1 and L_2).

The azo ligands (L_3 and L_4) from 2-aminobenzothiazole is shown in Scheme (3-2). First step in this reaction including of benzothiazole diazonium salt, than coupling with the ethyl alcohol solution of the selected agents.

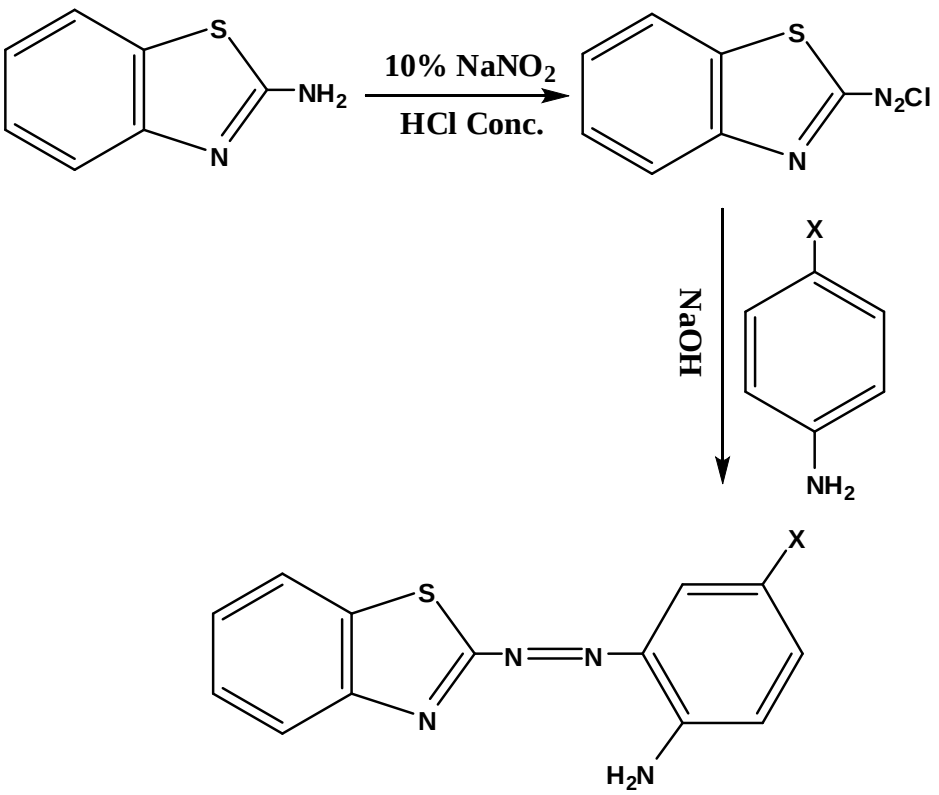

L_3 , X = $COCH_3$, L_4 , X = NO_2

Scheme (3-2): synthesis of azo dyes ligands (L_3 and L_4).

The solubility of azo ligands (L_1-L_4) in various solvents is given in Table (3-1).

Table (3-1): Solubility of azo ligands in different solvents.

compounds	Ethanol	Acetone	Benzene	CH_2Cl_2	DMF	DMSO	Distal water
L_1	+	+	÷	÷	+	+	÷
L_2	+	+	÷	÷	+	+	÷
L_3	+	+	÷	÷	+	+	÷
L_4	+	+	÷	÷	+	+	÷

Soluble (+), sparingly (÷)

The ligands were identified on the basis of elemental analysis, were in real identical with the calculated values and agree well with the proposed formula of azo ligands and the data included in Table (3-2).

Table (3-2): Microelemental analysis results of the azo ligands (L_1-L_4).

Compounds	Analysis Calc (Found)				
	C%	H%	N%	O%	S%
L_1	67.85 (66.18)	5.95 (4.56)	16.66 (15.92)	9.52 (8.77)	-
L_2	65.32 (64.78)	5.44 (4.85)	20.05 (19.91)	9.17 (8.76)	-
L_3	60.81 (59.93)	4.05 (3.88)	18.91 (17.96)	5.40 (4.91)	10.81 (10.32)
L_4	52.17 (51.94)	3.01 (2.45)	23.41 (22.27)	10.70 (9.01)	10.70 (9.23)

The azo ligands also characterized by thermal analysis, (FTIR, UV-Vis, LC-Mass and ^{1}H, ^{13}C NMR) spectra.

3.2. Mass spectra of azo dyes ligands

Spectrum of each ligand appears a well defined parent peak and the same fragmented ion pattern.

3.2.1. Mass spectrum of the ligand (L_1)

The mass spectrum of the azo ligand (L_1) showed peak centered at m/z=336 due to the formula $C_{19}H_{20}N_4O_2$. The general pattern of fragmentation are summarized in Scheme (3-3), see Figure (3-1).

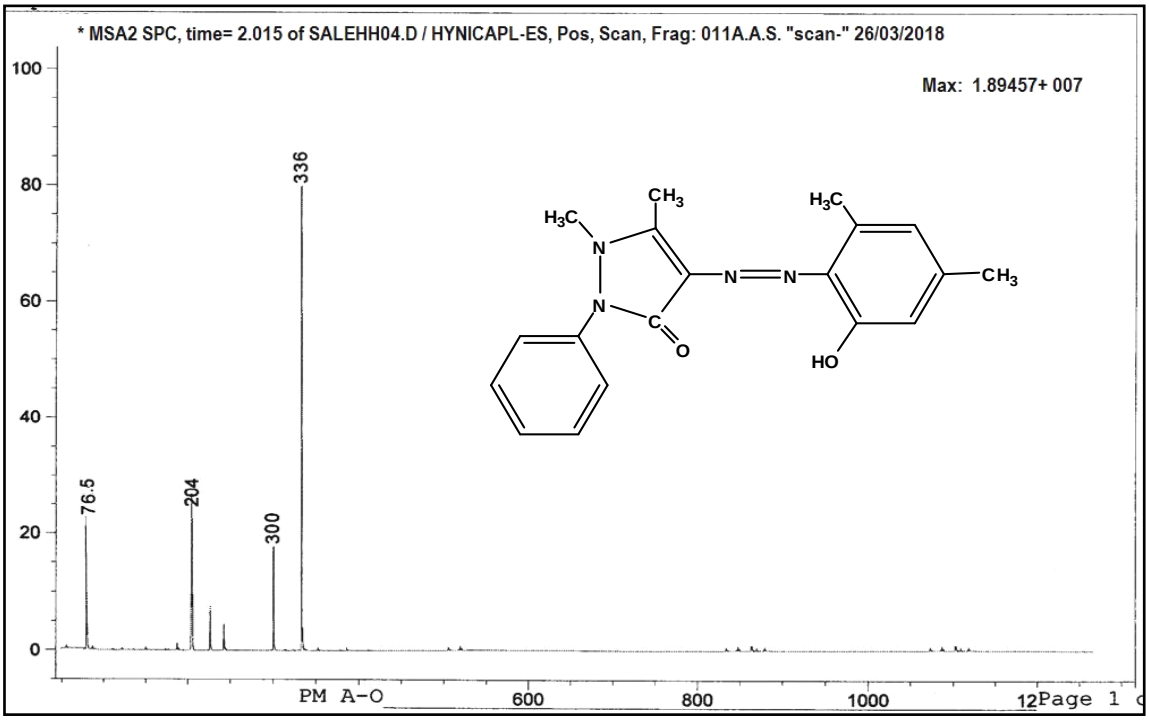

Figure (3-1): Mass spectrum of the ligand (L_1).

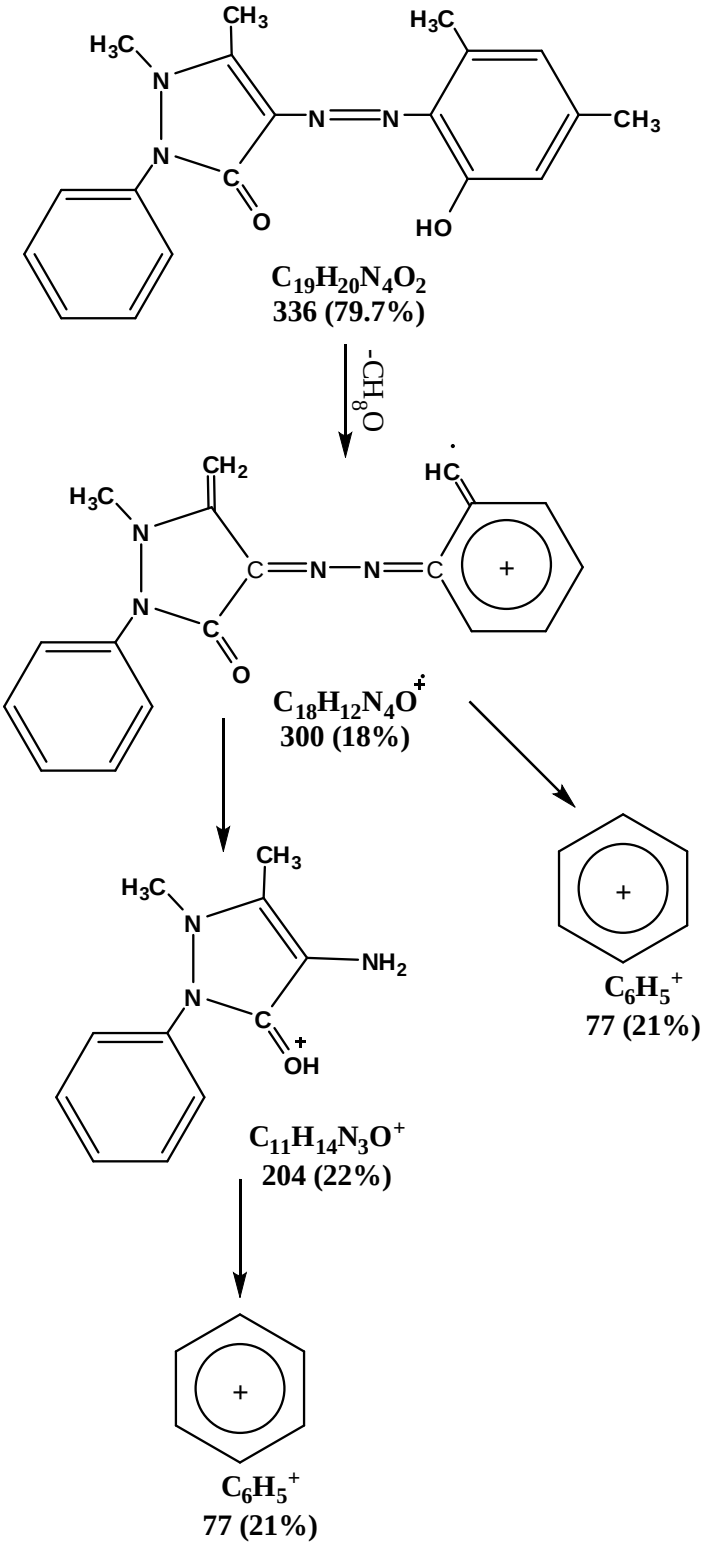

Scheme (3-3): Fragmentation pattern of the ligand (L_1).

3.2.2. Mass spectrum of the ligand (L_2)

The mass spectrum of the ligand (L_2) is shown in Figure (3-2). General pattern of fragmentation are listed in Scheme (3-4), the spectrum show peak represent the parent fragment centered at m/z=348 corresponds with the formula $C_{19}H_{18}N_5O_2^+$.

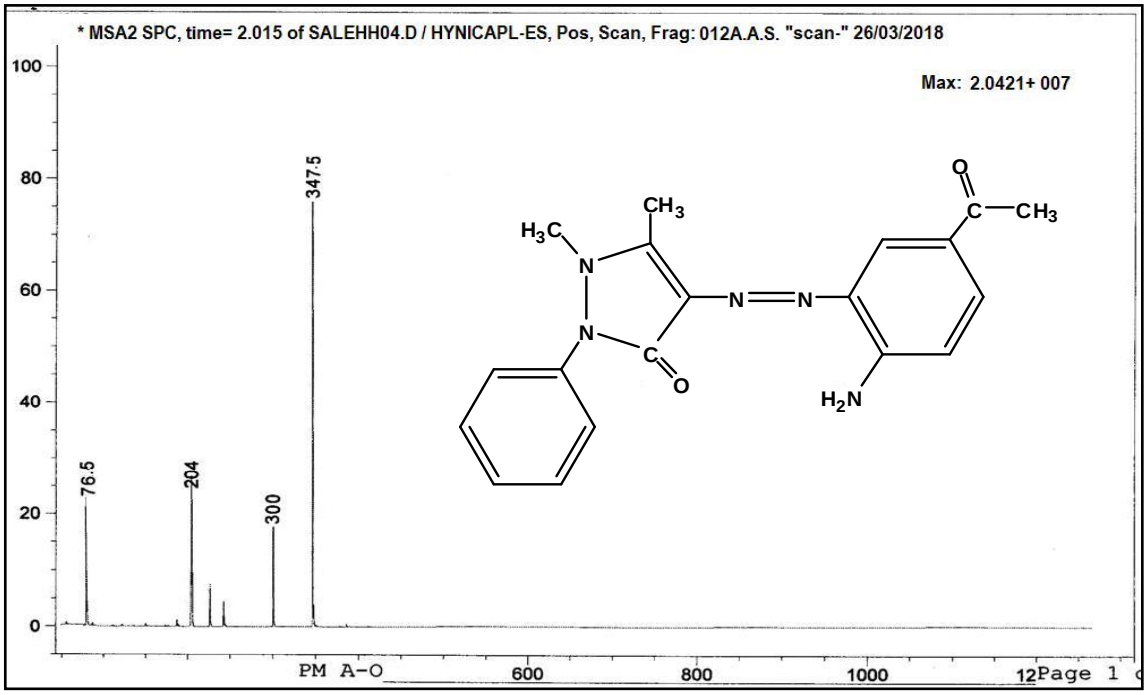

Figure (3-2): Mass spectrum of the ligand (L_2).

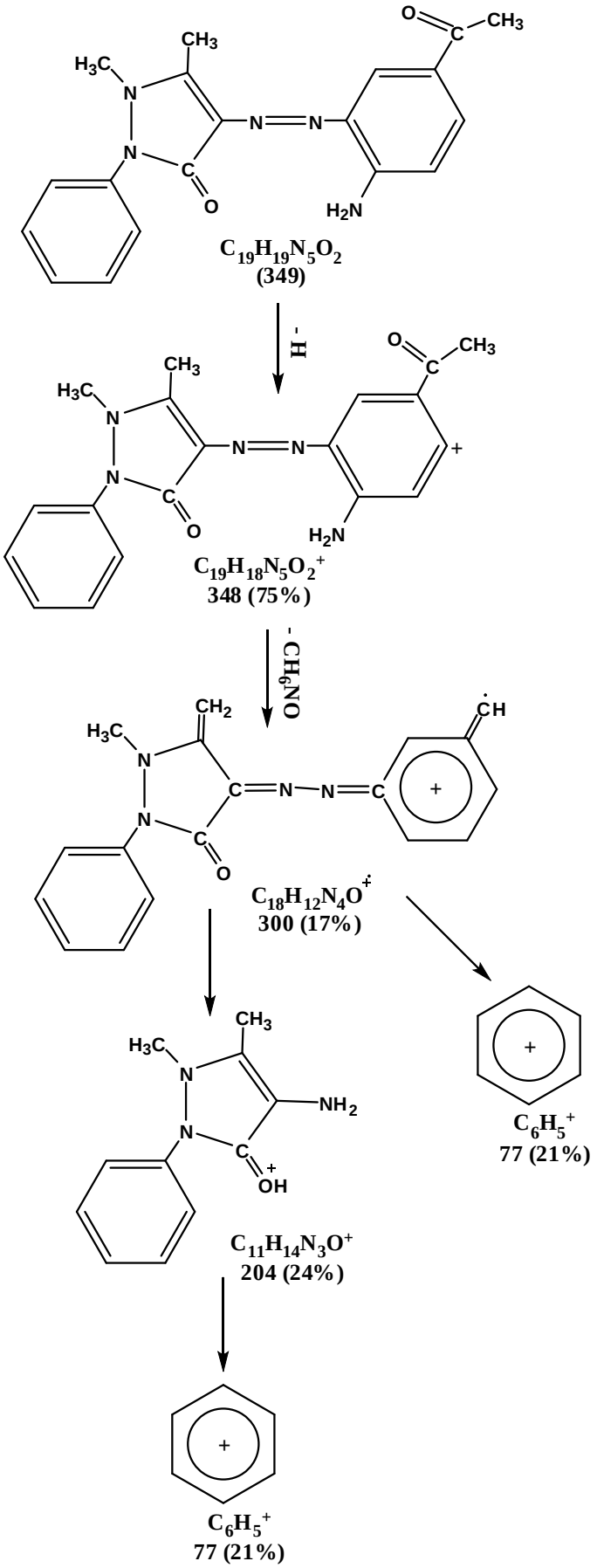

Scheme (3-4): Fragmentation pattern of the ligand (L_2).

3.2.3. Mass spectrum of the ligand (L_3)

The mass spectrum of the ligand (L_3) is shown in Figure (3-3). General pattern of fragmentation are listed in Scheme (3-5), the spectrum show peak represent the parent fragment centered at m/z=296 corresponds with the formula $C_{15}H_{12}N_4OS$.

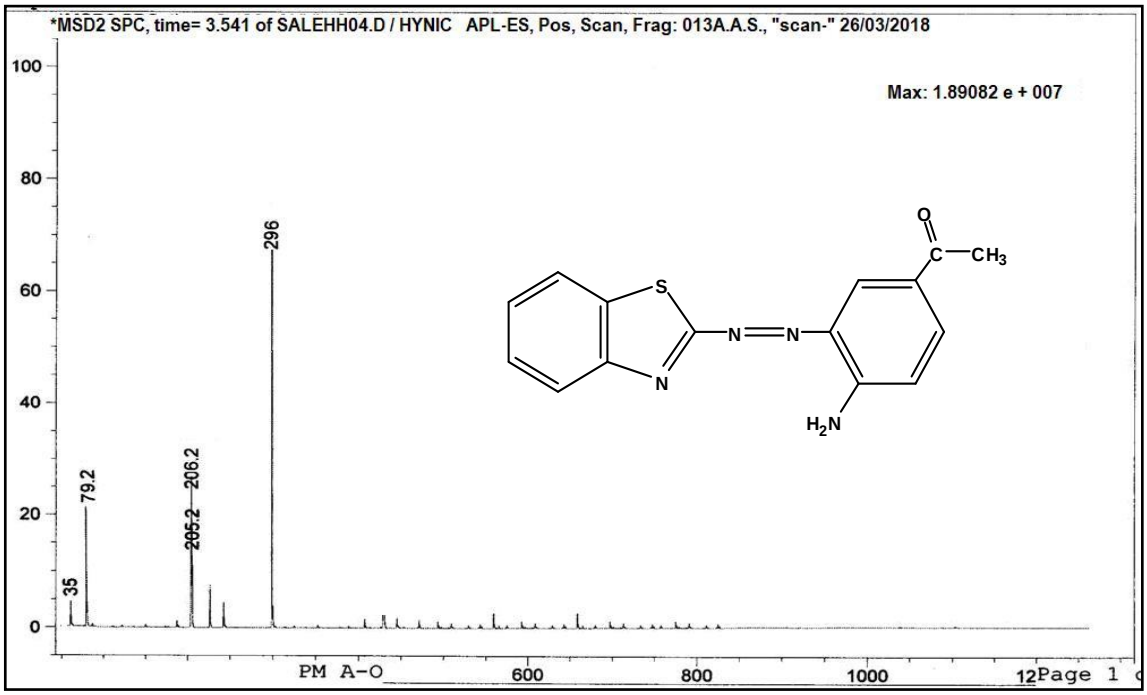

Figure (3-3): Mass spectrum of the ligand (L_3).

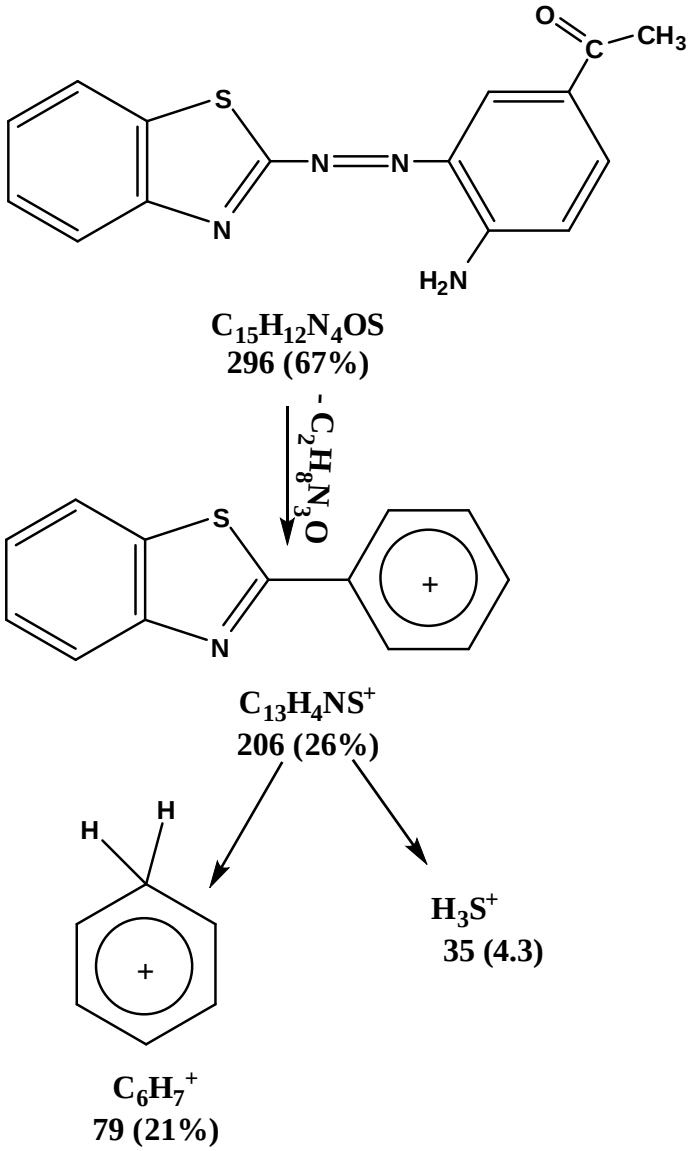

Scheme (3-5): Fragmentation pattern of the ligand (L_3).

3.2.4. Mass spectrum of the ligand (L_4)

The mass spectrum of the azo ligand (L_4) showed peak centered at m/z=299 due to the formula $C_{13}H_9N_5O_2S$. The general pattern of fragmentation are summarized in Scheme (3-6), see Figure (3-4).

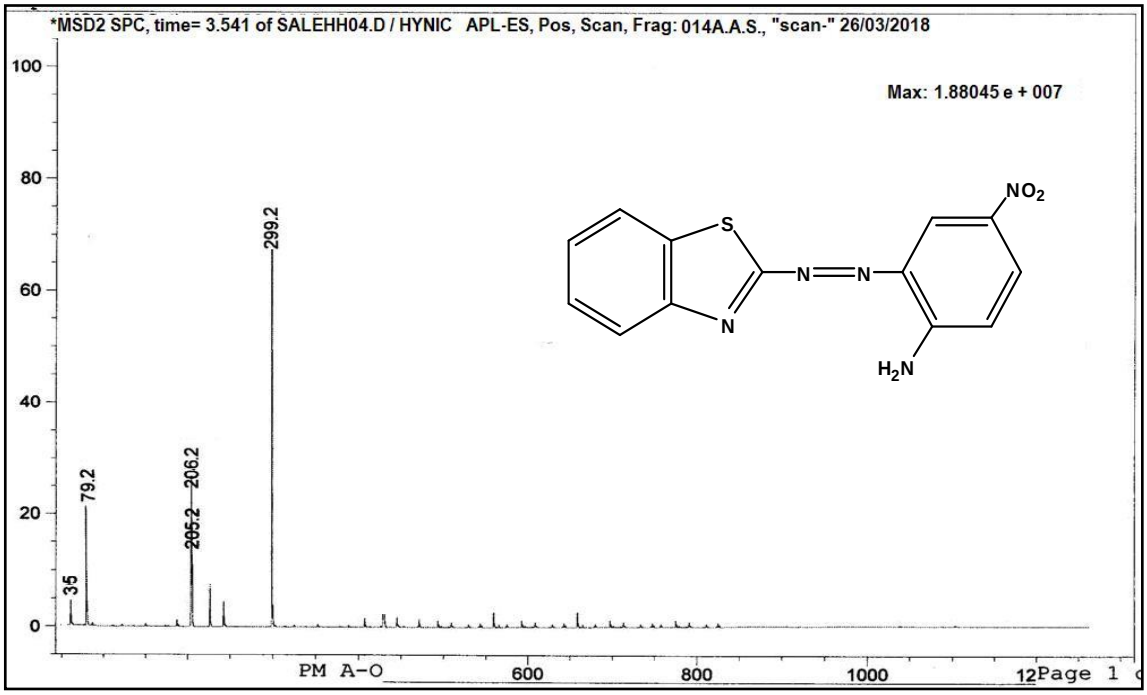

Figure (3-4): Mass spectrum of the ligand (L_4).

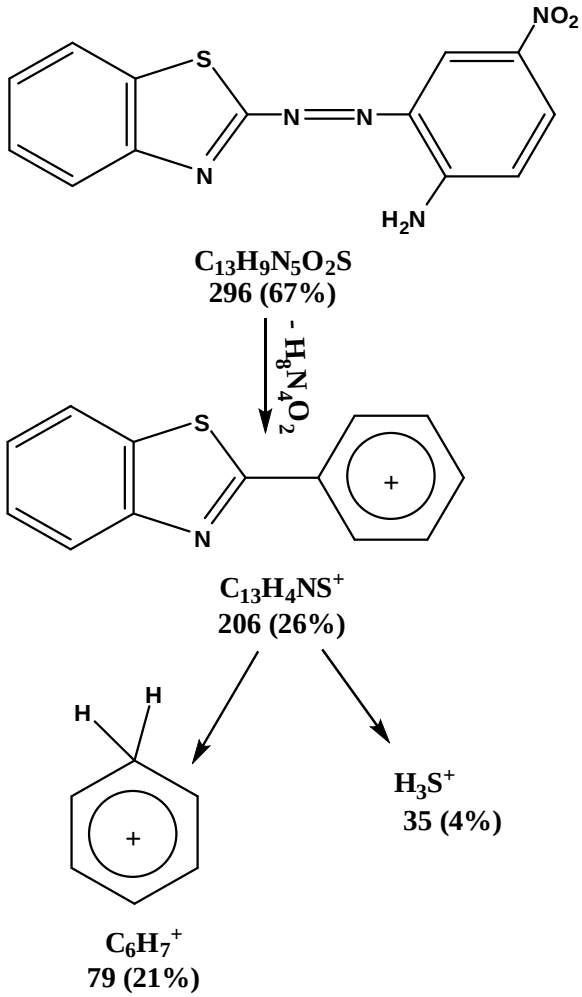

Scheme (3-6): Fragmentation pattern of the ligand (L_4).

3.3. Thermal analysis

The aim of thermal analysis is to obtain information concerning the thermal stability of the investigated for azo dyes ligands (L_1-L_4) as seen in Figures (3-5) to (3-8), the decomposition is shown in Scheme (3-7) and the data recorded in Table (3-3).

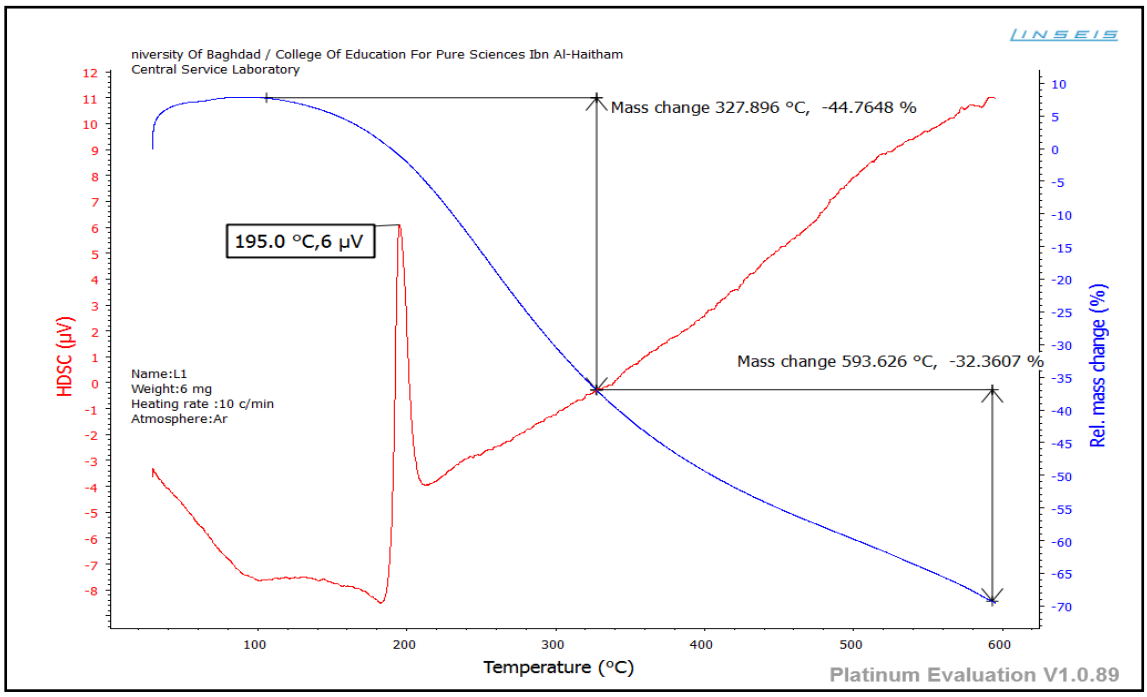

Figure (3-5): TG/DSC Thermogram of the ligand (L_1).

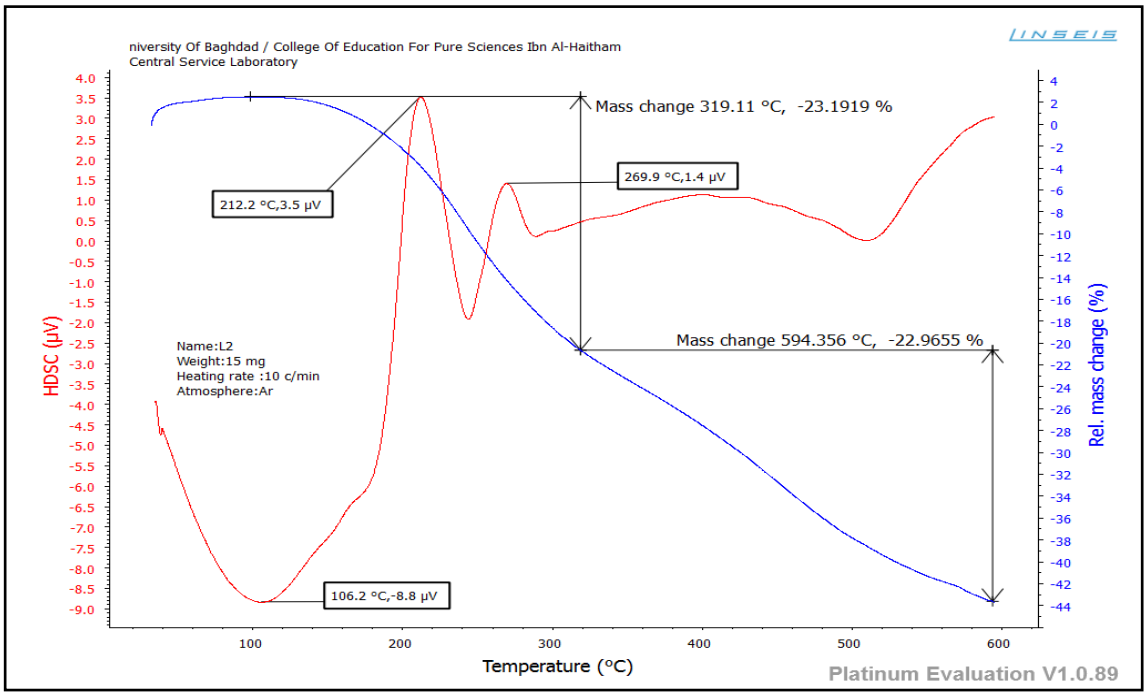

Figure (3-6): TG/DSC Thermogram of the ligand (L_2).

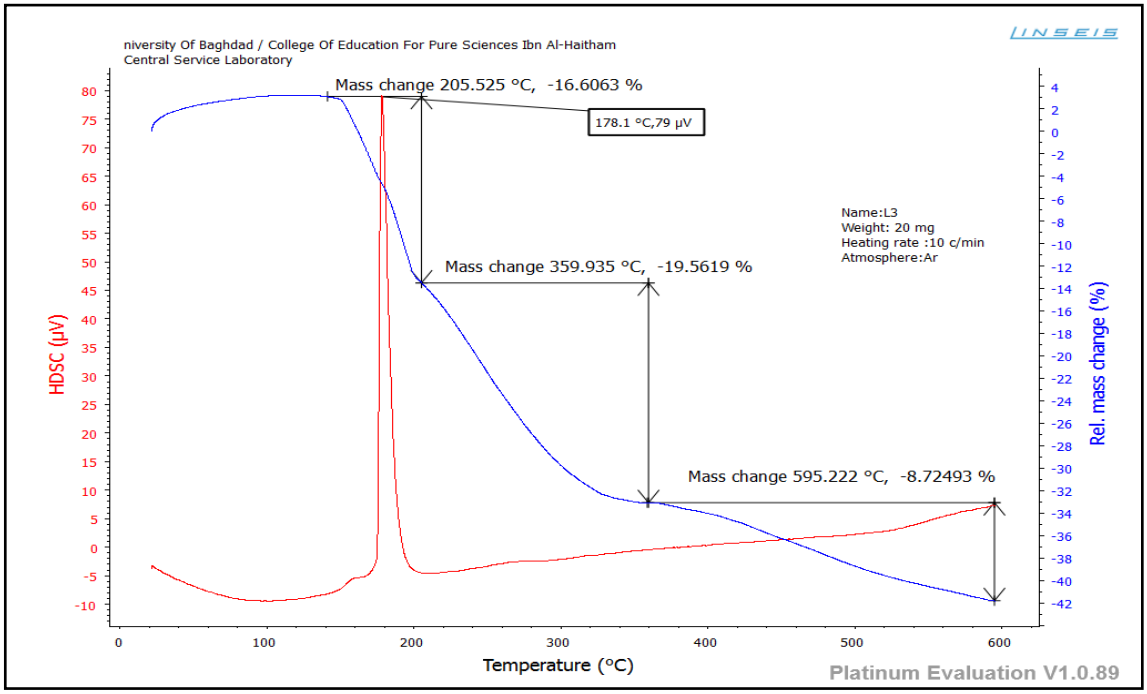

Figure (3-7): TG/DSC Thermogram of the ligand (L_3).

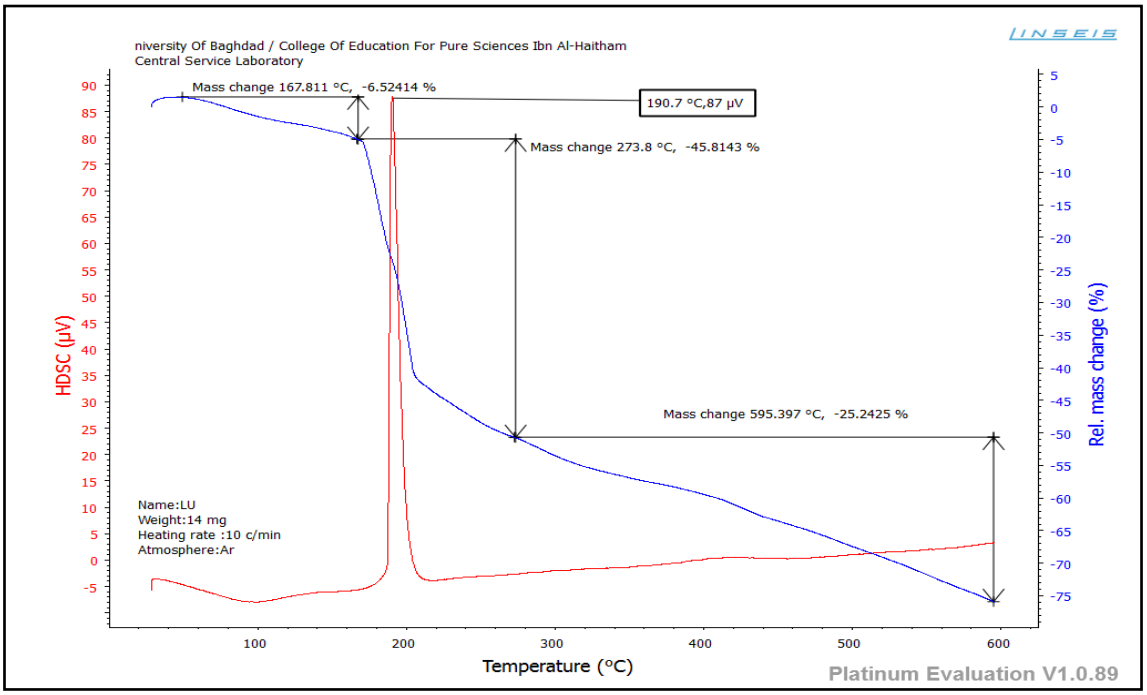

Figure (3-8): TG/DSC Thermogram of the ligand (L_4).

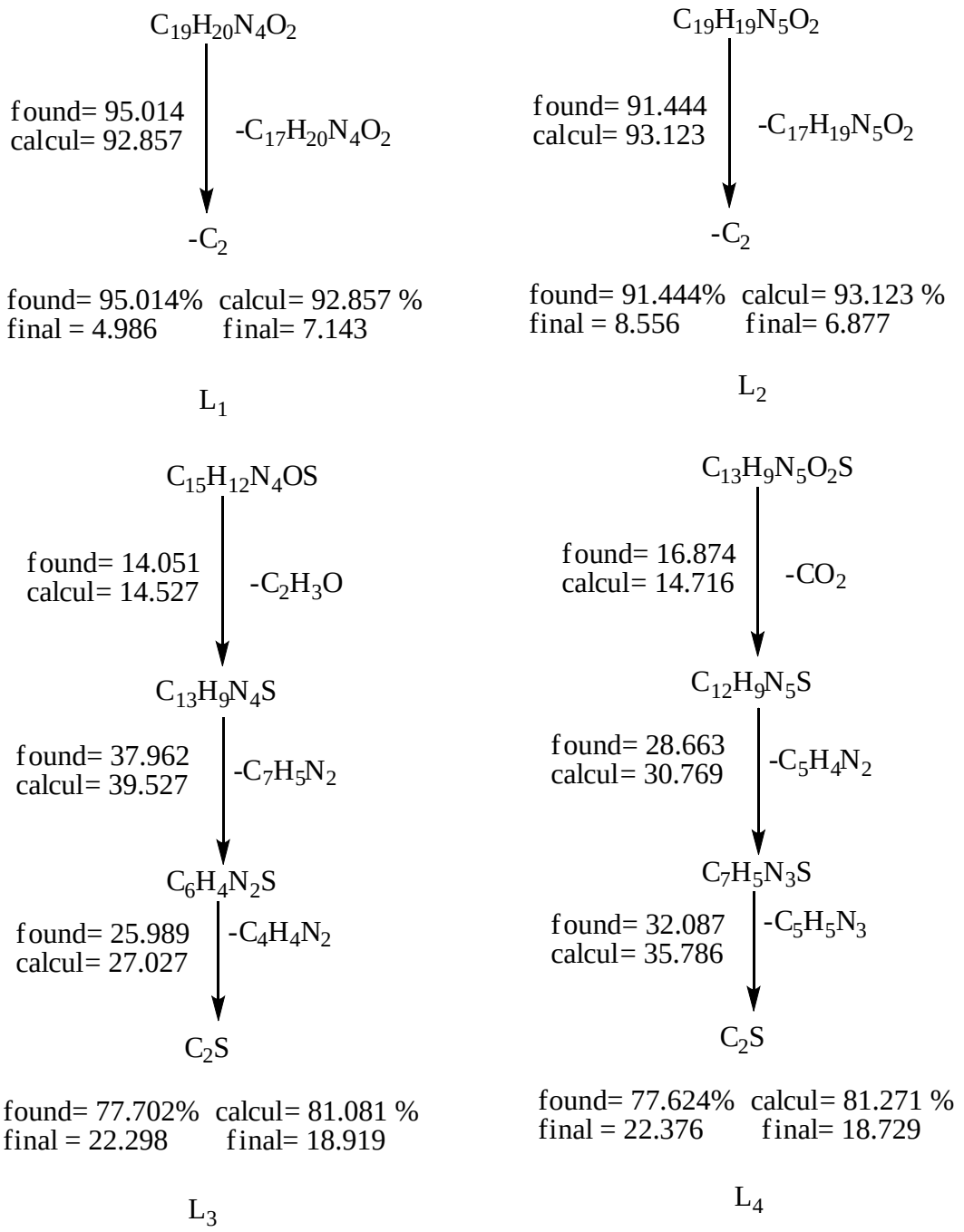

Scheme (3-7): Tentative decomposition reaction of ligands (L_1-L_4).

Table (3-3): Characterization parameters of thermal decomposition ($10°C\ min^{-1}$) ligands.

Ligand	Step	TGA				Reaction	Total mass loss%
		Ti/°C	T_f/°C	T_{DTGmax}	Weight mass loss% calc (found)		
L_1	1	114.5	599	347	92.857 (95.014)	$-C_{17}H_{20}O_2N_4$	92.857 (95.014)
						$-C_2$	
Wight experimental loss(95.014)%, final (4.986)% , wight theoretical loss (92.857)% and final(7.143)% with (C_2)							
L_2	1	122	569.5	289	93.123 (91.444)	$-C_{17}H_{19}N_5O_2$	93.123 (91.444)
						$-C_2$	
Wight experimental loss(91.444)% , final (8.556)% , wight theoretical loss (93.123)% and final(6.877)% with (C_2)							
L_3	1	141	201.5	167	14.527 (14.051)	$-COCH_3$	81.081 (77.702)
	2	205	334.5	257	39.527 (37.962)	$-C_7H_5N_2$	
	3	373.5	599	467.5	27.027 (25.989)	$-C_4H_4N_2$	
						$-C_2S$	
Wight experimental loss(77.702)%, final (22.298)%, wight theoretical loss (81.081)% and final (18.919)% with (C_2S)							
L_4	1	53.5	176.7	108	14.716 (16.874)	$-CO_2$	81.271 (77.624)
	2	177	254.8	207	30.769 (28.663)	$-C_5H_4N_2$	
	3	284	599	411	35.786 (32.087)	$-C_5H_5N_3$	
						$-C_2S$	
Wight experimental loss (77.624)%, final(22.376)%, wight theoretical loss (81.271)% and final (18.729)%							

3.4. ^{1}HNMR spectra of azo dyes ligands

Azo dyes ligands have been identified by ^{1}HNMR spectra using dimethylsulphoxide (DMSO-d_6) as the solvent and tetramethylsilane (TMS) as the reference.

3.4.1. ^{1}HNMR spectrum of the ligand (L_1)

The ^{1}HNMR spectrum of the ligand Figure (3-9) display various signals at (δ=6.688-7.618) ppm refers to aromatic protons[86]. The signal obtained at (δ=6.571) ppm lead to proton of phenol[87]. Finding, the signals at (δ=3.413) ppm and (δ=2.619) ppm describe to δ(N-CH_3) and δ(CH_3) of pyrazole respectively[88]. Signal at (δ=2.320) ppm was assigned to δ(CH_3) of phenol, the signals at (δ=4.506) ppm and (δ=2.50) ppm due to water and DMSO-d_6[89].

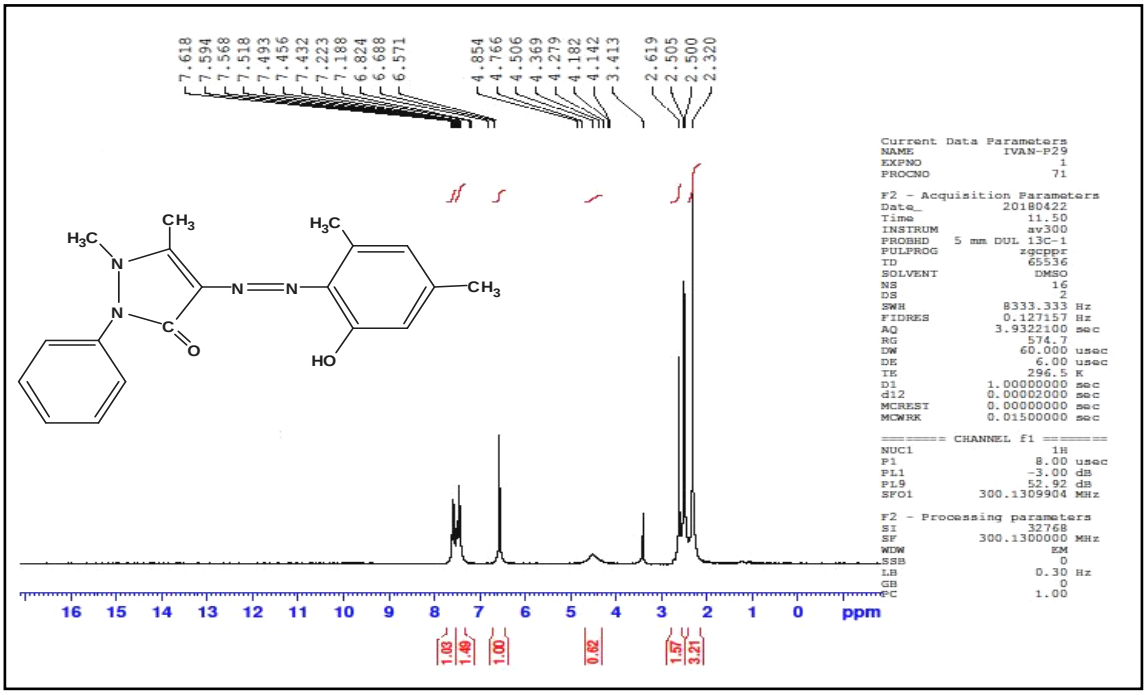

Figure (3-9): ^{1}HNMR spectrum of the ligand (L_1).

3.4.2. ^{1}HNMR spectrum of the ligand (L_2)

^{1}HNMR spectrum of the ligand Figure (3-10) show multiplet signals at (δ=7.389-8.126) ppm was assigned to aromatic protons[90]. The signals obtained at (δ=3.221) ppm and (δ=2.623) ppm due to δ(N-CH_3) and δ(CH_3) of pyrazole respectively[91] .Whereas, the signals at (δ=8.537) ppm and at (δ=2.937) ppm due to δ(NH_2) and δ(CH_3) of acetyl group. Signals obtained at (δ=4.084) ppm and (δ=2.50) ppm referred to water and DMSO-d_6[92].

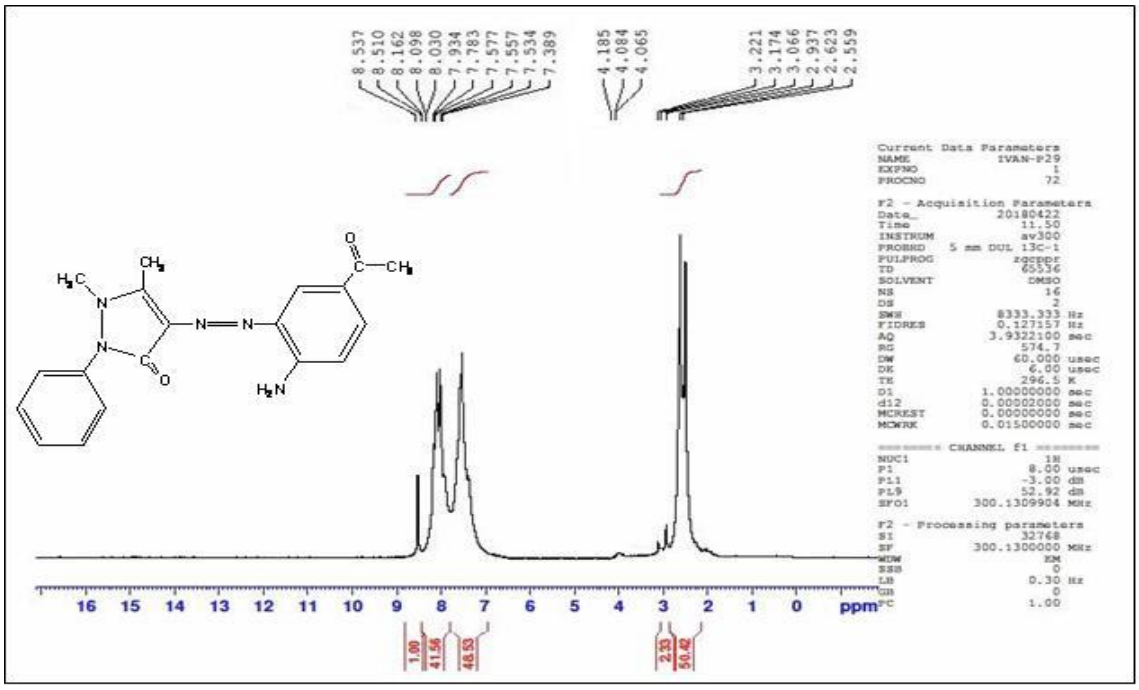

Figure (3-10): ^{1}HNMR spectrum of the ligand (L_2).

3.4.3. ^{1}HNMR spectrum of the ligand (L_3)

The ^{1}HNMR spectrum of the ligand display many signals at (δ=7.048-7.897) ppm assigned to aromatic protons[93]. Signals obtained at (δ=7.926) ppm and (δ=2.672) ppm due to δ(NH_2) and δ(CH_3) of acetyl group sequences[94], the signal observed at (δ=2.50) ppm lead to DMSO-d_6, see Figure (3-11).

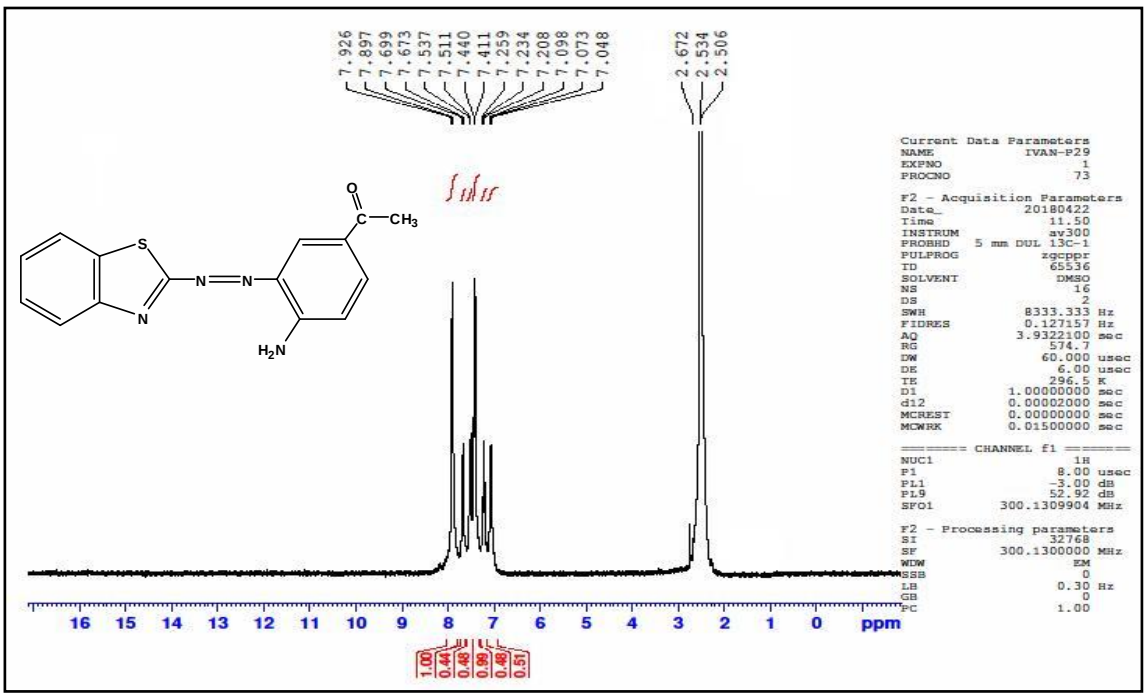

Figure (3-11): ^{1}HNMR spectrum of the ligand (L_3).

3.4.4. ^{1}HNMR spectrum of the ligand (L_4)

^{1}HNMR spectrum of the ligand display various signals at (δ=6.610-8.300) ppm described to aromatic protons[95]. The signals observed at (δ=8.449) ppm and (δ=2.50) ppm which were assigned to δ(NH_2) and DMSO-d_6[96], see Figure (3-12).

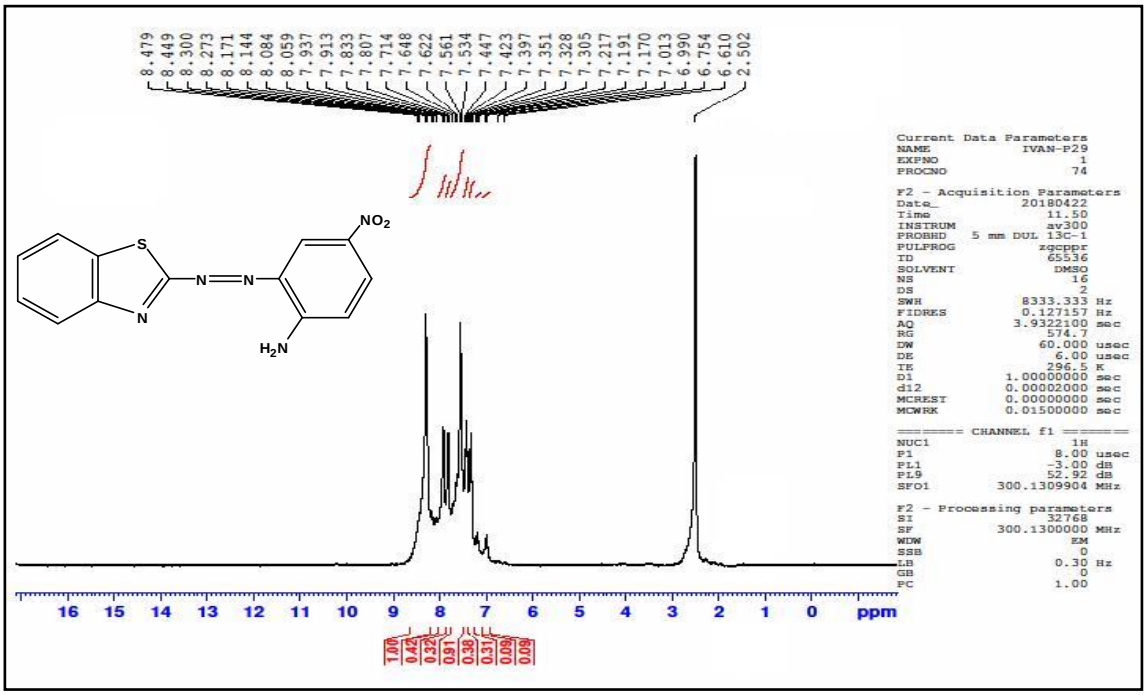

Figure (3-12): ^{1}HNMR spectrum of the ligand (L_4).

3.5. ^{13}CNMR spectra of azo dyes ligands

Azo dyes ligands have been characterized by ^{13}CNMR spectra using DMSO-d_6 as the solvent and TMS as the reference.

3.5.1. ^{13}CNMR spectrum of the ligand (L_1)

The ^{13}CNMR spectrum of the ligand display resonance at (δ=19.514) ppm and (δ=34.662) ppm due to carbon of (CH_3) in phenol ring. The resonance at (δ=10.444) ppm and (δ=38.016) ppm due to carbon of (CH_3) in pyrazole group. The various signals at (δ=156.295, 140.259, 139.618, 133.117, 129.676, 129.406, 128.501, 126.674, 122.805, 115.894 and 94.185) ppm attributed to carbon atoms of aromatic rings. Signals at (δ=157.127) ppm and (δ=151.140) ppm due to carbon of (C=O) and (C-OH) groups and the indicative in (δ=39.500) ppm due into DMSO-d_6[97,98], see Figure (3-13).

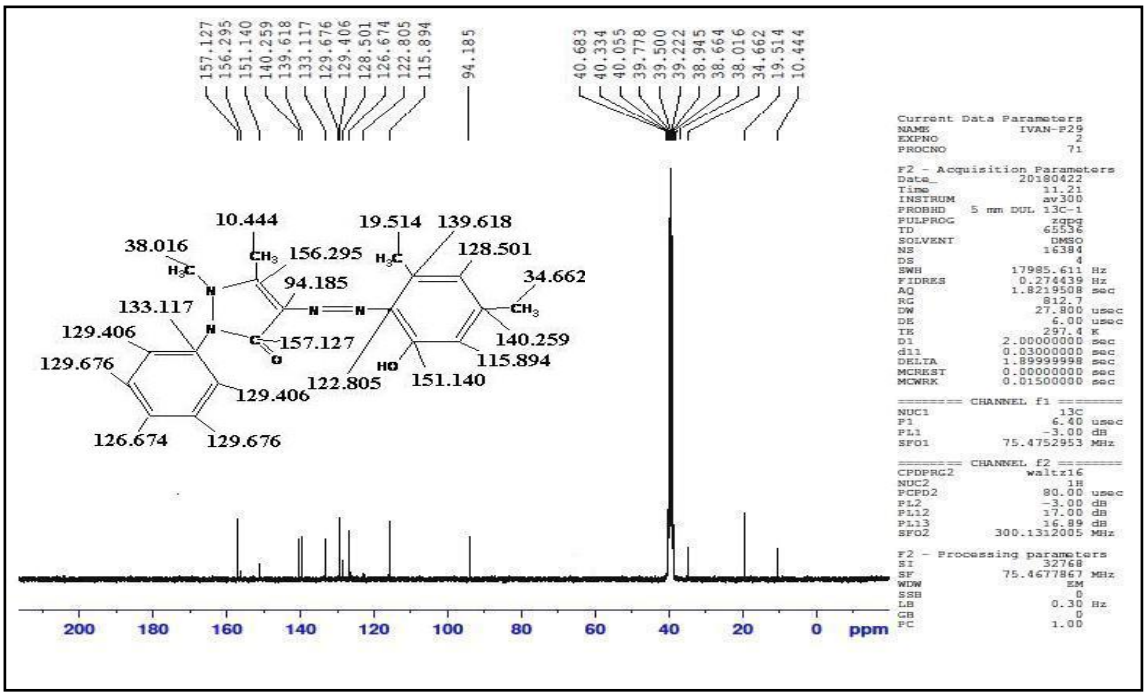

Figure (3-13): ^{13}CNMR spectrum of the ligand (L_1).

3.5.2. ^{13}CNMR spectrum of the ligand (L_2)

The ^{13}CNMR spectrum of the azo ligand Figure (3-14) show signals at (δ=197.307) ppm and (δ=164.183) ppm were assigned to carbon of (C=O) of acetyl and pyrazole groups sequences. The resonance at (δ=150.367) ppm due to carbon of amino group. The various signals at (δ=152.427, δ=134.850, δ=129.583, δ=126.266, δ=124.745, δ=123.576, δ=122.731, δ=119.531, δ=118.781, δ=114.729 and δ=100.881) ppm described to carbon atoms of aromatic rings. Resonance at (δ=13.550) ppm and (δ=36.115) ppm due to carbon of (CH_3) in pyrazole group. Signals at (δ=26.735) ppm and (δ=39.500) ppm due to carbon of (CH_3) in acetyl group and DMSO-d_6[99,100].

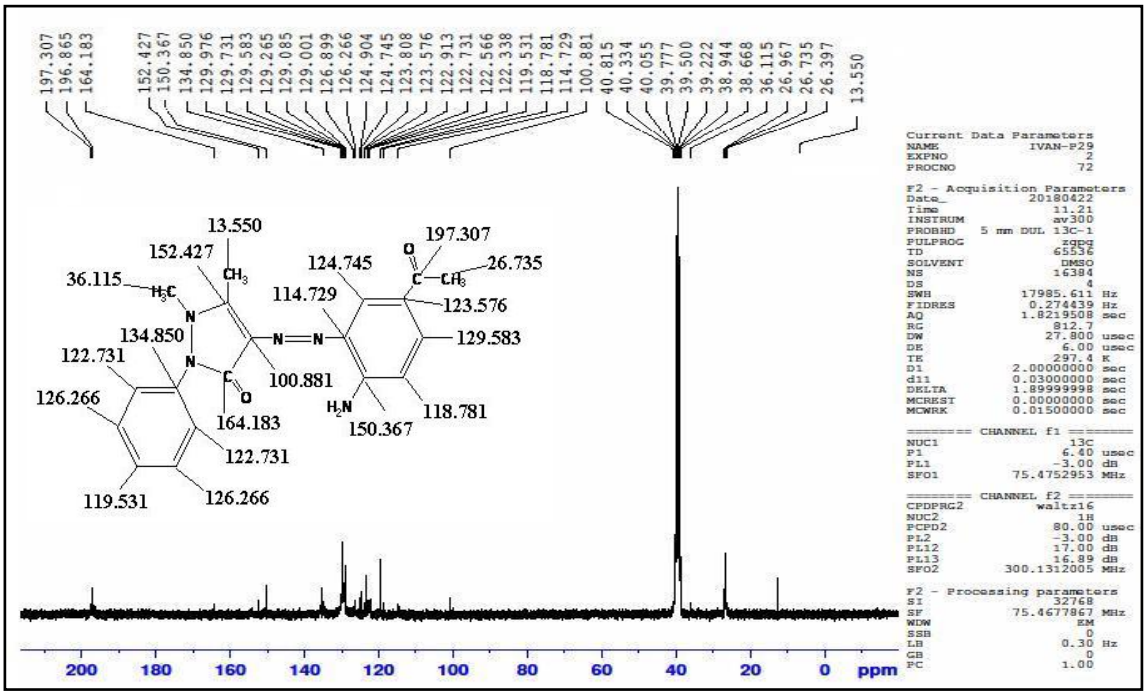

Figure (3-14): ^{13}CNMR spectrum of the ligand (L_2).

3.5.3. ^{13}CNMR spectrum of the ligand (L_3)

^{13}CNMR spectrum of the azo ligand Figure (3-15) shows resonance at (δ=196.370) ppm and (δ=152.921) ppm were described to carbon of (C=O) of acetyl and amino groups sequences. Various signals at (δ=155.030, δ=131.896, δ=131.743, δ=131.680, δ=129.543, δ=124.984, δ=121.719, δ=120.936, δ=119.533, δ=118.578 and δ=99.966) ppm lead to carbon atoms of aromatic rings. The resonance at (δ=26.381) ppm and (δ=39.783) ppm due to carbon of (CH_3) in acetyl group and DMSO-d_6[101,102].

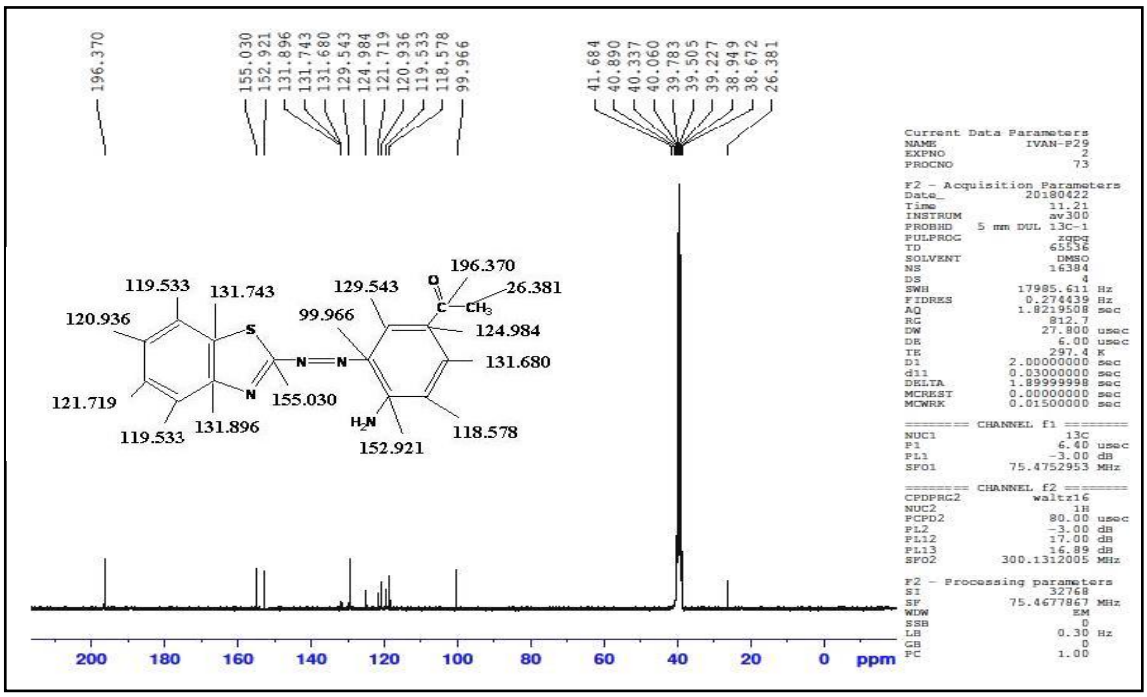

Figure (3-15): ^{13}CNMR spectrum of the ligand (L_3).

3.5.4. ^{13}CNMR spectrum of the ligand (L_4)

^{13}CNMR spectrum of the ligand appear resonance at (δ=149.960) ppm which was assigned to carbon of amino group. The various signals at (δ=151.591,δ=143.039, δ=132.192, δ=130.739, δ=126.346, δ=126.257, δ=125.348,δ=124.672,δ=124.011, δ=123.043, δ=121.721 and δ=120.802) ppm attributed to carbon atoms of aromatic rings. Signal at (δ=39.751) ppm due into DMSO-d_6[103], see Figure (3-16).

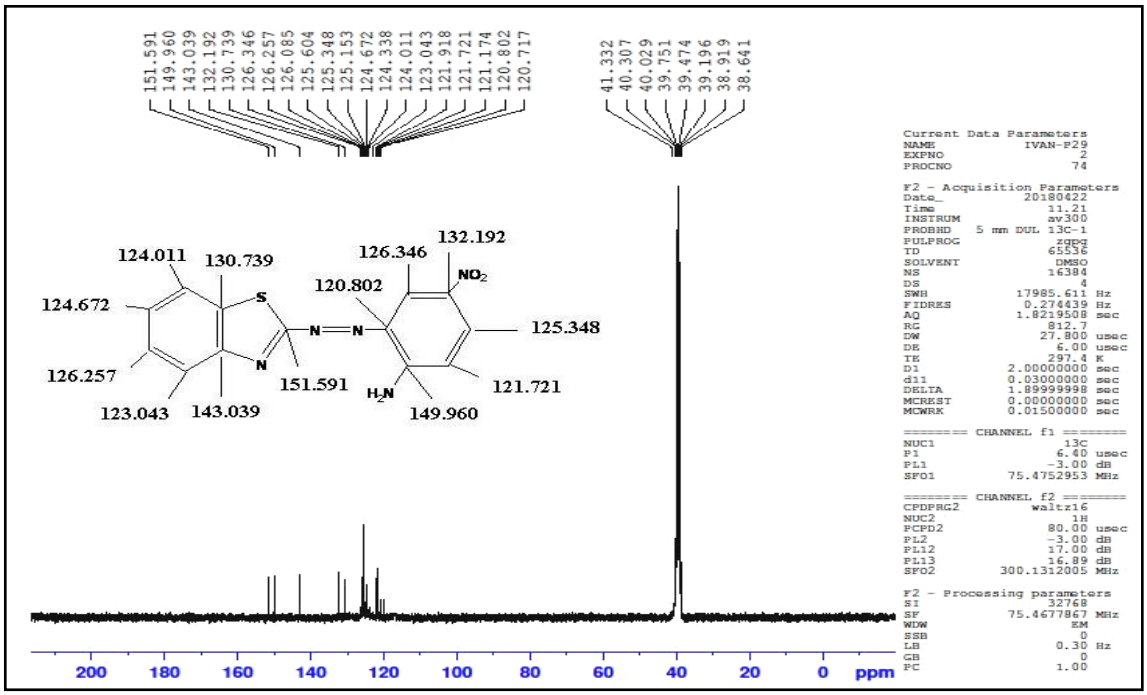

Figure (3-16): ^{13}CNMR spectrum of the ligand (L_4).

3.6. FTIR spectra of azo dyes ligands

Azo dyes ligands were characterized by FTIR spectra with samples produced as KBr discs.

3.6.1. FTIR spectrum of the ligand (L_1)

IR spectrum of starting material 4-aminoantipyrine Figure (3-17) show bands at 3433 cm^{-1} and 3325 cm^{-1} due to $\upsilon(NH_2)$ asymmetric and symmetric respectively[104]. The bands at 1743 cm^{-1} and 1589 cm^{-1} assigned to υ(C=O) and υ(C=C) respectively[105]. Bands at (1496, 1450 and 1354) cm^{-1} lead to bending vibration of $\delta(CH_3)$[106]. Figure (3-18) display the starting material 3,5-dimetylphenol, which appear broad band a 3251 cm^{-1} described to υ(OH), while the bands at (1616, 1593, 1473, 1442, 1346 and 1307) cm^{-1} due to stretching vibration of υ(C=C) and bending frequency of $\delta(CH_3)$ sequences[107,108].

The FTIR spectrum of the ligand (L_1), Figure (3-19) exhibited sharp band at 3410 cm^{-1} described to stretching vibration of υ(OH)

phenol. The bands at 1666 cm^{-1} and 1585 cm^{-1} which were assigned to vibration of υ(C=O) and υ(N=N) respectively, bands at (1496, 1442, 1415, 1369 and 1319) cm^{-1} lead to bending frequency of δ(CH_3) groups[109-111].

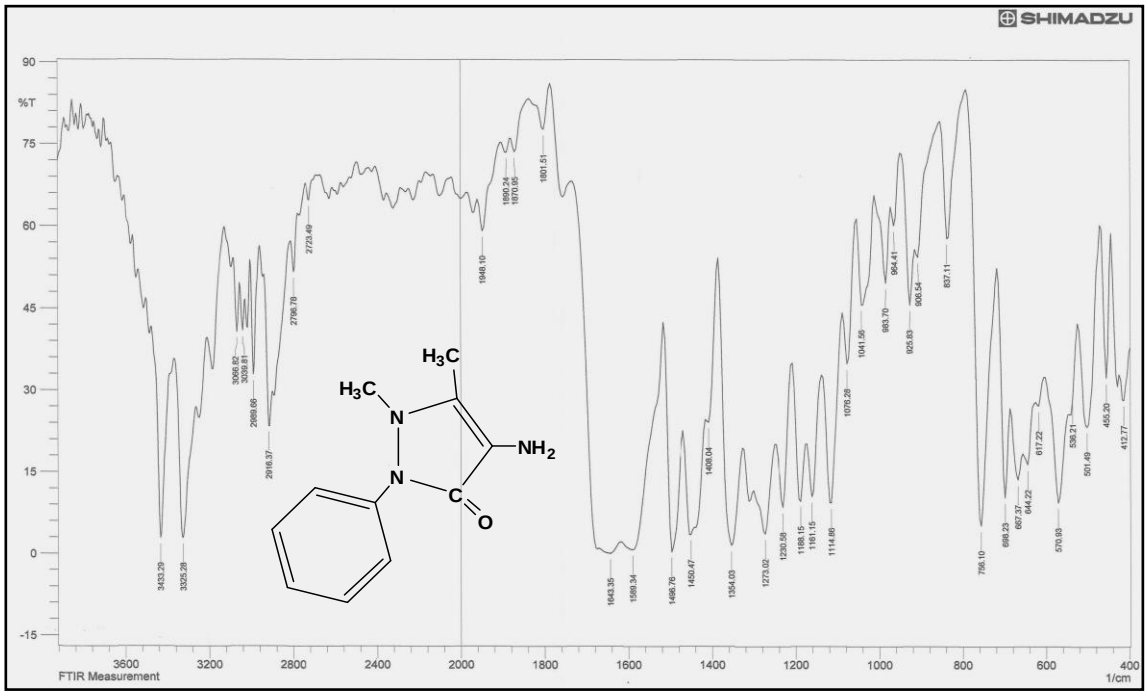

Figure (3-17): FTIR spectrum of 4-aminoantipyrine.

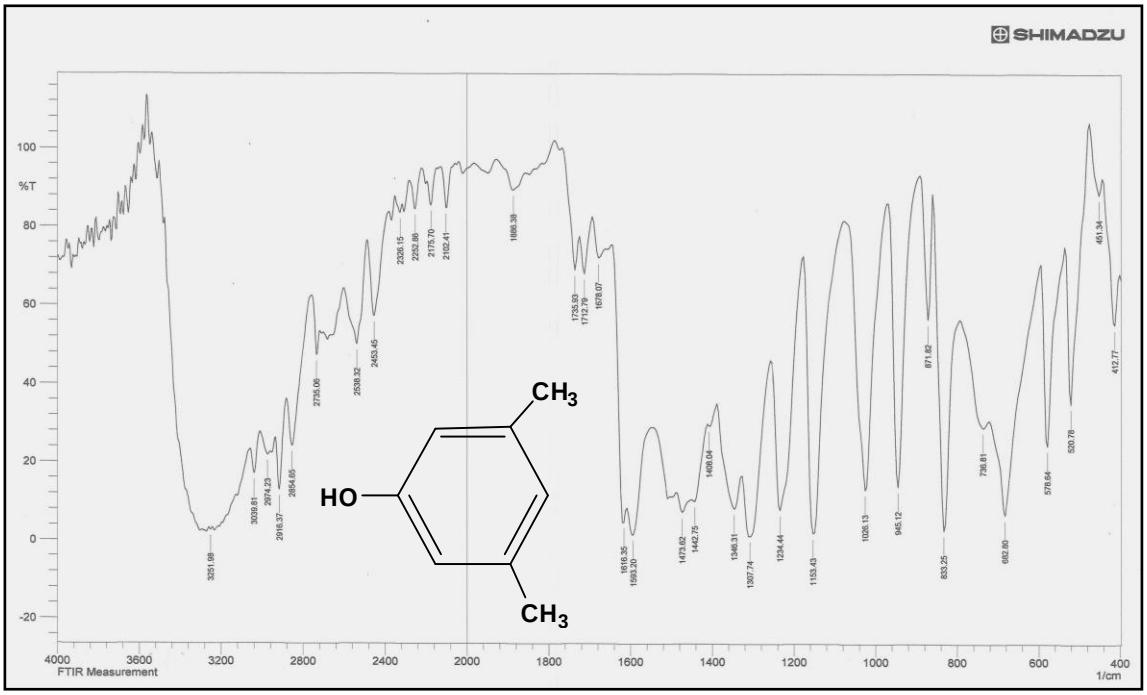

Figure (3-18): FTIR spectrum of 3,5-dimethyphenol.

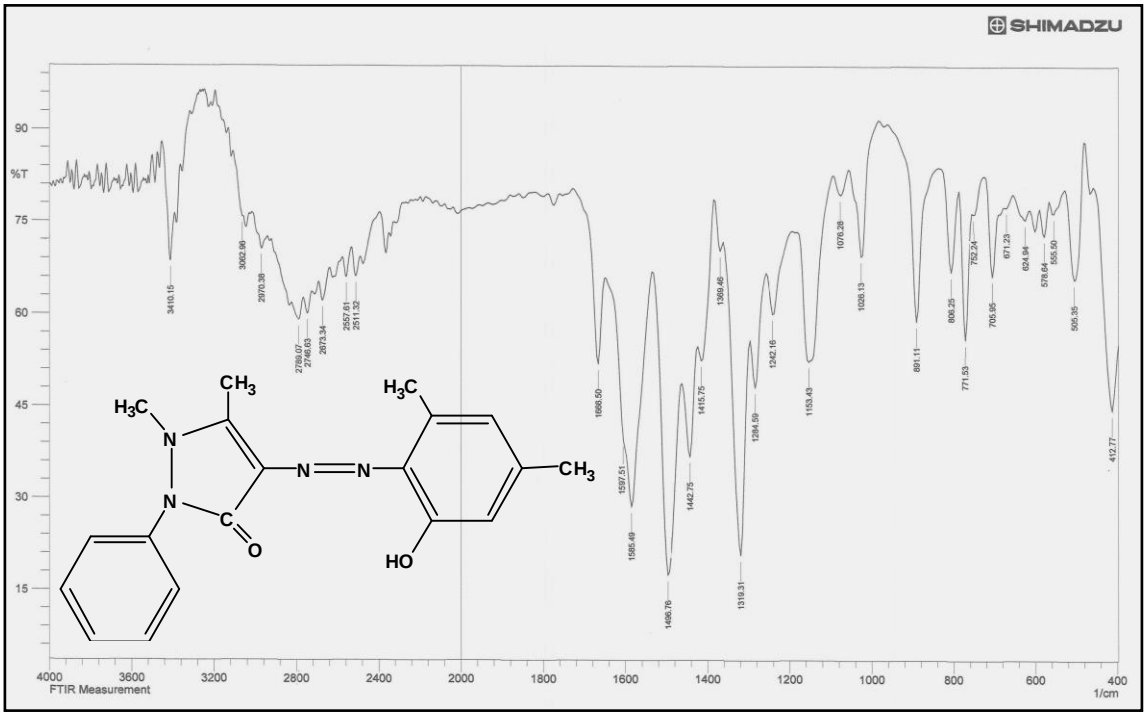

Figure (3-19): FTIR spectrum of the ligand (L_1).

3.6.2. FTIR spectrum of the ligand (L_2)

Figure (3-20) display the starting material 4-aminoacetophenone, which exhibited bands at 3394 cm^{-1} and 3332 cm^{-1} described to stretching frequency asymmetric and symmetric of $\upsilon(NH_2)$respectively, while the band at 1647 cm^{-1} lead to υ(C=O)[112]. Bands at (1589, 1562, 1438 and 1361) cm^{-1} due to stretching vibration of υ(C=C) and bending frequency of $\delta(CH_3)$ sequences[113]. Spectrum of the ligand (L_2) shows bands at 3487 cm^{-1} and 3414 cm^{-1} which were assigned to stretching frequency asymmetric and symmetric of $\upsilon(NH_2)$[114]. The bands at 1678 cm^{-1} and 1657 cm^{-1} due to carbonyl υ(C=O) of acetyl and pyrazole groups respectively [115]. The bands at 1597 cm^{-1} and 1512 cm^{-1} due to vibration of υ(C=C) and υ(N=N) sequences, bands at (1496, 1454, 1411, 1357 and 1307) cm^{-1} lead to bending frequency of $\delta(CH_3)$ groups[116], see Figure (3-21).

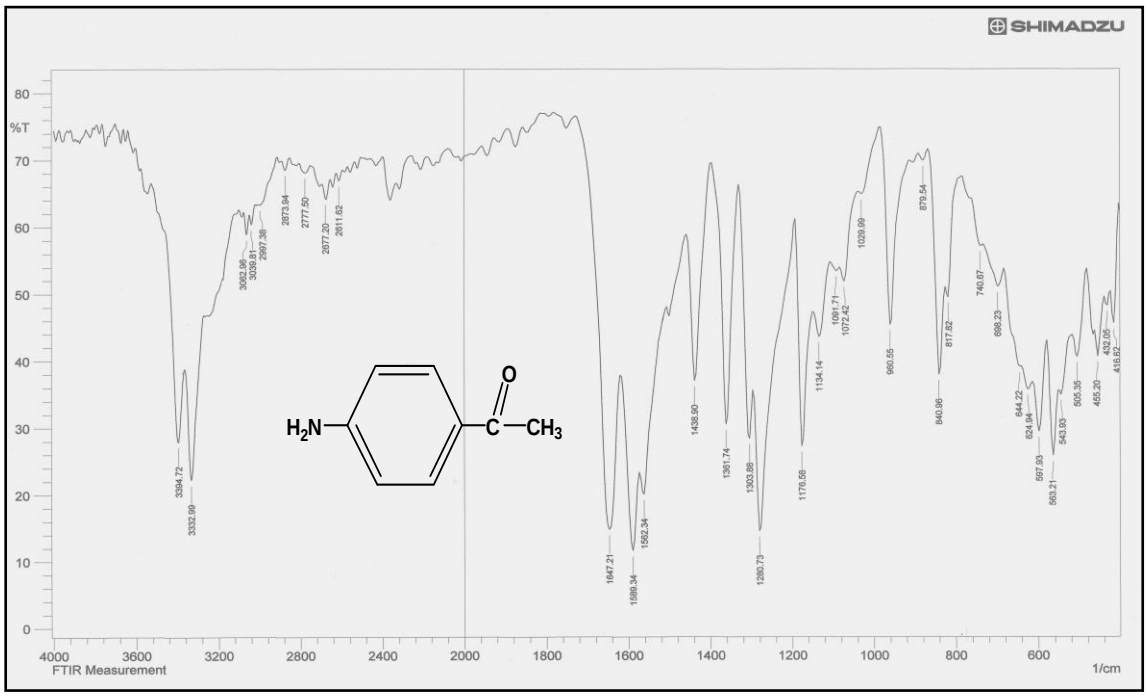

Figure (3-20): FTIR spectrum of 4-aminoacetophenone.

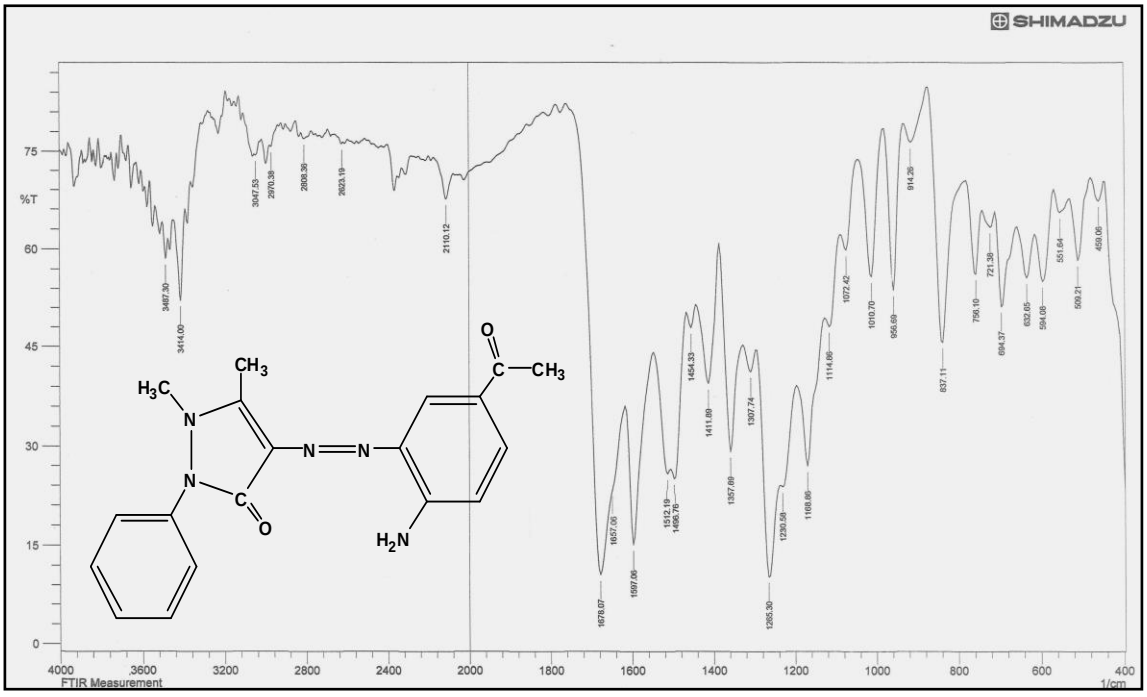

Figure (3-21): FTIR spectrum of the ligand (L_2).

3.6.3. FTIR spectrum of the ligand (L_3)

IR spectrum of starting material 2-aminobenzothiazole Figure (3-22) display bands at 3414 cm^{-1} and 3356 cm^{-1} due to $\upsilon(NH_2)$ asymmetric and symmetric respectively. bands at 1631 cm^{-1} and (1589, 1543) cm^{-1} assigned to υ(C=N) and υ(C=C) respectively[117]. Spectrum of the ligand (L_3), Figure (3-23) exhibited bands at 3483 cm^{-1} and 3414 cm^{-1} which were assigned to stretching vibration of $\upsilon(NH_2)$[118]. Bands at 1678 cm^{-1} and 1654 cm^{-1} due to carbonyl υ(C=O) of acetyl and υ(C=N) of thiazole groups sequences[119]. The band at 1531 cm^{-1} due to vibration of υ(N=N), bands at 1589 cm^{-1} and 1570 cm^{-1} attributed to υ(C=C). The bands at (1442, 1423, 1396 and 1342) cm^{-1} lead to bending vibration of $\delta(CH_3)$ group[120]..

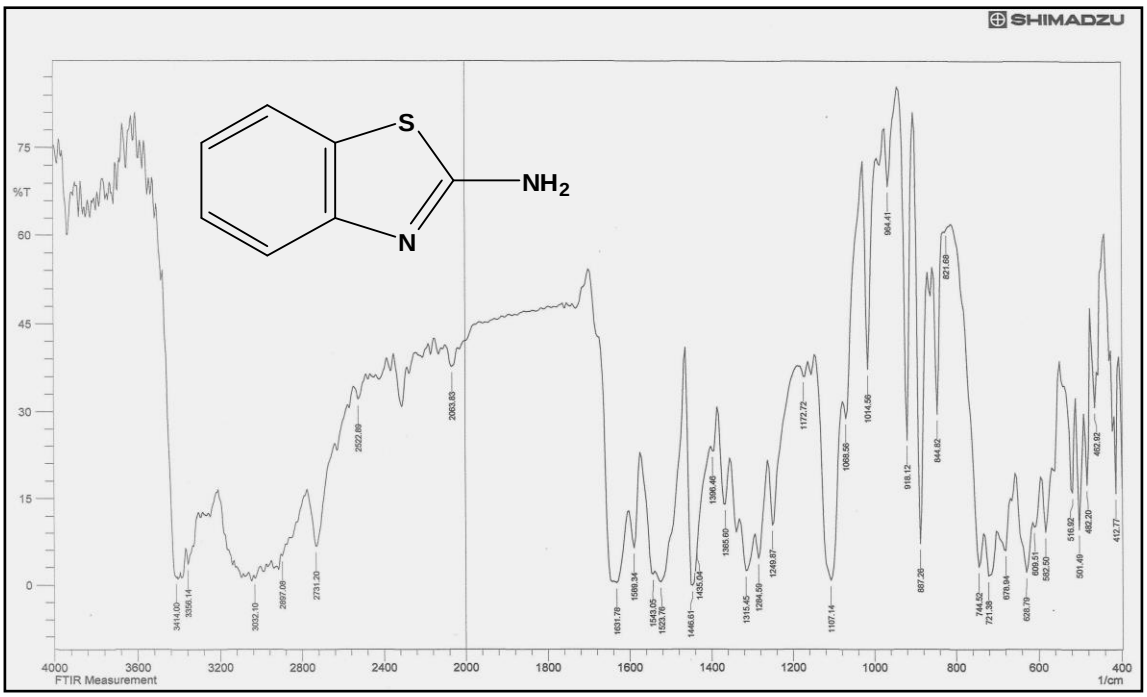

Figure (3-22): FTIR spectrum of 2-aminobenzothiazole.

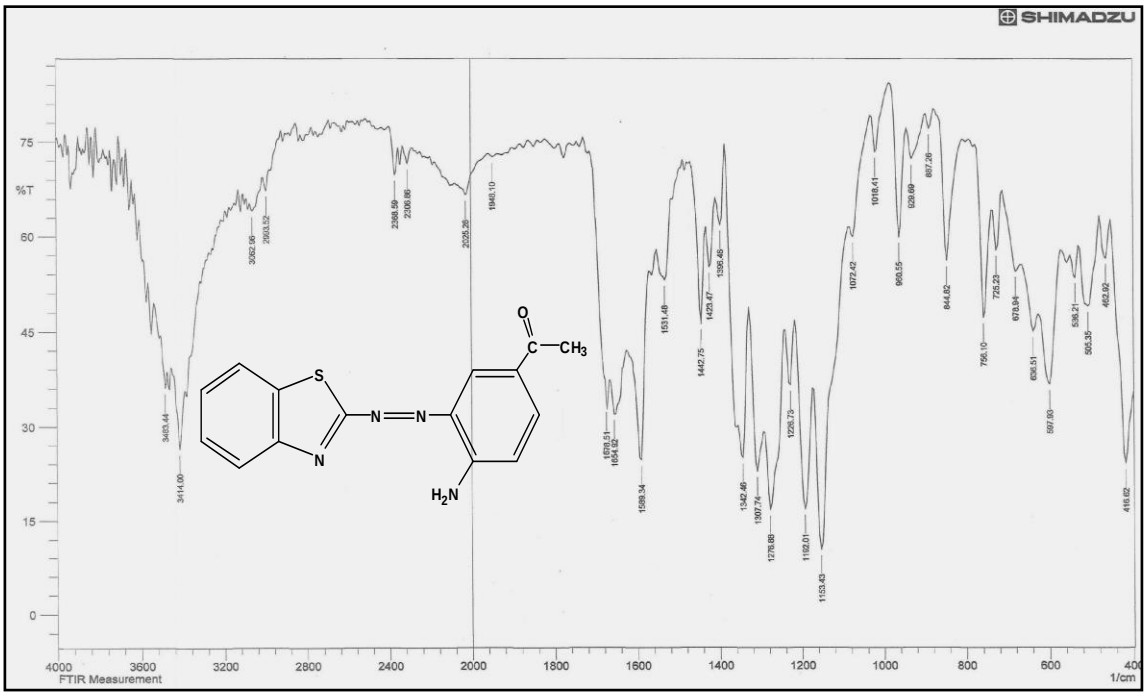

Figure (3-23): FTIR spectrum of the ligand (L_3).

3.6.4. FTIR spectrum of the ligand (L_4)

Figure (3-24), show the starting material 4-nitroaniline, which exhibited bands at 3479 cm^{-1} and 3360 cm^{-1} due to asymmetric and symmetric frequency of $\upsilon(NH_2)$, while the bands at 1632 cm^{-1} and 1593 cm^{-1} lead to υ(C=C). Bands at 1500 cm^{-1} and 1332 cm^{-1} due to stretching vibration asymmetric and symmetric of $\upsilon(NO_2)$[121,122].The ligand (L_4) exhibited bands at 3484 cm^{-1} and 3414 cm^{-1} which were assigned to frequency asymmetric and symmetric of $\upsilon(NH_2)$[123].The band at 1639 cm^{-1} due to υ(C=N) group[124]. Bands at 1593 cm^{-1} and 1562 cm^{-1} described to vibration of υ(C=C), the band at 1446 cm^{-1} lead to frequency of υ(N=N). The bands at 1508 cm^{-1} and 1332 cm^{-1} which assigned to vibration of asymmetric and symmetric of $\upsilon(NO_2)$[125], see Figure (3-25).

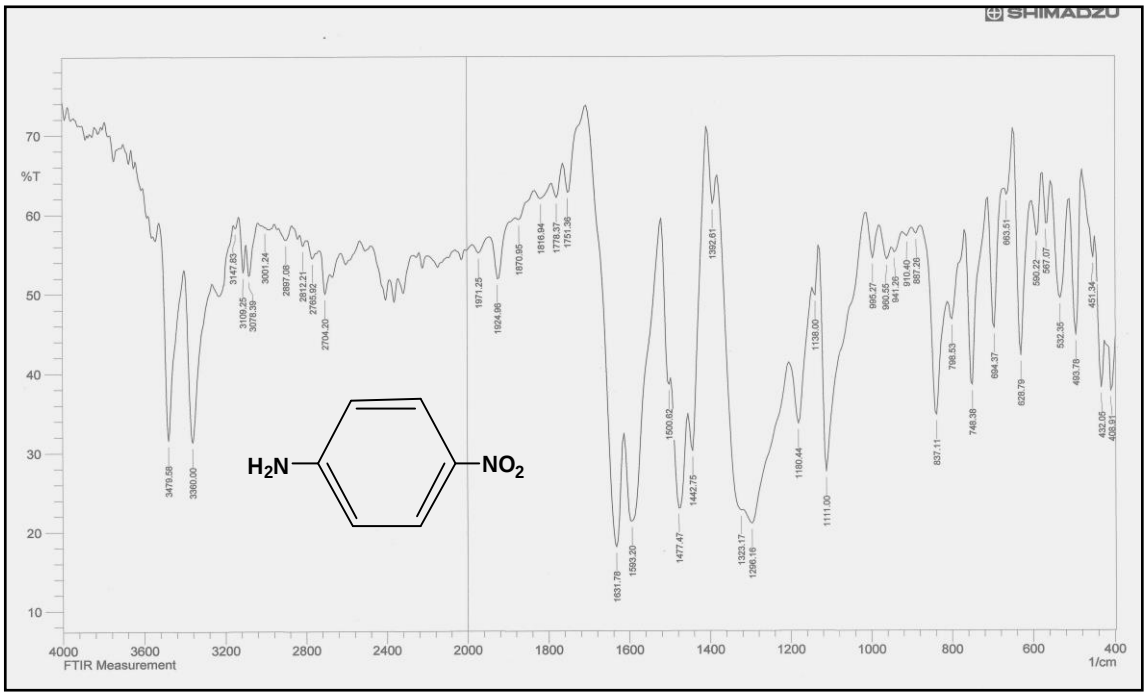

Figure (3-24): FTIR spectrum of 4-nitroaniline.

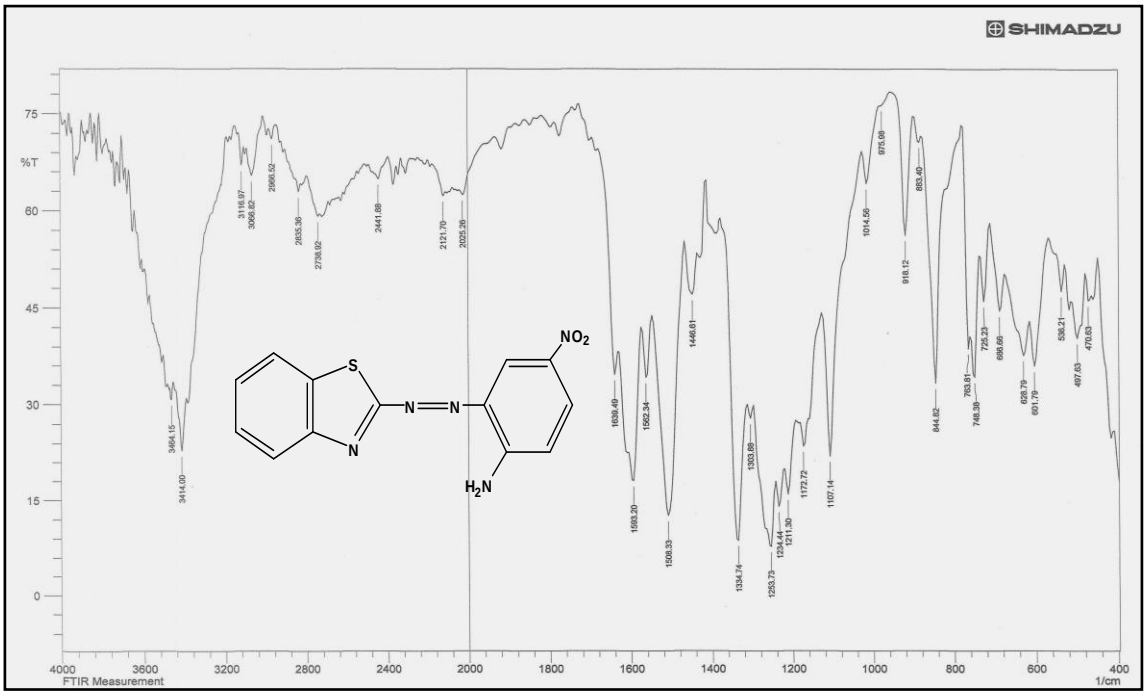

Figure (3-25): FTIR spectrum of the ligand (L_4).

3.7. UV-Vis spectra of azo dyes ligands

The electronic spectra of ligands under investigation were carried out in ethyl alcohol (10^{-3} mole/L).

3.7.1. UV-Vis spectrum of the ligand (L_1)

The spectrum, Figure (3-26) display intense absorption peaks at (242 nm) (41322 cm^{-1}) (ε_{max}=1894 $l.mole^{-1}.cm^{-1}$) and (356 nm) (28089 cm^{-1}) (ε_{max}=1853 $l.mole^{-1}.cm^{-1}$) which were assigned to (π-π^*), other peak at (414 nm) (24154 cm^{-1}) (ε_{max}=1177 $l.mole^{-1}.cm^{-1}$) due to electronic transition (n-π^*)[126,127].

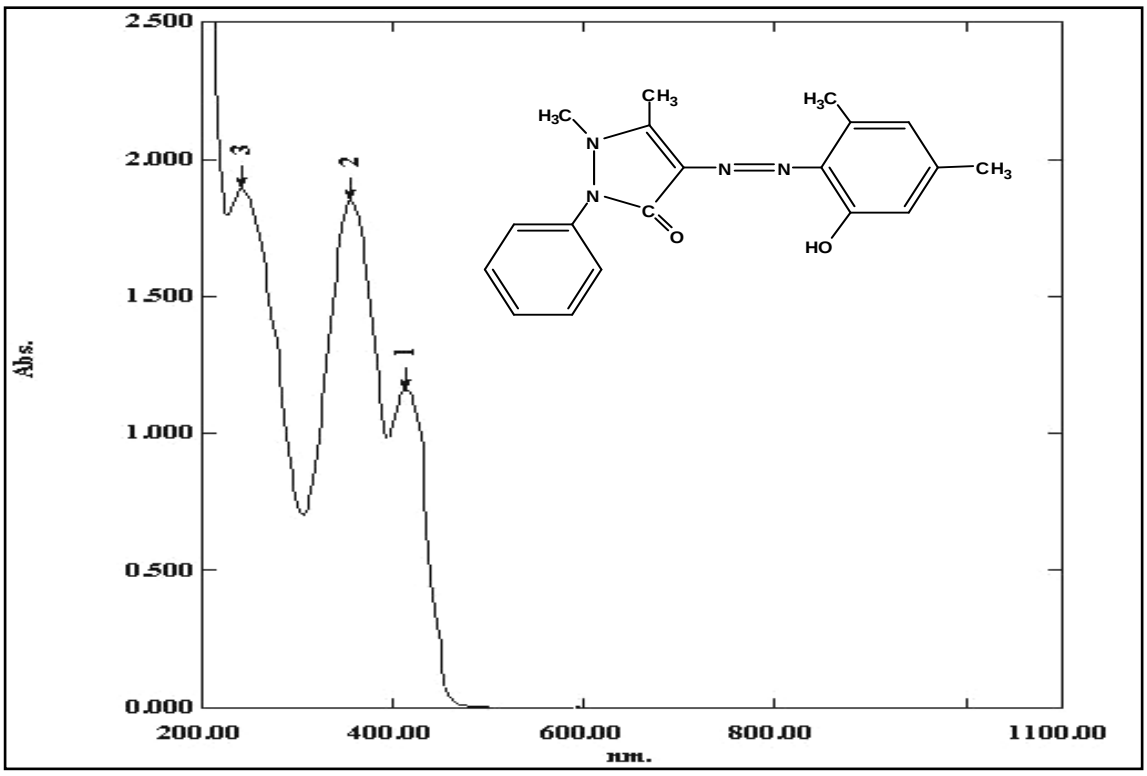

Figure (3-26): UV-Vis spectrum of the ligand (L_1).

3.7.2. UV-Vis spectrum of the ligand (L_2)

Figure (3-27) display the spectrum of azo ligand (L_2), which exhibited peaks at (298 nm) (33557 cm^{-1}) (ε_{max}=2272 $l.mole^{-1}.cm^{-1}$) and (432 nm) (23148 cm^{-1}) (ε_{max}=1479 $l.mole^{-1}.cm^{-1}$) which were assigned to (π-π^*) and (n-π^*) for (-N=N-) group[128,129].

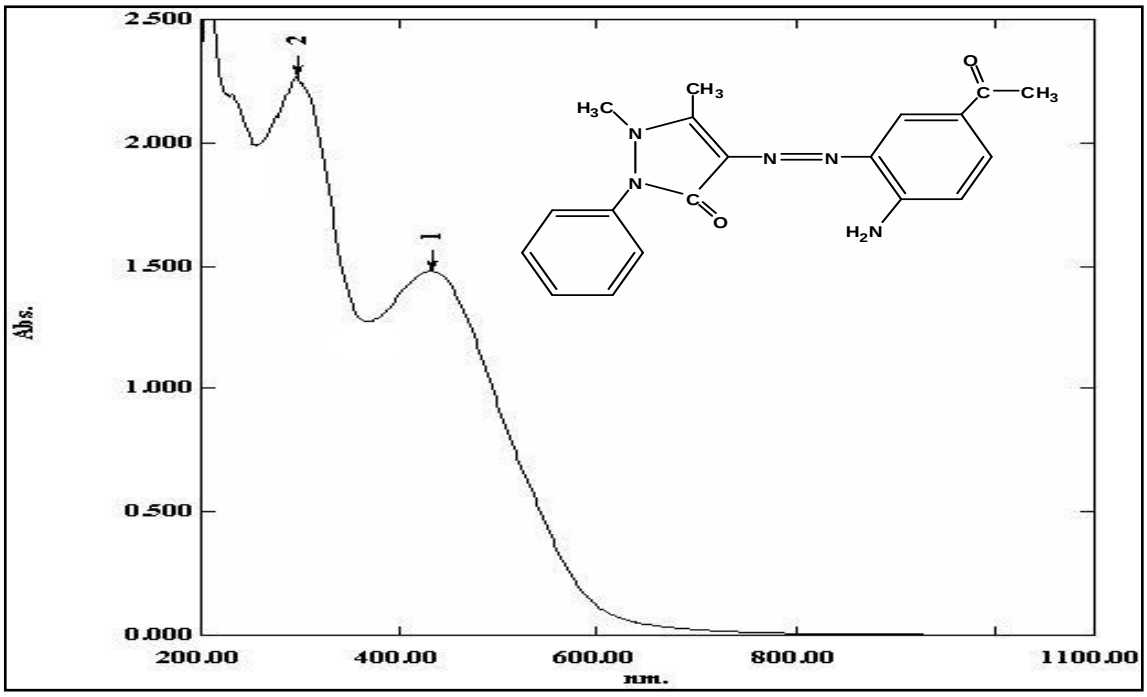

Figure (3-27): UV-Vis spectrum of the ligand (L_2).

3.7.3. UV-Vis spectrum of the ligand (L_3)

Figure (3-28), represents the spectrum of ligand (L_3) which exhibited peaks at (218 nm) (45871 cm^{-1}) (ε_{max}=1950 $l.mole^{-1}.cm^{-1}$), (270 nm) (37037 cm^{-1}) (ε_{max}=1066 $l.mole^{-1}.cm^{-1}$) and (396 nm) (25252 cm^{-1}) (ε_{max}=2039 $l.mole^{-1}.cm^{-1}$) lead to electronic transition (π-π^*)[130,131].

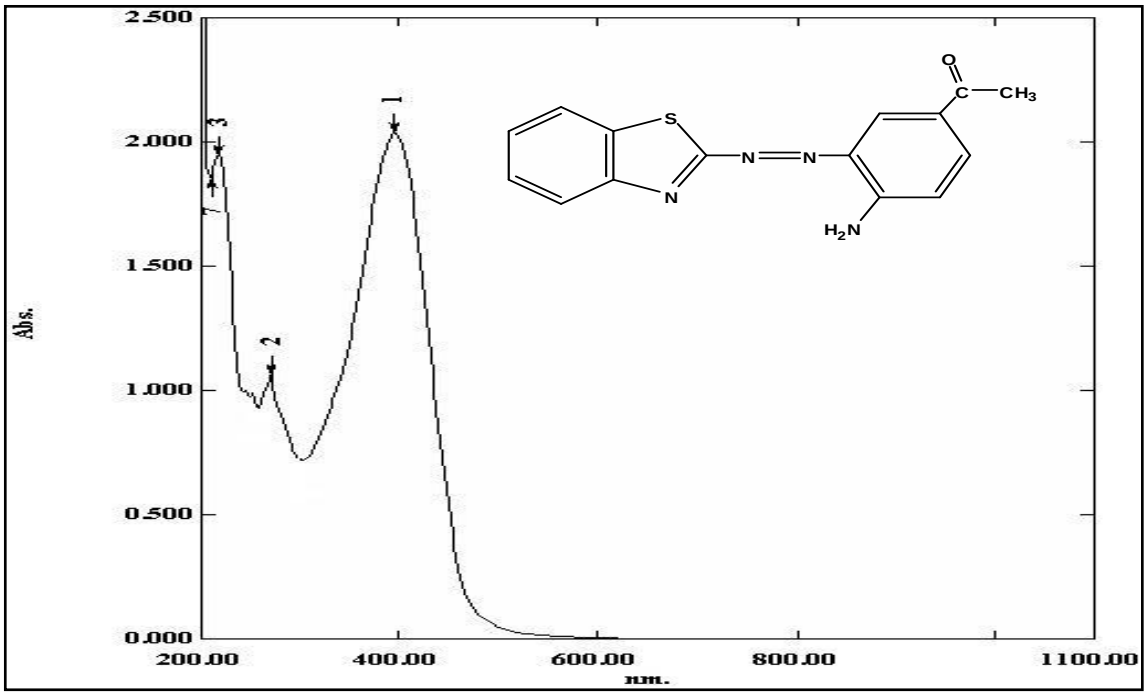

Figure (3-28): UV-Vis spectrum of the ligand (L_3).

3.7.4. UV-Vis spectrum of the ligand (L_4)

Figure (3-29), which exhibited peaks at (218 nm) (45871 cm^{-1}) (ε_{max}=2198 $l.mole^{-1}.cm^{-1}$), (290 nm) (34482 cm^{-1}) (ε_{max}=785 $l.mole^{-1}.cm^{-1}$) and (410 nm) (24390 cm^{-1}) (ε_{max}=2340 $l.mole^{-1}.cm^{-1}$) described to electronic transition (π-π^*)[132,133].

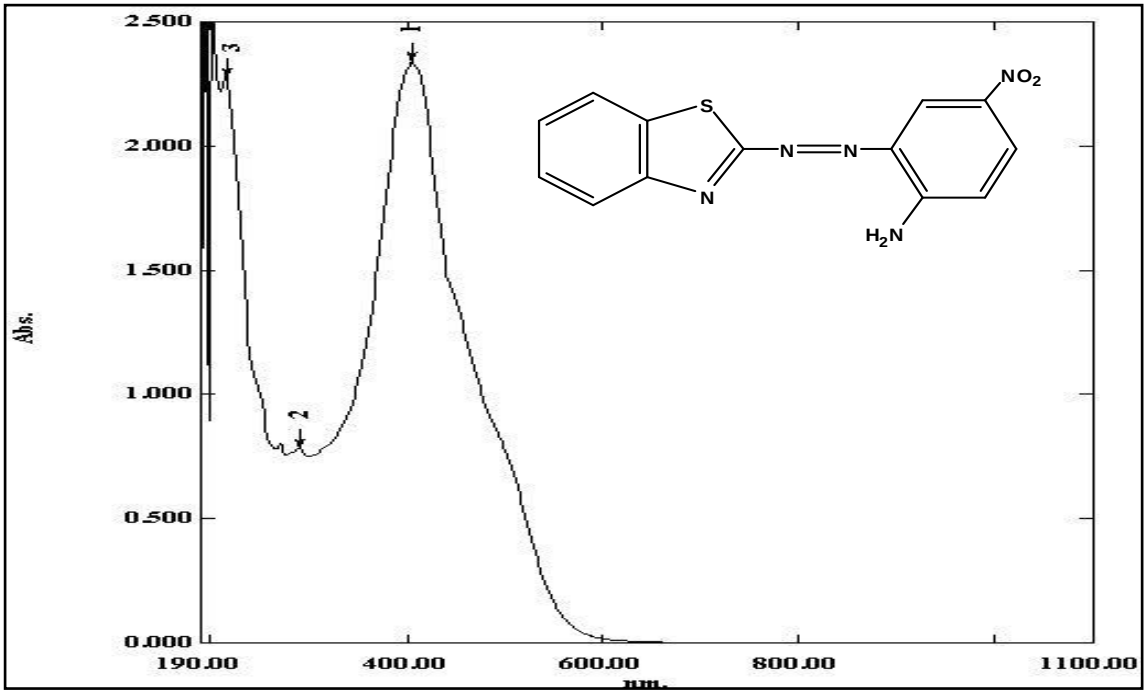

Figure (3-29): UV-Vis spectrum of the ligand (L_4).

3.8. UV-Vis spectral studies

The colored contained from the reaction of metal ions with azo ligands are very important for electronic spectral studies. Because of the presence of high and sharp absorption peak which belong to the metal complex, this peak shift in the visible region was detected in solution of complex spectra with respect to ligand may be due to good indicated for coordination and formation of the complex. see figure (3-30), which exhibited comparison between free ligand (L_2) solution with Cu-L_2 mixed solution and free ligand (L_4) solution with Co- L_4 mixed solution .

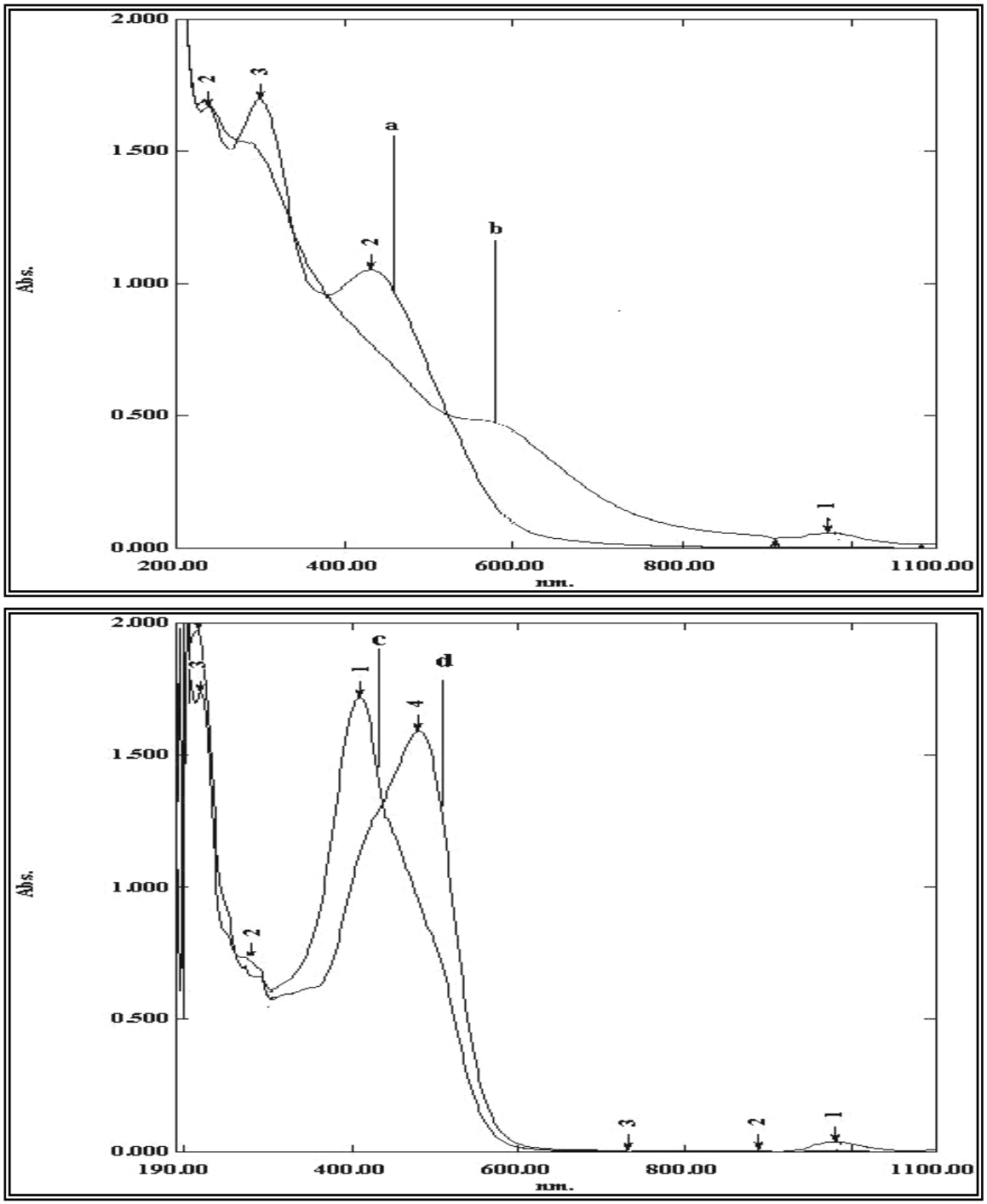

Figure (3-30): UV-Vis spectra:

a) Free ligand (L_2) solution, b) Cu-L_2 mixed solution

c) Free ligand (L_4) solution, d) Co-L_4 mixed solution

3.8.1. Effect of pH and concentration

Electronic spectra were measured for the mixed solutions obtaining equal quantities of metal ions dissolved in buffer solution and ligands dissolved in ethanol at the same concentration.

Molar concentration studied at the range (10^{-2}- 10^{-5} mole/L), while the pH range at (5- 9). These concentration are not all suitable in UV-Vis measurements. The solutions of (10^{-2} mole/L) were turbid, on other than out of scale absorbance were measured by (10^{-3} mole/L), in the same time the color of (10^{-3} mole/L) solutions make it very hard to study. Only reach (1- 3×10^{-4} mole/L) concentration followed Beer's law and appeared obvious intense color. Best fit straight lines were happened with correlation factor (R> 0.99) as shown in Figure (3-31), and the results obtained is given in Table (3-4). Perfect concentration was chosen for complex solution based on which solution gives the highest absorbance at constant (λ_{max}) at different pH, and results are described in Table (3-5). The trial results evidence that the absorbance of all prepared complexes are maximum and constant in a buffer solution of ammonium acetate at pH extent (5- 9). It was found that all prepared complexes had perfect pH as is shown in Figure (3-32).

Table (3-4): Absorbance at (λ_{max}) for molar concentration of mixed solutions of metal ions with azo ligands.

Absorbance Metal ion (λ_{max})	Ligands				
	Molar Conc. $\times 10^{-4}$				
	3.0	**2.5**	**2.0**	**1.5**	**1.0**
Co(II) (460)/ L_1	0.038	0.047	0.073	0.093	0.116
Ni(II) (458)/ L_1	0.036	0.055	0.076	0.098	0.109
Cu(II) (481)/ L_1	0.033	0.053	0.072	0.090	0.112
Zn(II) (450)/ L_1	0.037	0.052	0.078	0.091	0.107
Co(II) (442)/ L_2	0.017	0.032	0.048	0.055	0.057
Ni(II) (440)/ L_2	0.046	0.057	0.098	0.107	0.125
Cu(II) (560)/ L_2	0.126	0.197	0.256	0.370	0.413
Zn(II) (476)/ L_2	0.030	0.020	0.062	0.054	0.036
Co(II) (458)/ L_3	0.451	0.381	0.317	0.226	0.155
Ni(II) (466)/ L_3	0.175	0.152	0.122	0.095	0.055
Cu(II) (470)/ L_3	0.124	0.109	0.077	0.064	0.042
Zn(II) (472)/ L_3	0.536	0.471	0.347	0.258	0.177
Co(II) (480)/ L_4	0.007	0.011	0.015	0.017	0.024
Ni(II) (478)/ L_4	0.283	0.382	0.510	0.700	0.764
Cu(II) (476)/ L_4	0.269	0.392	0.477	0.680	0.713
Zn(II) (478)/ L_4	0.016	0.025	0.028	0.036	0.048

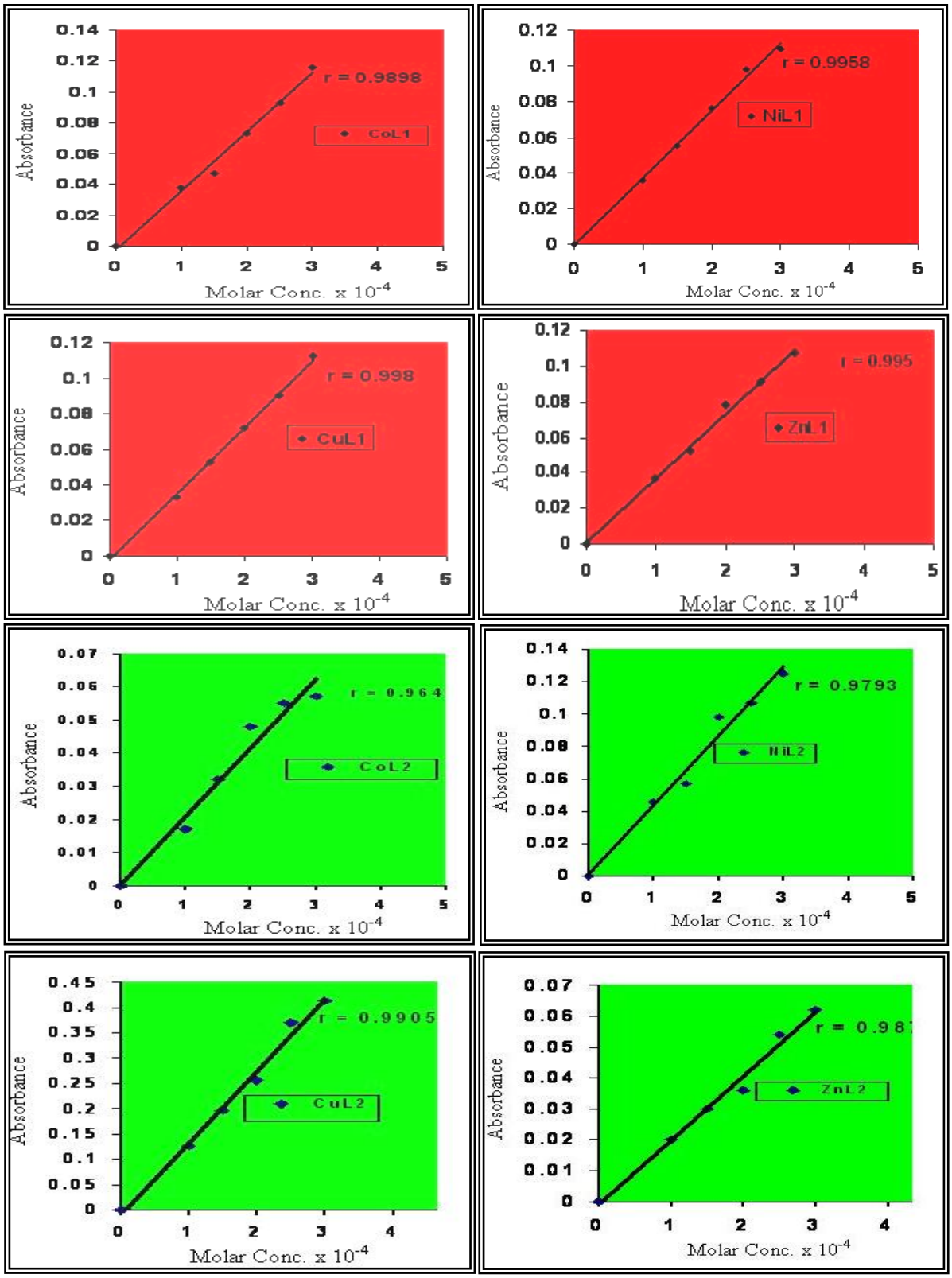

Figure (3-31): Linear correlation between molar concentration and absorbance for mixed solutions of metal ions with azo ligands.

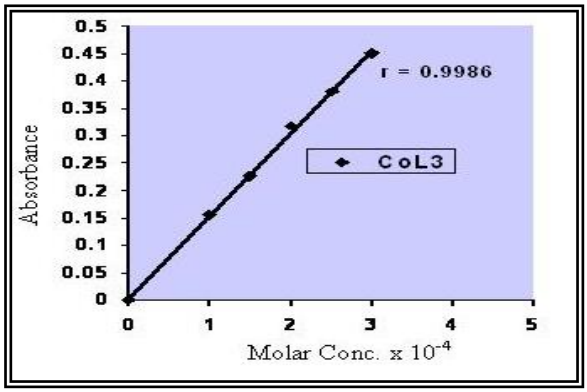
r = 0.9986
CoL3
Absorbance
Molar Conc. x 10-4

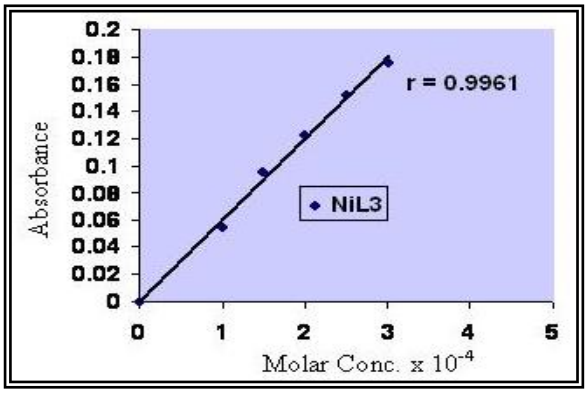
r = 0.9961
NiL3
Absorbance
Molar Conc. x 10-4

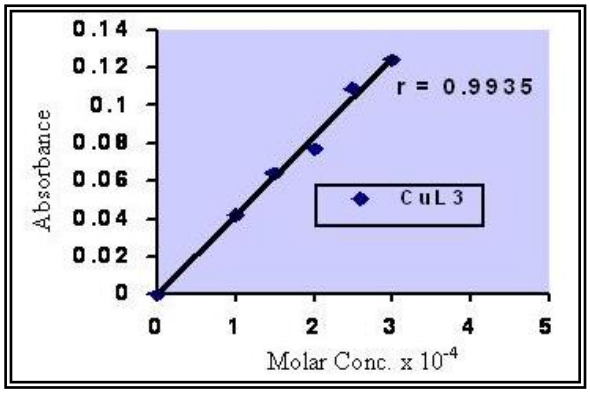
r = 0.9935
CuL3
Absorbance
Molar Conc. x 10-4

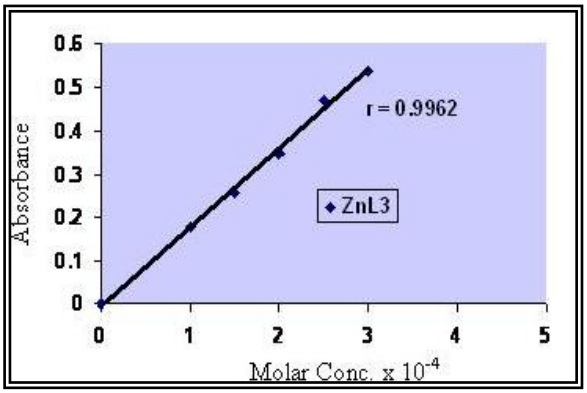
r = 0.9962
ZnL3
Absorbance
Molar Conc. x 10-4

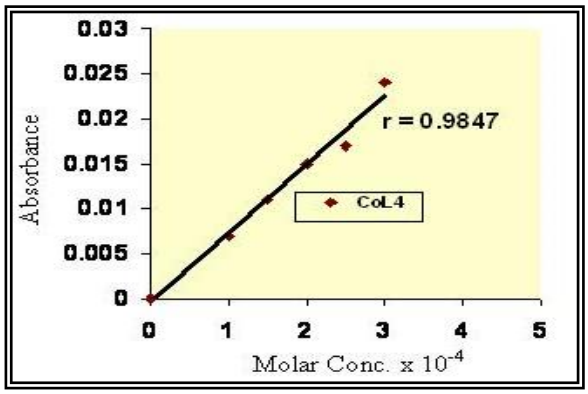
r = 0.9847
CoL4
Absorbance
Molar Conc. x 10-4

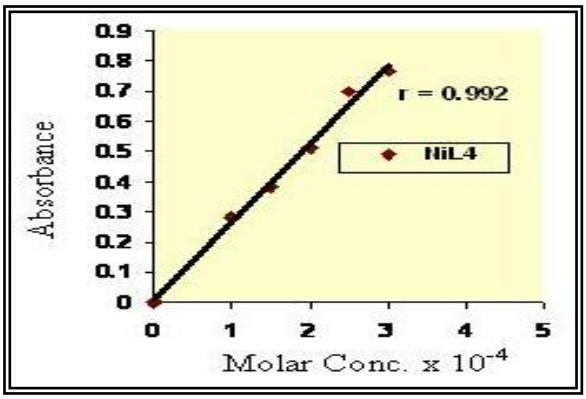
r = 0.992
NiL4
Absorbance
Molar Conc. x 10-4

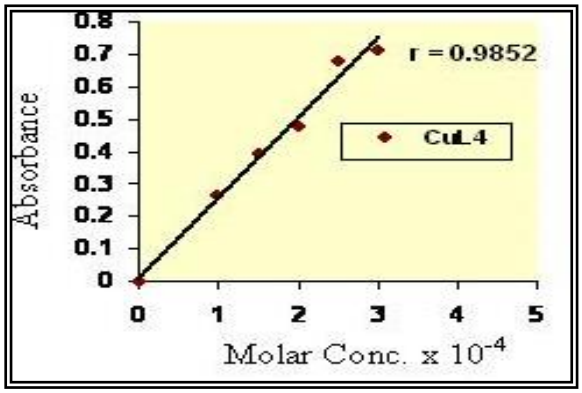
r = 0.9852
CuL4
Absorbance
Molar Conc. x 10-4

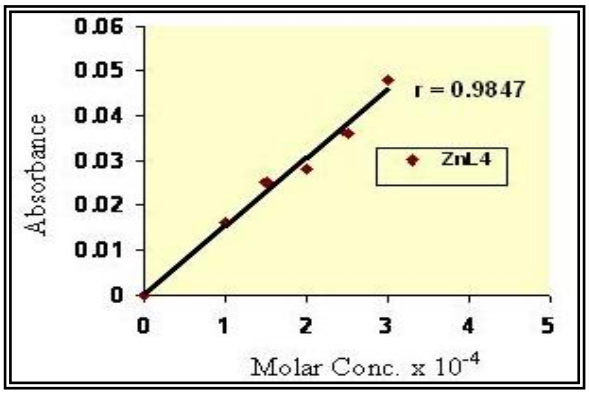
r = 0.9847
ZnL4
Absorbance
Molar Conc. x 10-4

Table (3-5): Absorbance at different pH and perfect concentration of mixed solutions of metal ions with azo ligands.

Ligands							
Metal Ion	**λ(max) (nm)**	**Molar Conc.×10^{-4}**	**Absorbance at pH**				
			5	**6**	**7**	**8**	**9**
Co(II)/L_1	460	2.5	0.048	0.071	0.093	0.075	0.053
Ni(II)/L_1	458	2.5	0.044	0.057	0.098	0.063	0.048
Cu(II)/L_1	481	2.5	0.058	0.073	0.090	0.082	0.061
Zn(II)/L_1	450	2.5	0.037	0.065	0.091	0.061	0.045
Co(II)/L_2	442	2.0	0.048	0.050	0.063	0.080	0.115
Ni(II)/L_2	440	2.5	0.125	0.137	0.162	0.173	0.185
Cu(II)/L_2	560	3.0	0.353	0.421	0.436	0.441	0.486
Zn(II)/L_2	476	2.5	0.020	0.028	0.041	0.066	0.085
Co(II)/L_3	458	2.5	0.117	0.226	0.288	0.326	0.381
Ni(II)/L_3	466	2.5	0.117	0.136	0.147	0.152	0.175
Cu(II)/L_3	470	2.5	0.109	0.253	0.396	0.708	0.815
Zn(II)/L_3	472	2.5	0.317	0.386	0.425	0.471	0.517
Co(II)/L_4	480	2.5	0.003	0.006	0.011	0.012	0.017
Ni(II)/L_4	478	2.5	0.323	0.377	0.484	0.572	0.700
Cu(II)/L_4	476	2.5	0.323	0.351	0.461	0.475	0.680
Zn(II)/L_4	478	2.5	0.011	0.016	0.027	0.030	0.036

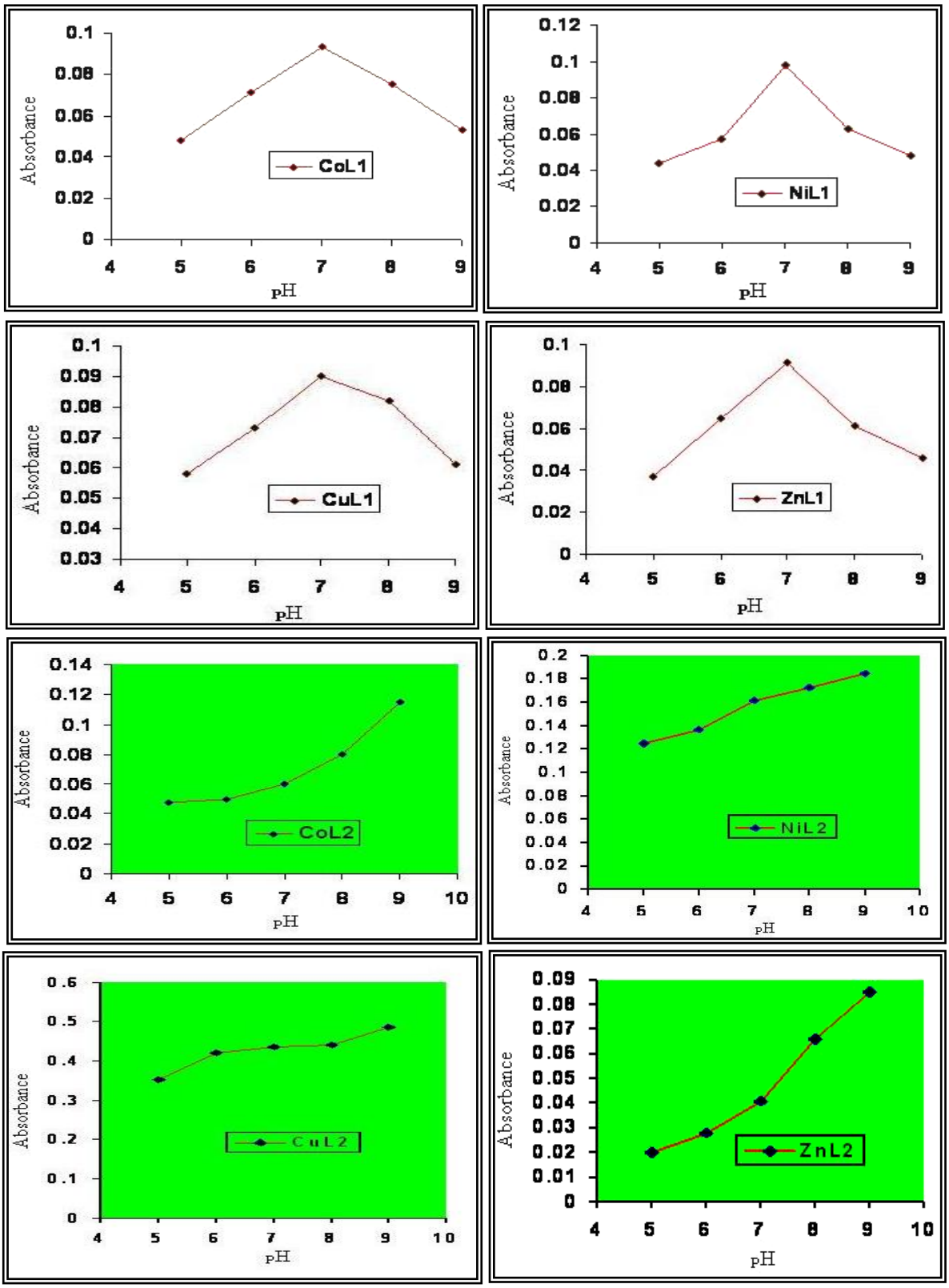

Figure (3-32): Effect of pH on absorbance at (λ_{max}) of mixed solutions of metal ions with azo ligands at perfect concentrations.

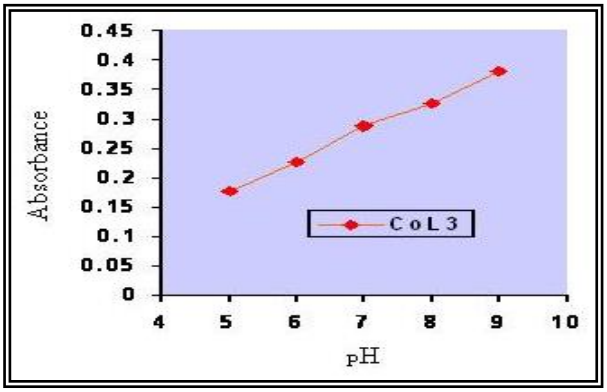
Absorbance
pH
CoL3

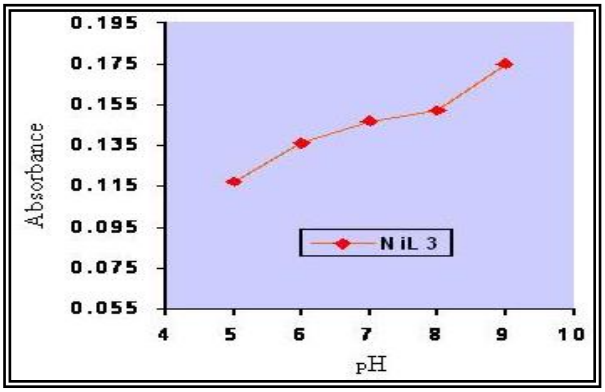
Absorbance
pH
NiL3

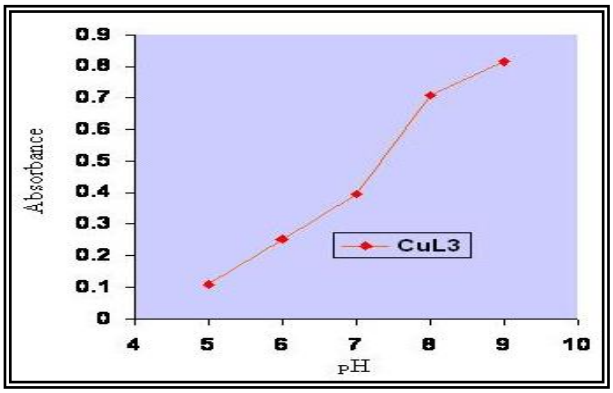
Absorbance
pH
CuL3

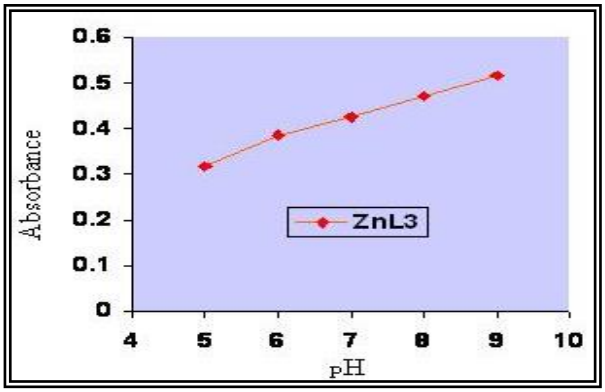
Absorbance
pH
ZnL3

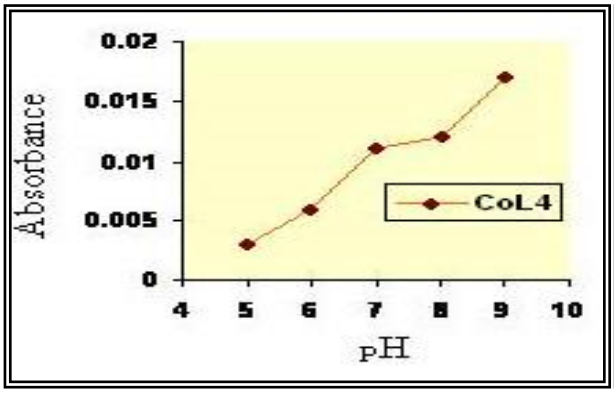
Absorbance
pH
CoL4

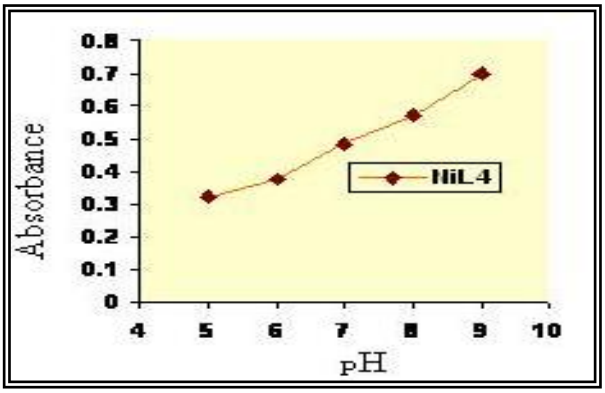
Absorbance
pH
NiL4

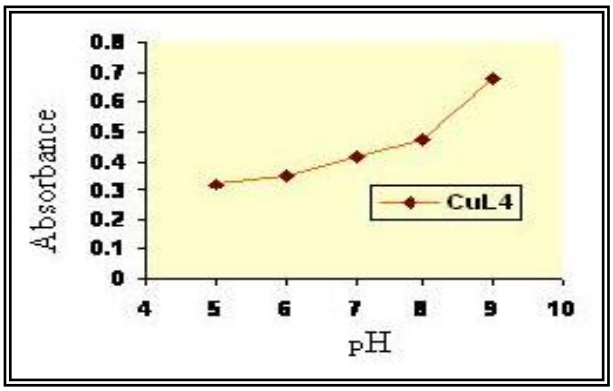
Absorbance
pH
CuL4

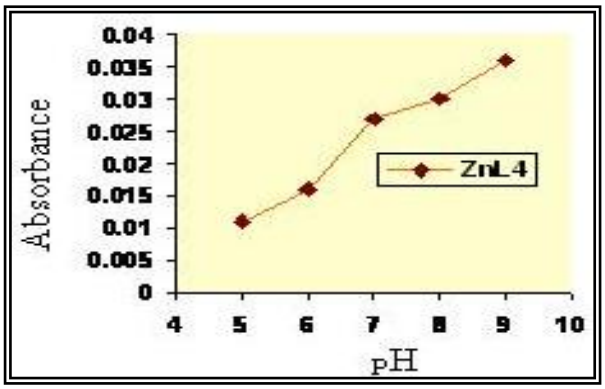
Absorbance
pH
ZnL4

3.8.2. Complexes nature

The nature of the complexes formed in solution without isolation are characterized by mole ratio method. This way dependent on plotting measured absorbance against molar ratios of two components of a complex when the concentration of one component is varied as the concentration of the other is constant, this way has been introduced by Yoe and Jones[134]. Measurements have been used at perfect pH, concentration and wavelength. The results describes the formation of (1:2) (Metal to Ligand) ratio for all ready complexes, Figure (3-33) display the relationship between absorbance and (Metal: Ligand) ratio, as well as the data are given in Table 3-6.

Other way used is job method, which modified by Vosbury and Copper[135]. This method depending measured absorbance when the concentration of two compound have been varied, the results are shown in Figure (3-34), and the data recorded in Table (3-7).

Table (3-6): UV-Vis spectral data at (λ_{max}) for mole ratio method at perfect pH and concentration of mixed solutions of metal ions with azo ligands.

			Ligands			
Metal Ion	**Co(II)/L_1**	**Ni(II)/L_1**	**Cu(II)/L_1**	**Zn(II)/L_1**	**Co(II)/L_2**	**Ni(II)/L_2**
Molar Conc.×10^{-4}	**2.5**	**2.5**	**2.5**	**2.5**	**2.0**	**2.5**
pH/λ_{max}	**7.0/460**	**7.0/458**	**7.0/481**	**7.0/450**	**9.0/442**	**9.0/440**
M:L	**Absorbance at (λ_{max})**					
1:0.25	0.012	0.011	0.021	0.021	0.021	0.013
1:0.50	0.034	0.025	0.037	0.035	0.038	0.066
1:0.75	0.044	0.036	0.046	0.047	0.047	0.087
1:1.00	0.052	0.047	0.073	0.066	0.063	0.144
1:1.25	0.061	0.059	0.085	0.078	0.085	0.710
1:1.50	0.074	0.072	0.098	0.096	0.095	0.188
1:1.75	0.089	0.088	0.110	0.108	0.095	0.203
1:2.00	0.113	0.108	0.122	0.117	0.122	0.218
1:2.25	0.113	0.108	0.122	0.177	0.122	0.218
1:2.50	0.113	0.103	0.114	0.119	0.124	0.235
1:2.75	0.108	0.102	0.116	0.118	0.127	0.222
1:3.00	0.108	0.107	0.124	0.115	0.122	0.212
1:3.25	0.110	0.108	0.123	0.116	0.124	0.221
1:3.50	0.116	0.103	0.122	0.117	0.124	0.218
1:3.75	0.110	0.108	0.115	0.114	0.127	0.223
1:4.00	0.113	0.108	0.112	0.117	0.122	0.218
Metal Ion	**Cu(II)/L_2**	**Zn(II)/L_2**	**Co(II)/L_3**	**Ni(II)/L_3**	**Cu(II)/L_3**	**Zn(II)/L_3**
Molar Conc.×10^{-4}	**3.0**	**2.5**	**2.5**	**2.5**	**2.5**	**2.5**
pH/λ_{max}	**9.0/560**	**9.0/472**	**9.0/458**	**9.0/466**	**9.0/470**	**9.0/472**
M:L	**Absorbance at (λ_{max})**					
1: 0.25	0.077	0.031	0.123	0.127	0.026	0.031
1:0.50	0.179	0.046	0.146	0.183	0.049	0.053
1:0.75	0.265	0.062	0.177	0.227	0.073	0.086
1:1.00	0.325	0.071	0.216	0.263	0.095	0.115

1:1.25	0.431	0.078	0.249	0.324	0.115	0.137
1:1.50	0.437	0.091	0.267	0.377	0.127	0.163
1:1.75	0.494	0.111	0.304	0.416	0.144	0.188
1:2.00	0.523	0.131	0.337	0.460	0.162	0.211
1:2.25	0.523	0.131	0.337	0.460	0.161	0.203
1:2.50	0.488	0.128	0.302	0.463	0.164	0.202
1:2.75	0.488	0.128	0.370	0.422	0.161	0.212
1:3.00	0.523	0.131	0.340	0.460	0.162	0.211
1:3.25	0.486	0.133	0.332	0.447	0.161	0.211
1:3.50	0.523	0.131	0.334	0.446	0.163	0.211
1:3.75	0.523	0.129	0.337	0.460	0.162	0.207
1:4.00	0.523	0.130	0.337	0.460	0.161	0.211
Metal Ion	**Co(II)/L_4**	**Ni(II)/L_4**	**Cu(II)/L_4**	**Zn(II)/L_4**		
Molar Conc.×10^{-4}	**2.5**	**2.5**	**2.5**	**2.5**		
pH/λ_{max}	**9.0/480**	**9.0/478**	**9.0/476**	**9.0/478**		
M:L	**Absorbance at (λ_{max})**					
1:0.25	0.388	0.763	1.264	0.883		
1:0.50	0.466	0.816	1.336	0.977		
1:0.75	0.527	0.875	1.421	1.036		
1:1.00	0.569	0.931	1.466	1.135		
1:1.25	0.627	0.973	1.527	1.266		
1:1.500	0.705	1.080	1.582	1.317		
1:1.75	0.755	1.180	1.677	1.386		
1:2.00	0.807	1.274	1.762	1.535		
1:2.25	0.806	1.279	1.762	1.532		
1:2.50	0.810	1.277	1.770	1.547		
1:2.75	0.798	1.278	1.718	1.532		
1:3.00	0.807	1.300	1.779	1.559		
1:3.25	0.787	1.291	1.776	1.568		
1:3.50	0.774	1.299	1.721	1.533		
1:3.75	0.807	1.274	1.788	1.532		
1:4.00	0.807	1.274	1.742	1.532		

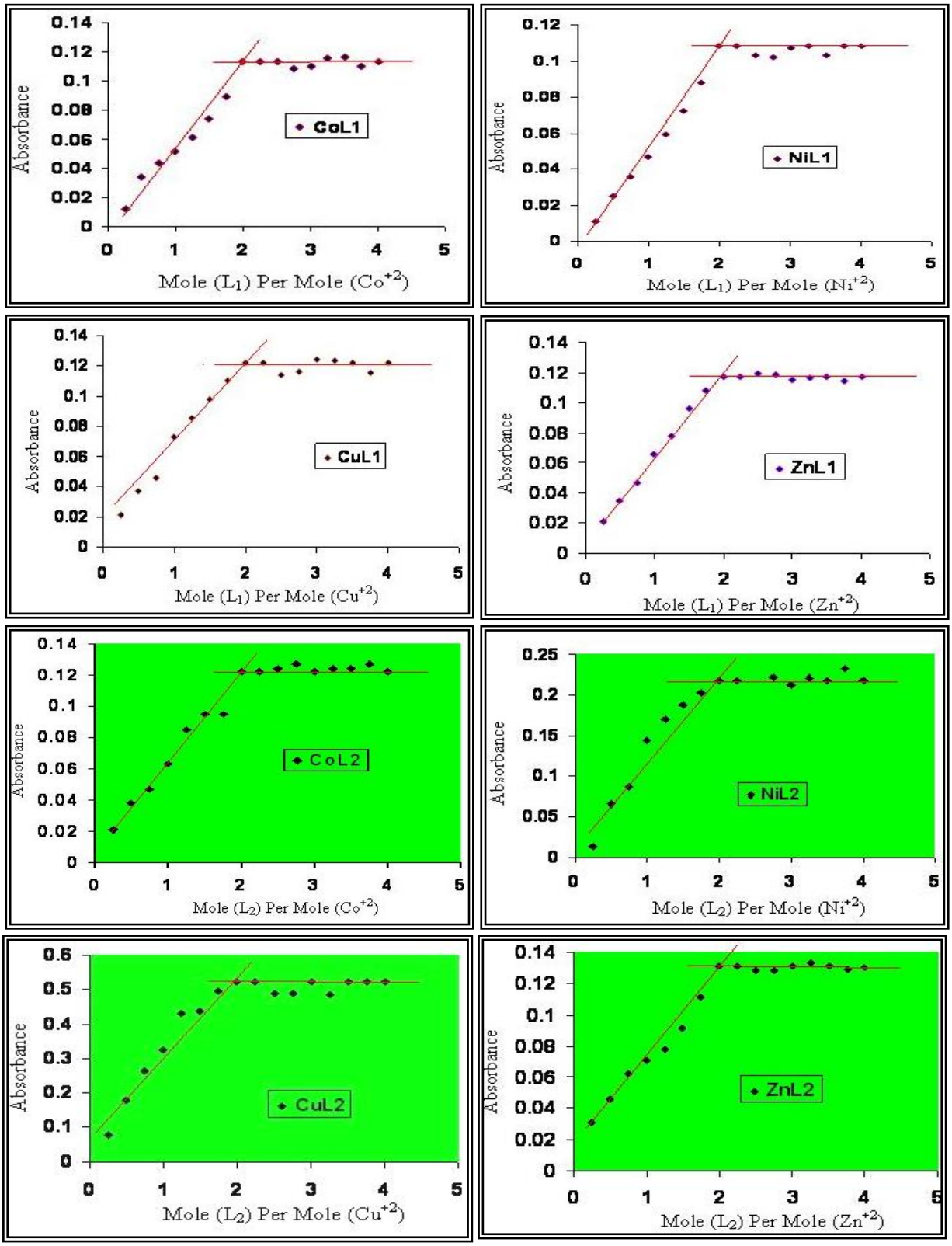

Figure (3-33): Mole ratio plot for (M:L) ratio at perfect pH and concentration of mixed solutions of metal ions with azo ligands.

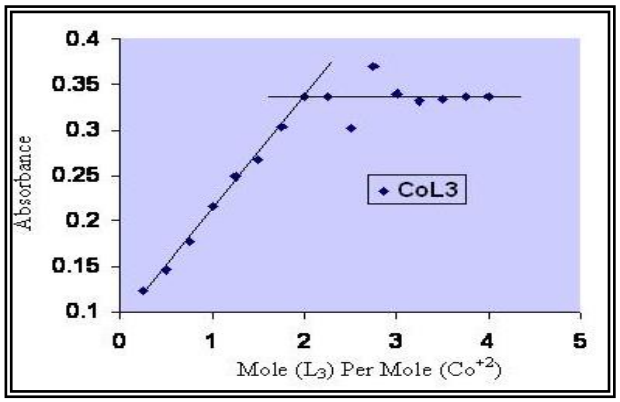
Absorbance
CoL3
Mole (L3) Per Mole (Co+2)

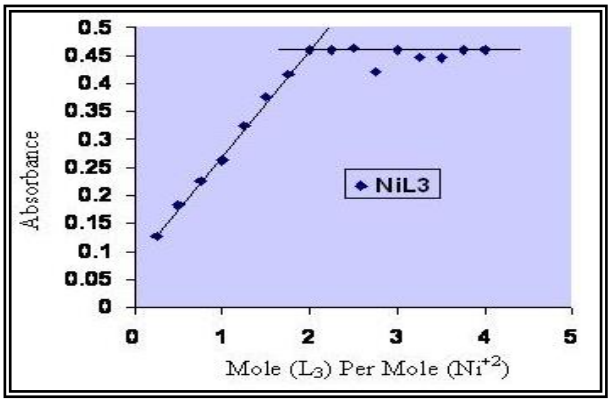
Absorbance
NiL3
Mole (L3) Per Mole (Ni+2)

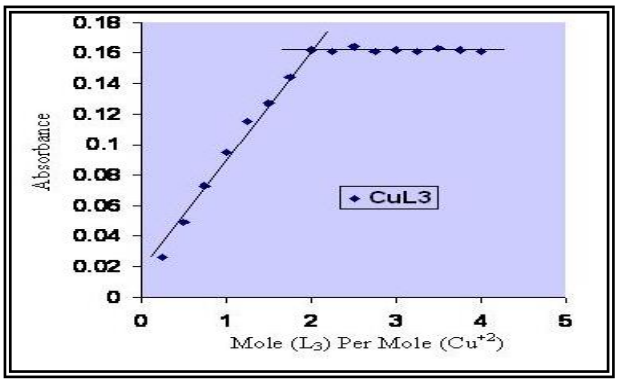
Absorbance
CuL3
Mole (L3) Per Mole (Cu+2)

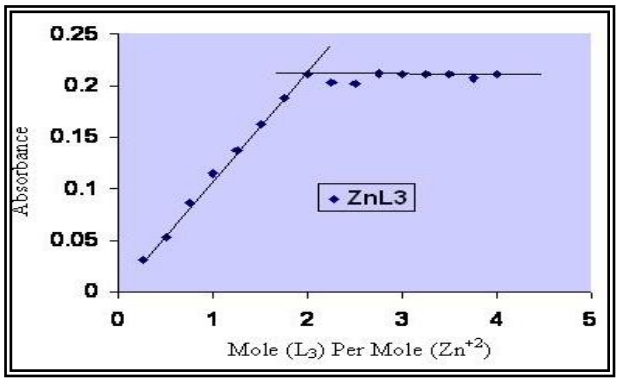
Absorbance
ZnL3
Mole (L3) Per Mole (Zn+2)

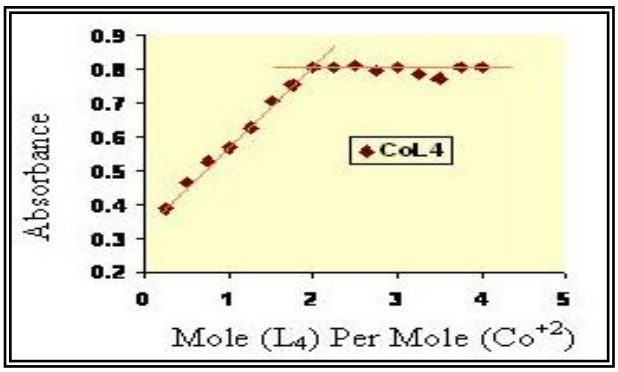
Absorbance
CoL4
Mole (L4) Per Mole (Co+2)

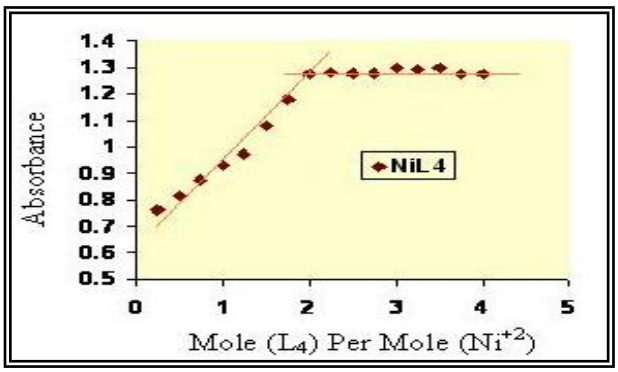
Absorbance
NiL4
Mole (L4) Per Mole (Ni+2)

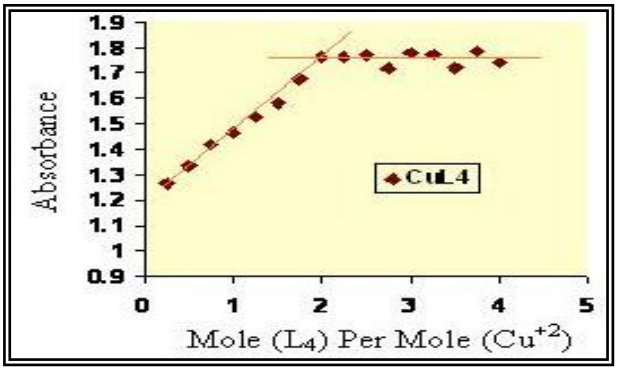
Absorbance
CuL4
Mole (L4) Per Mole (Cu+2)

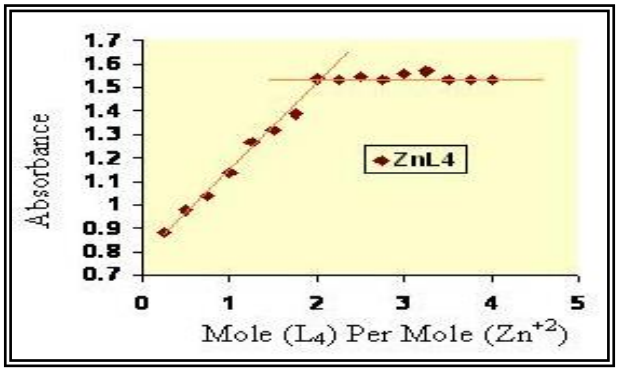
Absorbance
ZnL4
Mole (L4) Per Mole (Zn+2)

Table (3-7): UV-Vis spectra data at (λ_{max}) for job method at perfect pH and L_1concentration of mixed solutions of metal ions with azo ligands.

L_1				
Zn(II)	**Cu(II)**	**Ni(II)**	**Co(II)**	$\frac{V_m}{V_m + V_L}$
Absorbance at (λ_{max})				
0.033	0.037	0.035	0.037	0.1
0.075	0.074	0.062	0.074	0.2
0.117	0.121	0.108	0.113	0.3
0.117	0.120	0.107	0.113	0.4
0.096	0.105	0.088	0.097	0.5
0.077	0.085	0.063	0.075	0.6
0.057	0.063	0.042	0.054	0.7
0.037	0.042	0.026	0.036	0.8
0.017	0.022	0.015	0.016	0.9
L_2				
0.037	0.255	0.106	0.042	**0.1**
0.103	0.358	0.152	0.074	**0.2**
0.130	0.522	0.218	0.121	**0.3**
0.129	0.518	0.217	0.120	**0.4**
0.117	0.428	0.166	0.097	**0.5**
0.077	0.351	0.116	0.092	**0.6**
0.057	0.228	0.083	0.055	**0.7**
0.048	0.144	0.041	0.037	**0.8**
0.024	0.099	0.031	0.021	**0.9**
L_3				
0.146	0.104	0.317	0.227	**0.2**
0.211	0.160	0.461	0.337	**0.3**

0.208	0.160	0.460	0.335	**0.4**
0.173	0.133	0.377	0.274	**0.5**
0.138	0.103	0.315	0.225	**0.6**
0.109	0.073	0.218	0.166	**0.7**
0.066	0.046	0.155	0.144	**0.8**
0.036	0.022	0.077	0.057	**0.9**
L_4				
0.486	0.664	0.437	0.236	**0.1**
0.975	1.227	0.885	0.526	**0.2**
1.530	1.753	1.273	0.806	**0.3**
1.500	1.751	1.270	0.807	**0.4**
1.255	1.477	1.063	0.662	**0.5**
0.985	1.177	0.857	0.527	**0.6**
0.753	0.875	0.662	0.395	**0.7**
0.538	0.583	0.426	0.264	**0.8**
0.246	0.277	0.218	0.125	**0.9**

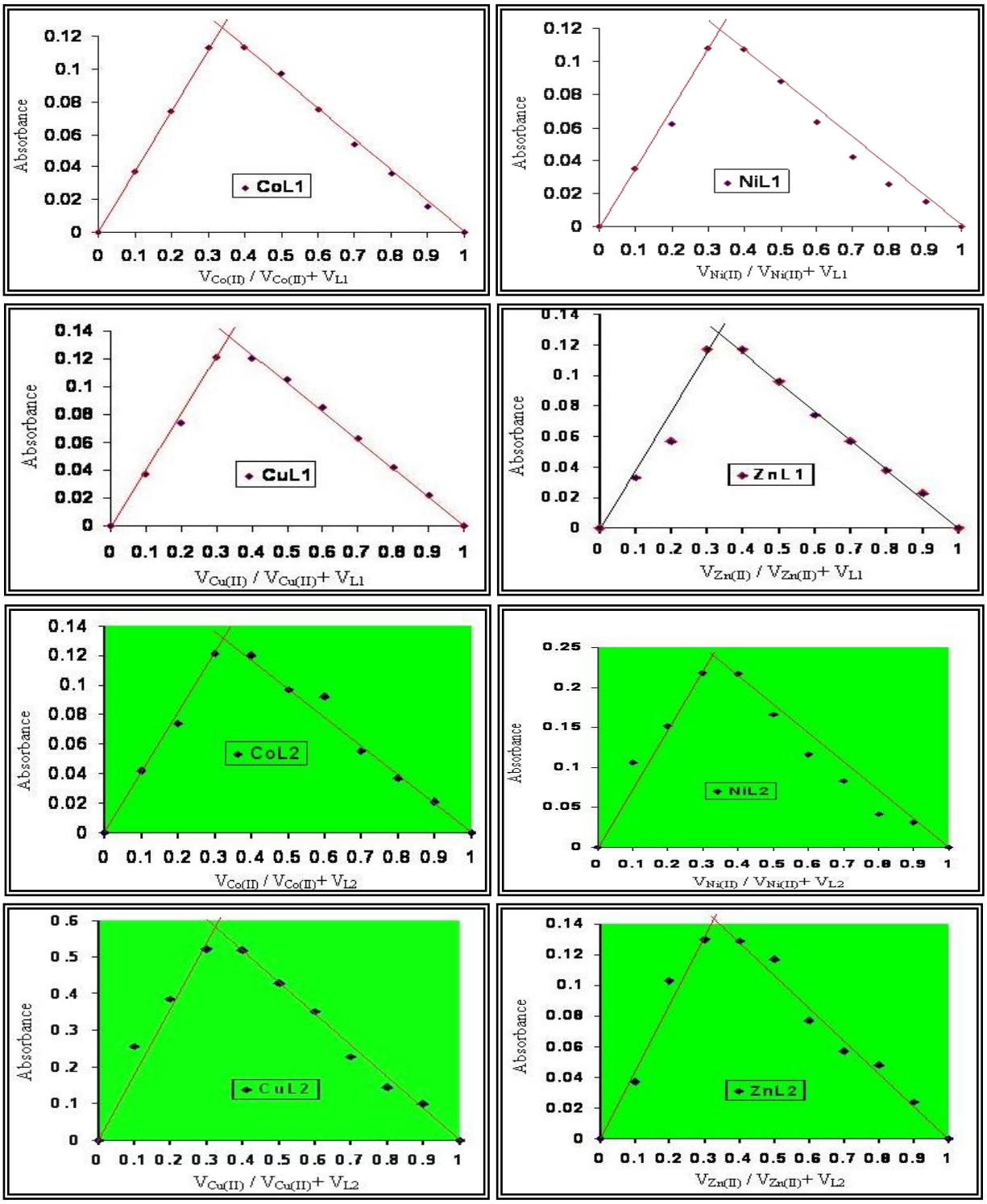

Figure (3-34): Job method plot for (M:L) ratio at perfect pH and concentration of mixed solutions of metal ions with azo ligands.

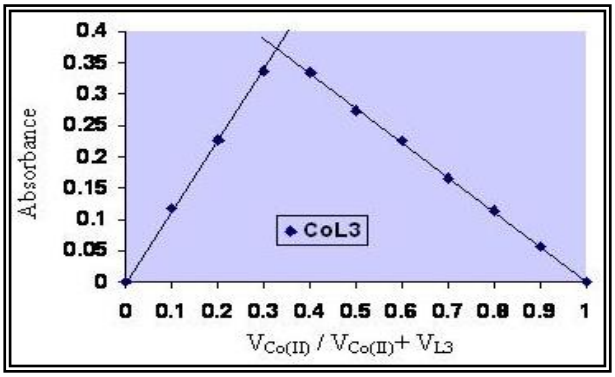
Absorbance
CoL3
$V_{Co(II)} / V_{Co(II)} + V_{L3}$

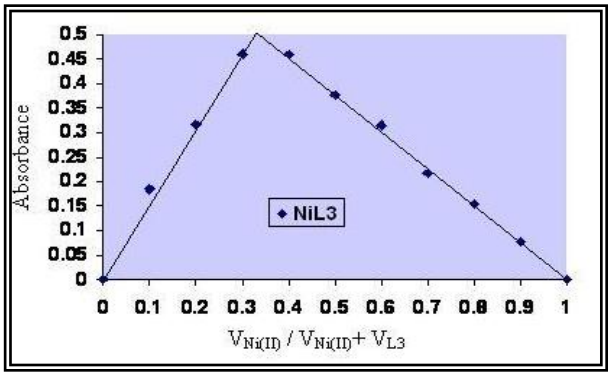
Absorbance
NiL3
$V_{Ni(II)} / V_{Ni(II)} + V_{L3}$

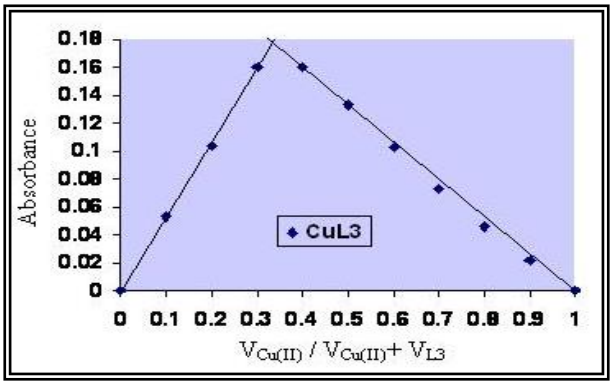
Absorbance
CuL3
$V_{Cu(II)} / V_{Cu(II)} + V_{L3}$

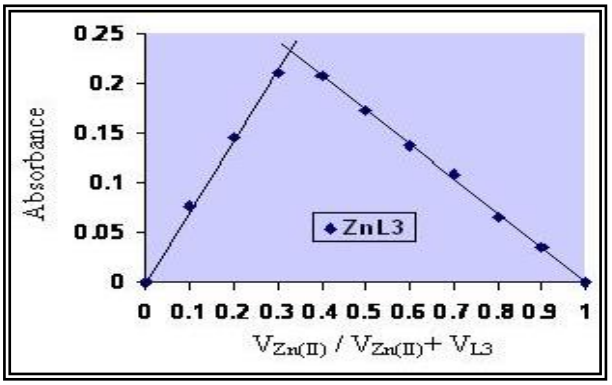
Absorbance
ZnL3
$V_{Zn(II)} / V_{Zn(II)} + V_{L3}$

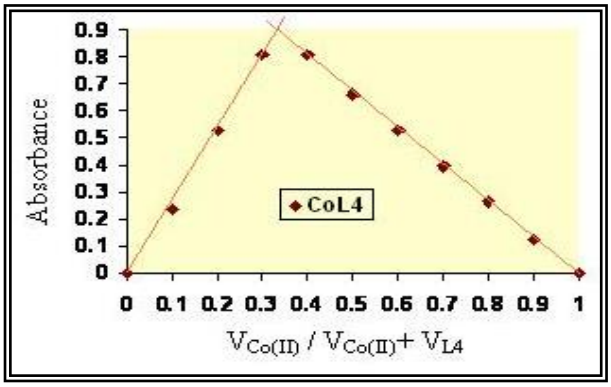
Absorbance
CoL4
$V_{Co(II)} / V_{Co(II)} + V_{L4}$

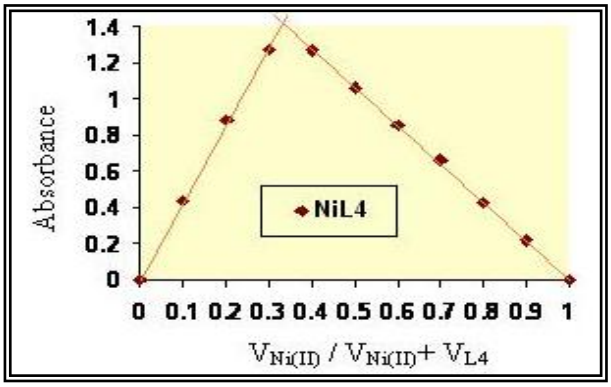
Absorbance
NiL4
$V_{Ni(II)} / V_{Ni(II)} + V_{L4}$

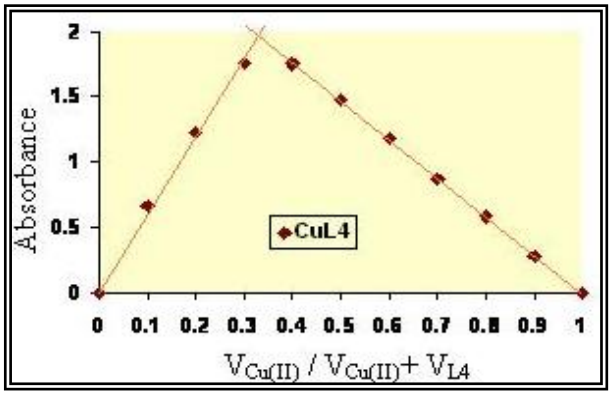
Absorbance
CuL4
$V_{Cu(II)} / V_{Cu(II)} + V_{L4}$

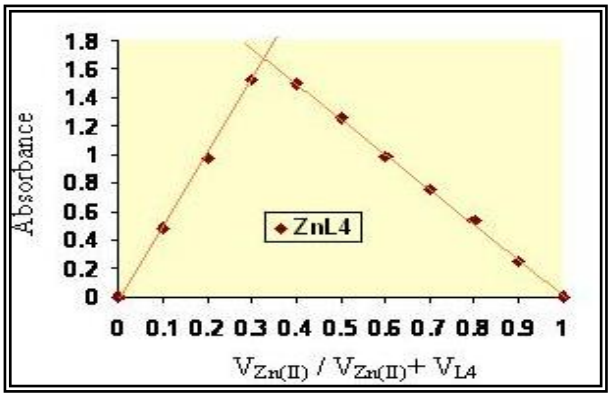
Absorbance
ZnL4
$V_{Zn(II)} / V_{Zn(II)} + V_{L4}$

3.8.3. Effect of time on absorbance

The effect of time have been studied for color complex solution under perfect condition (pH, concentration and wavelength), the reaction was complete in (5 min) at 25°C and continues stable for about (90 min), this shows that the ligands strong coordination with metal salts. The results are shown in Figure (3-35), and Table 3-8.

Table (3-8): Absorbance for mixed solutions of metal ions with azo ligands at the change of time.

L_1				
Zn(II)	**Cu(II)**	**Ni(II)**	**Co(II)**	**Time (min)**
Absorbance at (λ_{max})				
0.088	0.091	0.089	0.080	**0.0**
0.088	0.092	0.089	0.080	**5.0**
0.087	0.091	0.089	0.0780	**10**
0.088	0.091	0.089	0.079	**15**
0.087	0.091	0.089	0.079	**20**
0.087	0.091	0.090	0.078	**25**
0.089	0.092	0.090	0.080	**30**
0.088	0.092	0.089	0.080	**35**
0.088	0.091	0.089	0.080	**40**
0.088	0.090	0.090	0.080	**45**
0.088	0.088	0.089	0.080	**50**
0.087	0.091	0.089	0.078	**55**
0.088	0.091	0.089	0.077	**60**
0.089	0.090	0.089	0.076	**65**
0.088	0.089	0.089	0.080	**70**
0.088	0.093	0.090	0.080	**75**
0.088	0.091	0.090	0.080	**80**
L_2				

0.059	0.611	0.187	0.080	**0.0**
0.060	0.614	0.187	0.079	**5.0**
0.059	0.611	0.182	0.080	**10**
0.059	0.617	0.190	0.080	**15**
0.059	0.617	0.191	0.080	**20**
0.059	0.617	0.192	0.079	**25**
0.059	0.618	0.187	0.079	**30**
0.059	0.617	0.187	0.079	**35**
0.059	0.619	0.188	0.080	**40**
0.059	0.618	0.186	0.079	**45**
0.059	0.619	0.187	0.080	**50**
0.059	0.617	0.187	0.080	**55**
0.059	0.616	0.190	0.080	**60**
0.059	0.616	0.193	0.080	**65**
0.059	0.615	0.187	0.080	**70**
0.059	0.617	0.188	0.080	**75**
0.059	0.610	0.190	0.080	**80**
0.059	0.610	0.187	0.080	**85**
0.059	0.610	0.187	0.080	**90**
L_3				
0.914	0.386	0.232	0.687	**0.0**
0.914	0.388	0.232	0.688	**5.0**
0.913	0.386	0.231	0.688	**10**
0.914	0.383	0.232	0.684	**15**
0.913	0.384	0.221	0.685	**20**
0.899	0.385	0.223	0.679	**25**
0.906	0.378	0.232	0.697	**30**
0.914	0.382	0.232	0.688	**35**
0.919	0.377	0.230	0.699	**40**
0.914	0.379	0.231	0.694	**45**
0.914	0.382	0.232	0.688	**50**

0.914	0.386	0.232	0.683	**55**
0.915	0.385	0.232	0.677	**60**
0.920	0.369	0.232	0.674	**65**
0.919	0.377	0.232	0.670	**70**
0.917	0.367	0.232	0.666	**75**
0.914	0.386	0.232	0.663	**80**
0.915	0.386	0.231	0.658	**85**
0.914	0.386	0.232	0.662	**90**
L_4				
1.015	2.225	1.553	0.708	**0.0**
1.015	2.208	1.553	0.688	**5.0**
1.054	2.224	1.583	0.711	**10**
1.040	2.224	1.552	0.703	**15**
1.040	2.250	1.552	0.711	**20**
1.017	2.223	1.550	0.705	**25**
1.023	2.176	1.580	0.702	**30**
1.033	2.185	1.580	0.705	**35**
1.004	2.150	1.585	0.725	**40**
1.042	2.195	1.588	0.725	**45**
1.048	2.165	1.611	0.708	**50**
1.050	2.223	1.585	0.718	**55**
1.019	2.253	1.571	0.713	**60**
1.015	2.230	1.525	0.717	**65**
1.011	2.226	1.607	0.709	**70**
1.021	2.226	1.525	0.636	**75**
1.021	2.226	1.613	0.682	**80**
1.028	2.208	1.532	0.685	**85**
1.018	2.226	1.535	0.676	**90**

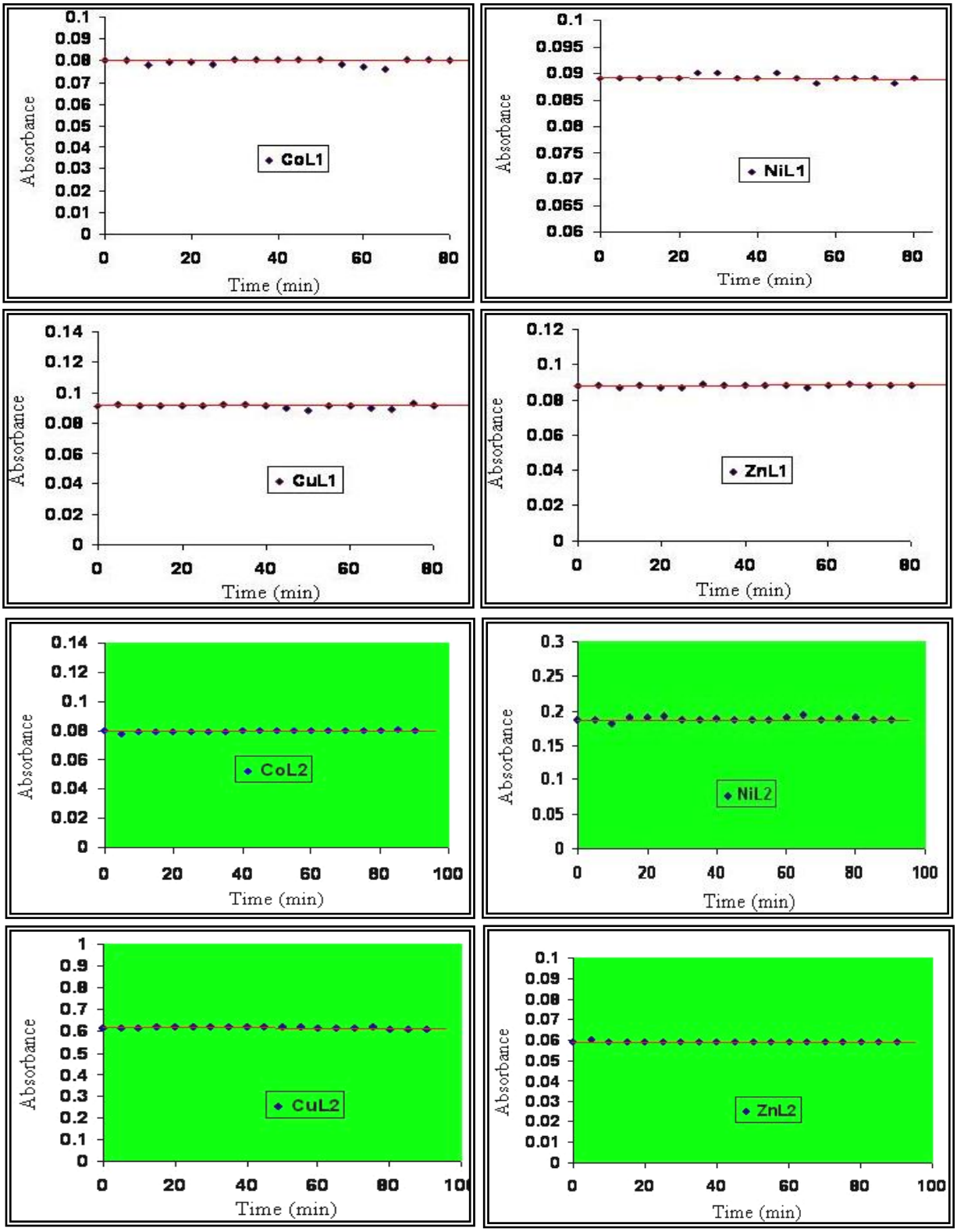

Figure (3-35): Time effect for mixed solutions of metal ions with azo ligands (L_1-L_4).

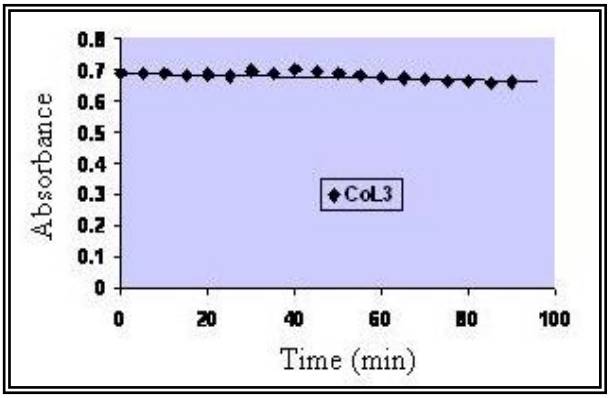
Absorbance
Time (min)
CoL3

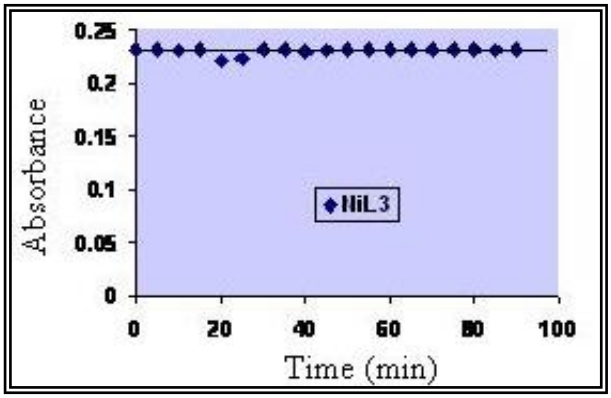
Absorbance
Time (min)
NiL3

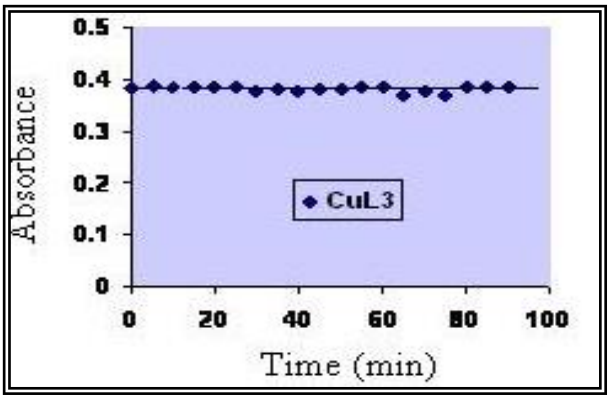
Absorbance
Time (min)
CuL3

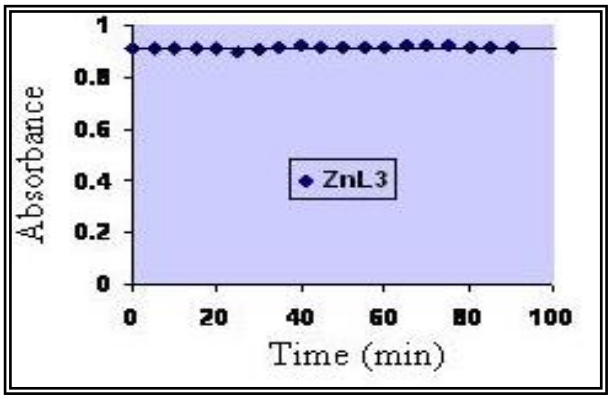
Absorbance
Time (min)
ZnL3

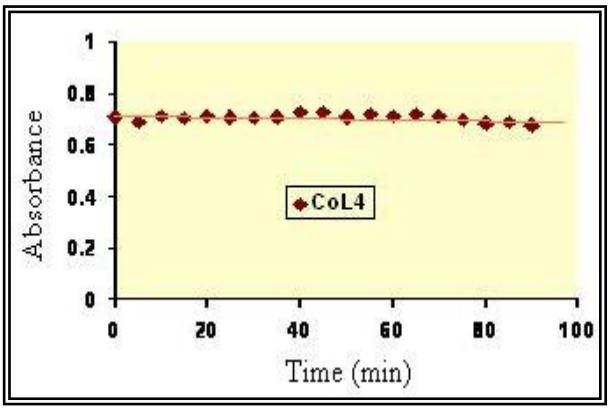
Absorbance
Time (min)
CoL4

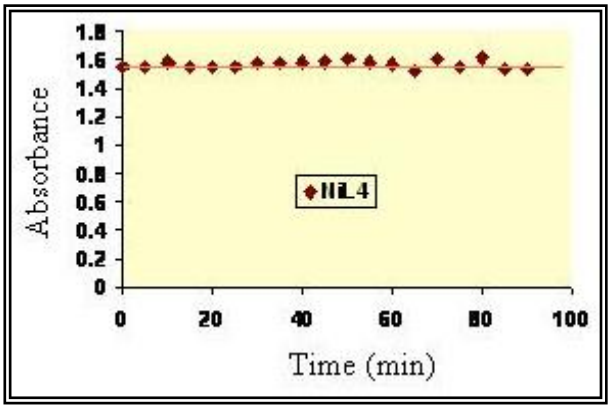
Absorbance
Time (min)
NiL4

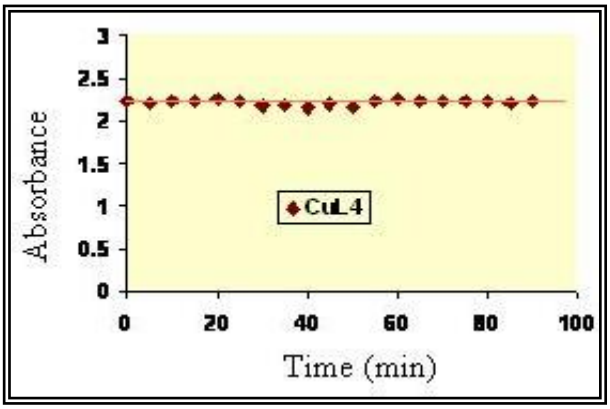
Absorbance
Time (min)
CuL4

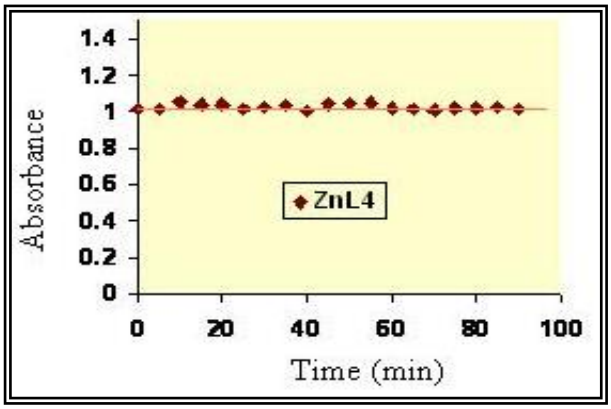
Absorbance
Time (min)
ZnL4

3.8.4. Stability constant

The sequent stability constant (K) to the (1:2) metal to ligand compound can be computed according to the equations.

$$K = \frac{1-\alpha}{4\alpha^3 C^2} \quad ; \qquad \alpha = \frac{A_m - A_s}{A_m}$$

Where *c*= concentration to the compound solution at mole/ L α= degree for dissociation, As= Absorption in solution containing same amount of ligand and metal ion and Am= the absorption of solution containing the selfsame quantities for metal and surplus for ligand. High values for (K) refers to high constancy for produced complexes[136]. Thermodynamic parameters of Gibbs free energy (ΔG°) were also studied. The ΔG° data have been reckoned from the equation[137].

$$\Delta G° = - R\ T\ Ln\ k$$

Where; R= gas constant= 8.3 $J.mol^{-1}.K^{-1}$, T= absolute temperature (Kelvin), the negative value of (ΔG°) due to the reaction between azo dyes ligands and metal ions understudy are spontaneous. All results were listed in Table (3-9).

Table (3-9): Stability constant and Gibbs free energy of the prepared complexes with azo dyes ligands (L_1-L_4).

Complexes	A_s	A_m	α	k	Ln k	ΔG° kJ.mol^{-1}
$[Co(L_1)_2]$	0.052	0.113	0.539	12.13×10^6	16.311	-40.411
$[Ni(L_1)_2]$	0.047	0.108	0.564	9.90×10^6	16.108	-39.908
$[Cu(L_1)_2]$	0.073	0.122	0.401	39.93×10^6	17.502	-43.362
$[Zn(L_1)_2]$	0.066	0.117	0.435	28.25×10^6	17.156	-42.505
$Co(L)_2].H_2O$	0.063	0.122	0.483	28.72×10^6	17.173	-42.547
$[Ni(L)_2].H_2O$	0.144	0.218	0.339	73.44×10^6	18.111	-44.871
$[Cu(L)_2].H_2O$	0.325	0.523	0.378	32.73×10^6	17.303	-42.869
$[Zn(L)_2].H_2O$	0.071	0.131	0.458	22.58×10^6	16.932	-41.950
$[Co(L_3)_2]$	0.216	0.337	0.359	58.27×10^6	17.880	-44.298
$[Ni(L_3)_2]$	0.263	0.460	0.428	30.10×10^6	17.220	-42.663
$[Cu(L_3)_2]$	0.095	0.162	0.413	34.53×10^6	17.357	-43.003
$[Zn(L_3)_2]$	0.115	0.211	0.454	23.74×10^6	16.982	-42.074
$[Co(L_4)_2]$	0.569	0.807	0.295	117.50×10^6	18.581	-46.035
$[Ni(L_4)_2]$	0.931	1.274	0.269	182.75×10^6	19.023	-47.130
$[Cu(L_4)_2]$	1.466	1.762	0.168	832.00×10^6	20.539	-50.886
$[Zn(L_4)_2]$	1.135	1.535	0.260	18.50×10^6	16.733	-41.457

3.9. Characterization of solid complexes techniques

Metal chelates have been identified by reaction of ethyl alcohol for azo dyes ligands with metal ions dissolved at perfect pH in a (1:2) (metal: ligand) molar ratio, other than metal content and (C.H.N.S.O) analysis are listed in Table (3-10).

Table (3-10): Metal content and (C.H.N.S.O) analysis data for prepared compounds.

Compounds	Analysis Calc (Found)					
	M%	C%	H%	N%	O%	S%
$[Co(L_1)_2]$	8.09 (7.94)	62.55 (61.85)	5.21 (4.97)	15.36 (14.88)	8.77 (7.83)	-
$[Ni(L_1)_2]$	7.96 (7.12)	62.63 (61.98)	5.21 (4.84)	15.38 (14.79)	8.79 (8.04)	-
$[Cu(L_1)_2]$	8.71 (7.92)	62.12 (61.83)	5.17 (4.96)	15.25 (14.92)	8.71 (8.11)	-
$[Zn(L_1)_2]$	8.84 (8.06)	62.04 (61.68)	5.17 (4.92)	15.23 (14.78)	8.70 (7.98)	-
$[Co(L_2)_2].H_2O$	7.63 (7.11)	58.99 (57.93)	4.65 (4.03)	18.11 (17.85)	8.28 (7.84)	-
$[Ni(L_2)_2].H_2O$	7.51 (6.83)	59.06 (59.01)	4.66 (4.11)	18.13 (17.76)	8.29 (8.06)	-
$[Cu(L_2)_2].H_2O$	8.22 (7.79)	58.61 (58.04)	4.62 (3.96)	17.99 (16.92)	8.22 (7.76)	-
$[Zn(L_2)_2].H_2O$	8.34 (7.81)	58.53 (57.91)	4.62 (3.92)	17.77 (16.88)	8.21 (7.98)	-
$[Co(L_3)_2]$	9.09 (8.91)	55.46 (55.12)	3.38 (2.97)	17.25 (16.77)	4.93 (3.89)	9.86 (8.94)
$[Ni(L_3)_2]$	8.95 (7.88)	55.55 (54.91)	3.39 (2.87)	17.28 (16.92)	4.93 (4.36)	9.87 (8.86)
$[Cu(L_3)_2]$	9.78 (8.92)	55.04 (54.11)	3.36 (3.05)	17.12 (16.85)	4.89 (4.62)	9.78 (8.94)
$[Zn(L_3)_2]$	9.92 (8.86)	54.96 (54.11)	3.35 (2.92)	17.09 (16.78)	4.88 (4.22)	9.77 (8.85)

[Co(L_4)$_2$]	9.00 (8.85)	47.63 (46.86)	2.44 (1.97)	21.37 (20.79)	9.77 (8.88)	9.77 (8.92)
[Ni(L_4)$_2$]	8.86 (8.33)	47.70 (46.93)	2.44 (1.87)	21.40 (20.87)	9.78 (8.63)	9.78 (8.81)
[Cu(L_4)$_2$]	9.69 (8.92)	47.27 (46.77)	2.42 (2.05)	21.21 (20.85)	9.69 (8.83)	9.69 (8.96)
[Zn(L_4)$_2$]	9.83 (8.81)	47.20 (46.46)	2.42 (1.88)	21.18 (20.75)	9.68 (8.43)	9.68 (8.83)
[Co(L_1)(L_2)]	7.95 (6.76)	61.45 (60.88)	4.98 (3.95)	16.98 (15.76)	8.62 (7.82)	-
[Ni(L_1)(L_2)]	7.82 (6.82)	61.53 (60.13)	4.99 (3.04)	17.00 (16.39)	8.63 (7.07)	-
[Ni(L_1)(L_2)]	7.82 (6.82)	61.53 (60.13)	4.99 (3.04)	17.00 (16.39)	8.63 (7.07)	-
[Co(L_3)(L_4)]	9.04 (8.75)	51.53 (50.66)	2.91 (1.87)	19.32 (18.82)	7.36 (6.73)	9.81 (8.90)
[Ni(L_3)(L_4)]	8.90 (7.78)	51.61 (50.89)	2.91 (2.04)	19.35 (18.96)	7.37 (6.54)	9.83 (8.85)
[Cu(L_3)(L_4)]	9.74 (8.91)	51.14 (50.51)	2.89 (2.67)	19.17 (18.88)	7.30 (6.60)	9.74 (8.91)
[Zn(L_3)(L_4)]	9.87 (8.87)	51.06 (50.74)	2.88 (2.03)	19.14 (18.77)	7.29 (6.38)	9.72 (8.73)

3.9.1. Thermal analysis

TGA/DSC analysis are more useful techniques investigating the thermal decomposition for metal chelates as seen in Figures (3-36) to (3-39), the decomposition is shown in Schemes (3-8) to (3-11), the data are listed in Table (3-11).

Table (3-11): Characterization parameters of thermal decomposition ($10°C\ min^{-1}$) metal complexes.

Compounds	Step	TGA				Reaction	Total mass loss%
		Ti/°C	T_f/°C	T_{DTGmax}	Weight mass loss % calc (found)		
NiL_1	1	95.6	282	227	18.681 (20.016)	$-C_8H_{10}N_2$	75.549 (75.030)
	2	411	599	486	56.868 (55.014)	$-C_{24}H_{22}N_4O_3$	
						-NiO, $C_6H_6N_2$	
Wight experimental loss (75.030)% , final (24.970)%, wight theoretical loss (75.549)% and Final (24.451)% with (NiO, $C_6H_6N_2$)							
ZnL_3	1	78	578.6	289.4	70.076 (69.008)	$-C_{28}H_{11}N_8$	70.076 (69.008)
						$-ZnO_2C_2S_2$	
Wight experimental loss (69.008)%, final (30.992)%, wight theoretical loss (70.076)% and Final (29.924)% with ($ZnO_2C_2S_2$)							
CuL_4	1	61.3	336	187.5	29.242 (30.012)	$-CO_2\ C_6\ H_5N_2$	76.969 (75.571)
	2	335	599	436.5	47.727 (45.559)	$-C_{16}H_{11}N_8$	
						$-CuC_2S$	
Wight experimental loss (75.571)%, final (24.429)%, Wight theoretical loss (76.969)% and Final (23.031)% with (CuC_2S)							
NiL_2	1	76	272.5	153.4	28.456 (30.502)	$-H_2O$, $C_8H_{10}NO_2$	81.872 (80.633)
	2	279.5	411	337.4	31.501 (29.972)	$-C_{13}H_{10}N_4O$	
	3	411	598	480	21.915 (20.159)	$-C_9H_9N_4$	
						-NiO, C_8H_8N	
Wight experimental loss (80.633)%, final (19.367)%, Wight theoretical loss (81.872)% and Final (18.128)% with (NiO,$C_8\ H_7N$)							

$$C_{38}H_{38}N_8O_4Ni$$

found = 20.016
calcul = 18.681

$$\downarrow - C_8H_{12}N_2$$

$$C_{30}H_{28}N_6O_4Ni$$

found = 55.014
calcul = 56.868

$$\downarrow - C_{24}H_{22}N_4O_3$$

$$C_6H_6N_2, NiO$$

found = 75.030 % calcul = 75.549 %
final= 24.970 % final = 24.451 %

Scheme (3-8): The tentative decomposition reaction of $[Ni(L_1)_2]$ complex.

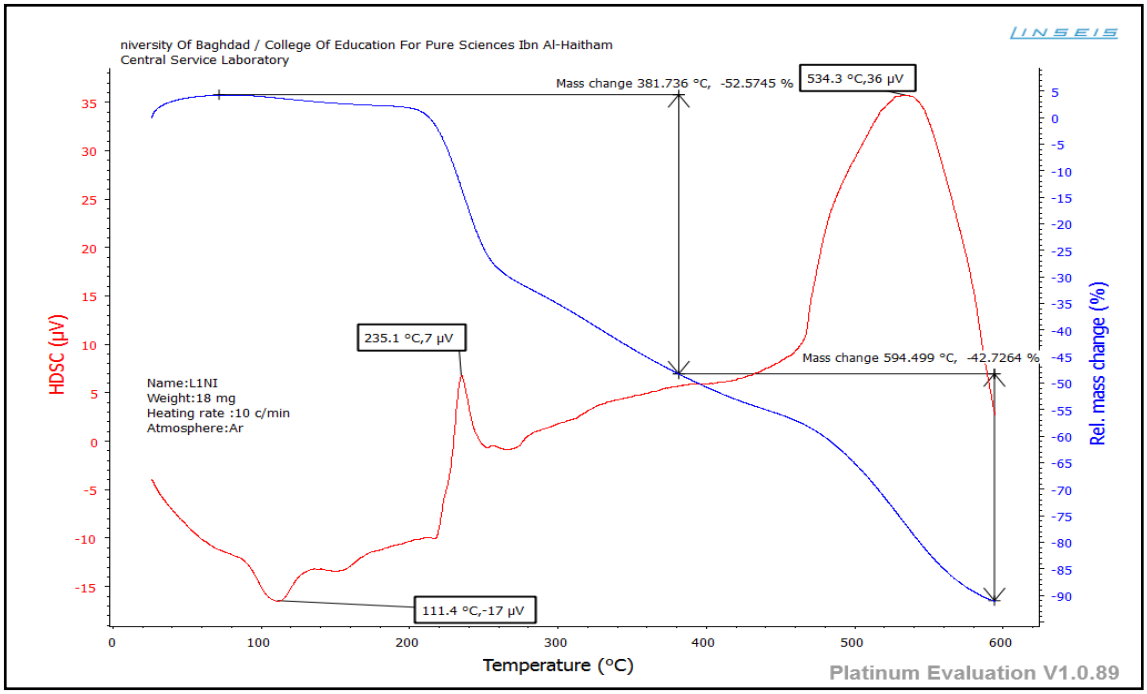

Figure (3-36): TG/DSC Thermogram of $[Ni(L_1)_2]$ complex.

$$C_{38}H_{38}N_{10}O_5Ni$$

found = 30.502
calcul = 28.456
$\downarrow$ - H_2O, $C_8H_{10}NO_2$

$$C_{30}H_{26}N_9O_2Ni$$

found = 29.972
calcul = 31.501
$\downarrow$ - $C_{13}H_{10}N_4O$

$$C_{17}H_{16}N_5ONi$$

found = 20.159
calcul = 21.915
$\downarrow$ - $C_9H_9N_4$

$$C_8H_7NONi$$

found = 80.633 % calcul = 81.872%
final= 19.367 % final = 18.128 %

Scheme (3-9): The tentative decomposition reaction of $[Ni(L_2)_2].H_2O$ complex.

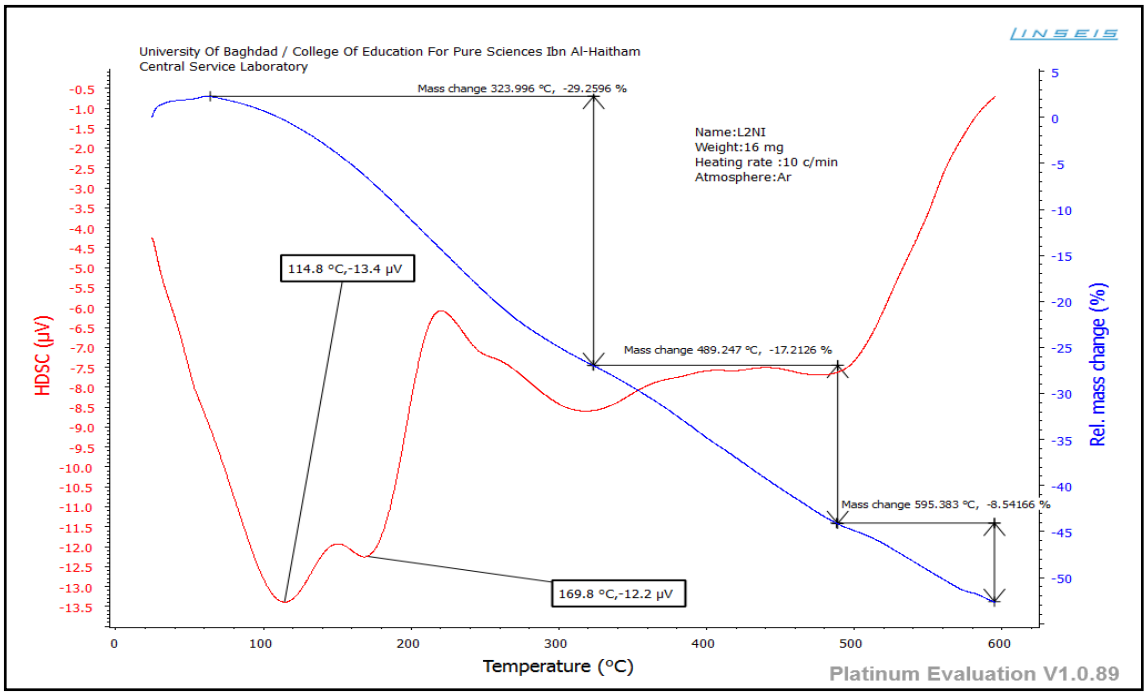

Figure (3-37): TG/DSC Thermogram of $[Ni(L_2)_2].H_2O$ complex.

$$C_{30}H_{11}N_8O_2S_2Zn$$

found = 69.008
calcul = 70.076

$$\downarrow \; - C_{28}H_{11}N_8$$

$$C_2S_2O_2Zn$$

found = 69.008 % calcul = 70.076 %
final= 30.992 % final = 29.924 %

Scheme (3-10): The tentative decomposition reaction of $[Zn(L_3)_2]$ complex.

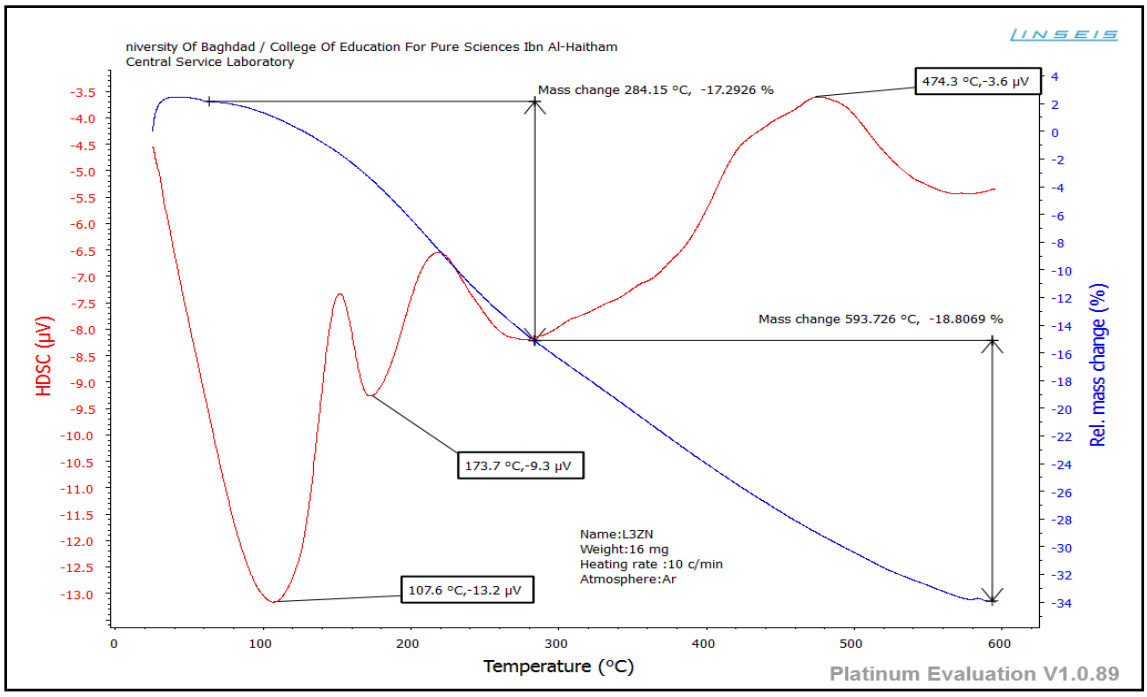

Figure (3-38): TG/DSC Thermogram of $[Zn(L_3)_2]$ complex.

$$C_{26}H_{16}N_{10}O_4S_2Cu$$

found = 30.012
calcul = 29.242

$$\downarrow \; - 2CO_2,\ C_6H_5N_2$$

$$C_{18}H_{11}N_8S_2Cu$$

found = 45.559
calcul = 47.727

$$\downarrow \; - C_{16}H_{11}N_8$$

$$CuC_2S_2$$

found = 75.571 % calcul = 76.969%
final= 24.429 % final = 23.031 %

Scheme (3-11): The tentative decomposition reaction of $[Cu(L_4)_2]$ complex.

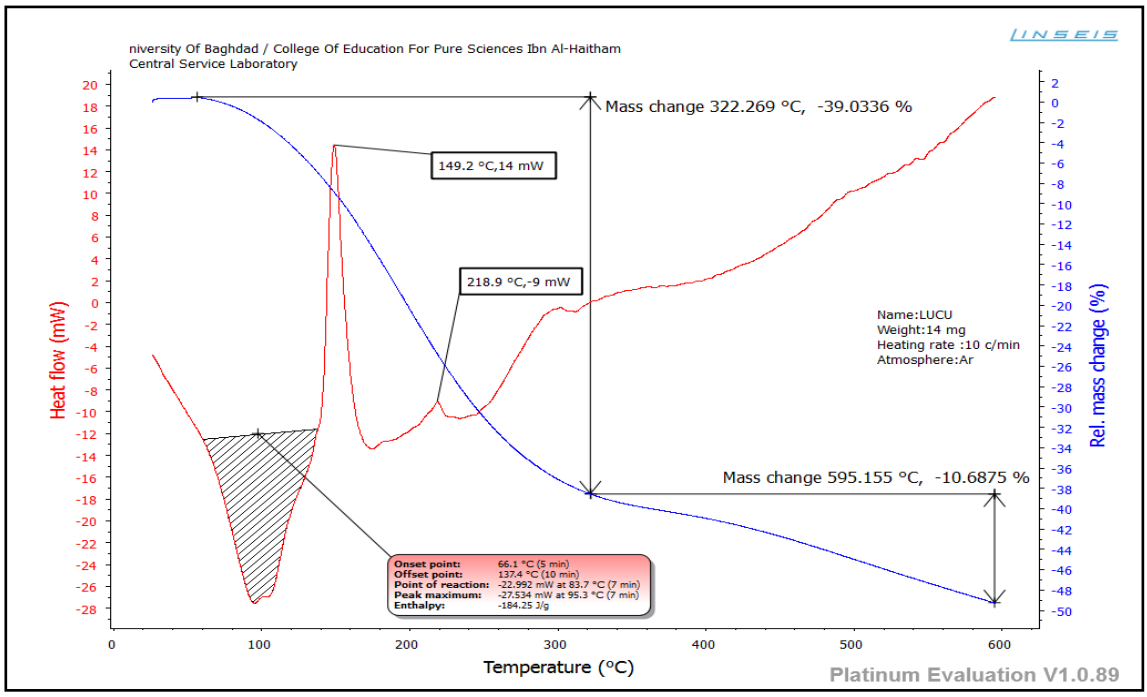

Figure (3-39): TG/DSC Thermogram of $[Cu(L_4)_2]$ complex.

3.9.2. Mass spectra of metal chelates

The mass spectra of the complexes displays peaks centered at m/z= 729, 772, 654, 661, 741 and 656 due to the formulas $C_{38}H_{38}N_8O_4Co$, $C_{38}H_{36}N_{10}O_4Ni.H_2O$, $C_{30}H_{22}N_8S_2O_2Cu$, $C_{26}H_{16}N_{10}S_2O_4Zn$, $C_{38}H_{37}N_9O_4Ni$ and $C_{28}H_{18}N_9S_2O_3Cu$ respectively. The general pattern of fragmentation are summarized in Schemes (3-12) to (3-17), see Figures (3-40) to (3-45).

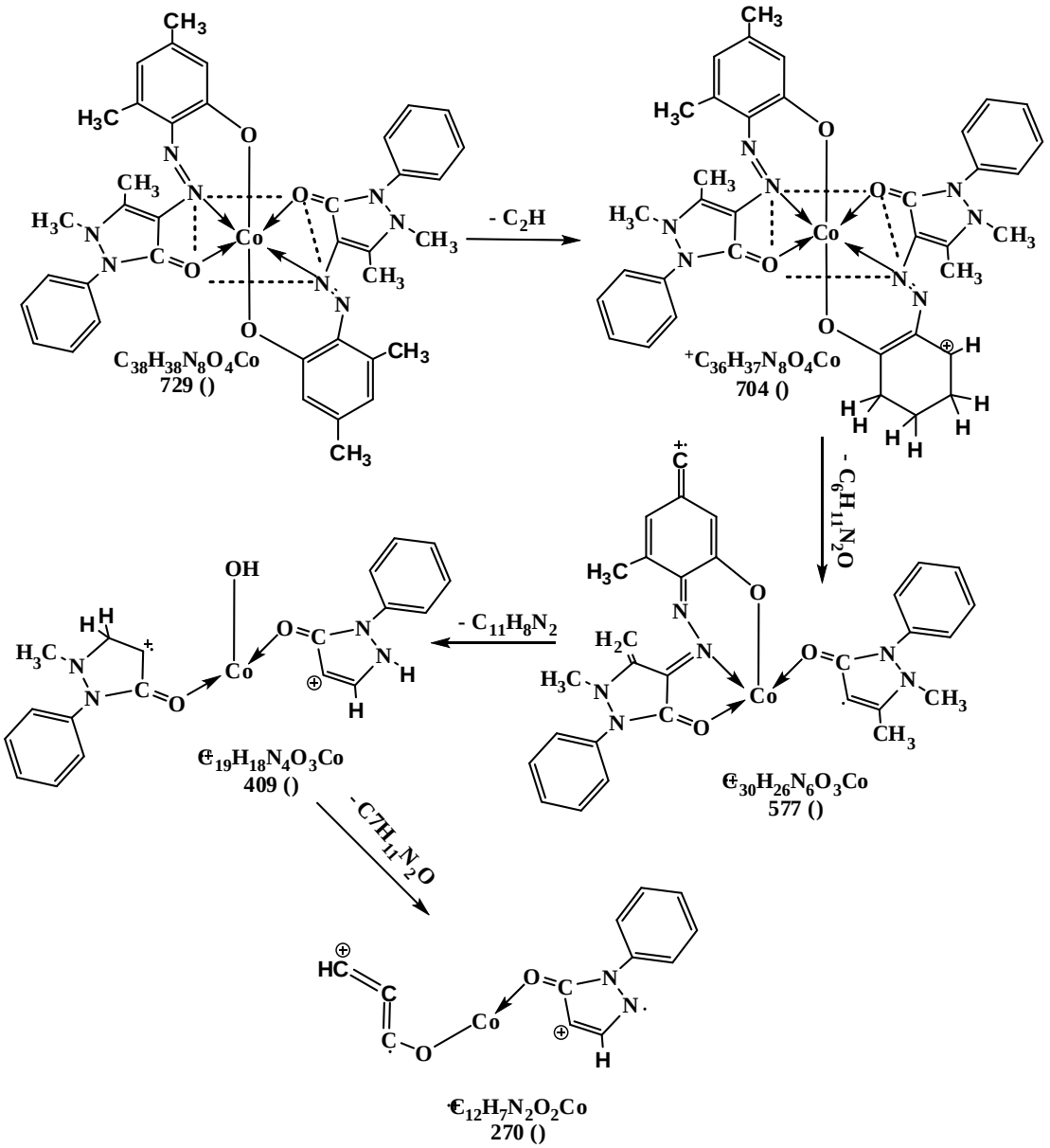

Scheme (3-12): Fragmentation pattern for $[Co(L_1)_2]$ complex.

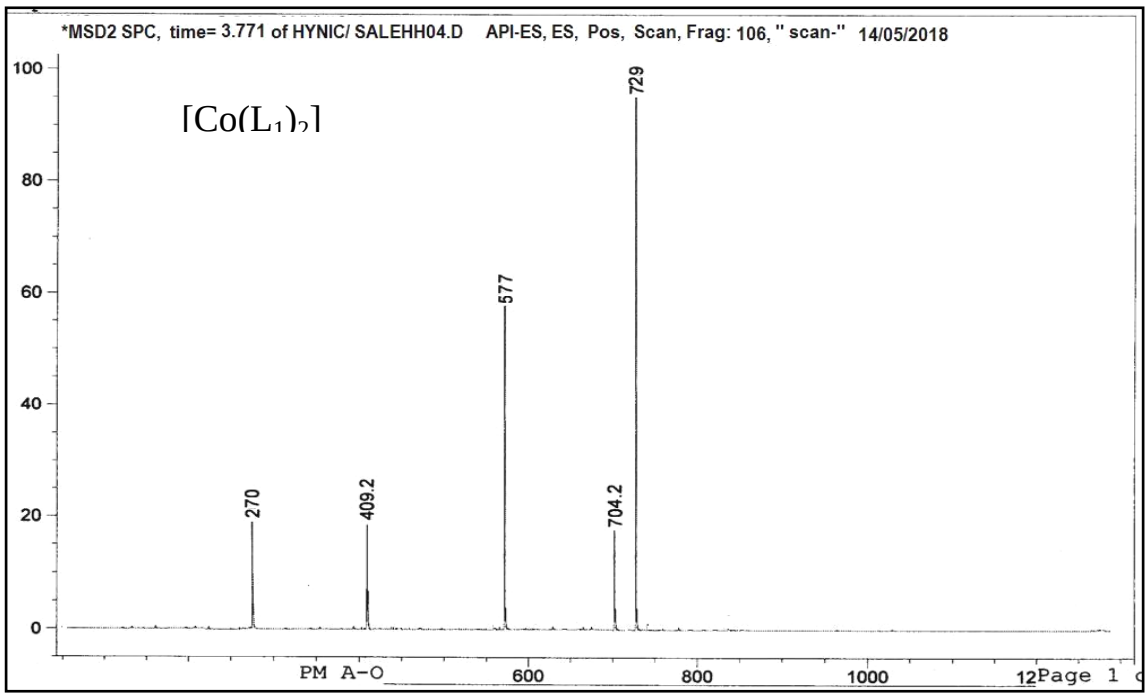

Figure (3-40): Mass spectrum for $[Co(L_1)_2]$ complex.

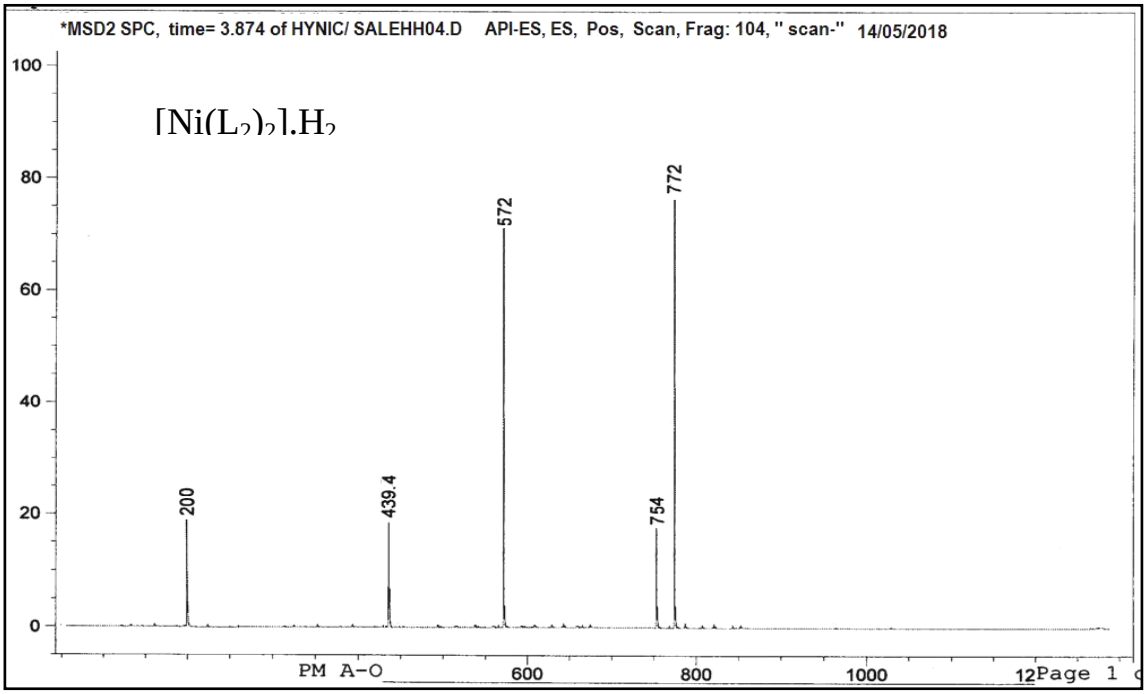

Figure (3-41): Mass spectrum for $[Ni(L_2)_2].H_2O$ complex.

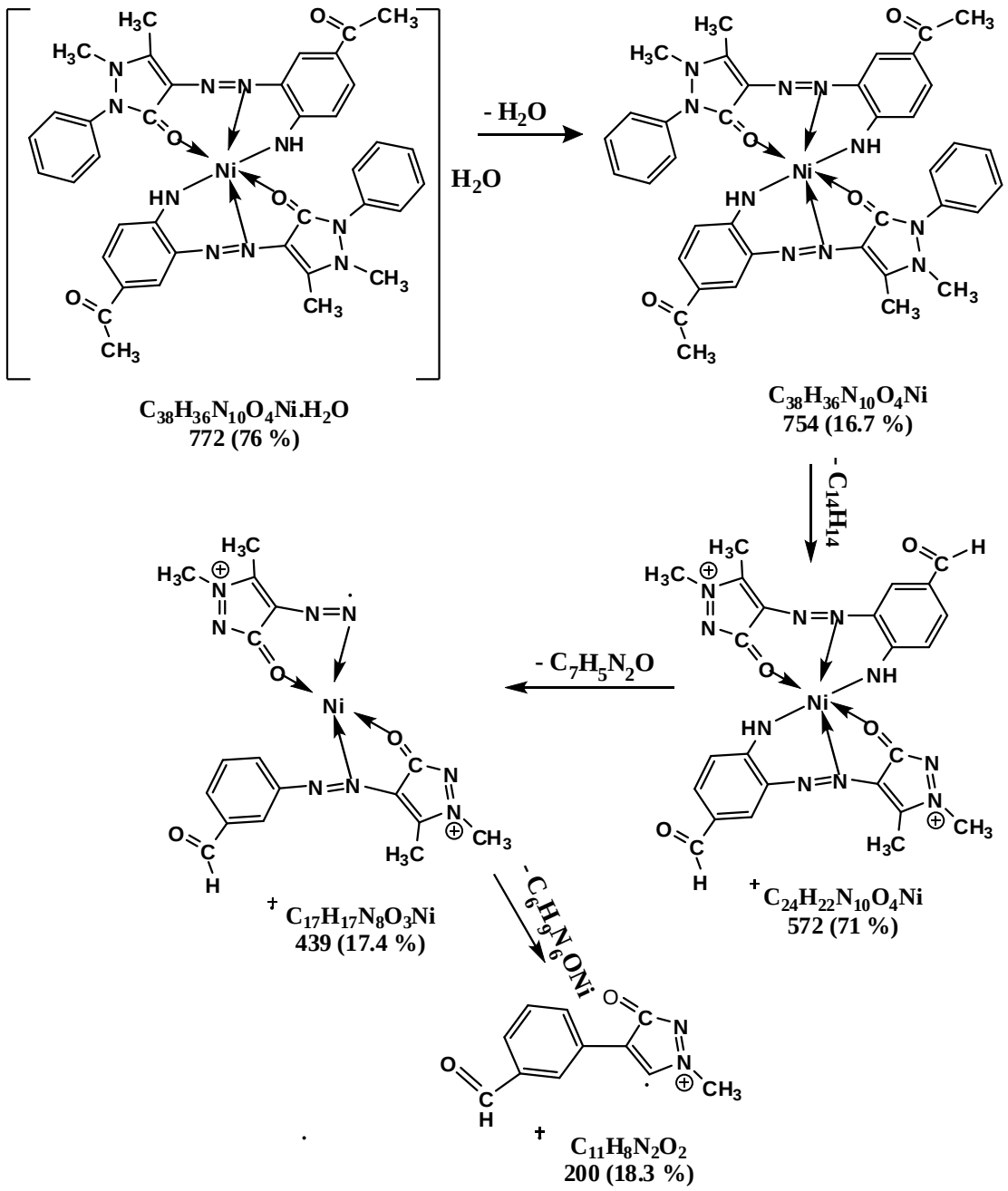

Scheme (3-13): Fragmentation pattern for $[Ni(L_2)_2].H_2O$ complex.

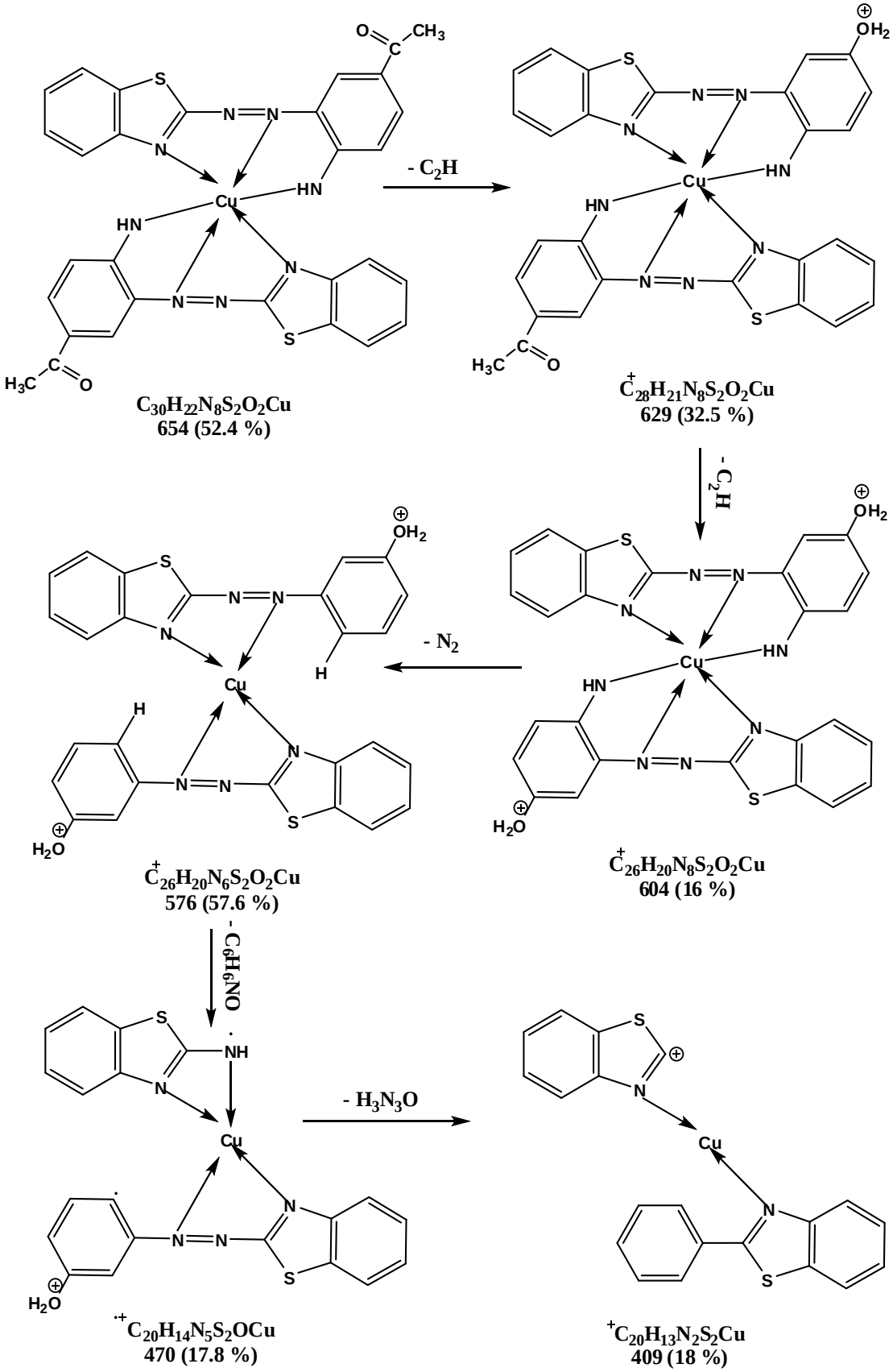

Scheme (3-14): Fragmentation pattern for $[Cu(L_3)_2]$ complex.

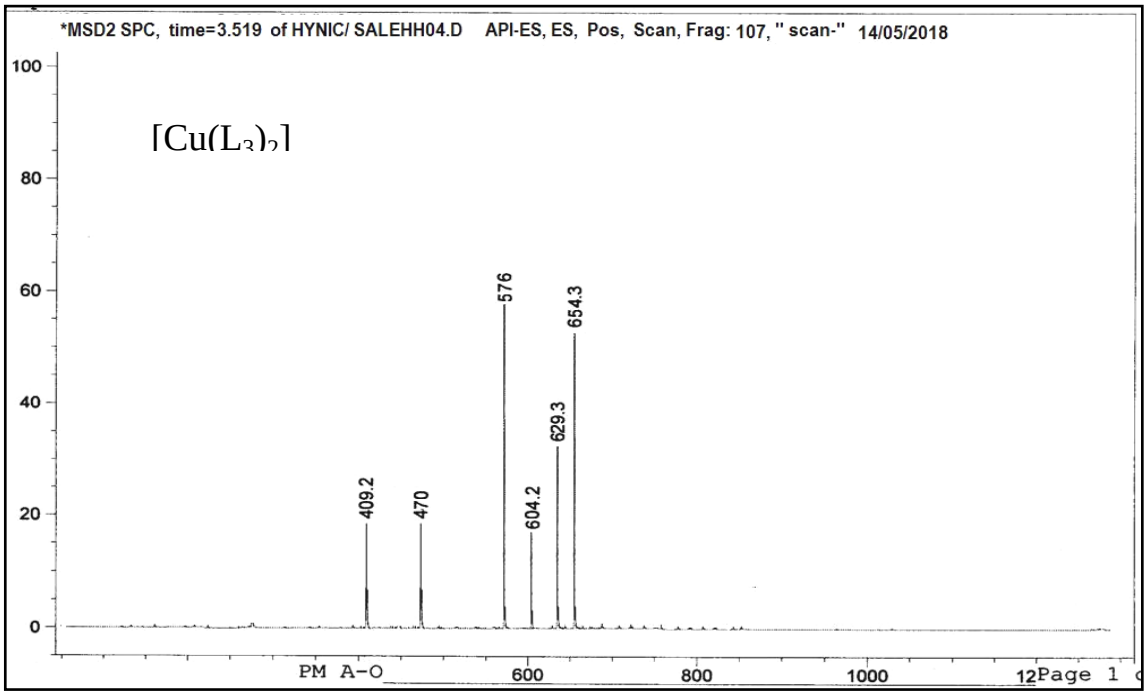

Figure (3-42): Mass spectrum for $[Cu(L_3)_2]$ complex.

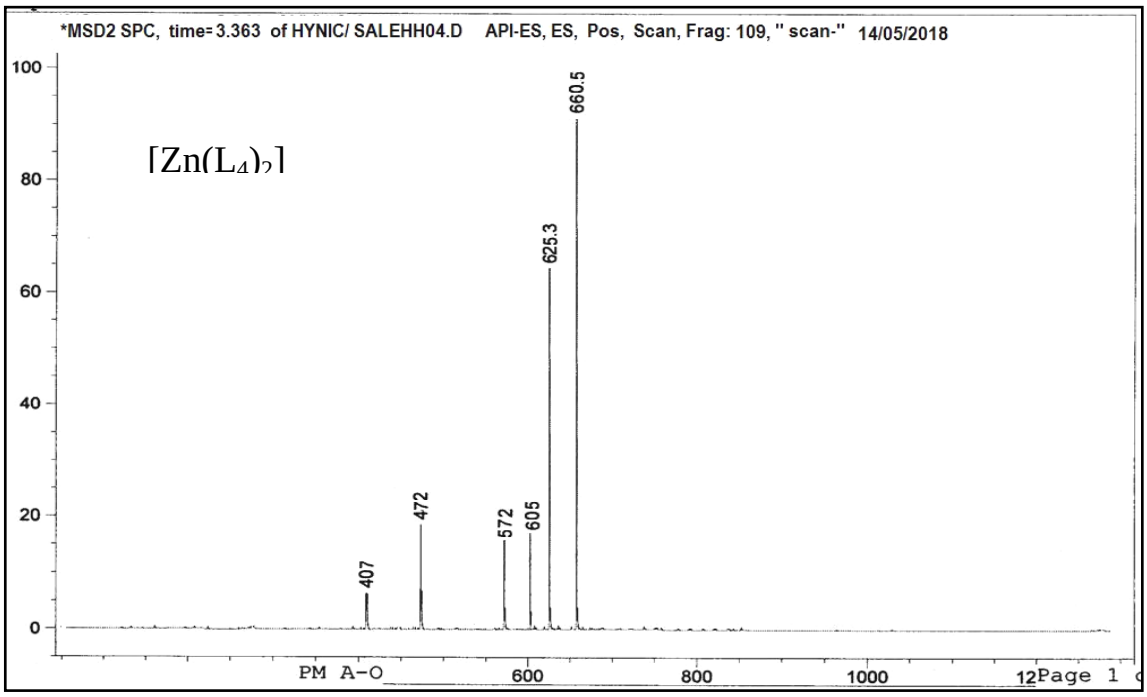

Figure (3-43): Mass spectrum for $[Zn(L_4)_2]$ complex.

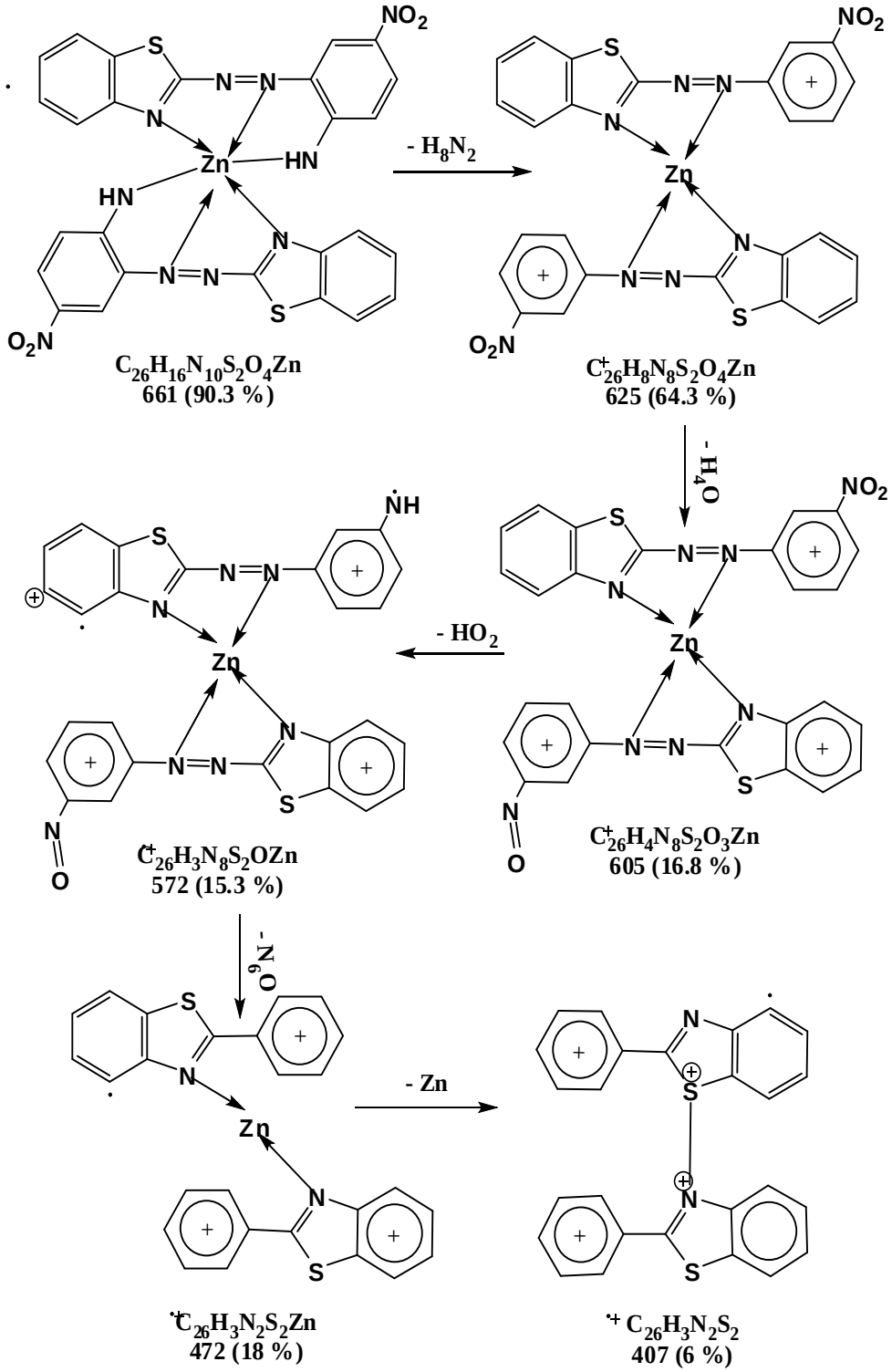

Scheme (3-15): Fragmentation pattern for $[Zn(L_4)_2]$ complex.

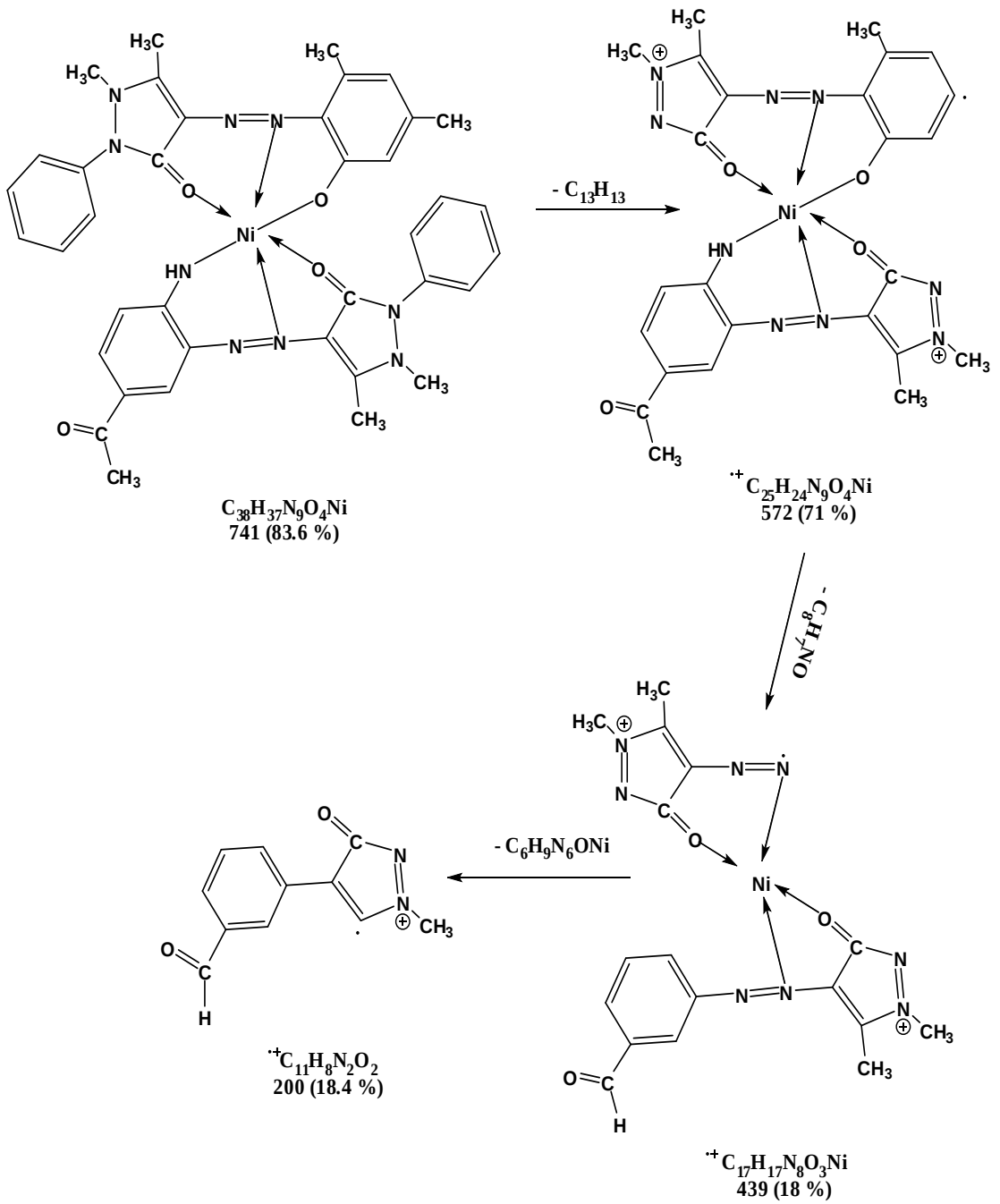

Scheme (3-16): Fragmentation pattern for [Ni(L_1)(L_2)] complex.

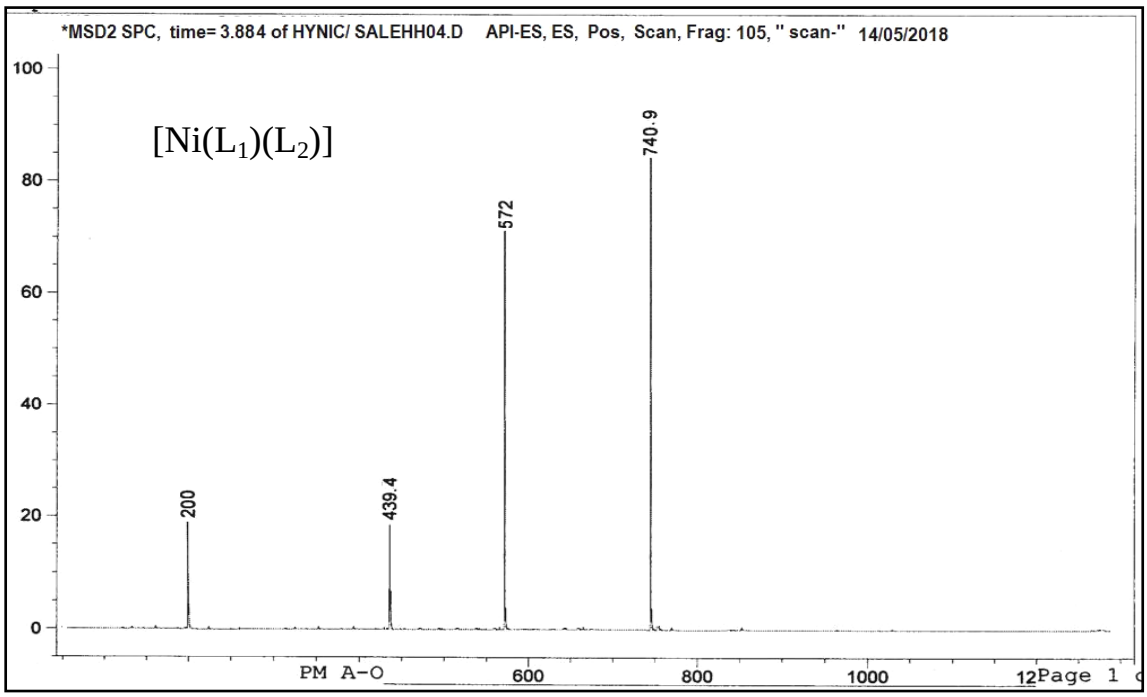

Figure (3-44): Mass spectrum for [Ni(L_1)(L_2)] complex.

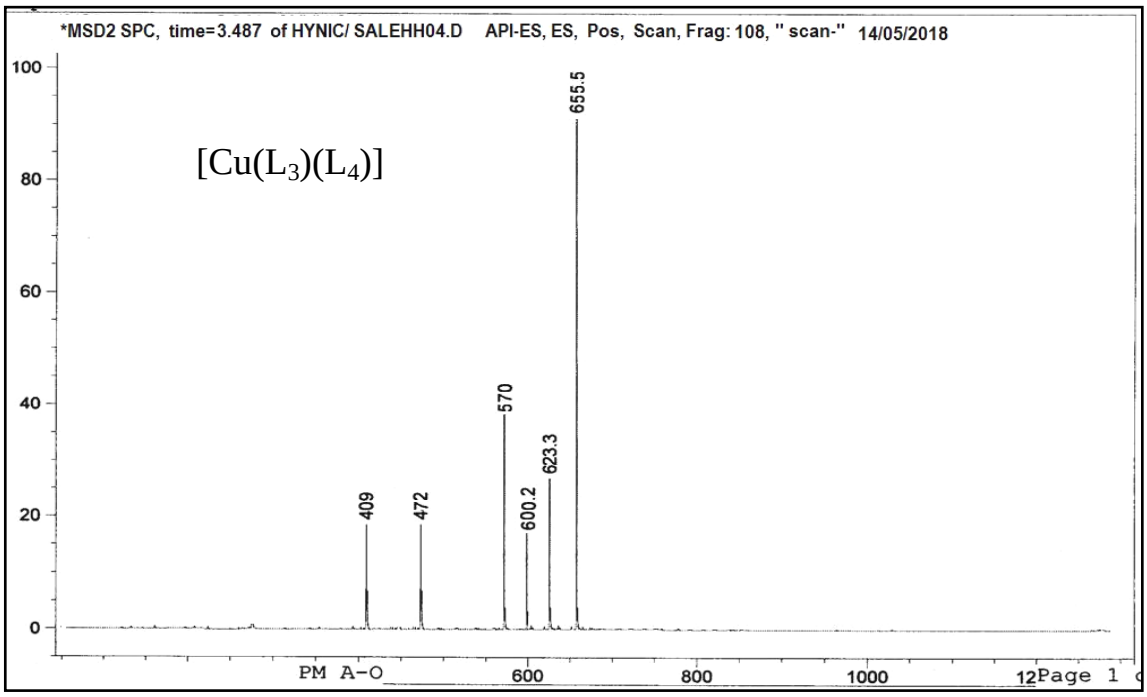

Figure (3-45): Mass spectrum for [Cu(L_3)(L_4)] complex.

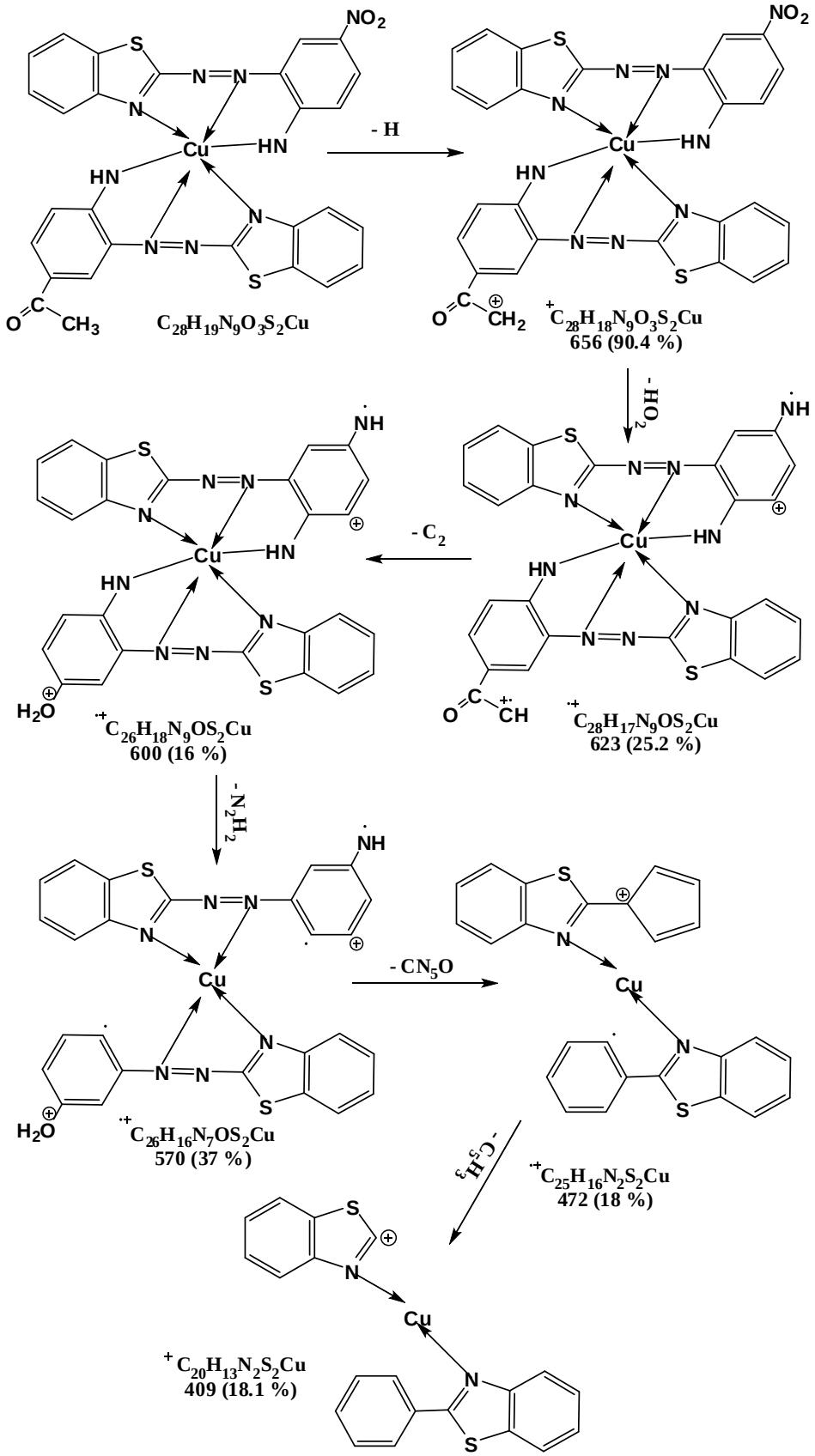

Scheme (3-17): Fragmentation pattern for [Cu(L_3)(L_4)] complex.

3.9.3. Solubility

Table (3-12), summarized the solubility of metal chelates in various solvents.

Table (3-12): Solubility for complexes in different solvents.

Compounds	Ethanol	Acetone	Benzene	CH_2Cl_2	DMF	DMSO	Distal water
$[Co(L_1)_2]$	+	+	÷	÷	+	+	÷
$[Ni(L_1)_2]$	+	+	÷	÷	+	+	÷
$[Cu(L_1)_2]$	+	+	÷	÷	+	+	÷
$[Zn(L_1)_2]$	+	+	÷	÷	+	+	÷
$[Co(L_2)_2].H_2O$	+	+	÷	÷	+	+	÷
$[Ni(L_2)_2].H_2O$	+	+	÷	÷	+	+	÷
$[Cu(L_2)_2].H_2O$	+	+	÷	÷	+	+	÷
$[Zn(L_2)_2].H_2O$	+	+	÷	÷	+	+	÷
$[Co(L_3)_2]$	+	+	÷	÷	+	+	÷
$[Ni(L_3)_2]$	+	+	÷	÷	+	+	÷
$[Cu(L_3)_2]$	+	+	÷	÷	+	+	÷
$[Zn(L_3)_2]$	+	+	÷	÷	+	+	÷
$[Co(L_4)_2]$	+	+	÷	÷	+	+	÷
$[Ni(L_4)_2]$	+	+	÷	÷	+	+	÷
$[Cu(L_4)_2]$	+	+	÷	÷	+	+	÷
$[Zn(L_4)_2]$	+	+	÷	÷	+	+	÷
$[Co(L_1)(L_2)]$	+	+	÷	÷	+	+	÷
$[Ni(L_1)(L_2)]$	+	+	÷	÷	+	+	÷
$[Cu(L_1)(L_2)]$	+	+	÷	÷	+	+	÷
$[Zn(L_1)(L_2)]$	+	+	÷	÷	+	+	÷
$[Co(L_3)(L_4)]$	+	+	÷	÷	+	+	÷
$[Ni(L_3)(L_4)]$	+	+	÷	÷	+	+	÷
$[Cu(L_3)(L_4)]$	+	+	÷	÷	+	+	÷
$[Zn(L_3)(L_4)]$	+	+	÷	÷	+	+	÷

Soluble (+), sparingly (÷)

3.9.4. Molar conductivity

Molar conductance values for metal chelates in dimethysulphoxide (DMSO), (10^{-3} mole/L) have been measured at room temperature. The molar conductance scopes contained for these complexes, Table (3-14) are in a good agreement with that recorded in the literature for non electrolyte type[138], see Table (3-13)

Table (3-13): Molar conductance data at different solvents.

Solvent	Non-Electrolyte	Electrolyte type			
		1:1	1:2	1:3	1:4
Water	0.0	120	240	360	480
Ethanol	0– 20	35 – 45	70 – 90	120	160
Nitro methane	0– 20	75 – 95	150-180	220-260	290-330
Methyl cyanide	0– 30	120-160	220-300	340-420	500
DMF	0– 30	65 – 90	130-170	200-240	300
DMSO	0– 20	30 – 40	70 – 80	_____	_____

Table (3-14): Molar conductance for metal chelates in dimethylsulphoxide (DMSO) (10^{-3} mole/L).

Λ_m ($S.cm^2.mol^{-1}$) In DMSO	Complexes
19.20	**$[Co(L_1)_2]$**
15.00	**$[Ni(L_1)_2]$**
16.81	**$[Cu(L_1)_2]$**
18.30	**$[Zn(L_1)_2]$**
14.11	**$[Co(L_2)_2].H_2O$**
19.20	**$[Ni(L_2)_2].H_2O$**
16.20	**$[Cu(L_2)_2].H_2O$**
10.93	**$[Zn(L_2)_2].H_2O$**
16.77	**$[Co(L_3)_2]$**
13.70	**$[Ni(L_3)_2]$**
18.32	**$[Cu(L_3)_2]$**
17.70	**$[Zn(L_3)_2]$**
12.63	**$[Co(L_4)_2]$**
13.42	**$[Ni(L_4)_2]$**
17.80	**$[Cu(L_4)_2]$**
11.50	**$[Zn(L_4)_2]$**
19.60	**$[Co(L_1)(L_2)]$**
16.50	**$[Ni(L_1)(L_2)]$**
18.21	**$[Cu(L_1)(L_2)]$**
11.67	**$[Zn(L_1)(L_2)]$**
13.90	**$[Co(L_3)(L_4)]$**
15.30	**$[Ni(L_3)(L_4)]$**
18.80	**$[Cu(L_3)(L_4)]$**
8.46	**$[Zn(L_3)(L_4)]$**

3.9.5. Magnetic properties

Magnetic susceptibility for prepared complexes was measured and the data were listed in Table (3-15), the values of effective magnetic moment (μ_{eff}) for Co(II), Ni(II) and Cu(II) complexes corresponded to high spin octahedral geometry around metal ion, except Zn(II) complexes are diamagnetic in nature ($3d^{10}$)[139,140].

The total magnetic moment has been characterized by the spin quantum number (S) and orbital angular momentum (L) according to:-

$$\mu_{S+L} = \sqrt{4S(S+1)+L(L+1)} \qquad B.M$$

At first transition metal series, magnetic moment has been calculated for spin only according to:-

$$\mu_S = \sqrt{4S(S+1)} \qquad B.M, S = n/2,$$

$$\mu_S = \sqrt{n(n+2)} \qquad B.M$$

The results obtained from magnetic balance have been corrected for diamagnetic effect using the following relationship, see Table (3-15).

$$\mu_{eff} = 2.828\sqrt{X_A.T} \qquad B.M$$

$X_A = X_m - D$

$X_m = X_g.Mwt$

μ_{eff}= effective magnetic moment.

T= absolute temperature (Kelvin).

X_A= atomic susceptibility.

X_m= molar magnetic susceptibility.

X_g= gram magnetic susceptibility.

D= diamagnetic function ($gm^{-1}atom^{-1}$).

Table (3-15): Magnetic moments data for the prepared metal chelates at 296°K .

Complexes	$X_g.10^{-6}$	$X_m.10^{-6}$	$X_A.10^{-6}$	μ_{eff} (B.M) Exp.	D
$[Co(L_1)_2]$	11.50	8383.5	8619.46	4.51	-235.96
$[Ni(L_1)_2]$	4.67	3399.76	3635.72	2.93	=
$[Cu(L_1)_2]$	1.38	1012.92	1248.88	1.71	=
$[Co(L_2)_2].H_2O$	14.00	10822	11057.48	5.10	-235.48
$[Ni(L_2)_2].H_2O$	4.20	3281	3516.48	2.88	=
$[Cu(L_2)_2].H_2O$	1.35	1050.3	1285.78	1.74	=
$[Co(L_3)_2]$	14.30	9280.7	9444.48	4.72	-163.78
$[Ni(L_3)_2]$	5.67	3674.16	3837.94	3.01	=
$[Cu(L_3)_2]$	1.68	1098.72	1262.5	1.72	=
$[Co(L_4)_2]$	14.98	9811.9	9968.44	4.85	-156.54
$[Ni(L_4)_2]$	5.25	3433.5	3590.04	2.91	=
$[Cu(L_4)_2]$	1.70	1122	1278.54	1.73	=
$[Co(L_1)(L_2)]$	12.38	9185.96	9421.68	4.71	111.48 111.24
$[Ni(L_1)(L_2)]$	4.49	3327.09	3562.81	2.90	=
$[Cu(L_1)(L_2)]$	1.40	1045.58	1281.52	1.73	=
$[Co(L_3)(L_4)]$	12.33	8039.16	8199.32	4.39	-75.39 -71.77
$[Ni(L_3)(L_4)]$	5.19	3378.69	3538.85	2.89	=
$[Cu(L_3)(L_4)]$	1.64	1077.48	1237.64	1.71	=

3.9.6. FT-IR spectra of complexes

3.9.6.1. FT-IR spectra of azo ligand (L_1) metal chelates

FTIR spectra of azo ligand (L_1) and their metal chelates have been collated, and the data was scheduled in Table (3-16). The broad band in the spectrum of the ligand, Figure (3-19) at 3410 cm^{-1}, that was described into the stretching vibration from υ(OH) phenol, the disappearance of this band at the spectra with all produced compounds pointed out the deprotonation for phenol group to coordination with metal ion[141]. Spectrum presented band in 1666 cm^{-1} because of υ(C=O) vibration, on complexation, this band has been removed to lower frequency implying the coordination with metal ion[142]. Band differentiating of the azo group at 1585 cm^{-1} displaced into lower wave number for change during shape at spectra for all produced compounds[143]. The bands at the rate (1319-1496 cm^{-1}) due to bending frequency of (δCH_3)[144]. Stretching frequency bands to metal-nitrogen on other than metal-oxygen more[145,146] assured by the existence to the bands at rate 432-489 cm^{-1}, see Figures (3-46) to (3-49).

Table (3-16): Infrared spectral data for the azo ligand (L_1) and their metal chelates (cm^{-1}).

Compound	υ(OH)	υ(C=O)	υ(N=N)	$\delta(CH_3)_{as,s}$	υ(M-N) υ(M-O)
Ligand(L_1)	3410 br.	1666 sh.	1585 sh.	1496 sh. 1442 s. 1415 sho. 1369 sh. 1319 sh.	-
$[Co(L_1)_2]$	-	1627 s.	1581 s.	1492 sh. 1458 sh. 1396 sh. 1311 sh.	459 w. 439 w.
$[Ni(L_1)_2]$	-	1627 s.	1577 sho.	1492 sh. 1458 sh. 1419 sho. 1396 sh. 1311 sh.	474 w. 435 w.
$[Cu(L_1)_2]$	-	1627 sh.	1581 s.	1492 s. 1458 sh. 1400 sh. 1373 sho. 1311 sh.	489 w. 459 w.
$[Zn(L_1)_2]$	-	1627 sh.	1577 s.	1492 s. 1458 sh. 1400 sh. 1311 sh.	459 w. 432 w.

As= asymmetry, s= symmetry, br= broad, sh= sharp, s= strong, w= weak, sho=shoulder

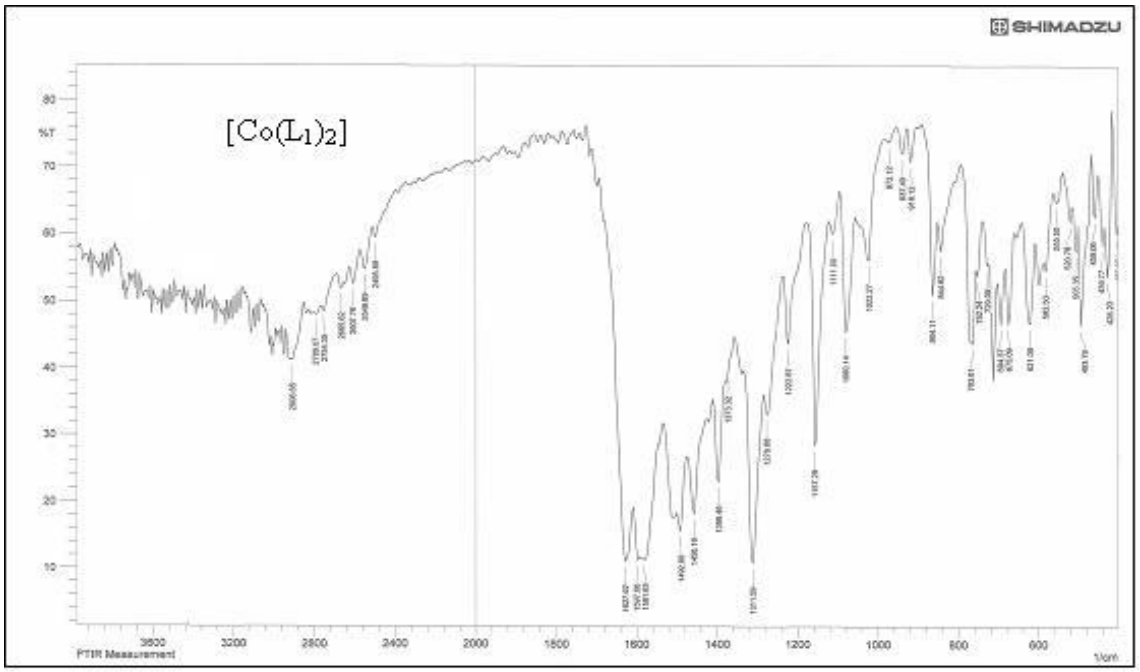

Figure (3-46): FTIR spectrum of the $[Co(L_1)_2]$ complex.

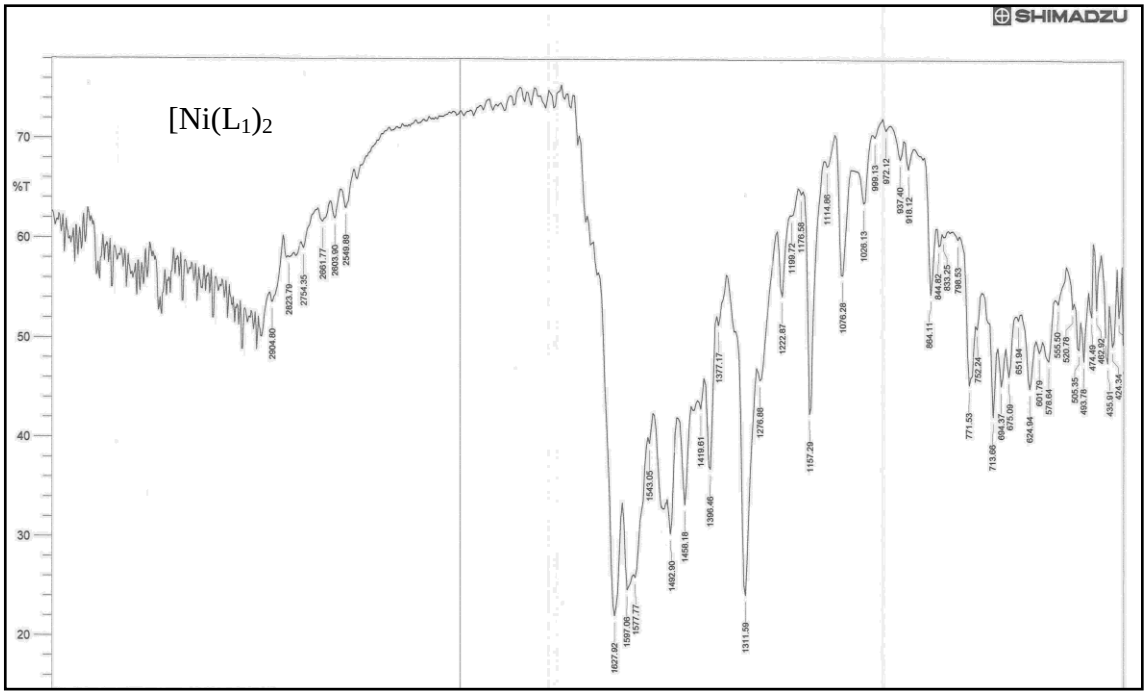

Figure (3-47): FTIR spectrum of the $[Ni(L_1)_2]$ complex.

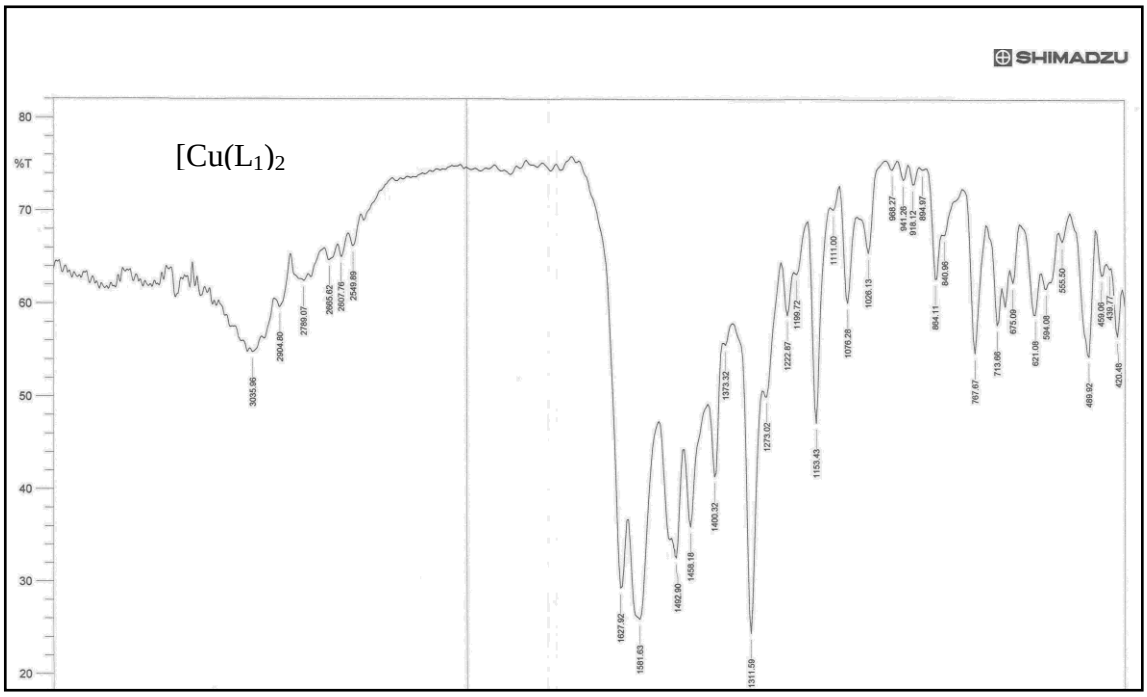

Figure (3-48): FTIR spectrum of the [Cu(L_1)$_2$] complex.

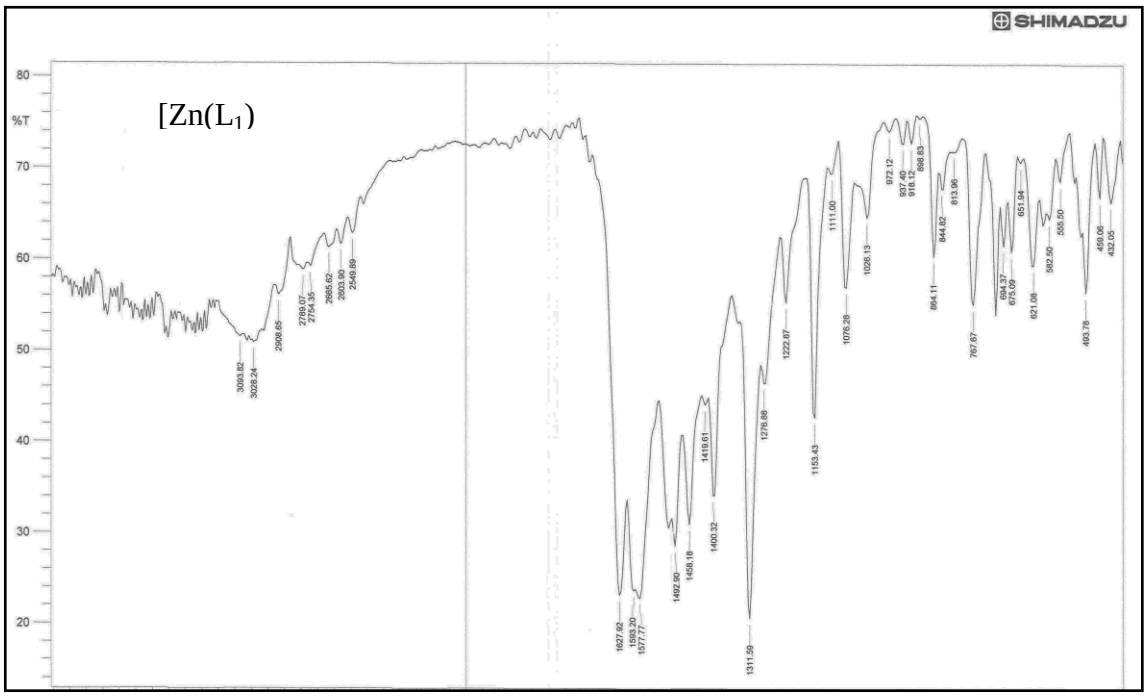

Figure (3-49): FTIR spectrum of the [Zn(L_1)$_2$] complex.

3.9.6.2. FT-IR spectra of azo ligand (L_2) metal chelates

Spectra for azo ligand (L_2) and their metal chelates have been collated, and the data was listed in Table (3-17). Spectrum of the ligand, Figure (3-21) exhibited bands at 3487 cm^{-1} and 3414 cm^{-1} were assigned to asymmetric and symmetric stretching vibration of $\upsilon(NH_2)$respectively, at the spectra of all produced compounds pointed out the deprotonation for amino group to υ(NH) group which appeared at lower frequency because of coordination with metal ion[147]. Band at 1678 cm^{-1} due to carbonyl υ(C=O) of acetyl group, no significant change in this band was noticed, the possibility that coordination occur via the donating atom in this group was excluded[148]. Band presented at 1657 cm^{-1} because of υ(C=O) vibration, on complexation this band has been removed to lower frequency implying the coordination with metal ion[149]. Band of the azo group at 1512 cm^{-1} displaced into higher wave number for change during shape at spectra for all produced metal chelates[150]. The bands at 1597 cm^{-1} and at (1496, 1454, 1411, 1357, 1307) cm^{-1} due to stretching vibration of υ(C=C) and bending frequency of (δCH_3) sequences[151]. The presence of hydrate water in the spectra of all complexes[152], were suggested by the very broad absorption around (3414-3525) cm^{-1}. Stretching frequency bands to metal-nitrogen on other than metal-oxygen more[153,154], assured by the existence to the bands at rate 455-497 cm^{-1}, see Figures (3-50) to (3-53).

Table (3-17): Infrared spectral data for the azo ligand (L_2) and their metal chelates (cm^{-1}).

Compounds	$\upsilon(NH_2)$ $\upsilon(NH)$	$\upsilon(C\text{-}O)$ acetyl pyrazole	$\upsilon(C=C)$ $\upsilon(N=N)$	$\delta(CH_3)_{as.s}$ $\upsilon(H_2O)$	$\upsilon(M–N)$ $\upsilon(M–O)$
Ligand (L_2)	3487 sh. 3414 sh. –	1678 s. 1657 sho.	1597 sh. 1512 sho.	1496 s. 1454 sh. 1411 s. 1357 sh. 1307 sh. –	–
$[Co(L_2)_2].H_2O$	3375 br. –	1678 s. 1631 sho.	1597 s. 1519 sho.	1492 sh. 1454 sh. 1408 s. 1357 sh. 1303 sho. 3417 br.	493 w. 474 w.
$[Ni(L_2)_2].H_2O$	– 3210 sho. –	1678 s. 1647 s.	1597 sh. 1516 sho.	1492 s. 1454 s. 1404 s. 1357 sh. 1307 sho. 3417 br.	489 w. 459 w.
$[Cu(L_2)_2].H_2O$	– 3174 br.	1681 s. 1643 sho.	1593 s. 1520 sho.	1492 sh. 1454 s. 1357 sh. 1303 s. 3414 br.	497 w. 455 w.
$[Zn(L_2)_2].H_2O$	– 3221 br.	1678 s. 1640 sho.	1597 sh. 1516 s.	1492 sh. 1454 sh. 1408 s. 1357 sh. 1303 sho. 3525 br.	474 w. 462 w.

As= asymmetry, s= symmetry, br= broad, sh= sharp, s= strong, w= weak, sho= shoulder

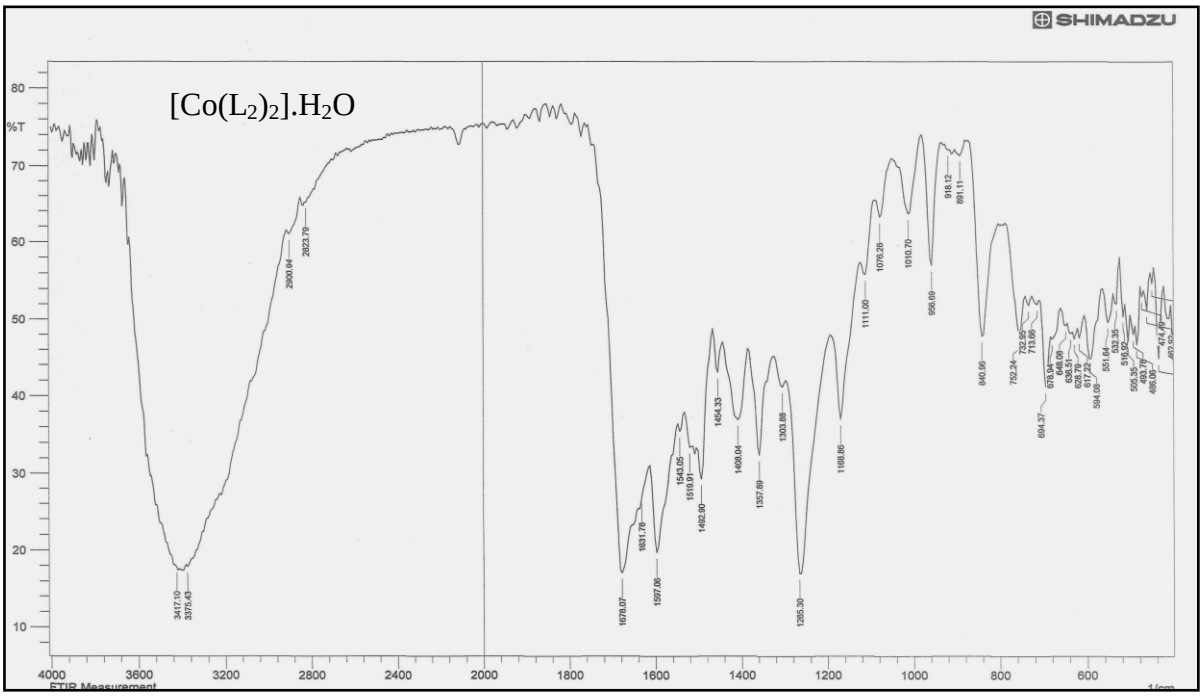

Figure (3-50): FTIR spectrum of the $[Co(L_2)_2].H_2O$ complex.

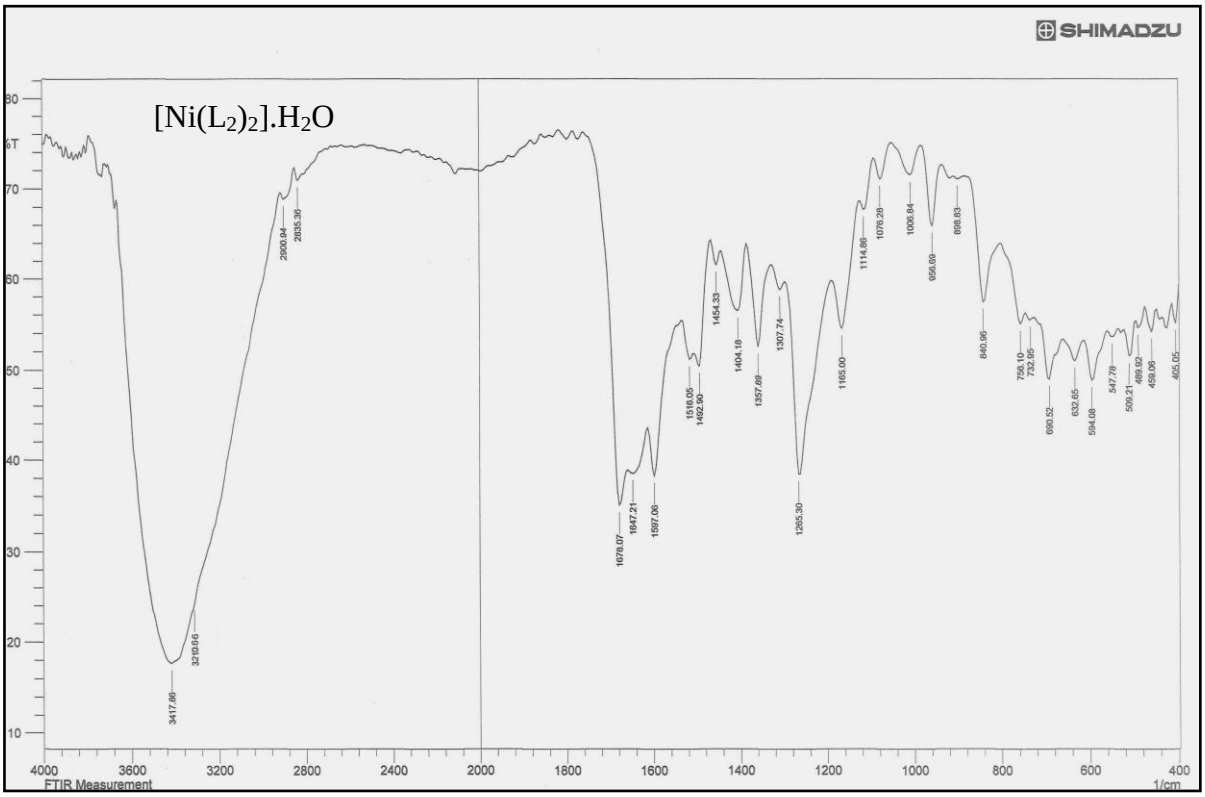

Figure (3-51): FTIR spectrum of the $[Ni(L_2)_2].H_2O$ complex.

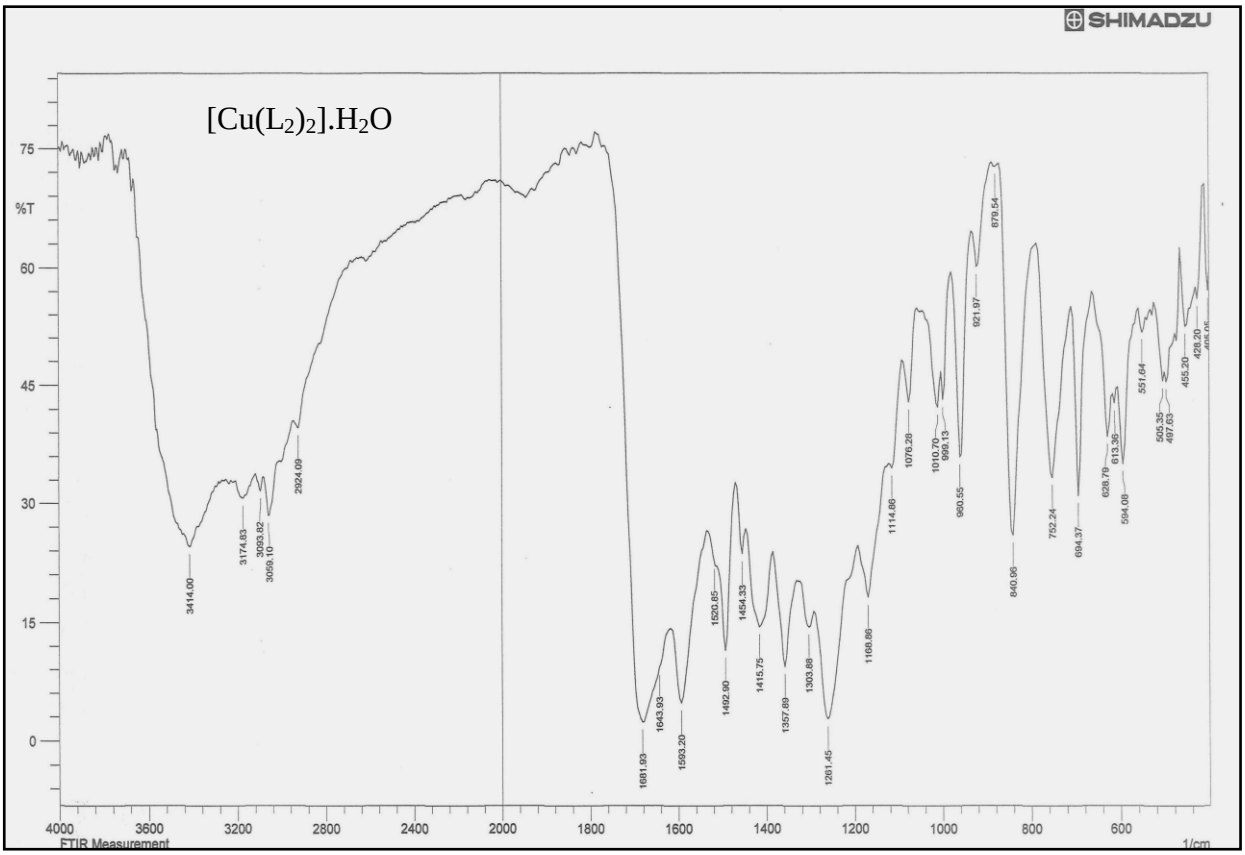

Figure (3-52): FTIR spectrum of the $[Cu(L_2)_2].H_2O$ complex.

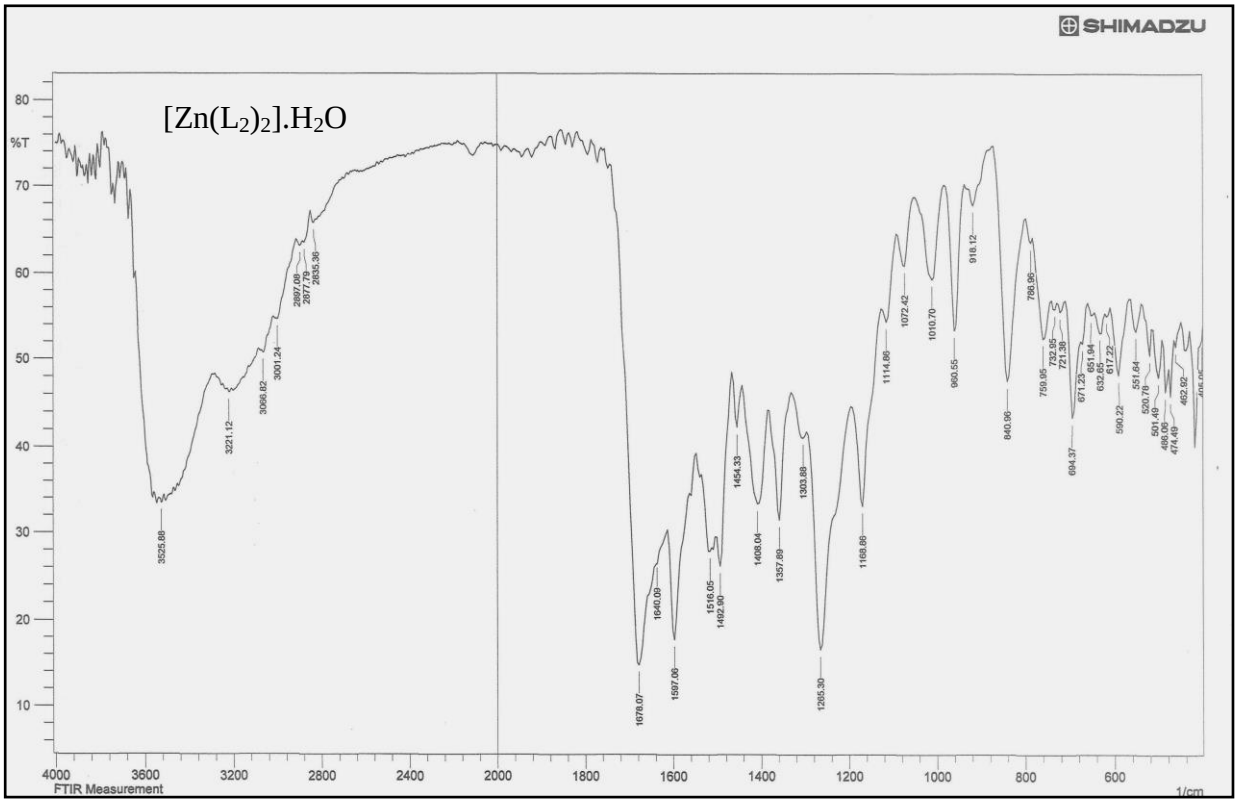

Figure (3-53): FTIR spectrum of the $[Zn(L_2)_2].H_2O$ complex.

3.9.6.3. FT-IR spectra of azo ligand (L_3) metal chelates

Spectra for azo ligand (L_3), Figure (3-23), and their metal chelates, Figures (3-54) to (3-57) have been collated, and the data was listed in Table (3-18). Ligand spectrum exhibited bands at 3483 cm^{-1} and 3414 cm^{-1} which were assigned to asymmetric and symmetric stretching vibration of $\upsilon(NH_2)$ respectively, at the spectra of all produced compounds pointed out the deprotonation for amino group to υ(NH) group which appeared at lower frequency because of coordination with metal ion[155]. Band at 1678 cm^{-1} due to carbonyl υ(C=O) of acetyl group, no significant change in this band was noticed, the possibility that coordination occur via the donating atom in this group was excluded[156]. Strong band at 1654 cm^{-1} described to υ(C=N) of thiazole ring, at the spectra of metal chelates this band has been removed to lower frequency implying the coordination with metal ion[157]. Band of the azo group at 1531 cm^{-1} displaced into lower wave number for change during shape at spectra for all produced compounds[158]. Bands at 1589 cm^{-1} and 1570 cm^{-1} attributed to υ(C=C), and the bands at (1442, 1423, 1396 and 1342) cm^{-1} lead to bending vibration of $\delta(CH_3)$ group[159]. Stretching frequency bands to metal-nitrogen more[160,161] assured by the existence to the bands at rate 432-484 cm^{-1}.

Table (3-18): Infrared spectral data for the azo ligand (L_3) and their metal chelates (cm^{-1}).

Compounds	υ(NH_2) υ(NH)	υ(C-O) υ(C=N)	υ(C=C) υ(N=N)	δ$(CH_3)_{as.s}$	υ(M–N)
Ligand(L_3)	3483 sh. 3414 sh. –	1678 sho. 1654 s.	1589 sh. 1570 sho. 1531 s.	1442 sh. 1423 sh. 1396 sh. 1342 sh.	–
[Co$(L_3)_2$]	– 3421 br.	1678 sh. 1635 sho.	15597 sh. 1570 sho. 1508 sh.	1446 sh. 1415 sh. 1346 s.	484 w. 455 w.
[Ni$(L_3)_2$]	– 3421 br.	1678 sh. 1639 s.	1597 sh. 1586 sho. 1512 sh.	1446 sh. 1419 sh. 1357 sh.	459 w. 432 w.
[Cu$(L_3)_2$]	– 3425 br.	1678 s. 1635 sho.	1597 sh. 1572 sho. 1519 sh.	1450 sh. 1423 sh. 1392 sh. 1357 s.	470 w. 451 w.
[Zn$(L_3)_2$]	– 3479 br.	1678 sh. 1620 sho.	1600 sh. 1558 sho. 1508 sh.	1454 sh. 1427 sh. 1396 sh. 1357 sh.	482 w. 451 w.

As= asymmetry, s= symmetry, br= broad, sh= sharp, s= strong, w= weak, sho =shoulder

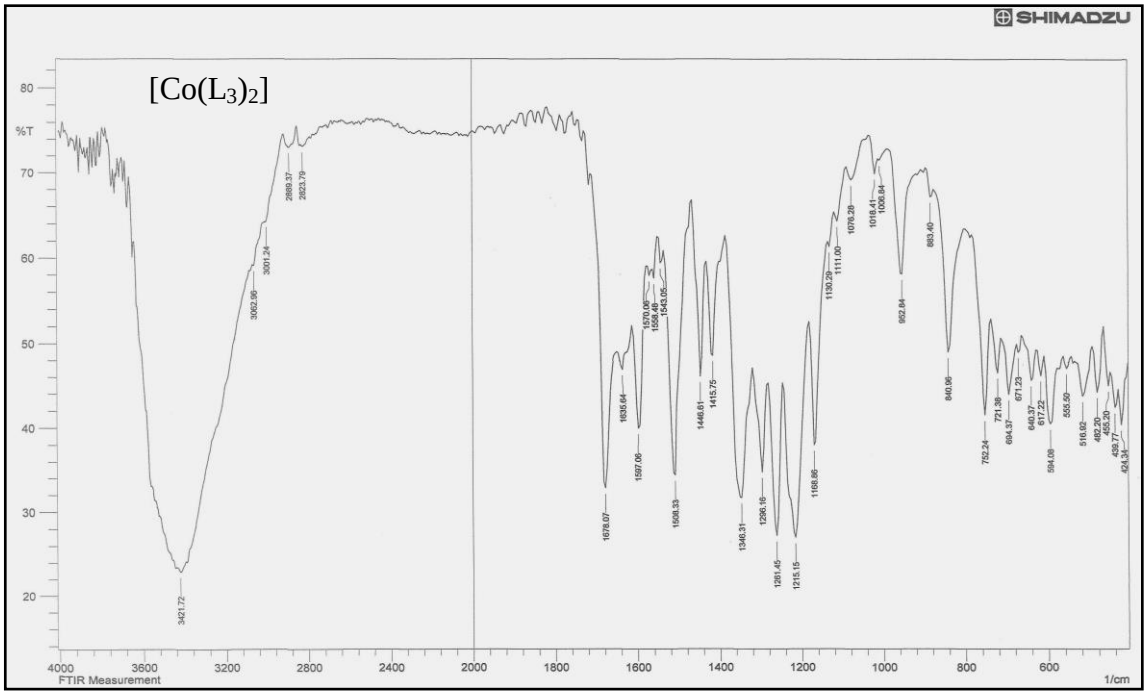

Figure (3-54): FTIR spectrum of the $[Co(L_3)_2]$ complex.

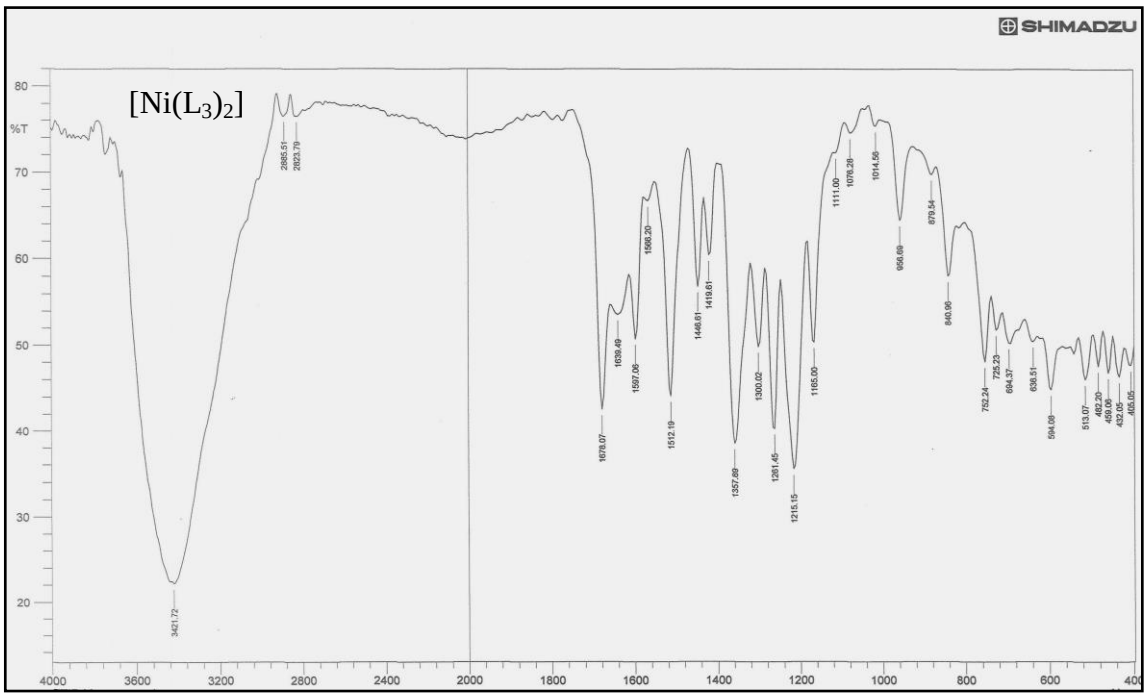

Figure (3-55): FTIR spectrum of the $[Ni(L_3)_2]$ complex.

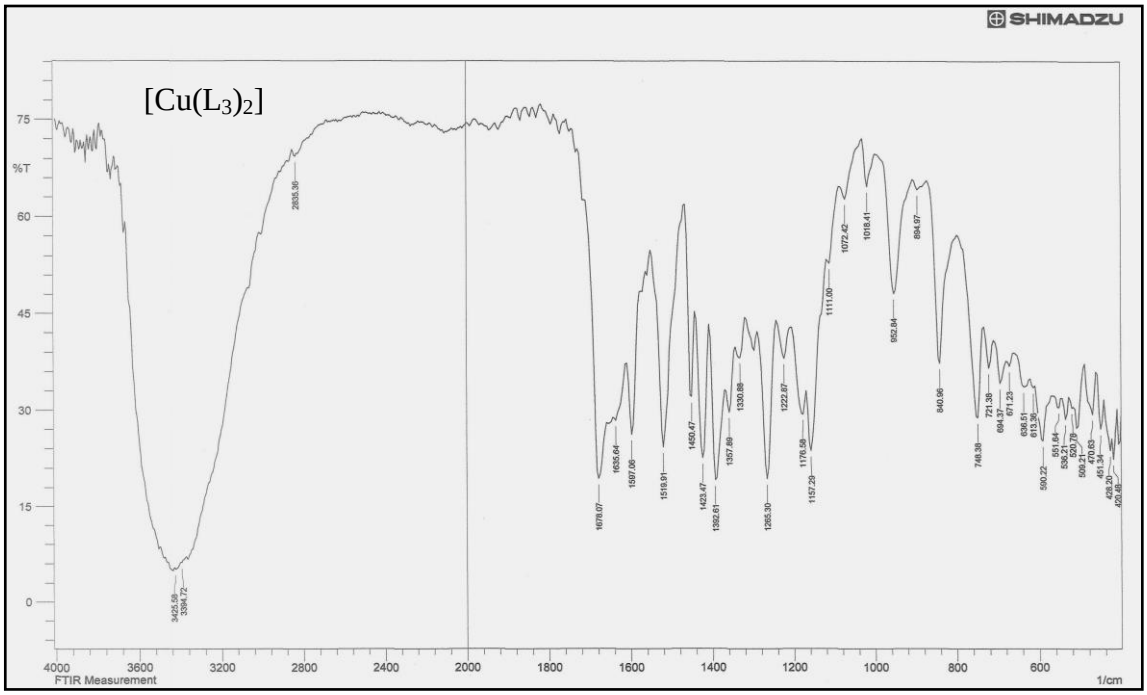

Figure (3-56): FTIR spectrum of the $[Cu(L_3)_2]$ complex.

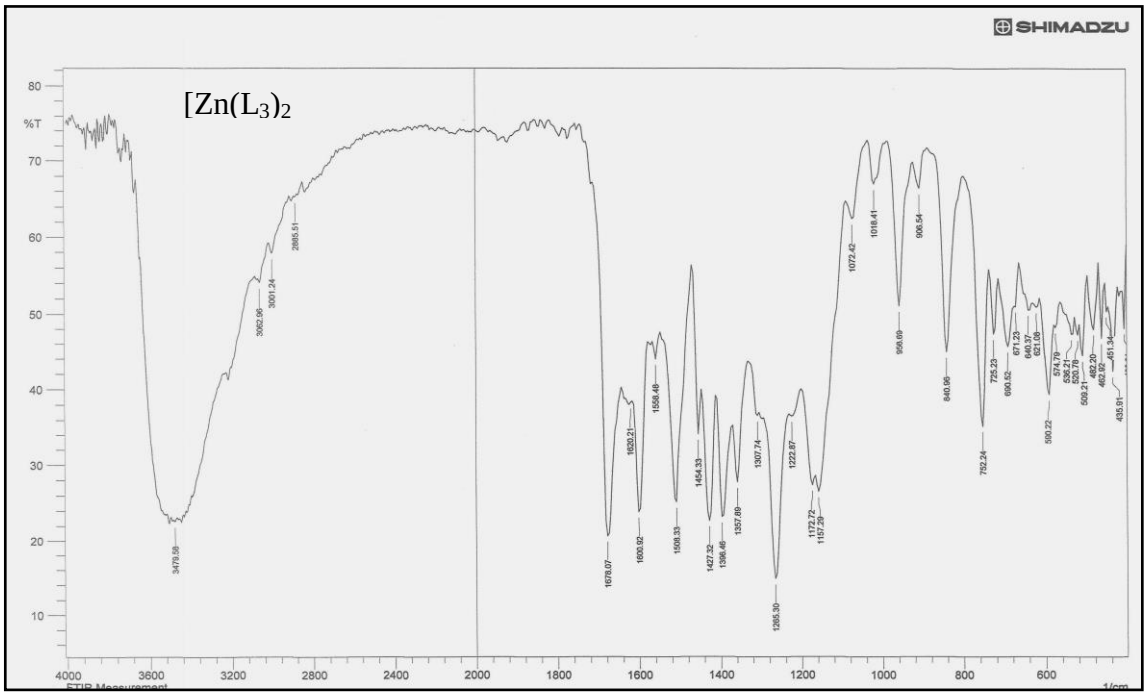

Figure (3-57): FTIR spectrum of the $[Zn(L_3)_2]$ complex.

3.9.6.4. FT-IR spectra of azo ligand (L_4) metal chelates

Azo ligand (L_4), Figure (3-25), and their metal chelates, Figures (3-58) to (3-61) have been collated, and the data was recorded in Table (3-19). Ligand spectrum exhibited bands at 3484 cm^{-1} and 3414 cm^{-1} which were assigned to asymmetric and symmetric stretching of $\upsilon(NH_2)$ respectively, at the spectra of all produced compounds pointed out the deprotonation for amino group toυ(NH) group which appeared at lower frequency because of coordination with metal ion[162]. The band at 1639 cm^{-1} due to υ(C=N) group, this band has been removed to lower frequency implying the coordination with metal ion[163]. Bands at 1593 cm^{-1} and 1562 cm^{-1} described to vibration of υ(C=C), the band at 1446 cm^{-1} lead to frequency of υ(N=N), into lower wave number for change during shape at spectra for all produced compounds [164]. Bands at 1508 cm^{-1} and 1332 cm^{-1} which assigned to vibration of asymmetric and symmetric of $\upsilon(NO_2)$[125]. Stretching frequency bands to metal-nitrogen more assured by the existence to the bands at rate 424-486 cm^{-1}[165,166].

Table (3-19): Infrared spectral data for the azo ligand (L_4) and their metal chelates (cm^{-1}).

Compounds	$\upsilon(NH_2)$ $\upsilon(NH)$	$\upsilon(C=N)$	$\upsilon(C=C)$ $\upsilon(N=N)$	$\delta(NO_2)_{as.s}$	(M–N)
Ligand(L_4)	3484 s. 3414 sh. –	1639 sh.	1593 sh. 1562 sh. 1446 s.	1508 sh. 1334 sh.	–
$[Co(L_4)_2]$	– 3383 br.	1617 sh.	1593 sh. 1560 sho. 1427 sh.	1512 sh. 1338 s.	486 w. 474 w.
$[Ni(L_4)_2]$	– 3394 br.	1630 sho.	1593 s. 1561 sho. 1427 sh.	1512 sh. 1338 sh.	455 w. 424 w.
$[Cu(L_4)_2]$	– 3379 br.	1627 sh.	1593 sh. 1558 sh. 1427 sh.	1512 sh. 1334 sh.	474 w. 462 w.
$[Zn(L_4)_2]$	– 3352 br.	1608 sh.	1597 s. 1558 sh. 1427 sh.	1512 s. 1338 s.	462 w. 435 w.

As= asymmetry, s= symmetry, br= broad, sh= sharp, s= strong, w= weak, sho= shoulder

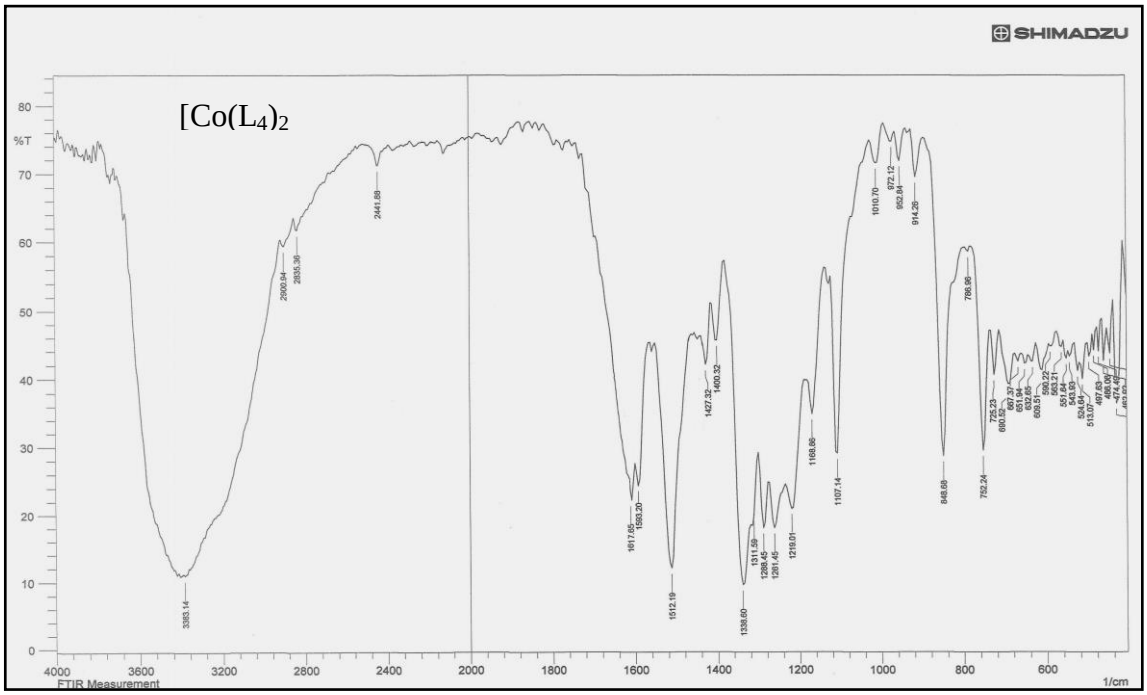

Figure (3-58): FTIR spectrum of the $[Co(L_4)_2]$ complex.

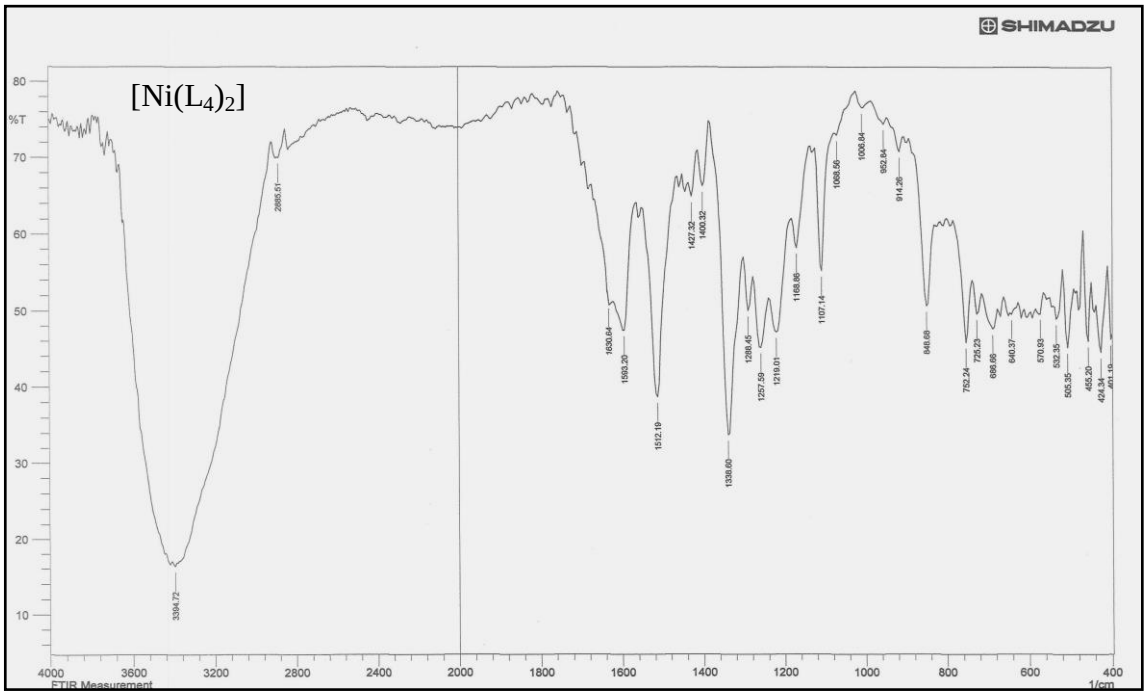

Figure (3-59): FTIR spectrum of the $[Ni(L_4)_2]$ complex.

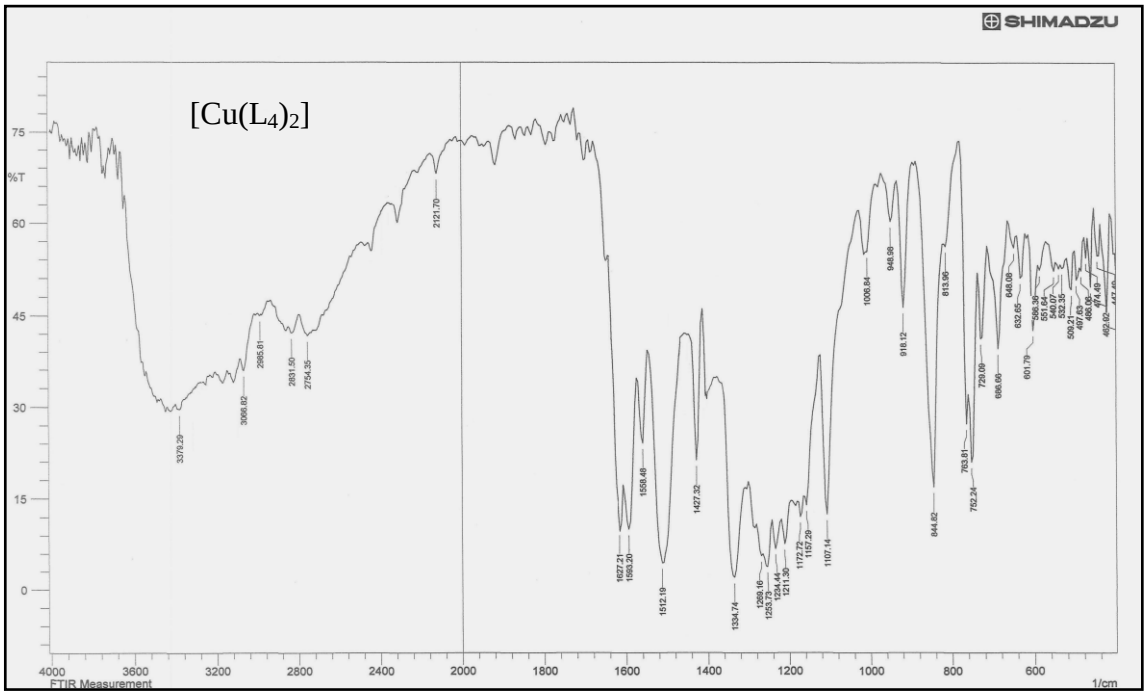

Figure (3-60): FTIR spectrum of the $[Cu(L_4)_2]$ complex.

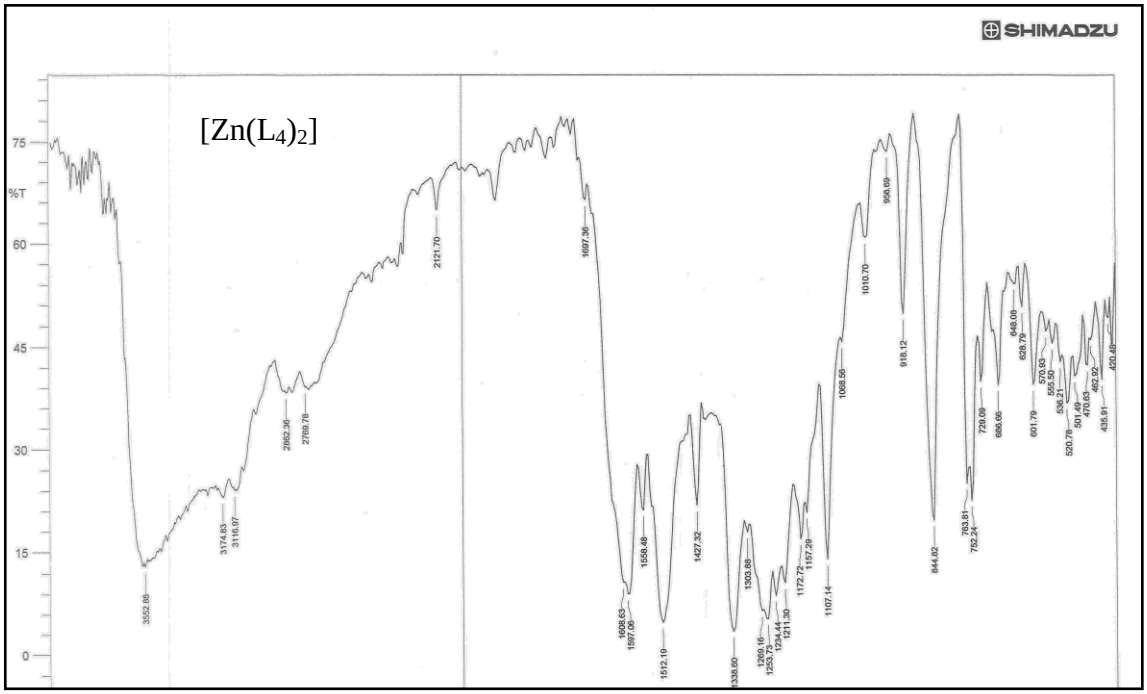

Figure (3-61): FTIR spectrum of the $[Zn(L_4)_2]$ complex.

3.9.6.5. FT-IR spectra of mixed ligand (L_1, L_2) metal chelates

Mixed ligands metal chelates, Figures (3-62) to (3-65) shows disappearance of υ(OH) frequency in ligand (L_1) and deprotonation for amino group in ligand (L_2) at the spectra of all produced compounds lead to coordinate with metal ion[167]. Band at 1674 cm^{-1} due to υ(C=O) of acetyl group, no significant change in this band was noticed, the possibility that coordination occur via the donating atom in this group was excluded[168]. Bands presented at (1593-1624) cm^{-1} because of υ(C=O) of pyrazole ring, removed to lower frequency implying the coordination with metal ion[169]. Bands at (1487-1527) cm^{-1} lead to frequency of υ(N=N)[170]. Stretching frequency bands to metal-nitrogen on other than metal-oxygen more[171,172] assured by the existence to the bands at rate 439-497 cm^{-1}, see Table (3-20).

Table (3-20): Infrared spectral data for mixed ligand (L_1, L_2) metal chelates (cm^{-1}).

Compounds	υ(NH_2) υ(NH)	υ(OH)	υ(C=O) acetyl υ(C=O) amide	υ(N=N)	υ(M–N) υ(M–O)
Ligand(L_1)	– –	3410 br.	– 1666 sh.	1585 sh.	–
Ligand(L_2)	3487 sh. 3414 sh.	–	1678 s. 1657 sho.	1512 sho.	–
[Co(L_1)(L_2)]	– 3448 br.	–	1674 s. 1624 sho. 1600 s.	1519 s. 1489 sh.	476 w. 443 w.
[Ni(L_1)(L_2)]	– 3433 br.	–	1674 s. 1622 s. 1593 s.	1512 sh. 1488 sho.	476 w. 447 w.
[Cu(L_1)(L_2)]	– 3360 br.	–	1674 s. 1612 s. 1593 sho.	1516 sh. 1488 sho.	482 w. 439 w.
[Zn(L_1)(L_2)]	– 3479 br.	–	1674 sho. 1624 s. 1597 s.	1527 s. 1487 s.	497 w. 478 w.

br = broad, sh = sharp, s = strong, w = weak, sho =shoulder

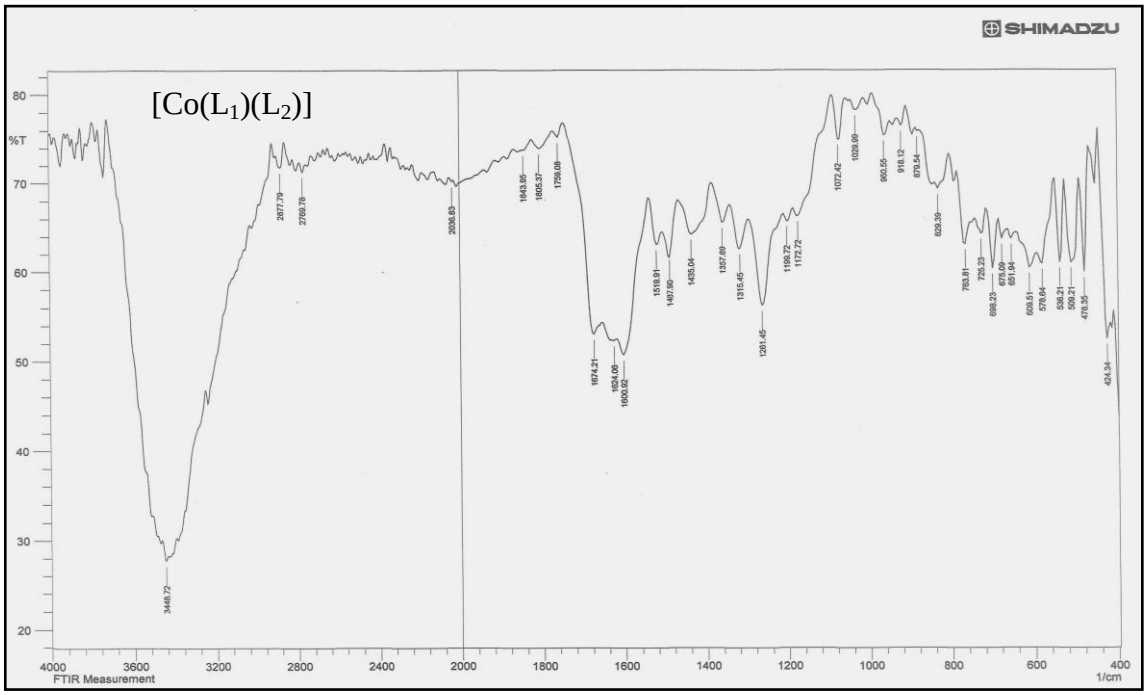

Figure (3-62): FTIR spectrum of the [Co(L_1)(L_2)] complex.

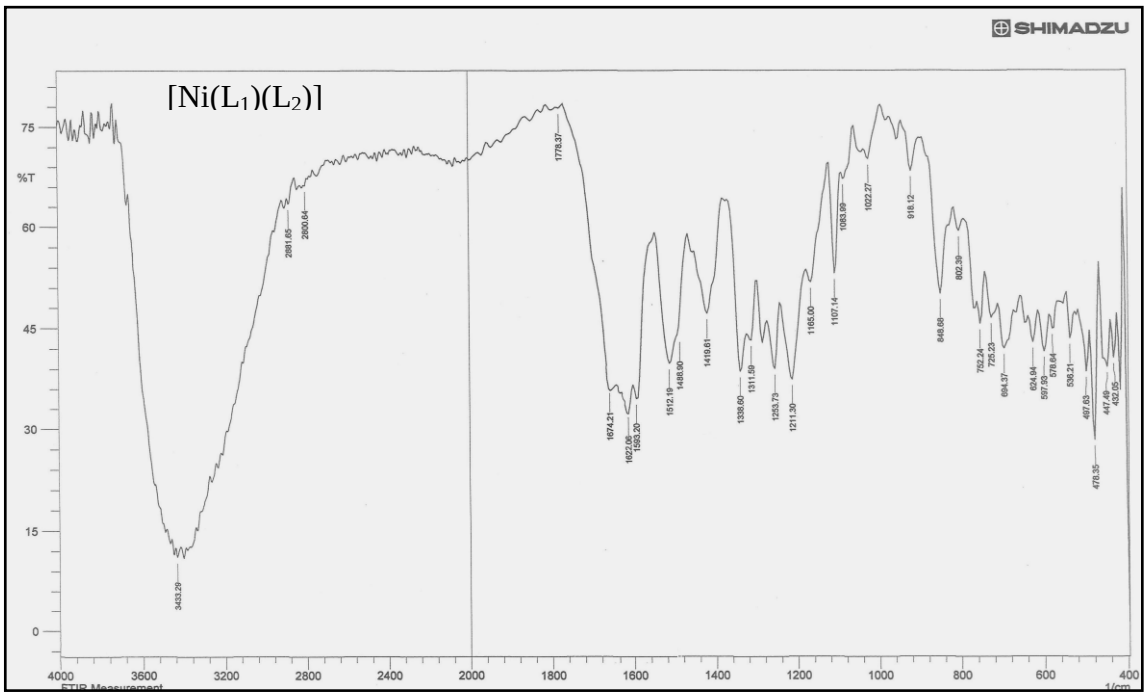

Figure (3-63): FTIR spectrum of the [Ni(L_1)(L_2)] complex.

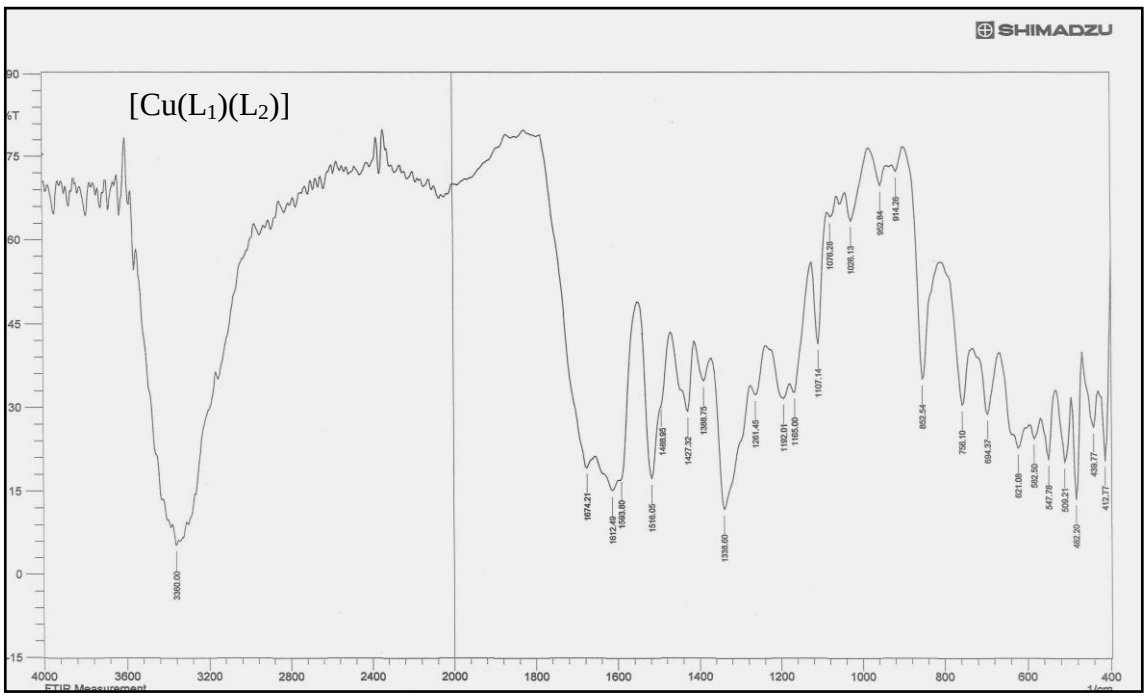

Figure (3-64): FTIR spectrum of the [Cu(L_1)(L_2)] complex.

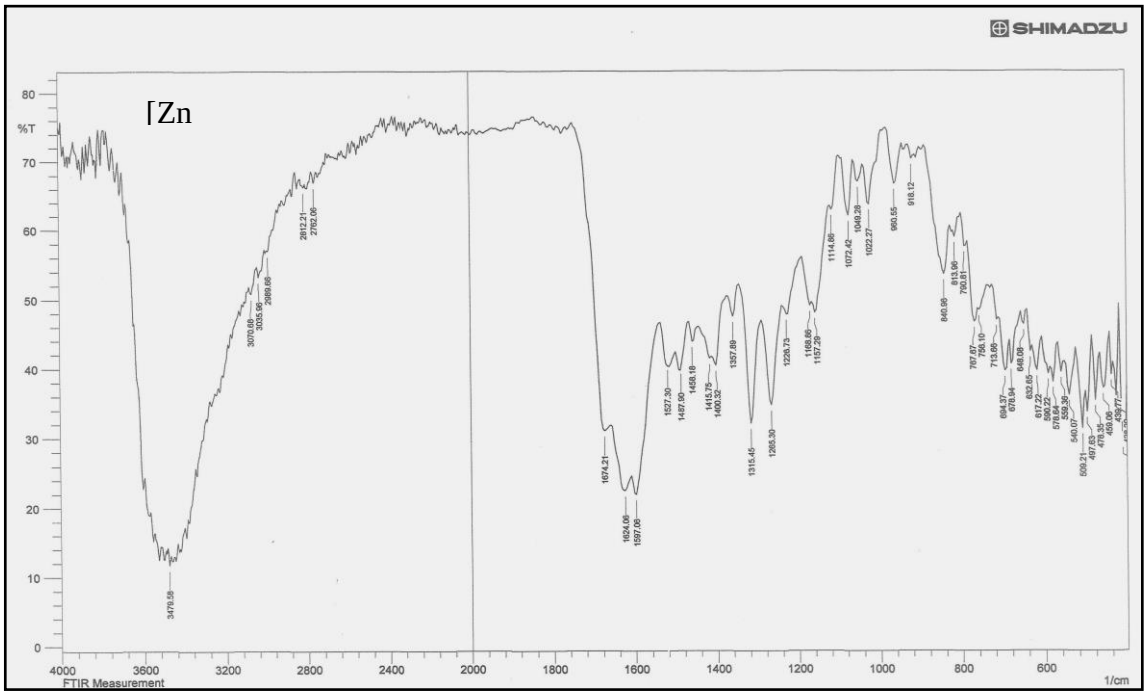

Figure (3-65): FTIR spectrum of the [Zn(L_1)(L_2)] complex.

3.9.6.6. FT-IR spectra of mixed ligand (L_3, L_4) metal chelates

Mixed ligands metal chelates, Table (3-21) and Figures (3-66) to (3-69) shows deprotonation for amino group at the spectra of all produced compounds described to coordinate with metal ion[173]. Band in spectrum of (L_3) at 1678 cm^{-1} due to υ(C=O) of acetyl group, no significant change in this band was noticed, the possibility that coordination occur via the donating atom in this group was excluded[174]. Bands presented at (1597-1643) cm^{-1} because of υ(C=N) of thiazole ring, removed to lower frequency implying the coordination with metal ion[175]. Bands at 1423 and 1427 cm^{-1} lead to υ(N=N) vibration[176]. Bands at 1334-1512 cm^{-1} assigned to vibration of asymmetric and symmetric of υ(NO_2)[125]. Frequency bands to metal-nitrogen assured by the existence to the bands at rate 443-493 cm^{-1}[177,178].

Table (3-21): Infrared spectral data for mixed ligand (L_3, L_4) metal chelates (cm^{-1}).

Compounds	$\upsilon(NH_2)$ $\upsilon(NH)$	$\upsilon(C=O)$	$\upsilon(C=N)$ $\upsilon(N=N)$	$\upsilon(NO_2)_{as.s}$	$\upsilon(M–N)$
Ligand(L_3)	3483 sh. 3414 sh. –	1678 sho.	1654 s. 1531 s.	–	–
Ligand(L_4)	3484 s. 3414 sh.	–	1639 sh. 1446 s.	1508 sh. 1334 sh.	–
[Co(L_3)(L_4)]	– 3421 br.	1670 s.	1642 sho. 1600 s. 1423 sh. 1400 sh.	1512 sh. 1338 sh.	482 w. 443 w.
[Ni(L_3)(L_4)]	– 3417 br.	1678 sh.	1643 sh. 1597 sh. 1423 sh.	1512 sh. 1334 sh.	486 w. 451 w.
[Cu(L_3)(L_4)]	– 3448 br.	1674 sho.	1635 s. 1597 sho. 1450 sh. 1427 sh.	1516 s. 1338 s.	455 w. 443 w.
[Zn(L_3)(L_4)]	– 3448 br.	1674 sh.	1643 sho. 1600 s. 1454 sh. 1427 sh.	1512 sh. 1338 sh.	493 w. 459 w.

As= asymmetry, s= symmetry, br= broad, sh= sharp, s= strong, w= weak, sho=shoulder.

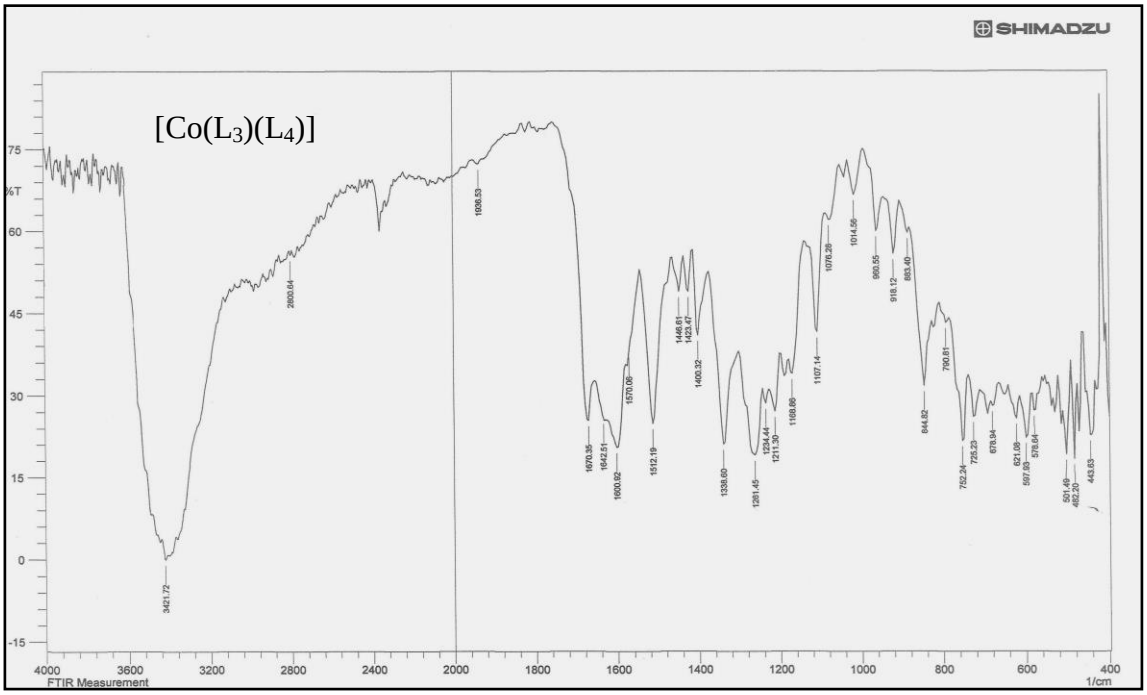

Figure (3-66): FTIR spectrum of the [Co(L_3)(L_4)] complex.

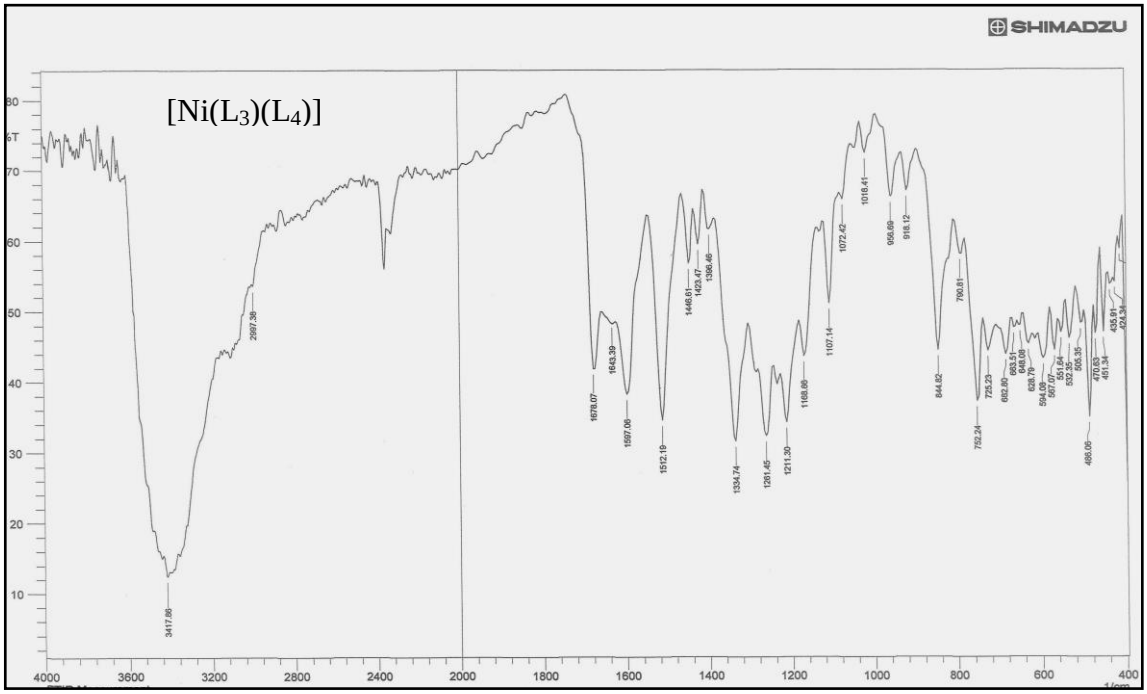

Figure (3-67): FTIR spectrum of the [Ni(L_3)(L_4)] complex.

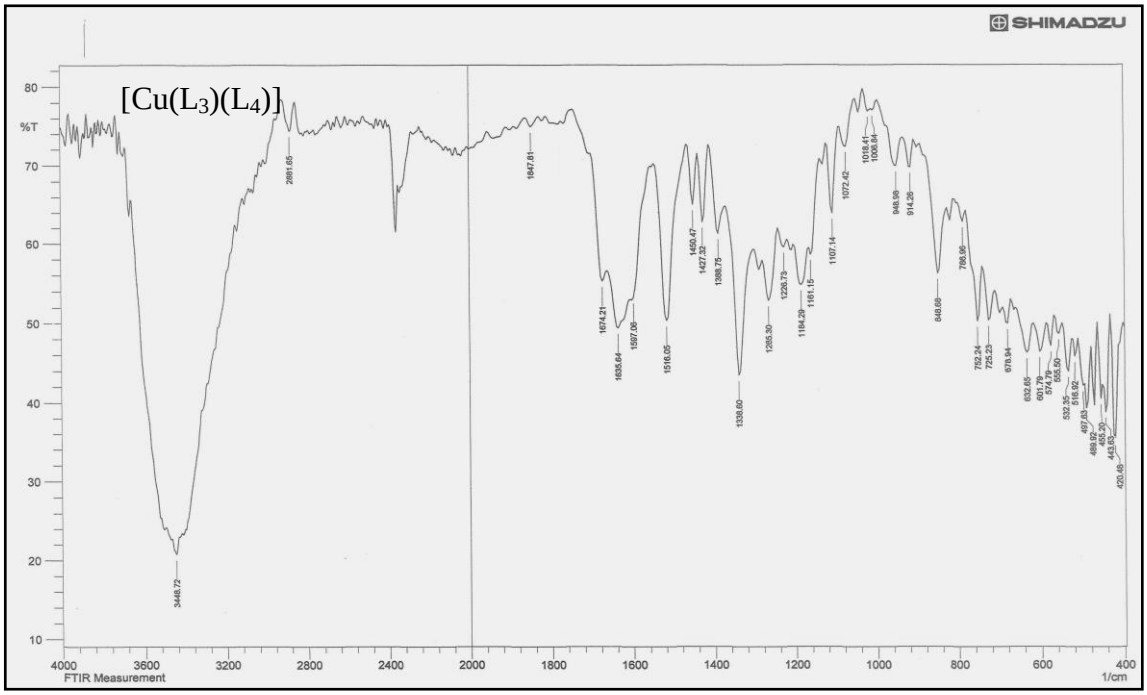

Figure (3-68): FTIR spectrum of the [Cu(L_3)(L_4)] complex.

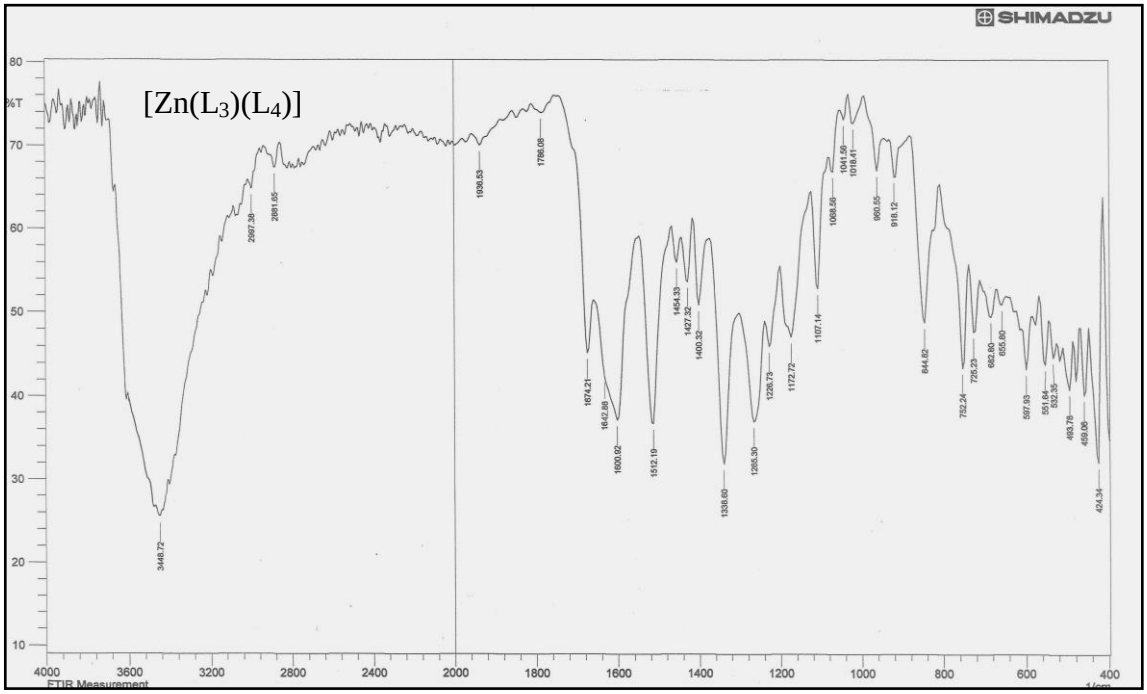

Figure (3-69): FTIR spectrum of the [Zn(L_3)(L_4)] complex.

3.9.7. UV-Vis spectra of complexes

3.9.7.1. UV-Vis spectra of azo ligand (L_1) metal chelates

UV-Vis spectra to the produced compounds melted at ethanol (10^{-3} mole/L) were gauged as well the datum formed are listed at Table (3-22), see Figures (3-70) to (3-73).

Co^{II} spectrum appeared three peaks at (244 nm) (40983 cm^{-1}) (ε_{max}=1760 $l.mole^{-1}.cm^{-1}$), (350 nm) (28571 cm^{-1}) (ε_{max}=2119 $l.mole^{-1}.cm^{-1}$) and (460 nm) (21739 cm^{-1}) (ε_{max}=2119 $l.mole^{-1}.cm^{-1}$) attributed to intra ligand and (M→L) charge transfer, new peaks at (732 nm) (13661 cm^{-1}) (ε_{max}=5 $l.mole^{-1}.cm^{-1}$), (868 nm) (11520 cm^{-1}) (ε_{max}=8 $l.mole^{-1}.cm^{-1}$) and (978 nm) (102240 cm^{-1}) (ε_{max}=90 $l.mole^{-1}.cm^{-1}$) described to electronic transition type $^4T_{1g(F)}\rightarrow{}^4T_{1g(P)}$ (υ_3), $^4T_{1g(F)}\rightarrow{}^4A_{2g(F)}$ (υ_2), and $^4T_{1g(F)}\rightarrow{}^4T_{2g(F)}$ (υ_1) respectively[179].

Ni^{II} complex exhibited three absorption peaks at (246 nm) (40650 cm^{-1}) (ε_{max}=1482 $l.mole^{-1}.cm^{-1}$), (354 nm) (28248 cm^{-1}) (ε_{max}=1775 $l.mole^{-1}.cm^{-1}$) and (458 nm) (21834 cm^{-1}) (ε_{max}=247 $l.mole^{-1}.cm^{-1}$) which were assigned to intra ligand and (M→L) charge transfer. Other peaks at (724 nm) (13812 cm^{-1}) (ε_{max}=19 $l.mole^{-1}.cm^{-1}$), (894 nm) (11185 cm^{-1}) (ε_{max}=3 $l.mole^{-1}.cm^{-1}$) and (982 nm) (10183 cm^{-1}) (ε_{max}=25 $l.mole^{-1}.cm^{-1}$) were assigned to electronic transition type $^3A_{2g}\rightarrow{}^3T_{1g(P)}$($\upsilon_3$), $^3A_{2g}\rightarrow{}^3T_{1g(F)}$ (υ_2) and $^3A_{2g}\rightarrow{}^3T_{2g(F)}$ (υ_1) respectively[180].

Cu^{II} complex showed peaks at (246 nm) (40650 cm^{-1}) (ε_{max}=1242 $l.mole^{-1}.cm^{-1}$), (352 nm) (28409 cm^{-1}) (ε_{max}=1570 $l.mole^{-1}.cm^{-1}$) and (481 nm) (20790 cm^{-1}) (ε_{max}=178 $l.mole^{-1}.cm^{-1}$) due to intra ligand and (M→ L) charge transfer, while peak at (980 nm) (10204 cm^{-1}) (ε_{max}=18 $l.mole^{-1}.cm^{-1}$) described to electronic transition type $^2E_g\rightarrow{}^2T_{2g}$[181] .

Spectrum of Zn^{II} complex showed peaks at (246 nm) (40650 cm^{-1}) (ε_{max}=1531 $l.mole^{-1}.cm^{-1}$), (354 nm) (28248 cm^{-1}) (ε_{max}=1914 $l.mole^{-1}.cm^{-1}$) and (450 nm) (22222 cm^{-1}) (ε_{max}=378 $l.mole^{-1}.cm^{-1}$) lead to intra ligand and (M→L) charge transfer. Magnetic susceptibility showed that the complex has diamagnetic moments, because d-d transition are not possible hence electronic spectra did not give any fruitful information, in fact this result is a good agreement with previous work of octahedral geometry[182].

Table (3-22): UV-Vis spectral data for azo ligand (L_1) metal chelates.

Compounds	λ_{max} (nm)	Abs.	Wave number (cm^{-1})	ε_{max} ($L.mol^{-1}.cm^{-1}$)	Transition Assignment
Ligand(L_1)	242	1.894	41322	1894	π-π^*
	356	1.853	28089	1853	π-π^*
	414	1.177	24154	1177	n-π^*
$[Co(L_1)_2]$	244	1.760	40983	1760	π-π^*
	350	2.119	28571	2119	π-π^*
	460	0.288	21739	288	(M→L)C.T
	732	0.005	13661	5	$^4T_{1g(F)} \rightarrow {}^4T_{1g(P)}$
	868	0.008	11520	8	$^4T_{1g(F)} \rightarrow {}^4A_{2g(F)}$
	978	0.090	10224	90	$^4T_{1g(F)} \rightarrow {}^4T_{2g(F)}$
$[Ni(L_1)_2]$	246	1.482	40650	1482	π-π^*
	354	1.775	28248	1775	π-π^*
	458	0.247	21834	247	(M→L)C.T
	724	0.019	13812	19	$^3A_{2g(F)} \rightarrow {}^3T_{1g(P)}$
	894	0.003	11185	3	$^3A_{2g(F)} \rightarrow {}^3T_{1g(F)}$
	982	0.025	10183	25	$^3A_{2g(F)} \rightarrow {}^3T_{2g(F)}$
$[Cu(L_1)_2]$	246	1.242	40650	1242	π-π^*
	352	1.570	28409	1570	π-π^*
	481	0.178	20790	178	(M→L)C.T
	980	0.018	10204	18	$^2E_g \rightarrow {}^2T_{2g}$
$[Zn(L_1)_2]$	246	1.531	40650	1531	π- π^*
	354	1.914	28248	1914	π- π^*
	450	0.368	22222	368	(M→L) C.T

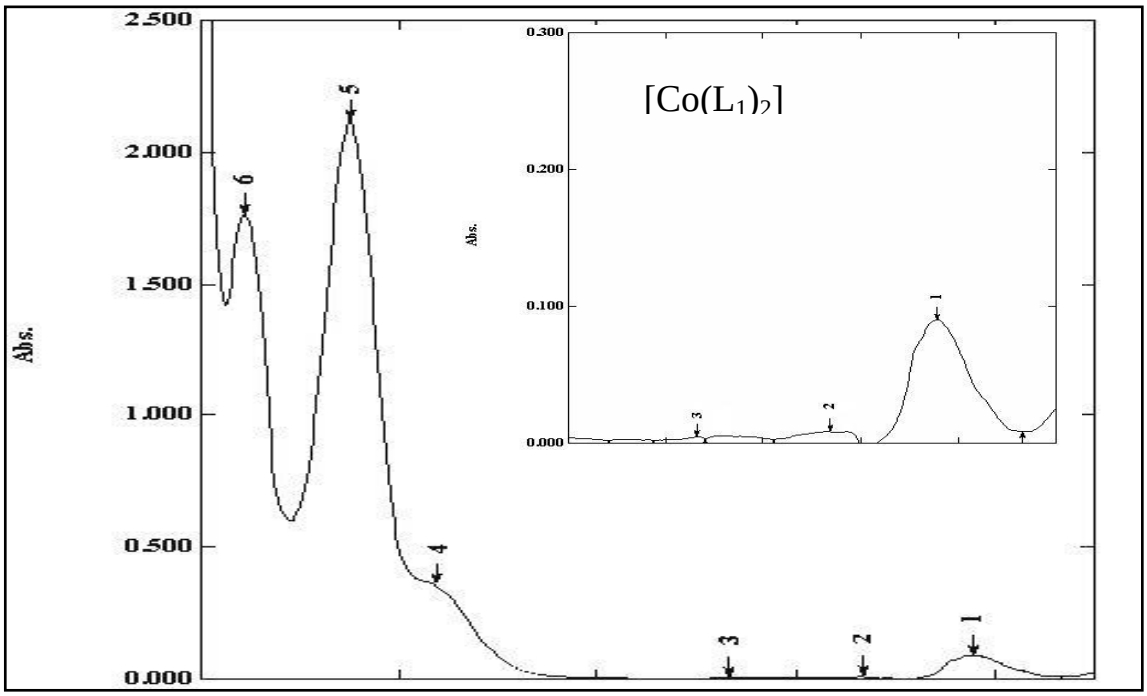

Figure (3-70): UV-Vis spectrum for $[Co(L_1)_2]$ complex.

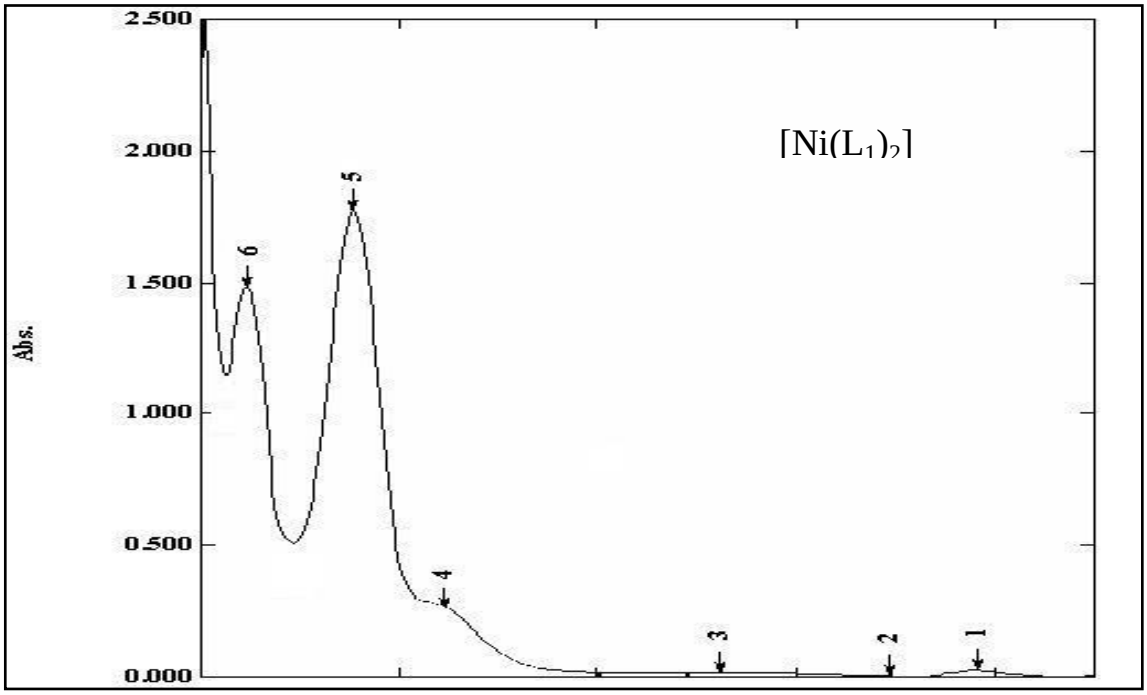

Figure (3-71): UV-Vis spectrum for $[Ni(L_1)_2]$ complex.

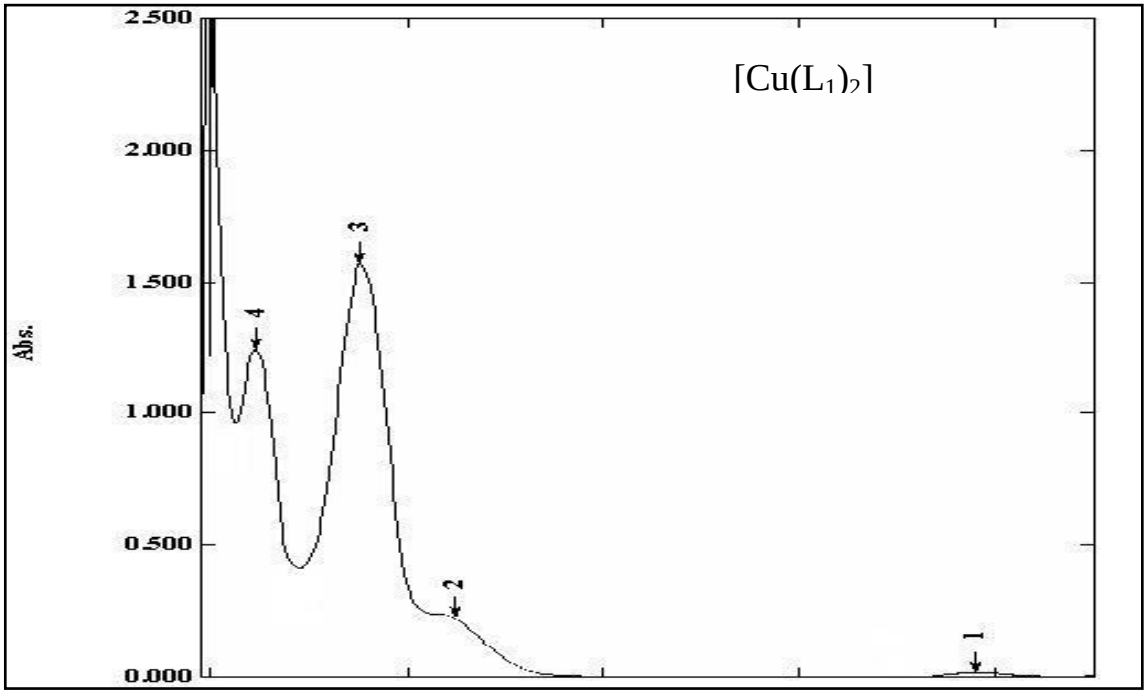

Figure (3-72): UV-Vis spectrum for $[Cu(L_1)_2]$ complex.

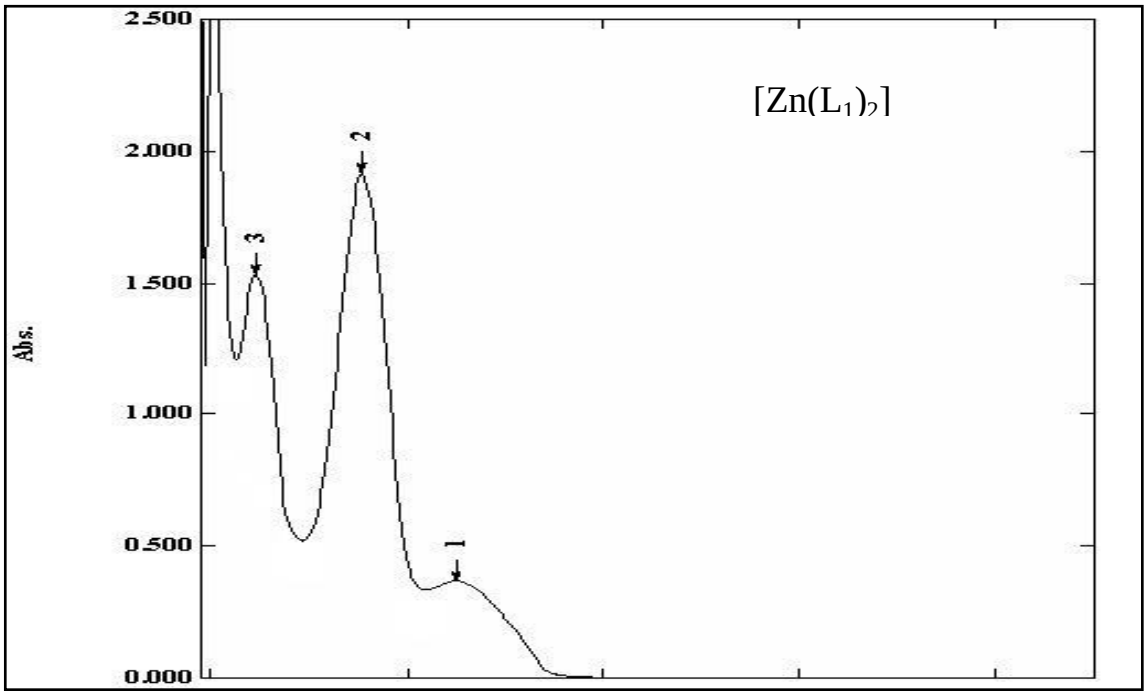

Figure (3-73): UV-Vis spectrum for $[Zn(L_1)_2]$ complex.

3.9.7.2. UV-Vis spectra of azo ligand (L_2) metal chelates

UV-Vis spectra to the produced azo ligand (L_2) and metal chelates melted at ethanol (10^{-3} mole/L) were gauged as well the datum formed are recorded at Table (3-23) and Figures (3-74) to (30-77).

Co^{II} spectrum appeared two peaks at (254 nm) (39370 cm^{-1}) (ε_{max}=817 $l.mole^{-1}.cm^{-1}$) and (442 nm) (22624 cm^{-1}) (ε_{max}=368 $l.mole^{-1}.cm^{-1}$) attributed to intra ligand and (M→L) charge transfer. New peaks at (572 nm) (17482 cm^{-1}) (ε_{max}=185 $l.mole^{-1}.cm^{-1}$), (858 nm) (11655 cm^{-1}) (ε_{max}=17 $l.mole^{-1}.cm^{-1}$) and (978 nm) (10224 cm^{-1}) (ε_{max}= 95 $l.mole^{-1}.cm^{-1}$) which were assigned to electronic transition type $^4T_{1g(F)}\rightarrow{}^4T_{1g(P)}(\upsilon_3)$, $^4T_{1g(F)}\rightarrow{}^4A_{2g}$ (υ_2) and $^4T_{1g(F)}\rightarrow{}^4T_{2g(F)}$ (υ_1) respectively[183].

Ni^{II} complex displayed three absorption peaks at (240 nm) (41666 cm^{-1}) (ε_{max}=1308 $l.mole^{-1}.cm^{-1}$), (298 nm) (33557 cm^{-1}) (ε_{max}=1361 $l.mole^{-1}.cm^{-1}$) and (440 nm) (22727 cm^{-1}) (ε_{max}=917 $l.mole^{-1}.cm^{-1}$) which described to intra ligand and (M→L) charge transfer. Peaks at (592 nm) (16891 cm^{-1}) (ε_{max}=341 $l.mole^{-1}.cm^{-1}$), (886 nm) (11286 cm^{-1}) (ε_{max}=20 $l.mole^{-1}.cm^{-1}$) and (978 nm) (10224 cm^{-1}) (ε_{max}=111 $l.mole^{-1}.cm^{-1}$) which were assigned to electronic transition type $^3A_{2g}\rightarrow{}^3T_{1g(P)}(\upsilon_3)$,$^3A_{2g}\rightarrow{}^3T_{1g(F)}$ (υ_2) and $^3A_{2g}\rightarrow{}^3T_{2g(F)}$ (υ_1) respectively[184].

Cu^{II} complex showed peaks at (236 nm) (42372 cm^{-1}) (ε_{max}=2155 $l.mole^{-1}.cm^{-1}$), (296 nm) (33783 cm^{-1}) (ε_{max}=17857 $l.mole^{-1}.cm^{-1}$) and (560 nm) (17857 cm^{-1}) (ε_{max}=640 $l.mole^{-1}.cm^{-1}$) due to intra ligand and (M→L) charge transfer, while peak at (974 nm) (10266 cm^{-1}) (ε_{max}=137 $l.mole^{-1}.cm^{-1}$) attributed to electronic transition type $^2E_g\rightarrow{}^2T_{2g}$[185].

Zn^{II} complex showed peaks at (294 nm) (34013 cm^{-1}) (ε_{max}=1571 $l.mole^{-1}.cm^{-1}$) and (476 nm) (21008 cm^{-1}) (ε_{max}=505 $l.mole^{-1}.cm^{-1}$) lead to intra ligand and (M→L) charge transfer, and the magnetic susceptibility

shows that the complex has diamagnetic moments, because d-d transition are not possible hence electronic spectra did not give any fruitful information, in fact this result is a good agreement with previous work of octahedral geometry[186].

Table (3-23): UV-Vis spectral data for azo ligand (L_2) metal chelates.

Compounds	λ_{max} (nm)	Abs.	Wave number (cm^{-1})	ε_{max} ($L.mol^{-1}.cm^{-1}$)	Transition Assignment
Ligand(L_2)	298	2.272	33557	2272	π-π^*
	432	1.479	23148	1479	n-π^*
$[Co(L_2)_2].H_2O$	254	0.817	39370	817	π-π^*
	442	0.368	22624	368	(M→L) C.T
	572	0.185	17482	185	$^4T_{1g(F)}\rightarrow{}^4T_{1g(P)}$
	858	0.017	11655	17	$^4T_{1g(F)}\rightarrow{}^4A_{2g(F)}$
	978	0.095	10224	95	$^4T_{1g(F)}\rightarrow{}^4T_{2g(F)}$
$[Ni(L_2)_2].H_2O$	240	1.308	41666	1308	π-π^*
	298	1.361	33557	1361	π-π^*
	440	0.917	22727	917	(M→L) C.T
	592	0.341	16891	341	$^3A_{2g(F)}\rightarrow{}^3T_{1g(P)}$
	886	0.020	11286	20	$^3A_{2g(F)}\rightarrow{}^3T_{1g(F)}$
	978	0.111	10224	111	$^3A_{2g(F)}\rightarrow{}^3T_{2g(F)}$
$[Cu(L_2)_2].H_2O$	236	2.155	42372	2155	π-π^*
	296	1.677	33783	1677	π-π^*
	560	0.640	17857	640	(M→L) C.T
	974	0.137	10266	137	$^2E_g\rightarrow{}^2T_{2g}$
$[Zn(L_2)_2].H_2O$	294	1.571	34013	1571	π- π^*
	476	0.505	21008	505	(M→L) C.T

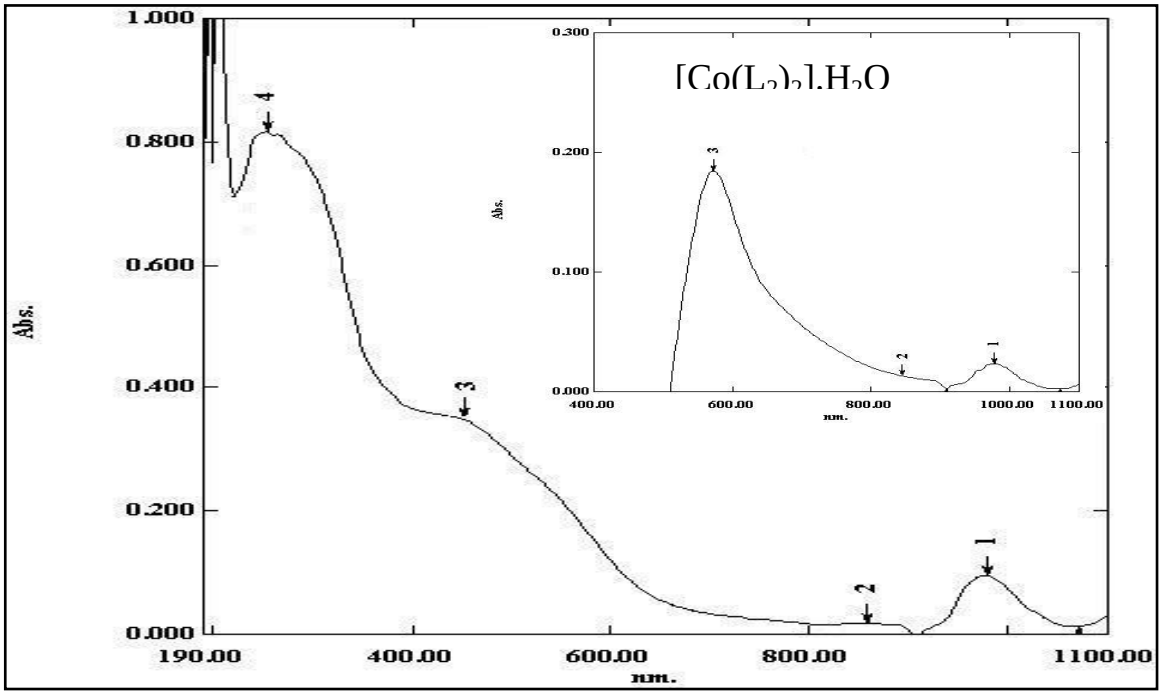

Figure (3-74): UV-Vis spectrum for $[Co(L_2)_2].H_2O$ complex.

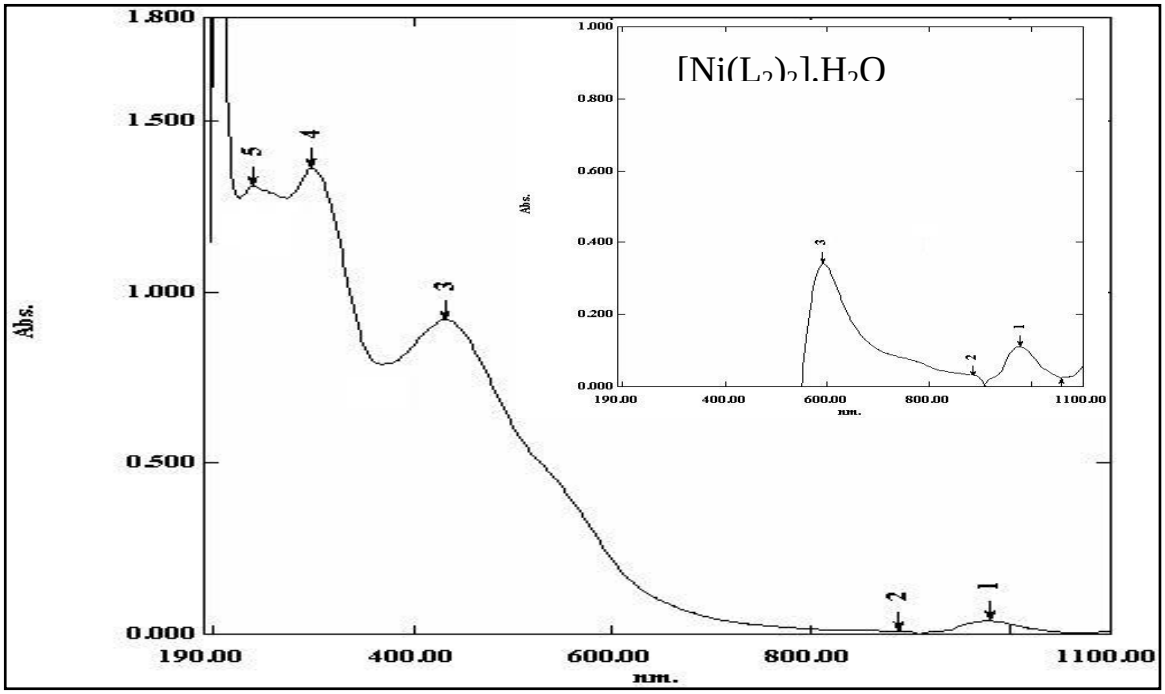

Figure (3-75): UV-Vis spectrum for $[Ni(L_2)_2].H_2O$ complex.

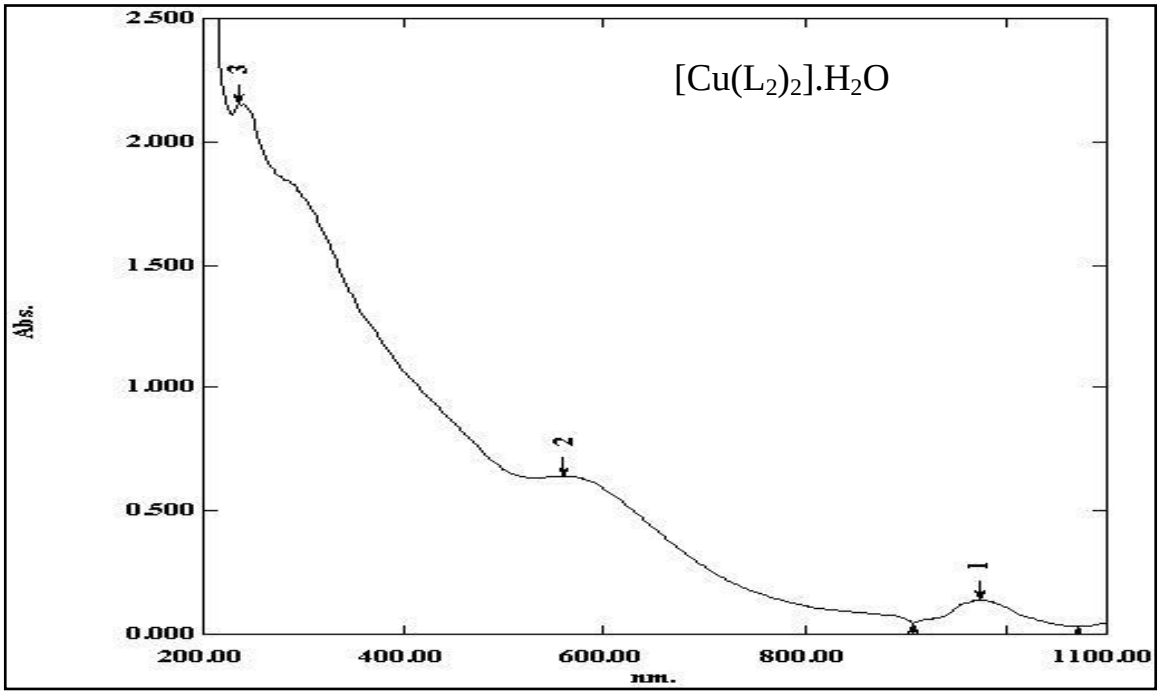

Figure (3-76): UV-Vis spectrum for $[Cu(L_2)_2].H_2O$ complex.

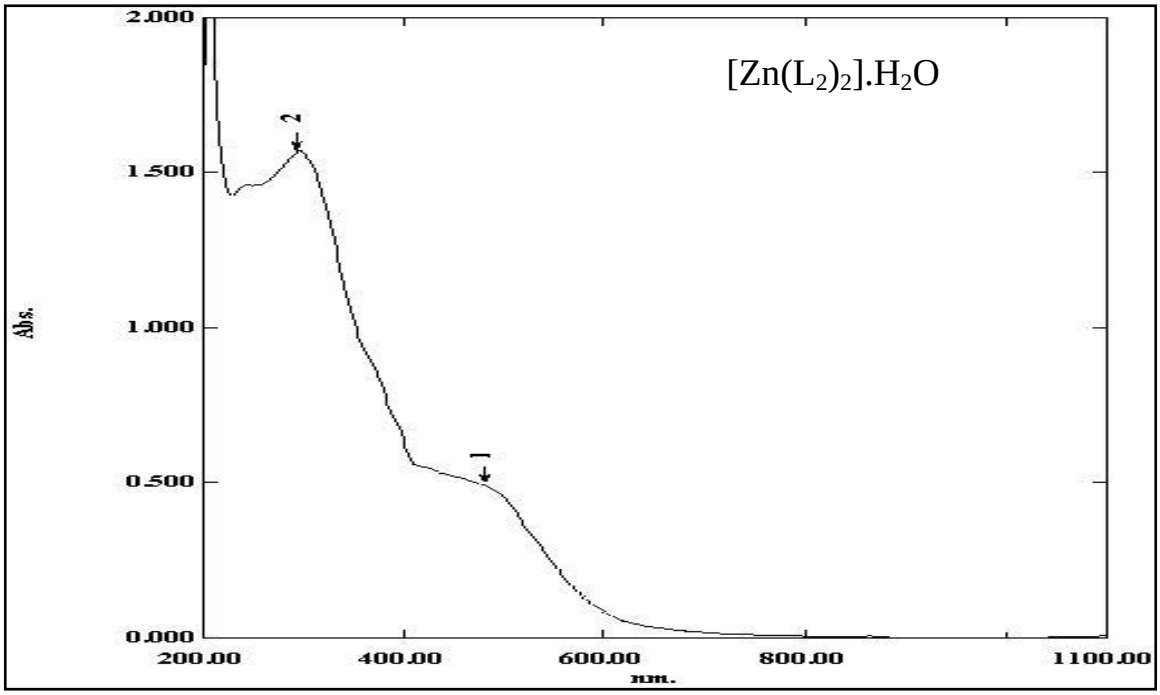

Figure (3-77): UV-Vis spectrum for $[Zn(L_2)_2].H_2O$ complex.

3.9.7.3. UV-Vis spectra of azo ligand(L_3) metal chelates

UV-Vis spectra for the ligand and their metal chelates melted at ethanol (10^{-3} mole/L) were gauged as well the datum formed are listed at Table (3-24).

Co^{II} spectrum showed peaks at (217 nm) (46082 cm^{-1}) (ε_{max}=914 $l.mole^{-1}.cm^{-1}$), (271 nm) (36900 cm^{-1}) (ε_{max}=587 $l.mole^{-1}.cm^{-1}$), (418 nm) (23923 cm^{-1}) (ε_{max}=961 $l.mole^{-1}.cm^{-1}$) and (458 nm) (21834 cm^{-1}) (ε_{max}=618 $l.mole^{-1}.cm^{-1}$) attributed to intra ligand and (M→L) charge transfer, other peaks at (754 nm) (13262 cm^{-1}) (ε_{max}=6 $l.mole^{-1}.cm^{-1}$), (864 nm) (11574 cm^{-1}) (ε_{max}=9 $l.mole^{-1}.cm^{-1}$) and (978 nm) (10224 cm^{-1}) (ε_{max}=96 $l.mole^{-1}.cm^{-1}$) due to electronic transition type $^4T_{1g(F)}\rightarrow{}^4T_{1g(P)}(\upsilon_3)$, $^4T_{1g(F)}\rightarrow{}^4A_{2g}$ (υ_2) and $^4T_{1g(F)}\rightarrow{}^4T_{2g(F)}$ (υ_1), respectively[187].

Ni^{II} complex exhibited fourth absorption peaks at (220 nm) (45454 cm^{-1}) (ε_{max}=1829 $l.mole^{-1}.cm^{-1}$), (272 nm) (36764 cm^{-1}) (ε_{max}=1118 $l.mole^{-1}.cm^{-1}$), (400 nm) (25000 cm^{-1}) (ε_{max}=2276 $l.mole^{-1}.cm^{-1}$) and (466 nm) (21459 cm^{-1}) (ε_{max}=500 $l.mole^{-1}.cm^{-1}$) which were described to intra ligand and (M→L) charge transfer. New peaks at (732 nm) (13661 cm^{-1}) (ε_{max}=4 $l.mole^{-1}.cm^{-1}$), (886 nm) (11286 cm^{-1}) (ε_{max}=6 $l.mole^{-1}.cm^{-1}$) and (972 nm) (10288 cm^{-1}) (ε_{max}=62 $l.mole^{-1}.cm^{-1}$) were assigned to electronic transition type $^3A_{2g}\rightarrow{}^3T_{1g(P)}$ (υ_3), $^3A_{2g}\rightarrow{}^3T_{1g(F)}$ (υ_2) and $^3A_{2g}\rightarrow{}^3T_{2g(F)}$ (υ_1) respectively[188].

Cu^{II} complex appeared peaks at (220 nm) (45454 cm^{-1}) (ε_{max}=1877 $l.mole^{-1}.cm^{-1}$), (272 nm) (36764 cm^{-1}) (ε_{max}=1138 $l.mole^{-1}.cm^{-1}$), (404 nm) (24752 cm^{-1}) (ε_{max}=1817 $l.mole^{-1}.cm^{-1}$) and (470 nm) (21276 cm^{-1}) (ε_{max}=725 $l.mole^{-1}.cm^{-1}$) lead to intra ligand and (M→L) charge transfer,

other than peak at (886 nm) (11286 cm^{-1}) (ε_{max}=75 $l.mole^{-1}.cm^{-1}$) described to electronic transition type $^2E_g \rightarrow {}^2T_{2g}$[189].

Zn^{II} complex displayed peaks at (218 nm) (45871 cm^{-1}) (ε_{max}=843 $l.mole^{-1}.cm^{-1}$), (271 nm) (36496 cm^{-1}) (ε_{max}=489 $l.mole^{-1}.cm^{-1}$), (398 nm) (25125 cm^{-1}) (ε_{max}=799 $l.mole^{-1}.cm^{-1}$) and (472 nm) (21186 cm^{-1}) (ε_{max}=247 $l.mole^{-1}.cm^{-1}$) lead to intra ligand and (M→L) charge transfer, and the magnetic susceptibility shows that the complex has diamagnetic moments, because d-d transition are not possible hence electronic spectra did not give any fruitful information, in fact this result is a good agreement with previous work of octahedral geometry[190], see Figures (3-78) to (3-81).

Table (3-24): UV-Vis spectral data for azo ligand (L_3) metal chelates.

Compounds	λ_{max} (nm)	Abs.	Wave number (cm^{-1})	ε_{max} ($L.mol^{-1}.cm^{-1}$)	Transition Assignment
Ligand(L_3)	218	1.950	45871	1950	π-π^*
	270	1.066	37037	1066	π-π^*
	396	2.039	25252	2039	π-π^*
$[Co(L_3)_2]$	217	0.914	46082	914	π-π^*
	271	0.587	36900	587	π-π^*
	418	0.961	23923	961	π-π^*
	458	0.618	21834	618	(M→L) C.T
	754	0.006	13262	6	$^4T_{1g(F)}\rightarrow{}^4T_{1g(P)}$
	864	0.009	11574	9	$^4T_{1g(F)}\rightarrow{}^4A_{2g(F)}$
	978	0.096	10224	96	$^4T_{1g(F)}\rightarrow{}^4T_{2g(F)}$
$[Ni(L_3)_2]$	220	1.829	45454	1829	π-π^*
	272	1.118	36764	1118	π-π^*
	400	2.276	25000	2276	π-π^*
	466	0.500	21459	500	(M→L) C.T
	732	0.004	13661	4	$^3A_{2g(F)}\rightarrow{}^3T_{1g(P)}$
	886	0.006	11286	6	$^3A_{2g(F)}\rightarrow{}^3T_{1g(F)}$
	972	0.062	10288	62	$^3A_{2g(F)}\rightarrow{}^3T_{2g(F)}$
$[Cu(L_3)_2]$	220	1.877	45454	1877	π-π^*
	272	1.138	36764	1138	π-π^*
	404	1.817	24752	1817	π-π^*
	470	0.725	21276	725	(M→L) C.T
	886	0.075	11286	75	$^2E_g\rightarrow{}^2T_{2g}$
$[Zn(L_3)_2]$	218	0.843	45871	843	π-π^*
	274	0.489	36496	489	π-π^*
	398	0.799	25125	799	π-π^*
	472	0.247	21186	247	(M→L) C.T

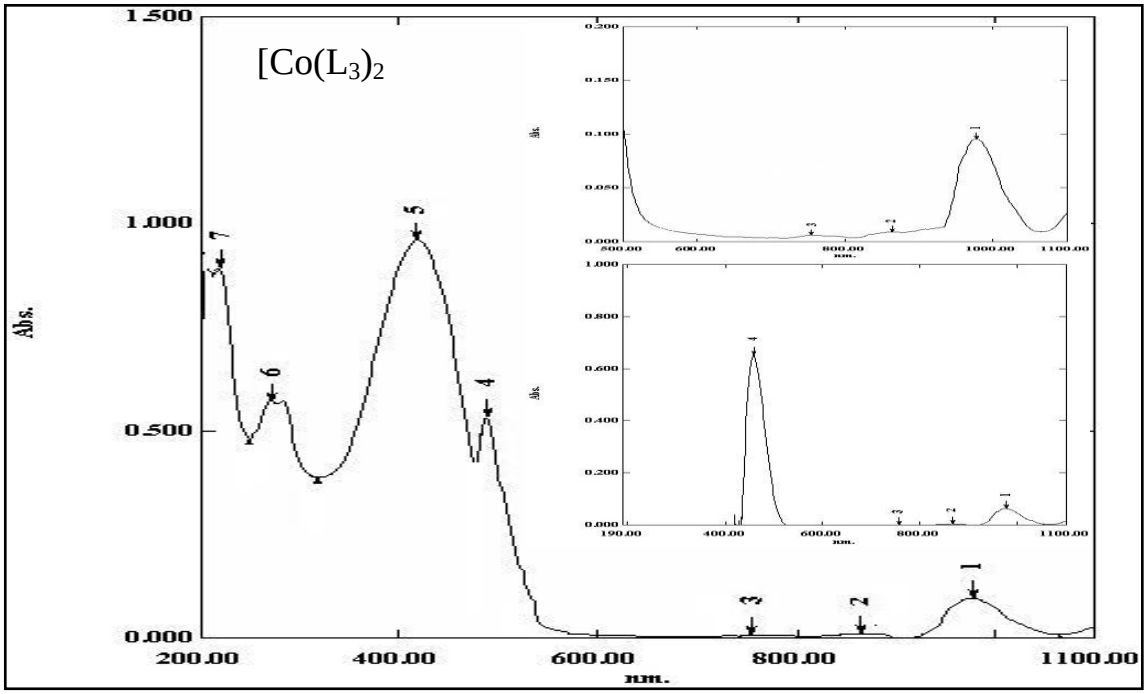

Figure (3-78): UV-Vis spectrum for $[Co(L_3)_2]$ complex.

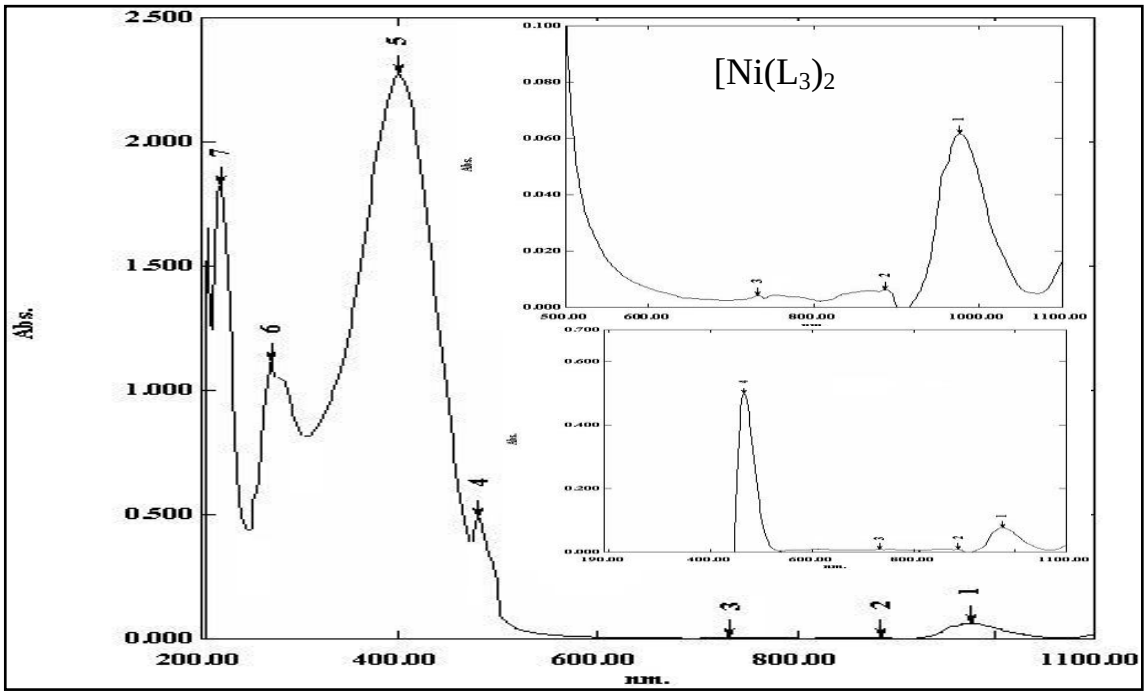

Figure (3-79): UV-Vis spectrum for $[Ni(L_3)_2]$ complex.

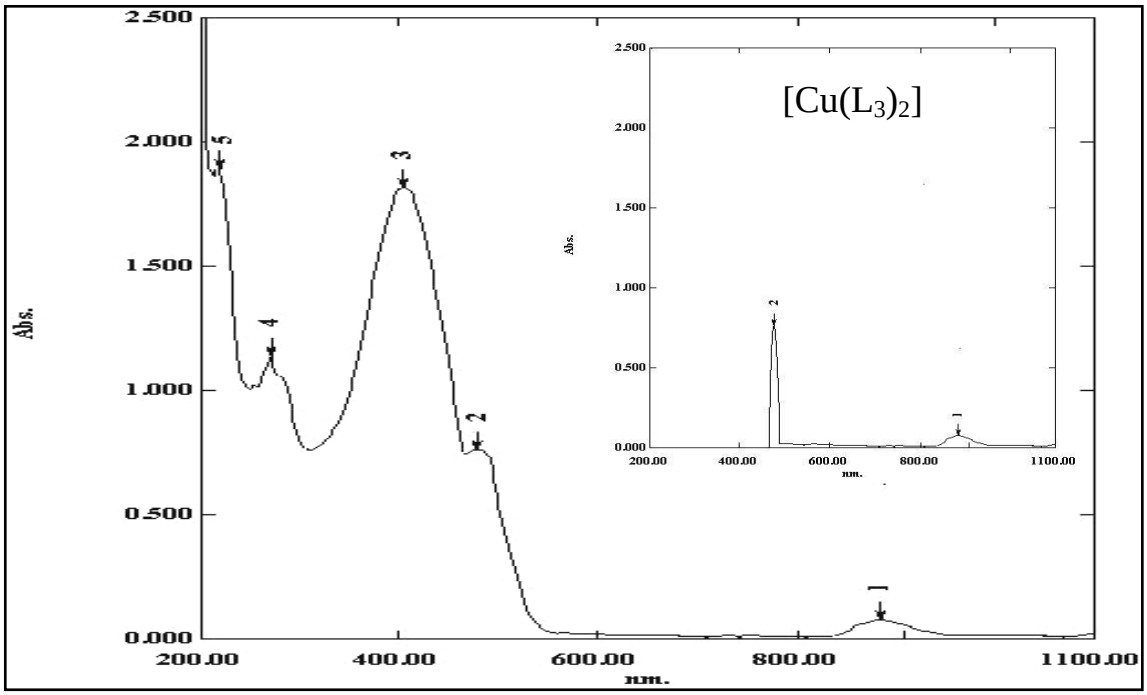

Figure (3-80): UV-Vis spectrum for $[Cu(L_3)_2]$ complex

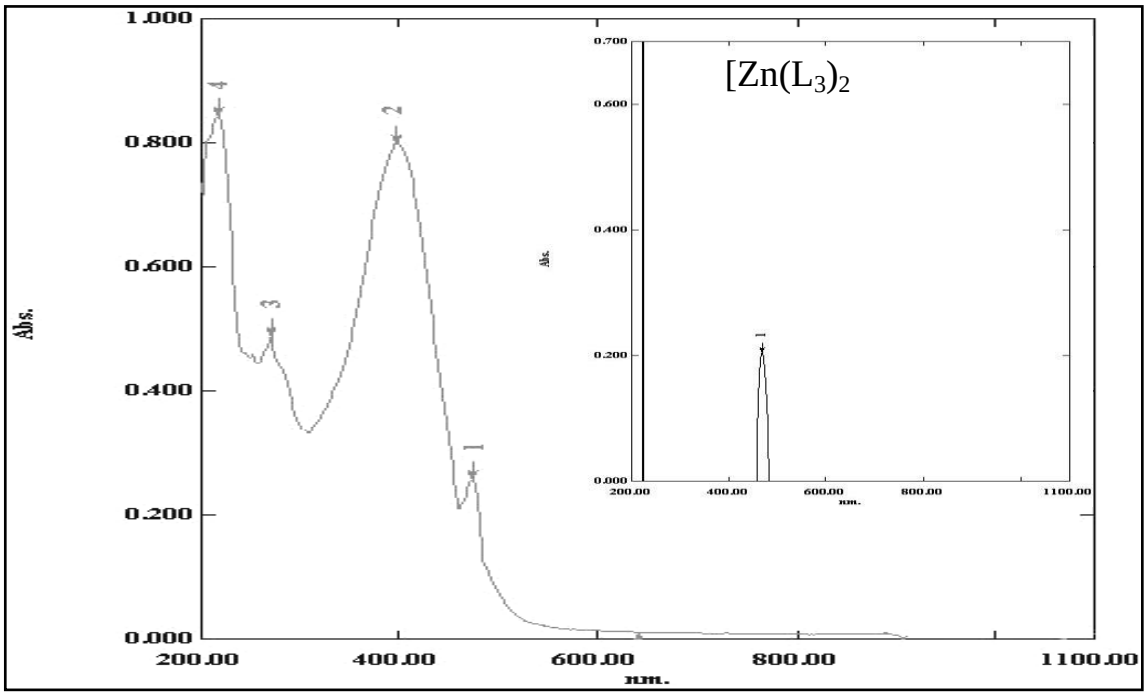

Figure (3-81): UV-Vis spectrum for $[Zn(L_3)_2]$ complex.

3.9.7.4. UV-Vis spectra of azo ligand (L_4) metal chelates

UV-Vis spectra for the ligand and their metal chelates melted at ethanol (10^{-3} mole/L) were gauged as well the datum formed are listed at Table (3-25).

Co^{II} complex showed peaks at (220 nm) (45454 cm^{-1}) (ε_{max}=1738 $l.mole^{-1}.cm^{-1}$), (278 nm) (35971 cm^{-1}) (ε_{max}=637 $l.mole^{-1}.cm^{-1}$) and (480 nm) (20833 cm^{-1}) (ε_{max}=1593 $l.mole^{-1}.cm^{-1}$) attributed to intra ligand and (M→L) charge transfer, other new peaks at (732 nm) (13661 cm^{-1}) (ε_{max}=7 $l.mole^{-1}.cm^{-1}$), (886 nm) (11286 cm^{-1}) (ε_{max}=6 $l.mole^{-1}.cm^{-1}$) and (976 nm) (10245 cm^{-1}) (ε_{max}=37 $l.mole^{-1}.cm^{-1}$) assigned to electronic transition type $^4T_{1g(F)} \rightarrow {}^4T_{1g(P)}(\upsilon_3)$, $^4T_{1g(F)} \rightarrow {}^4A_{2g}(\upsilon_2)$ and $^4T_{1g(F)} \rightarrow {}^4T_{2g(F)}(\upsilon_1)$, respectively[191].

Ni^{II} complex exhibited absorption peaks at (291 nm) (34364 cm^{-1}) (ε_{max}=536 $l.mole^{-1}.cm^{-1}$) and (478 nm) (20920 cm^{-1}) (ε_{max}=1379 $l.mole^{-1}.cm^{-1}$) described to intra ligand and (M→L) charge transfer. Peaks at (672 nm) (14880 cm^{-1}) (ε_{max}=5 $l.mole^{-1}.cm^{-1}$), (888 nm) (11261 cm^{-1}) (ε_{max}=2 $l.mole^{-1}.cm^{-1}$) and (978 nm) (10224 cm^{-1}) (ε_{max}= 33 $l.mole^{-1}.cm^{-1}$) were described to electronic transition type $^3A_{2g} \rightarrow {}^3T_{1g(P)}(\upsilon_3)$, $^3A_{2g} \rightarrow {}^3T_{1g(F)}$ (υ_2) and $^3A_{2g} \rightarrow {}^3T_{2g(F)}$ (υ_1) respectively[192].

Cu^{II} complex appeared peaks at (291 nm) (34364 cm^{-1}) (ε_{max}=1177 $l.mole^{-1}.cm^{-1}$), (414 nm) (24154 cm^{-1}) (ε_{max}=2255 $l.mole^{-1}.cm^{-1}$) and (476 nm) (21008 cm^{-1}) (ε_{max}=1974 $l.mole^{-1}.cm^{-1}$) due to intra ligand and (M→L) charge transfer, other than peak at (890 nm) (11235 cm^{-1}) (ε_{max}=23 $l.mole^{-1}.cm^{-1}$) described to electronic transition type $^2E_g \rightarrow {}^2T_{2g}$[193].

Zn^{II} complex displayed peaks at (219 nm) (45662 cm^{-1}) (ε_{max}=1218 $l.mole^{-1}.cm^{-1}$), (288 nm) (34722 cm^{-1}) (ε_{max}=617 $l.mole^{-1}.cm^{-1}$), (332 nm)

(30120 cm^{-1}) (ε_{max}=440 $l.mole^{-1}.cm^{-1}$) and (478 nm) (20920 cm^{-1}) (ε_{max}=1333 $l.mole^{-1}.cm^{-1}$) lead to intra ligand and (M→L) charge transfer, and the magnetic susceptibility shows that the complex has diamagnetic moments, because d-d transition are not possible hence electronic spectra did not give any fruitful information, in fact this result is a good agreement with previous work of octahedral geometry[194], see Figures (3-82) to (3-85).

Table (3-25): UV-Vis spectral data for azo ligand(L_4) metal chelates.

Compounds	λ_{max} (nm)	Abs.	Wave number (cm^{-1})	ε_{max} ($L.mol^{-1}.cm^{-1}$)	Transition Assignment
Ligand(L_4)	218	2.198	45871	2198	π-π^*
	290	0.785	34482	785	π-π^*
	410	2.340	24390	2340	π-π^*
$[Co(L_4)_2]$	220	1.738	45454	1738	π-π^*
	278	0.637	35971	637	π-π^*
	480	1.593	20833	1593	(M→L) C.T
	732	0.007	13661	7	$^4T_{1g(F)} \rightarrow {}^4T_{1g(P)}$
	886	0.006	11286	6	$^4T_{1g(F)} \rightarrow {}^4A_{2g(F)}$
	976	0.037	10245	37	$^4T_{1g(F)} \rightarrow {}^4T_{2g(F)}$
$[Ni(L_4)_2]$	292	0.536	34246	536	π-π^*
	478	1.379	20920	1379	(M→L) C.T
	672	0.005	14880	5	$^3A_{2g(F)} \rightarrow {}^3T_{1g(P)}$
	888	0.002	11261	2	$^3A_{2g(F)} \rightarrow {}^3T_{1g(F)}$
	978	0.033	10224	33	$^3A_{2g(F)} \rightarrow {}^3T_{2g(F)}$
$[Cu(L_4)_2]$	291	1.177	34264	1177	π-π^*
	414	2.255	24154	2255	π-π^*
	476	1.974	21008	1974	(M→L) C.T
	890	0.023	11235	23	$^2E_g \rightarrow {}^2T_{2g}$
$[Zn(L_4)_2]$	219	1.218	45662	1218	π-π^*
	288	0.617	34722	617	π-π^*
	332	0.440	30120	440	π-π^*
	478	1.333	20920	1333	(M→L) C.T

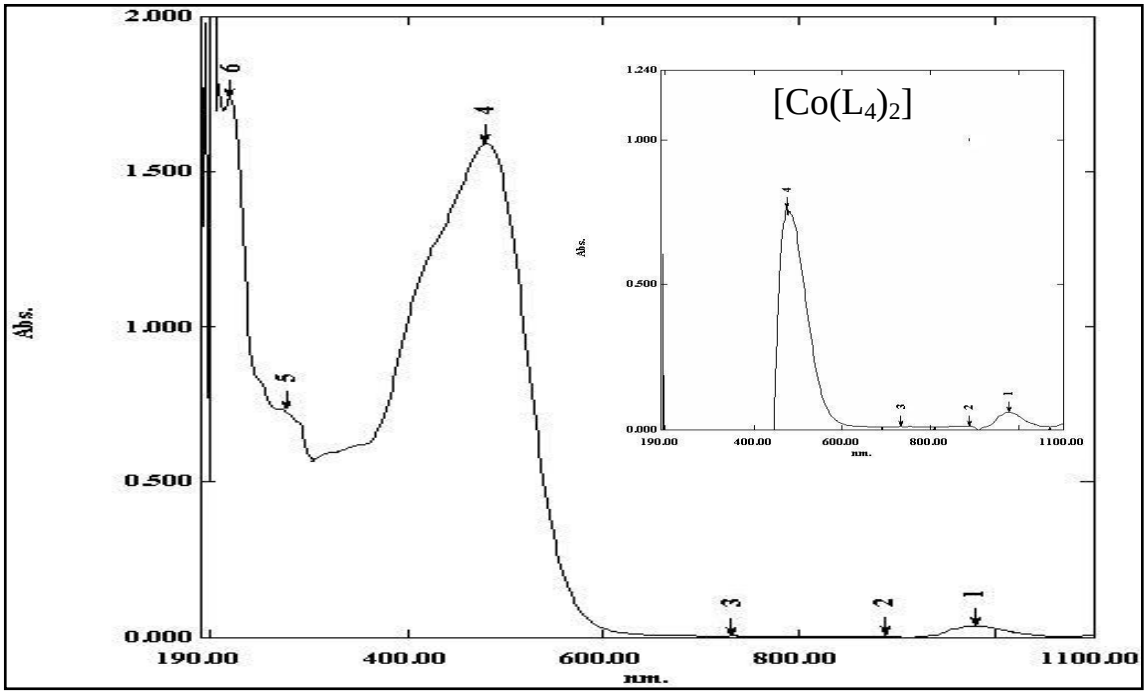

Figure (3-82): UV-Vis spectrum for $[Co(L_4)_2]$ complex.

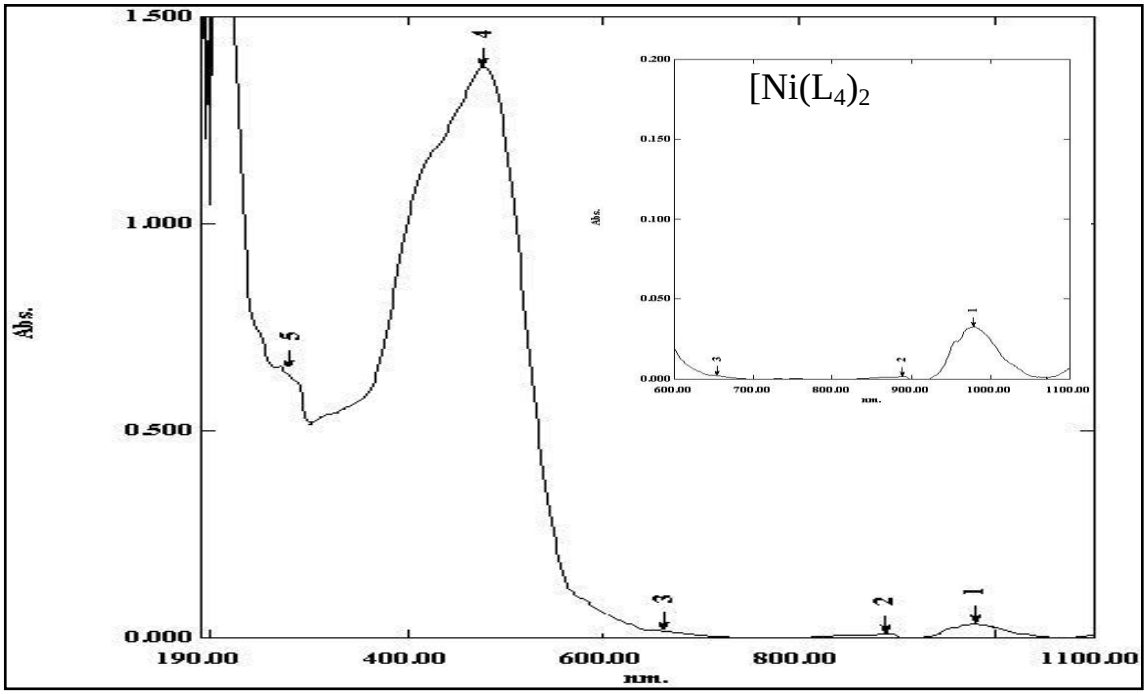

Figure (3-83): UV-Vis spectrum for $[Ni(L_4)_2]$ complex.

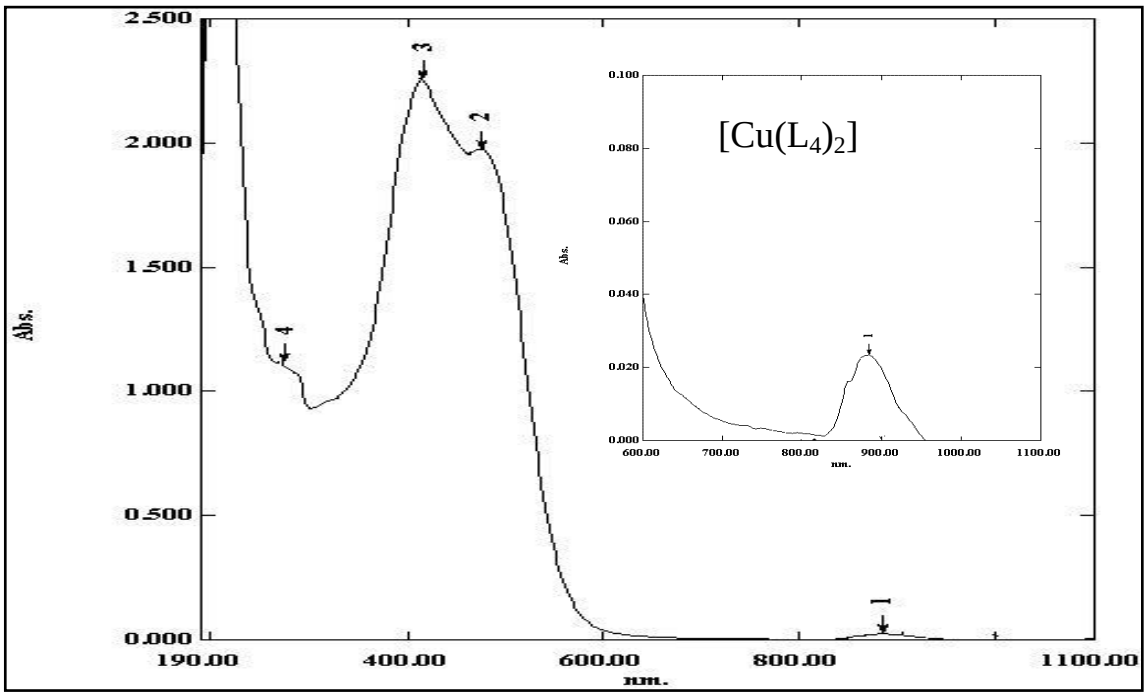

Figure(3-84): UV-Vis spectrum for $[Cu(L_4)_2]$ complex.

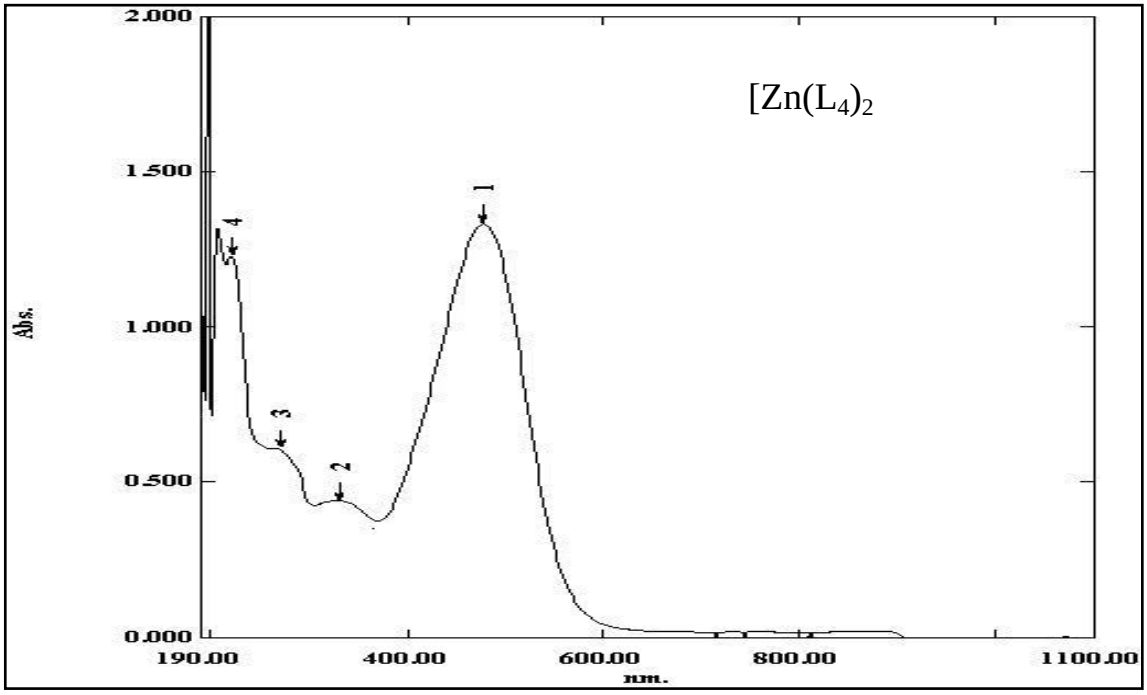

Figure (3-85): UV-Vis spectrum for $[Zn(L_4)_2]$ complex.

3.9.7.5. UV-Vis spectra of mixed azo ligand (L_1,L_2) metal chelates

UV-Vis spectra to the produced compounds melted at ethanol (10^{-3} mole/L) were gauged as well the datum formed are listed at Table (3-26), see Figures (3-86) to (3-89).

Co^{II} spectrum appeared three peaks at (243 nm) (41152 cm^{-1}) (ε_{max} =1270 $l.mole^{-1}.cm^{-1}$), (290 nm) (34482 cm^{-1}) (ε_{max}=1181 $l.mole^{-1}.cm^{-1}$) and (425 nm) (23529 cm^{-1}) (ε_{max}=612 $l.mole^{-1}.cm^{-1}$) attributed to intra ligand, new peaks at (751 nm) (13315 cm^{-1}) (ε_{max}=19 $l.mole^{-1}.cm^{-1}$), (884 nm) (11312 cm^{-1}) (ε_{max}=16 $l.mole^{-1}.cm^{-1}$) and (977 nm) (10235 cm^{-1}) (ε_{max}=123 $l.mole^{-1}.cm^{-1}$) described to electronic transition type $^4T_{1g(F)}\rightarrow{}^4T_{1g(P)}(\upsilon_3)$, $^4T_{1g(F)}\rightarrow{}^4A_{2g(F)}$ (υ_2) and $^4T_{1g(F)}\rightarrow{}^4T_{2g(F))}$ (υ_1) respectively[195].

Ni^{II} complex exhibited two absorption peaks at (270 nm) (37037 cm^{-1}) (ε_{max}=1462 $l.mole^{-1}.cm^{-1}$) and (429 nm) (23310 cm^{-1}) (ε_{max}=2007 $l.mole^{-1}.cm^{-1}$) were assigned to intra ligand. Other new peaks at (752 nm) (13297 cm^{-1}) (ε_{max}=13 $l.mole^{-1}.cm^{-1}$), (887 nm) (11273 cm^{-1}) (ε_{max}=14 $l.mole^{-1}.cm^{-1}$) and (980 nm) (10204 cm^{-1}) (ε_{max}=68 $l.mole^{-1}.cm^{-1}$) were assigned to electronic transition type $^3A_{2g}\rightarrow{}^3T_{1g(P)}$ (υ_3), $^3A_{2g}\rightarrow{}^3T_{1g(F)}$ (υ_2) and $^3A_{2g}\rightarrow{}^3T_{2g(F)}$ (υ_1), respectively[196].

Cu^{II} complex showed peaks at (247 nm) (40485 cm^{-1}) (ε_{max}=2315 $l.mole^{-1}.cm^{-1}$) and (425 nm) (23529 cm^{-1}) (ε_{max}=774 $l.mole^{-1}.cm^{-1}$) due to intra ligand, while peak at (886 nm) (11286 cm^{-1}) (ε_{max}=66 $l.mole^{-1}.cm^{-1}$) described to electronic transition type $^2E_g\rightarrow{}^2T_{2g}$[197] .

Spectrum of Zn^{II} complex showed peaks at (262 nm) (38167 cm^{-1}) (ε_{max}=1991 $l.mole^{-1}.cm^{-1}$), (407 nm) (24570 cm^{-1}) (ε_{max}=1978 $l.mole^{-1}.cm^{-1}$) and (537 nm) (18621 cm^{-1}) (ε_{max}=487 $l.mole^{-1}.cm^{-1}$) lead to intra

ligand and (M→L) charge transfer, and the magnetic susceptibility shows that the complex has diamagnetic moments, because d-d transition are not possible hence electronic spectra did not give any fruitful information, in fact this result is a good agreement with previous work of octahedral geometry[198].

Table (3-26): UV-Vis spectral data for mixed azo ligand (L_1, L_2) metal chelates

Compound	λ_{max} (nm)	Abs.	Wave number (cm^{-1})	ε_{max} ($L.mol^{-1}.cm^{-1}$)	Transition Assignment
Ligand(L_1)	242	1.894	41322	1894	π-π^*
	356	1.853	28089	1853	π-π^*
	414	1.177	24154	1177	π-π^*
Ligand(L_2)	298	2.272	33557	2272	π-π^*
	432	1.479	23148	1479	π-π^*
[Co(L_1)(L_2)]	243	1.270	41152	1270	π-π^*
	290	1.181	34482	1181	π-π^*
	425	0.612	23529	612	π-π^*
	751	0.019	13315	19	$^4T_{1g(F)}\rightarrow{}^4T_{1g(P)}$
	884	0.016	11312	16	$^4T_{1g(F)}\rightarrow{}^4A_{2g(F)}$
	977	0.123	10235	123	$^4T_{1g(F)}\rightarrow{}^4T_{2g(F)}$
[Ni(L_1)(L_2)]					π-π^*
	270	1.462	37037	1462	π-π^*
	429	2.007	23310	2007	π-π^*
	752	0.013	13297	13	$^3A_{2g(F)}\rightarrow{}^3T_{1g(P)}$
	887	0.014	11273	14	$^3A_{2g(F)}\rightarrow{}^3T_{1g(F)}$
	980	0.068	10204	68	$^3A_{2g(F)}\rightarrow{}^3T_{2g(F)}$
[Cu(L_1)(L_2)]	247	2.315	40485	2315	π-π^*
	425	0.774	23529	774	π-π^*
	886	0.066	11286	66	$^2E_g\rightarrow{}^2T_{2g}$
[Zn(L_1)(L_2)]	262	1.991	38167	1991	π-π^*
	407	1.978	24570	1978	π-π^*
	537	0.487	18621	487	(M→L) C.T

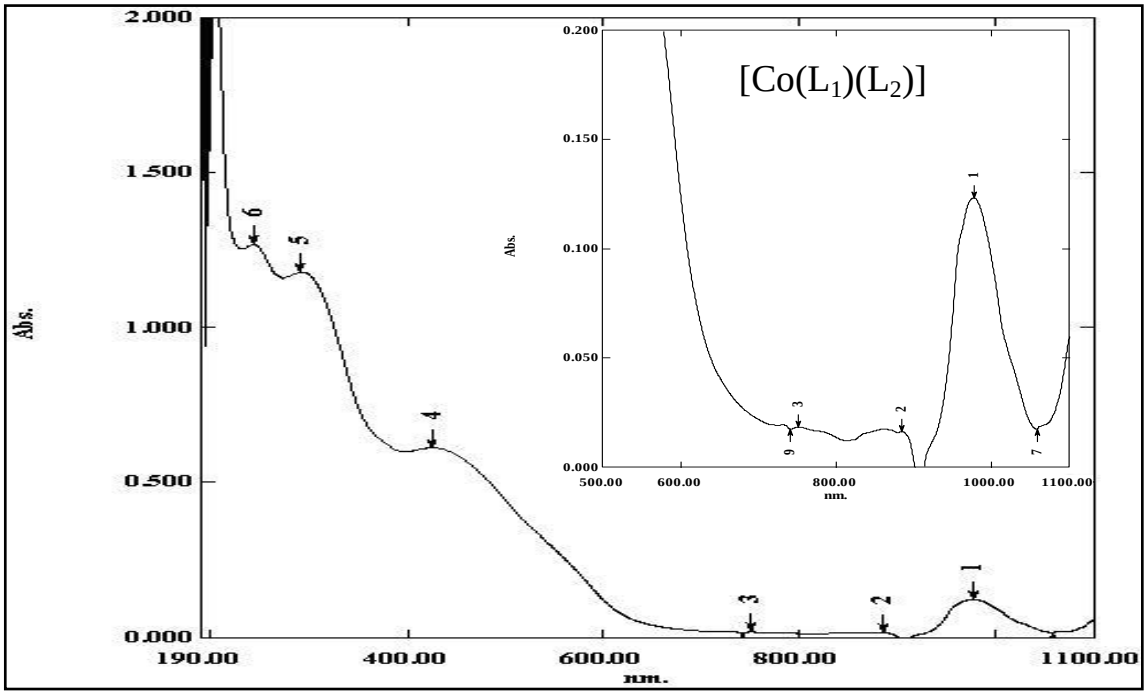

Figure (3-86): UV-Vis spectrum for [Co(L_1)(L_2)] complex.

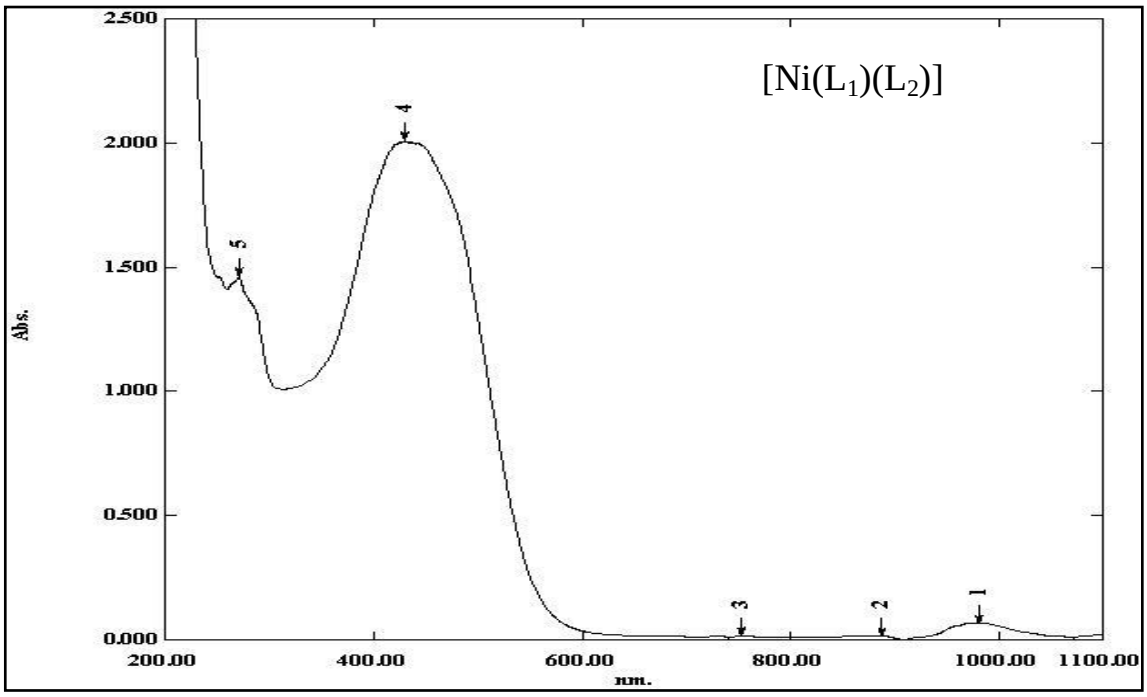

Figure (3-87): UV-Vis spectrum for [Ni(L_1)(L_2)] complex.

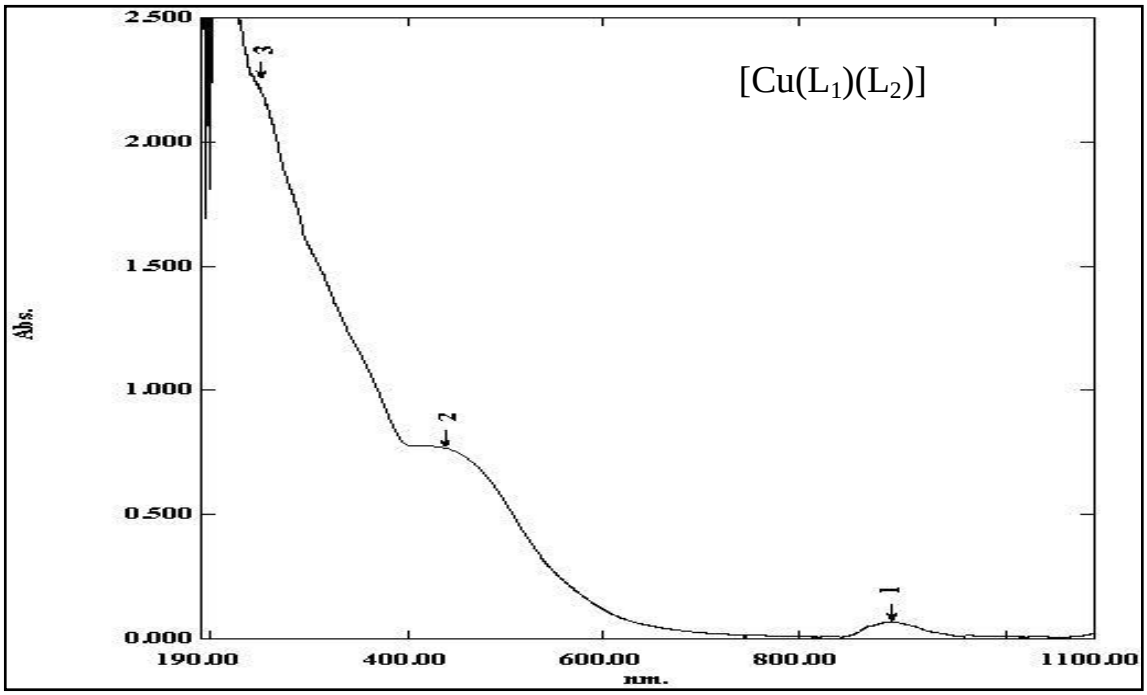

Figure (3-88): UV-Vis spectrum for [Cu(L_1)(L_2)] complex.

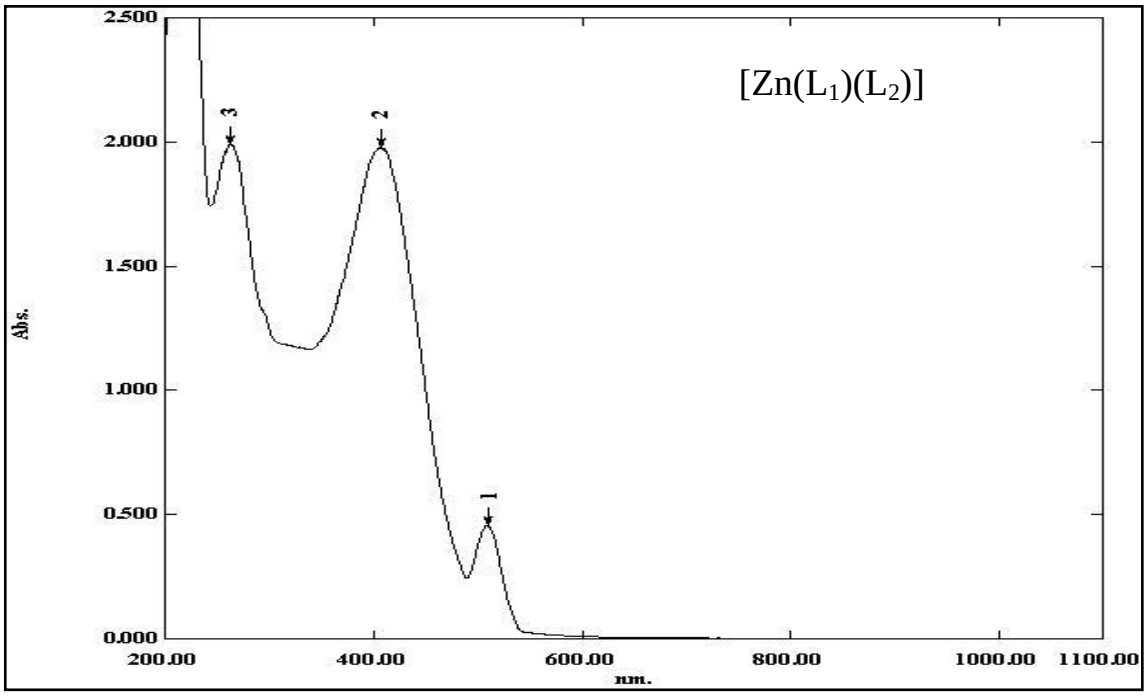

Figure (3-89): UV-Vis spectrum for [Zn(L_1)(L_2)] complex.

3.9.7.6. UV-Vis spectra of mixed azo ligand (L_3, L_4) metal chelates

UV-Vis spectra for the ligands and their metal chelates melted at ethanol (10^{-3} mole/L) were gauged as well the datum formed are listed at Table (3-27).

Co^{II} spectrum showed peaks at (270 nm) (37037 cm^{-1}) (ε_{max}=1388 $l.mole^{-1}.cm^{-1}$) and (415 nm) (24096 cm^{-1}) (ε_{max}=2116 $l.mole^{-1}.cm^{-1}$) attributed to intra ligand and (M→L) charge transfer, other new peaks at (752 nm) (13297 cm^{-1}) (ε_{max}=14 $l.mole^{-1}.cm^{-1}$), (885 nm) (11299 cm^{-1}) (ε_{max}=15 $l.mole^{-1}.cm^{-1}$) and (978 nm) (10224 cm^{-1}) (ε_{max}=73 $l.mole^{-1}.cm^{-1}$) due to electronic transition type $^4T_{1g(F)} \rightarrow {}^4T_{1g(P)}(\upsilon_3)$, $^4T_{1g(F)} \rightarrow {}^4A_{2g}$ (υ_2) and $^4T_{1g(F)} \rightarrow {}^4T_{2g(F)}$)(υ_1) respectively[199].

Ni^{II} complex exhibited three absorption peaks at (252 nm) (39682 cm^{-1}) (ε_{max}=1395 $l.mole^{-1}.cm^{-1}$), (270 nm) (37037 cm^{-1}) (ε_{max}=1444 $l.mole^{-1}.cm^{-1}$) and (452 nm) (22123 cm^{-1}) (ε_{max}=2266 $l.mole^{-1}.cm^{-1}$) which were described to intra ligand and (M→L) charge transfer. New peaks at (754 nm) (13262 cm^{-1}) (ε_{max}=6 $l.mole^{-1}.cm^{-1}$), (887 nm) (11273 cm^{-1}) (ε_{max}=7 $l.mole^{-1}.cm^{-1}$) and (979 nm) (10214 cm^{-1}) (ε_{max}=65 $l.mole^{-1}.cm^{-1}$) were assigned to electronic transition type $^3A_{2g} \rightarrow {}^3T_{1g(P)}(\upsilon_3)$, $^3A_{2g} \rightarrow {}^3T_{1g(F)}$ (υ_2), and $^3A_{2g} \rightarrow {}^3T_{2g(F)}$ (υ_1) respectively[200].

Cu^{II} complex appeared peaks at (270 nm) (37037 cm^{-1}) (ε_{max}=1406 $l.mole^{-1}.cm^{-1}$) and (454 nm) (22026 cm^{-1}) (ε_{max}=2318 $l.mole^{-1}.cm^{-1}$) lead to intra ligand and (M→L) charge transfer, other than peak at (979 nm) (10214 cm^{-1}) (ε_{max}=64 $l.mole^{-1}.cm^{-1}$) described to electronic transition type $^2E_g \rightarrow {}^2T_{2g}$[201].

Zn^{II} complex displayed peaks at (221 nm) (45248 cm^{-1}) (ε_{max}= 2314 $l.mole^{-1}.cm^{-1}$), (263 nm) (38022 cm^{-1}) (ε_{max}=1295 $l.mole^{-1}.cm^{-1}$), (394 nm) (25380 cm^{-1}) (ε_{max}=644 $l.mole^{-1}.cm^{-1}$) and (498 nm) (20080

cm^{-1}) (ε_{max}=274 $l.mole^{-1}.cm^{-1}$) lead to intra ligand and (M→L) charge transfer. Magnetic susceptibility showed that the complex has diamagnetic moments, because d-d transition are not possible hence electronic spectra did not give any fruitful information, in fact this result is a good agreement with previous work of octahedral geometry[202], see Figures (3-90) to (3-93).

Table (3-27): UV-Vis spectral data for mixed azo ligand (L_3, L_4) metal chelates.

Compound	λ_{max} (nm)	Abs.	Wave number (cm^{-1})	ε_{max} ($L.mol^{-1}.cm^{-1}$)	Transition Assignment
Ligand(L_3)	218	1.950	45871	1950	π-π^*
	270	1.066	37037	1066	π-π^*
	396	2.039	25252	2039	π-π^*
Ligand(L_4)	218	2.198	45871	2198	π-π^*
	290	0.785	34482	785	π-π^*
	410	2.340	24390	2340	π-π^*
[Co(L_3)(L_4)]	270	1.388	37037	1388	π-π^*
	415	2.116	24096	2116	(M→L) C.T
	752	0.014	13297	14	$^4T_{1g(F)} \rightarrow {}^4T_{1g(P)}$
	885	0.015	11299	15	$^4T_{1g(F)} \rightarrow {}^4A_{2g(F)}$
	978	0.073	10224	73	$^4T_{1g(F)} \rightarrow {}^4T_{2g(F)}$
[Ni(L_3)(L_4)]	252	1.395	39682	1395	π-π^*
	270	1.444	37037	1444	π-π^*
	452	2.266	22123	2266	(M→L) C.T
	754	0.006	13262	6	$^3A_{2g(F)} \rightarrow {}^3T_{1g(P)}$
	887	0.007	11273	7	$^3A_{2g(F)} \rightarrow {}^3T_{1g(F)}$
	979	0.065	10214	65	$^3A_{2g(F)} \rightarrow {}^3T_{2g(F)}$
[Cu(L_3)(L_4)]	270	1.406	37037	2315	π-π^*
	454	2.318	22026	774	(M→L) C.T
	979	0.064	10214	66	$^2E_g \rightarrow {}^2T_{2g}$
[Zn(L_1)(L_2)]	221	2.314	45248	2314	π-π^*
	263	1.295	38022	1295	π-π^*
	394	0.644	25380	644	π-π^*
	498	0.274	20080	274	(M→L) C.T

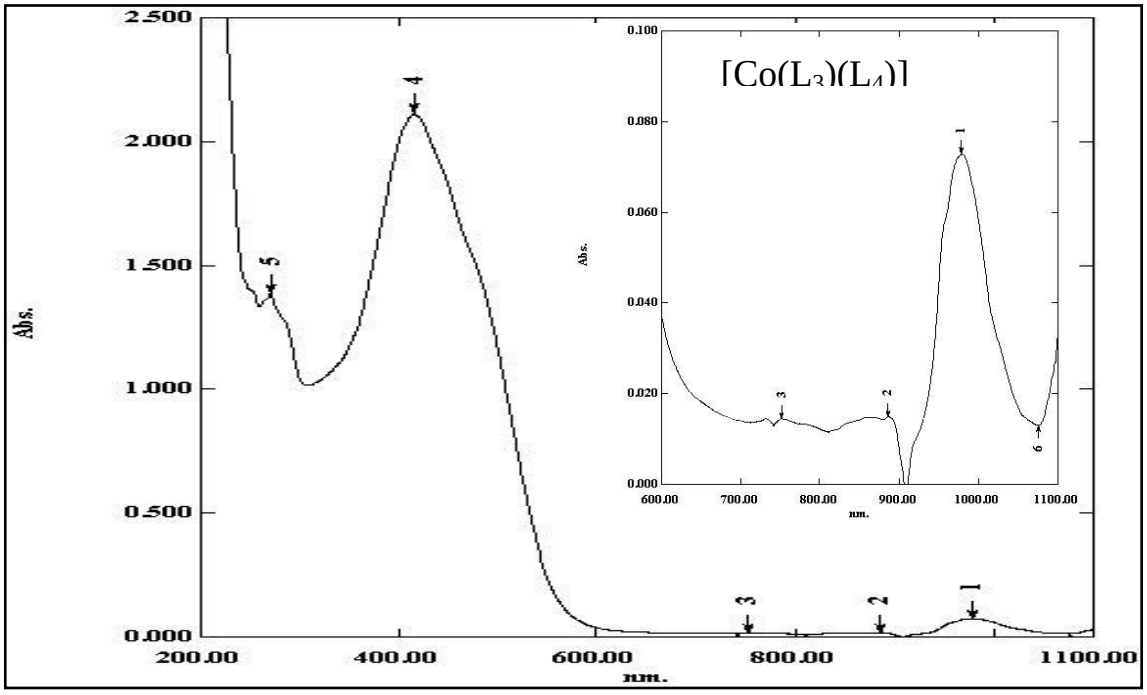

Figure (3-90): UV-Vis spectrum for [Co(L_3)(L_4)] complex.

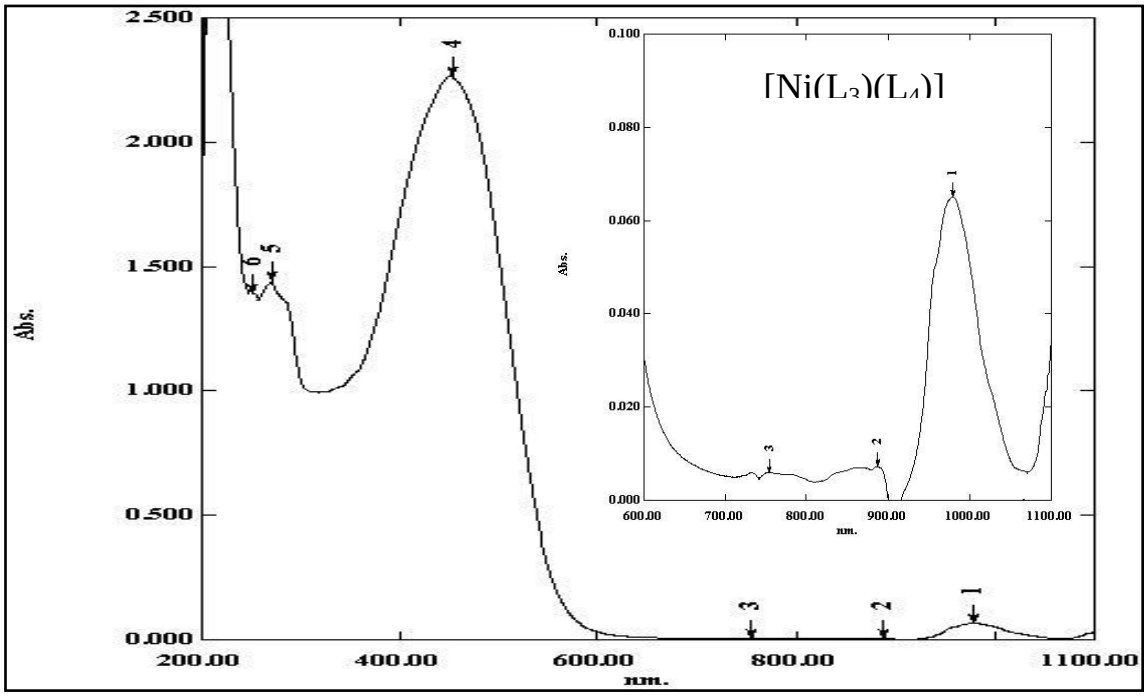

Figure (3-91): UV-Vis spectrum for [Ni(L_3)(L_4)] complex.

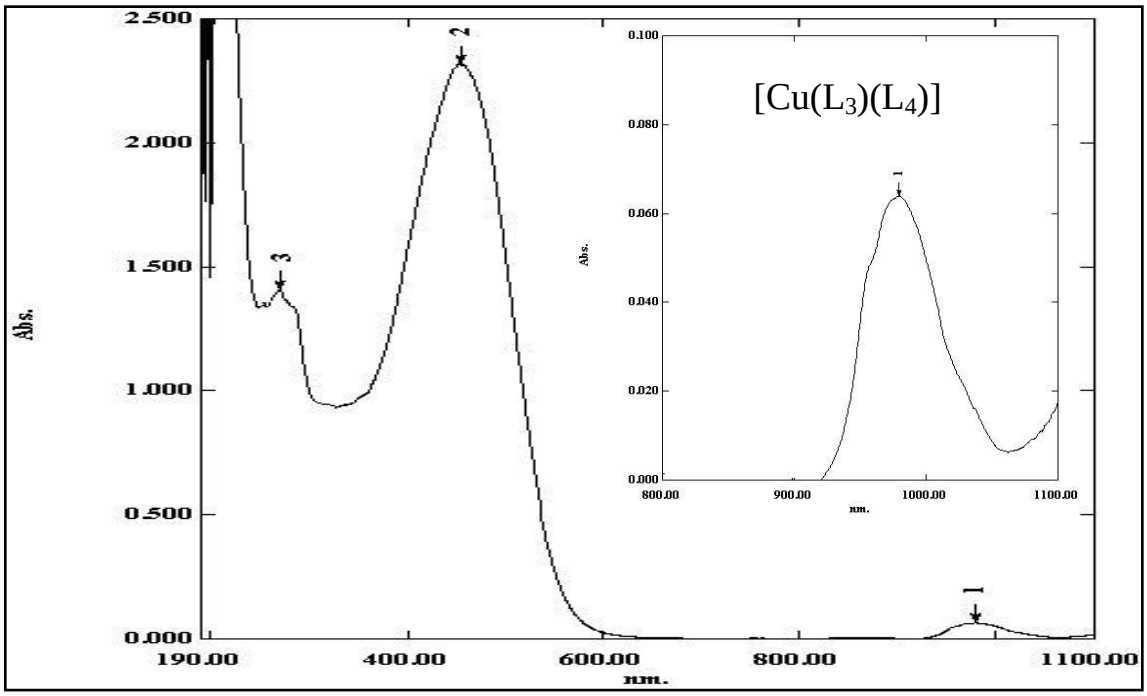

Figure (3-92): UV-Vis spectrum for [Cu(L_3)(L_4)] complex.

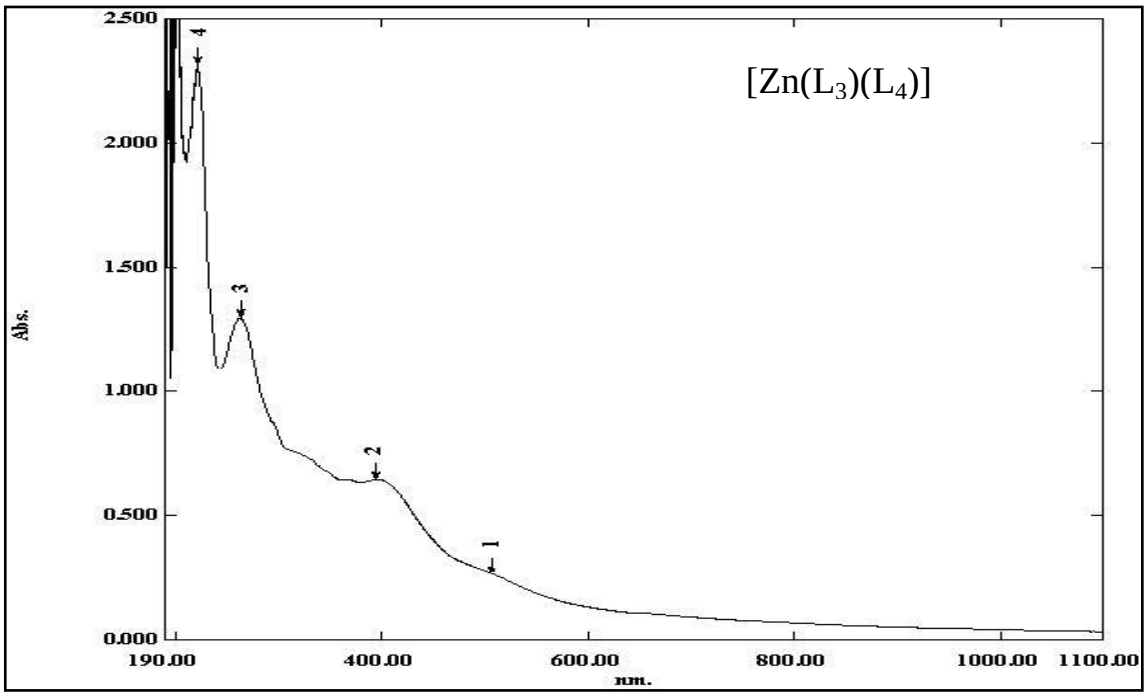

Figure (3-93): UV-Vis spectrum for [Zn(L_3)(L_4)] complex.

3.10. The Proposed molecular structures

Analytical physico-chemical data of the metal chelates due to hexacoordinate models, and the azo ligands acted as tridentate chelating react with metal ions through the azo group and the substance group in ortho position, other than the oxygen or nitrogen in five aromatic ring, see Figures (3-94) to (3-99).

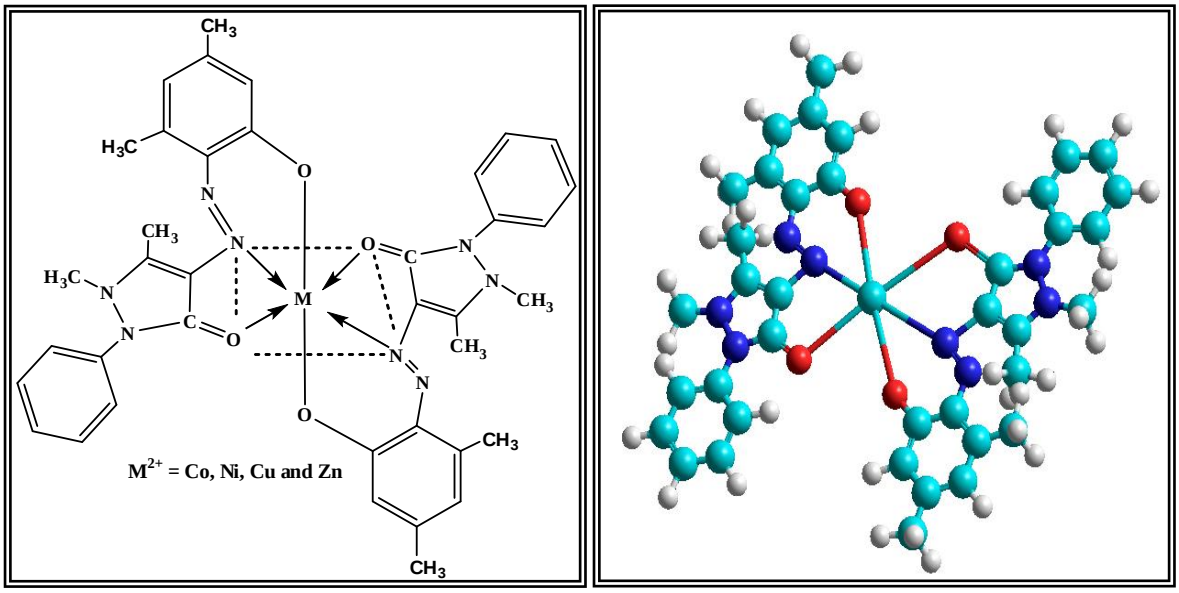

Figure (3-94): Suggested geometry for metal chelates of ligand (L_1).

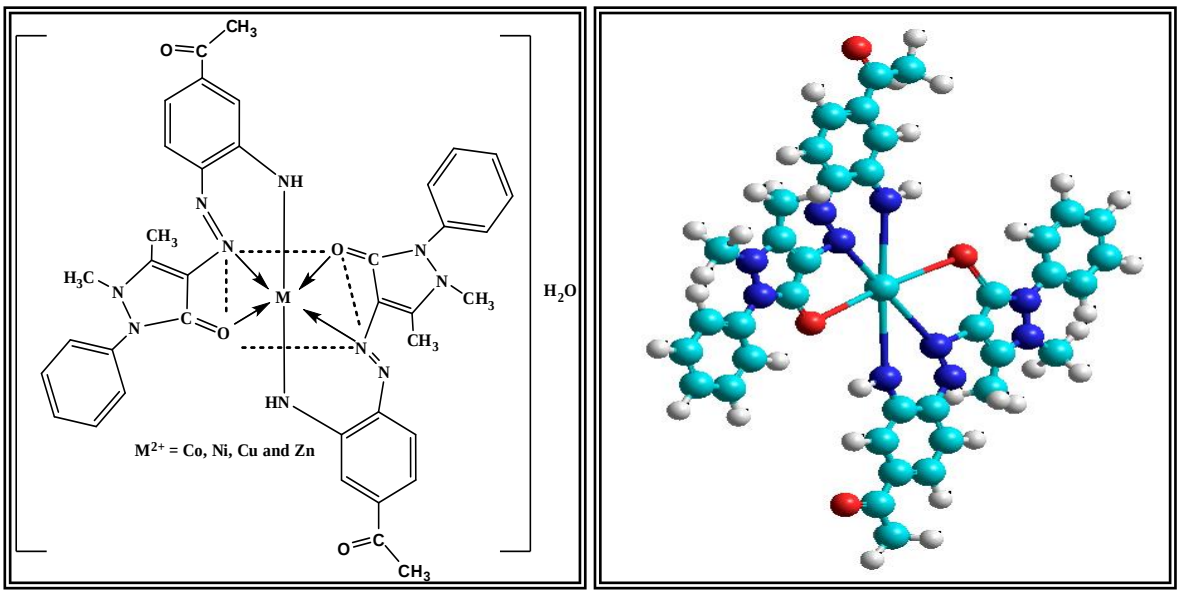

Figure (3-95): Suggested geometry for metal chelates of ligand (L_2).

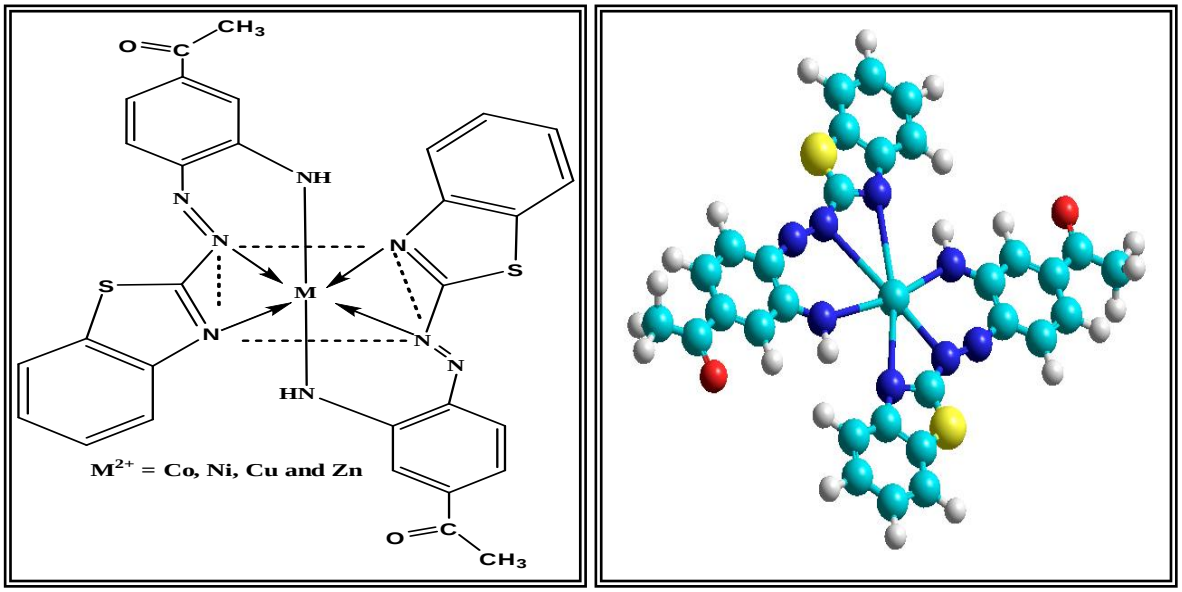

Figure (3-96): Suggested geometry for metal chelates of ligand (L_3).

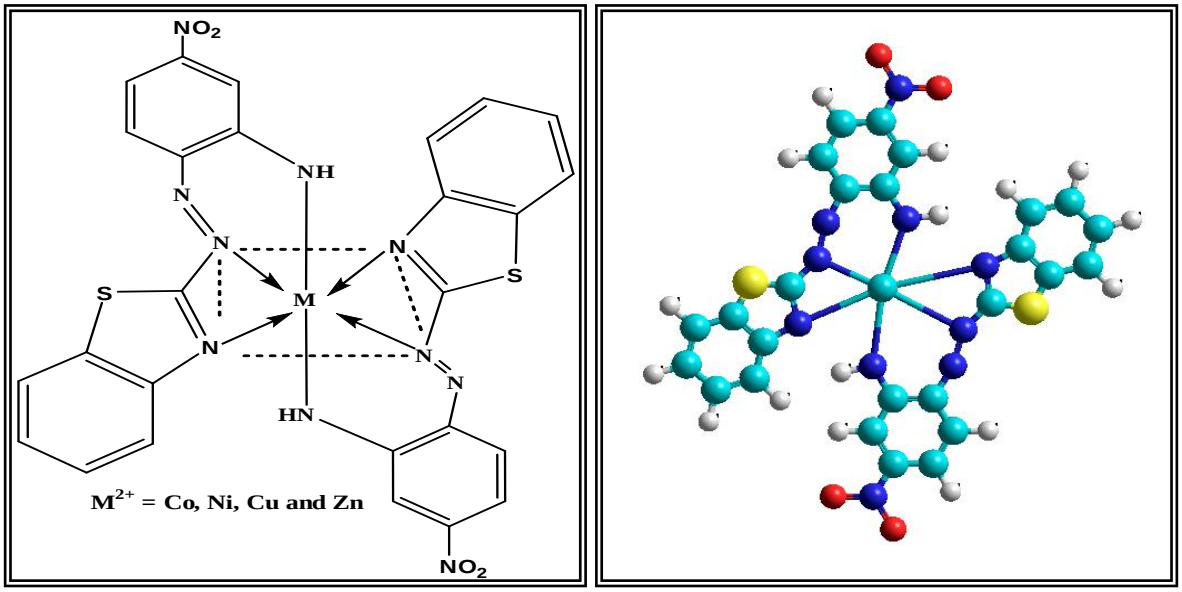

Figure (3-97): Suggested geometry for metal chelates of ligand (L_4).

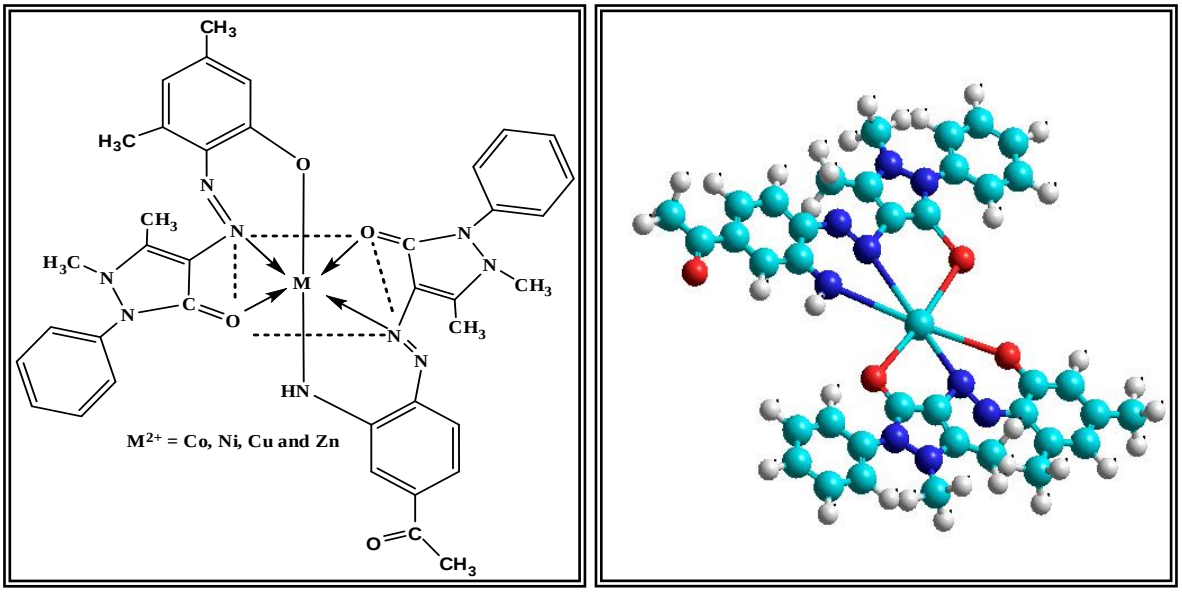

Figure (3-98): Suggested geometry for mixed azo ligand(L_1,L_2) metal chelates.

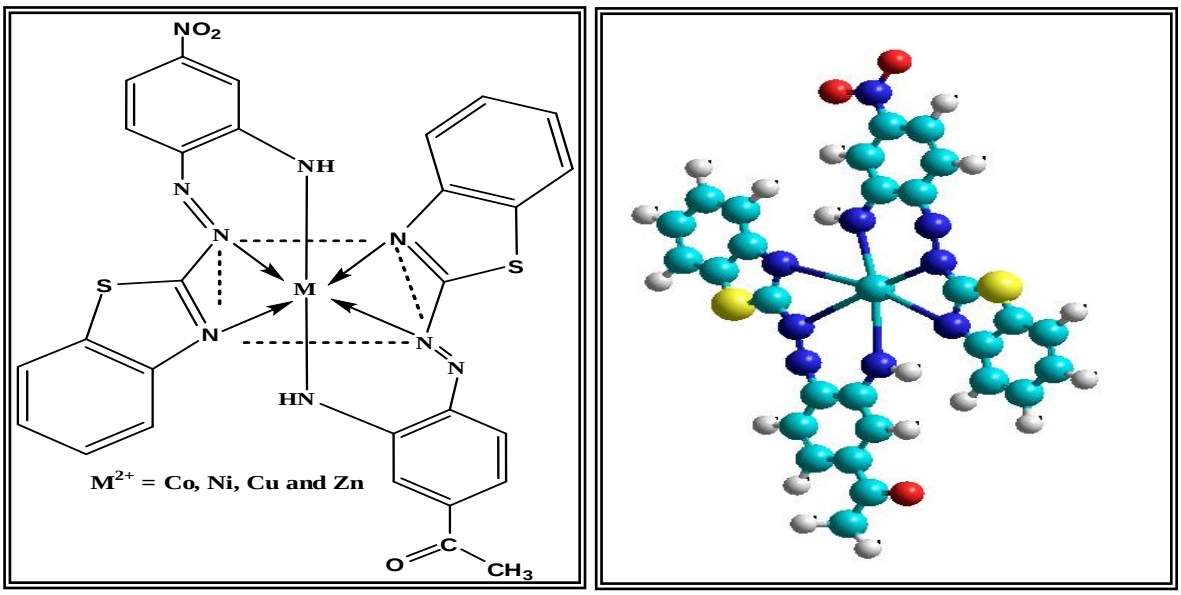

Figure (3-99): Suggested geometry for mixed azo ligand (L_3, L_4) metal chelates.

3.11. Biological activity

Qualitative screening for antimicrobial activities was performed preliminarily using the disc diffusion assay, in vitro microbial activities were measured from the diameter of clear inhibition zones caused by samples against the same bacteria and fungi under the same experimental condition. To verify the stability of new complexes in dimethylsulphoxide (DMSO) solution a long term. Microbial activity of the ligands and its metal chelates were tested on microorganisms. Bioactive were appreciated by measuring the growth inhibition zone against test organisms and minimal inhibition concentration[203]. It was found that the synthesized new metal complexes exhibited promising antibacterial and antifungal activity against: *Staphylococcus aureus*, *Esherichia Coli*, *Candida albicans* and *Candida tropicalis*, see Table (3-28) and Figures (3-100) to (3-103).

Table (3-28): Diameters (mm) at suppression for microbial activity to the azo ligands and compounds.

Compounds	Staphylococcus aureus	Esherichia coli	Candida albicans	Candida tropicalis
Ligand (L_1)	17	12	10	-
$[Co(L_1)_2]$	15	15	-	-
$[Ni(L_1)_2]$	14	13	16	-
$[Cu(L_1)_2]$	11	11	8	-
$[Zn(L_1)_2]$	15	11	11	-
Ligand (L_2)	12	12	-	11
$[Co(L_2)_2].H_2O$	-	15	-	-
$[Ni(L_2)_2].H_2O$	12	13	-	13
$[Cu(L_2)_2].H_2O$	15	14	-	19
$[Zn(L_2)_2].H_2O$	20	17	12	14
Ligand (L_3)	13	11	-	-
$[Co(L_3)_2]$	14	14	-	-
$[Ni(L_3)_2]$	11	14	15	10
$[Cu(L_3)_2]$	21	21	-	-
$[Zn(L_3)_2]$	13	12	-	-
Ligand (L_4)	16	14	-	-
$[Co(L_4)_2]$	13	15	-	-
$[Ni(L_4)_2]$	16	15	-	-
$[Cu(L_4)_2]$	15	15	-	-
$[Zn(L_4)_2]$	17	19	-	-
$[Co(L_1)(L_2)]$	15	-	-	-
$[Ni(L_1)(L_2)]$	14	14	-	-
$[Cu(L_1)(L_2)]$	15	12	-	-
$[Zn(L_1)(L_2)]$	14	21	-	-
$[Co(L_3)(L_4)]$	13	12	-	-
$[Ni(L_3)(L_4)]$	15	14	-	-
$[Cu(L_3)(L_4)]$	15	12	-	-
$[Zn(L_3)(L_4)]$	20	15	-	-

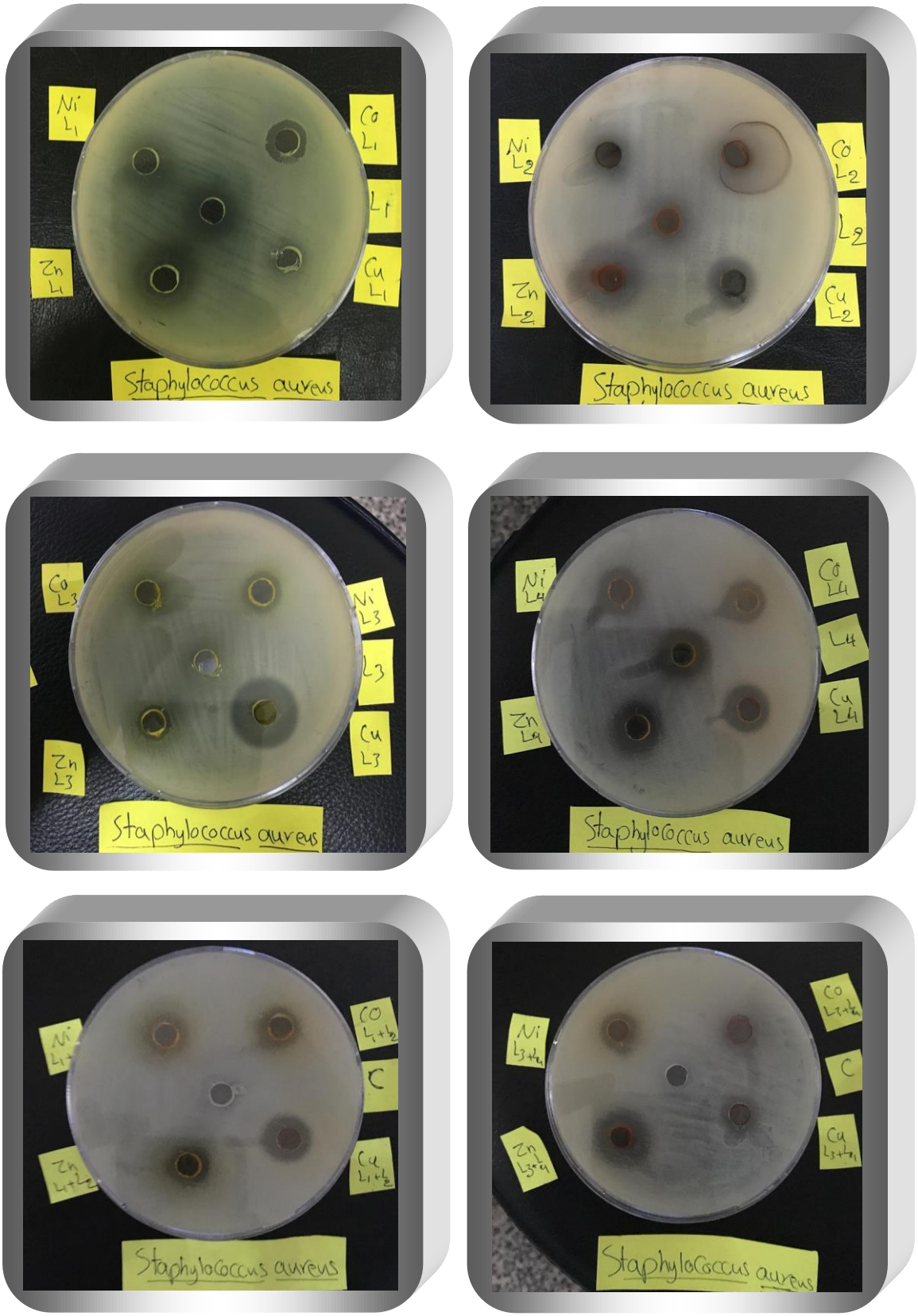

Figure (3-100): Bacterial activity for azo ligands and their metal chelates against *Staphylococcus aureus*.

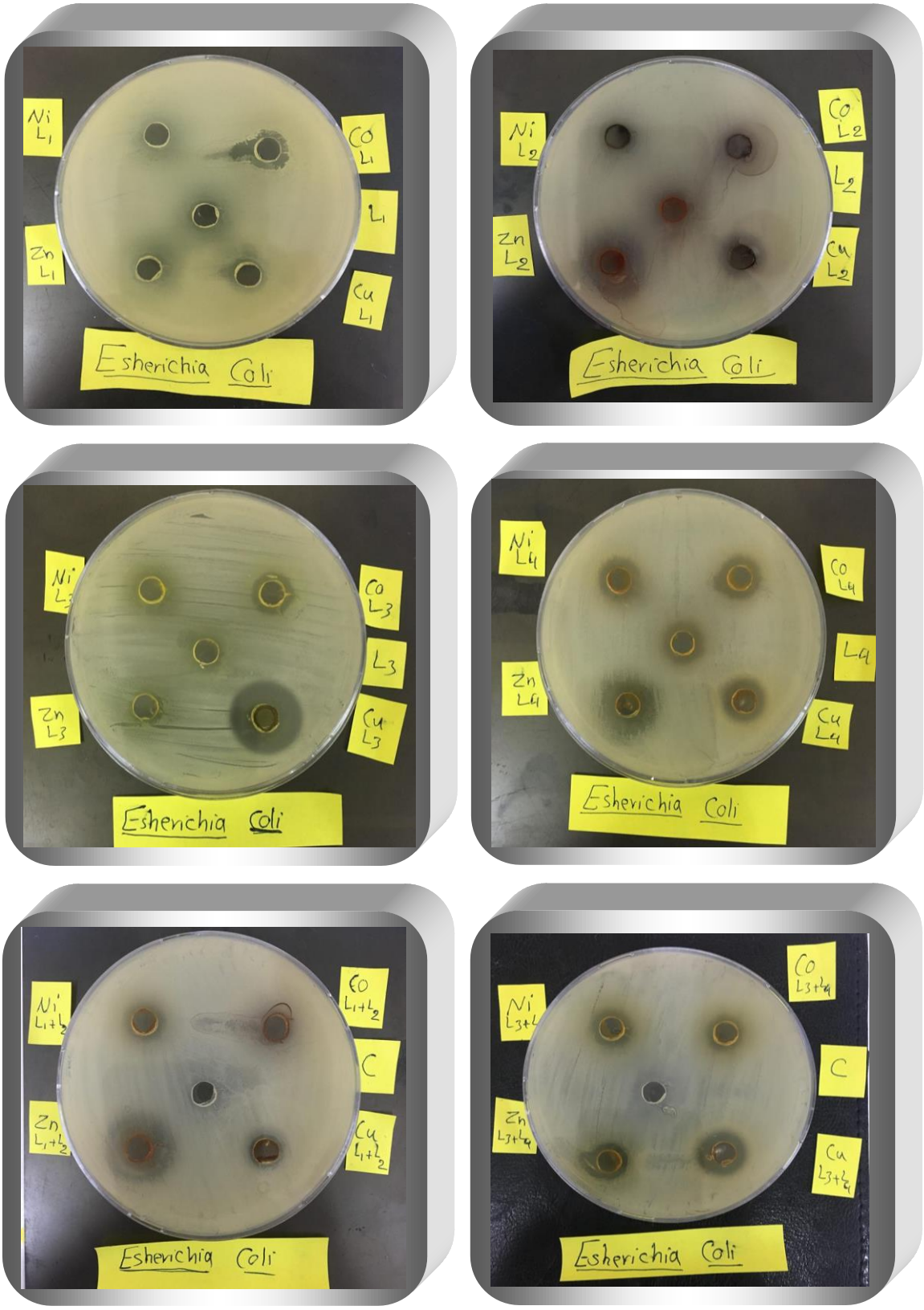

Figure (3-101): Bacterial activity for azo ligands and their metal chelates against *Esherichia coli*.

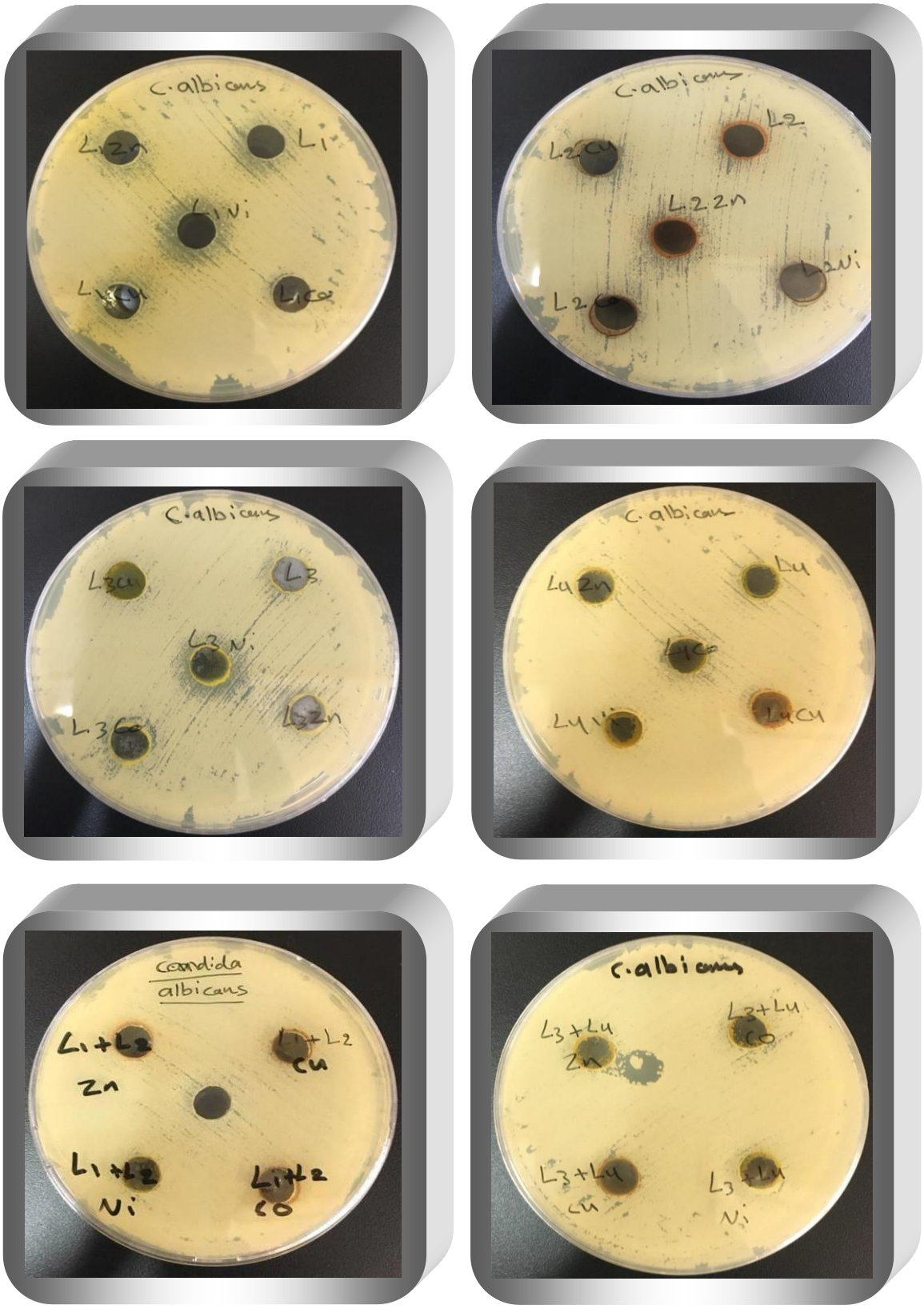

Figure (3-102): Antifungal activity for azo ligands and their metal chelates against *Candida albicans*.

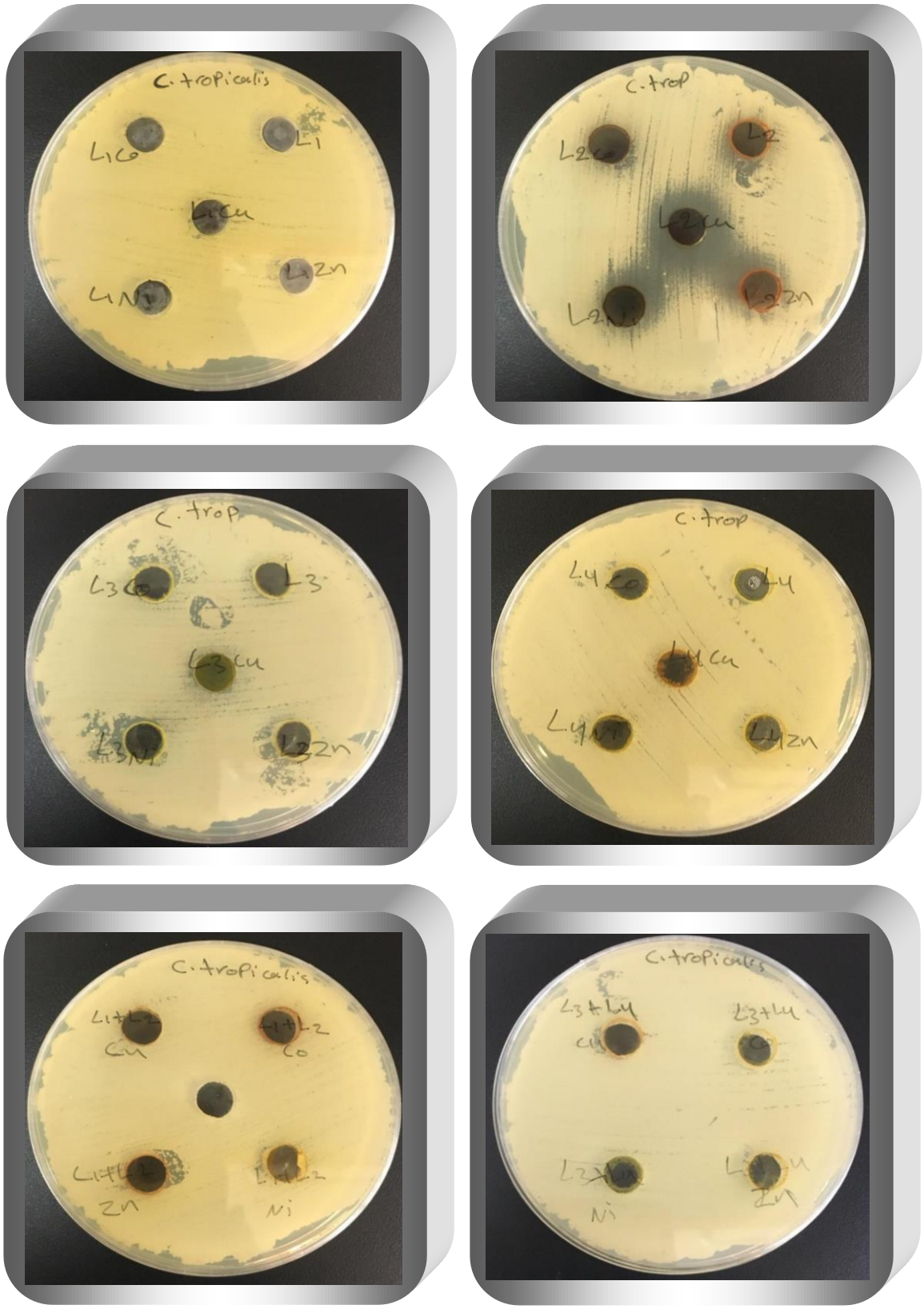

Figure (3-103): Antifungal activity for azo ligands and their metal chelates against *Candida tropicalis*.

3.12. Dyeing

Azo dyes are very important type of organic compounds, who use in scientific research. Synthetic these azo dyes have been used in different commercial application [204]. For many years, azo dyes have been used in various applications such as dyeing of textile fibres, coloring of various materials and advanced organic synthesis. It have been widely used as dyes for synthetic polyamide and as pigments[205].

Meal complexes of acidic azo dyes are very important role in industrial textile. Cr(III) and Co(III) complexes have been used for dyeing of wool and synthetic polyamides, metal chelate of azo dyes are applied for the wool by the treatment of dye wool with chromate or dichromate salts, Cr(IV)[206].

In 2015 Chhowala and Desai [207], synthesized a new Ni^{II} and Cu^{II} azo dye complexes having good light fastness on silk fabrics, see Figure (3-104).

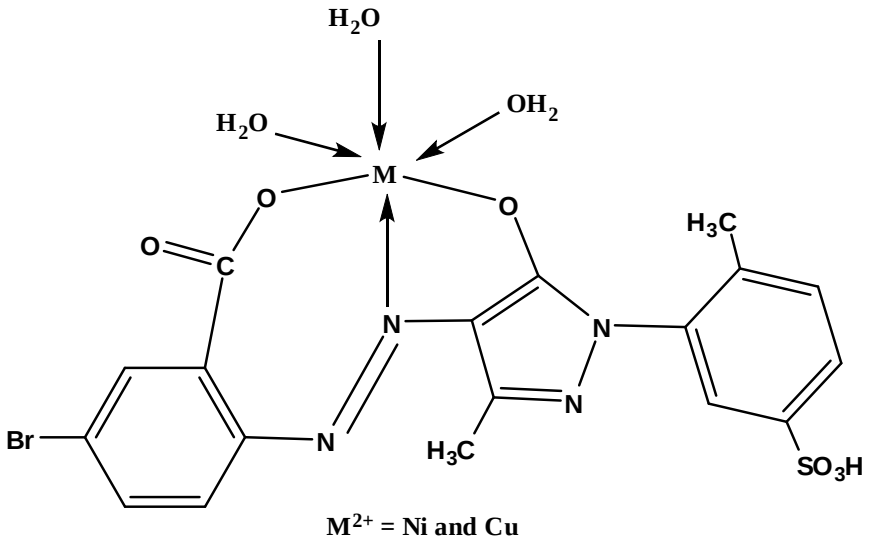

Figure (3-104): Ni^{II} and Cu^{II}-azo dye complexes.

In 2017 El-Wakiel, *et.al* [208], synthesized a new Co^{II}, Ni^{II} and Cu^{II} azo dye complexes having good light fastness on polyester fabrics, see Figure (3-105).

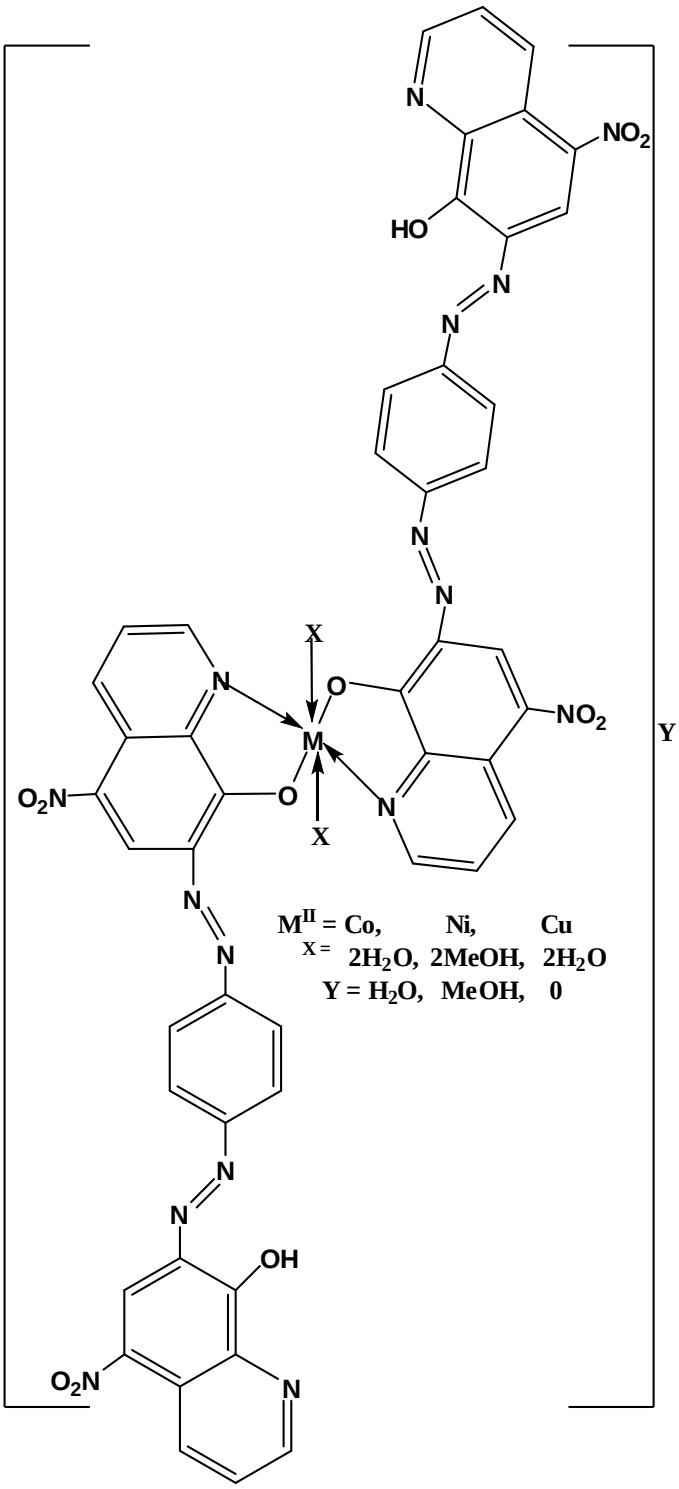

Figure (3-105): Co^{II}, Ni^{II} and Cu^{II}-azo dye complexes.

Recently, various heterocyclic azo dyes and their metal chelates have been synthesized and used in industrial textile were investigated [209,210]. Azo dyes ligands and their metal chelates have been tested on cotton fabric, the dyeing has been done due to experimental part (2-9), see Figures (3-106) to (3-111).

Figure (3-106): Textiles dyeing by azo ligand (L_1) and their metal chelates.

Figure (3-107): Textiles dyeing by azo ligand (L_2) and their metal chelates.

Figure (3-108): Textiles dyeing by azo ligand (L_3) and their metal chelates.

Figure (3-109): Textiles dyeing by azo ligand (L_4) and their metal chelates.

Figure (3-110): Textiles dyeing by mixed azo ligand (L_1,L_2) metal chelates.

Figure (3-111): Textiles dyeing by mixed azo ligand (L_3,L_4) metal chelates.

Conclusions

1. Produced azo dyes (L_1-L_4) appeared tridentate ligand with the metal ions to formation five and six rings.
2. Electronic spectra for metal chelates exhibited higher absorption peaks for (λ_{max}) in the ligand spectra which was assigned for coordination.
3. Metal chelates have been synthesized after perfect condition (concentration, pH and mole ratio).
4. Solid complexes have been recognized stable toward air and moisture as well higher melting points lead to stable for these metal chelates.

Prospective studies

1. Produced new metal complexes by using other metal ions.
2. Azo dyes are used in analytical chemistry for determination of metal ions.
3. Using X-ray technique to complete the characterized of the azo ligands and their metal complexes.
4. Investigated the possibility for using the azo ligands in separation of metal ions by column chromatography.
5. Studies the enzymes activity for the produced azo ligands and their metal chelates.

References

References

1. V.T. Yilmaz, V. Kars and C. Kazak; ***J. Coord. Chem.***, 59(2006): 1937-1944.
2. E.J. Baran and V.T. Yilmaz; ***Coord. Chem. Rev.***, 250(2006): 1980-1999.
3. B. Catikkas, E. Aktan and E. Yalcin; ***J. Mol. Struct.***, 1117(2016): 218-226.
4. J. Koh and A.J. Greaves; ***Dyes and Pigments***, 50(2001): 117-126.
5. A. Afkhami and M. Bahram; ***Spectrochim. Acta A***, 61(2005): 869-877.
6. E. Merino; ***Chem. Soc. Rev.***, 40(2011): 3835-3853.
7. H. Khanmohammadi, K. Rezaeian, M. Amini and S. Weng; ***Dyes and Pigments***, 98(2013): 557-564.
8. M.I. Abou-Dobara, A.Z. El-Sonbati and S.M. Morgan; ***World. J. Microbiol. Biotechnol.***, 29(2013): 119-126.
9. M. Jeburr; ***Innov. J. Sci.***, 2(2014): 1-5.
10. Y. Karaman, N. Menek, F.A. Bicer and H. Olmez; ***Int. J. Electrochem. Sci.***, 10(2015): 3106-3116.
11. N.M. Aljamali; ***Biochem. Anal. Biochem.***, 4(2015): 1-4.
12. M.E. Radulescu-Grad, S.G. Munteam, A. Todea, O. Verdes and A. Andelescu; Chem. Bull., 15(2015): 37-40.
13. A.R. Al-Rubaie and R.J. Mhessn; ***E-J. Chem.***, 9(2012): 465-470.
14. Y.B. Toura, S.M. Gumel, S. Habiba and J.L. Adam; ***IOSR J. Appl. Chem.***, 7(2014): 34-37.
15. A. Pandey, P. Singh and L. Iyengar; ***Int. Biodet. Biodeg.***, 59(2007): 73-84.

16. P.B. Makedonski, H.H. Johannes, J. Wichem, W. Grahn and W. Kowalsky; ***Dyes&Pigments***, 61(2004): 109-119.
17. A.M. Al-Jasser; ***Kuwait Med. J.***, 38(2006): 171-182.
18. R.H. Fayadh, A.A. Ali, F.M. Al-Jabri; ***Int. J. Engin. Techn. Res.***, 2(2015): 24-28.
19. M. W. Bes, S. F. Kettle, and D. B. Powell ; **SpectroChem. Acta** ., 1974, 30 (A), 139
20. A.M. Ali; ***Nat. J. Chem.***, 23(2006): 335-343.
21. I. Reva, B.J. Almeida, L. Lapinski and R. Fausto; ***J. Mol. Struct.***, 1025(2012): 74-82.
22. A.L. Valfredo, S.S. Elenir, S.S. Moacy and T.Y. Regino; ***Micro. Chim. Acta.***, 158(2007): 189-197.
23. M.M. Al-Rufaie; ***Mod. Chem. Appl.***, 4(2016): 1-5.
24. M.M. Al-Rufaie; ***Astur. J. Basic. Appl. Sci.***, 10(2016): 9-14.
25. U.S. Mothar, J.C. Ray, T.H. Wu and C. Sinha; ***J. Coord. Chem.***, 58(2005): 399-407.
26. S.T. Sad; ***Nat. J. Chem.***, 36(2009): 605-613.
27. A.A. Al-Hassani, A.H. Al-Khafagy and A.M. Ali; ***World. J. Pharm. Res.***, 3(2014): 218-231.
28. V.A. Modhavadiya; ***Asian. J. Biochem. Pharm. Res.***, 1(2011): 173-179.
29. C.V. Turcas and I. Sebe; ***U.P.B. Sci. Bull.,Series B***, 74(2012): 109-118.
30. D. Canakci, O.Y. Sariyik and S. Serin; ***Int. J. Sci. Res. Inno. Techn.***, 1(2014): 52-72.
31. Anith, K.R. Reddy and Fasiulla; ***Arch. Appl. Sci. Res.***,7(2015): 59-65.
32. Z.S. Kadhim; ***M.Sc., Thesis, University of Baghdad***, (2015).

33. A.L. Al-Ansary, N.S. Abdel-Kader, O.E. Sherif and A.G. Sayed; ***Inorg. Chem.***, 11(2016): 19-35.
34. A.J. Jarad and S.H. Quiasim; ***Res. J. Pharm. Bio. Chem. Sci.***, 9(2018): 613-642.
35. Z. Seferoglu; ***Arkivoc***, 7(2009): 42-57.
36. T. Mathur, U.S. Ray, J.C. Liou, J.S. Wu, T.H. Lu and C. Sinha; ***Polyhedron***, 24(2005): 739-746.
37. V.A. Lemos_, E.S. Santos, M.S. Santos, and R. T. Yamaki; ***Microchim Acta*** ,158 (2007):189–204.
38. K. Pyrzynska; ***Micro. Chim. Acta.***, 149(2005): 159-164.
39. M.M. Omar and G.G. Mohamed; ***Spectrochim. Acta A***, 61(2005): 929-936.
40. F. Karipcin and E. Kabalcilar; ***Acta. Chem. Slov.***, 54(2007): 242-247.
41. W.H. Mahmoud, F.N. Sayed and G.G. Mohamed; ***Appl. Organometal. Chem.***, Full paper, DOI 20.1002/qoc. 3529(2016).
42. A.N. Anlhemidis, D.G. Themelis and J.A. Stratis; ***Talanta.,*** 54(2001): 37-43.
43. N. Pourreza and S. Rastegarzadeh; ***Anal. Chem. Acta.***, 437(2001): 273.
44. V.Grdinie and Luterotti; **Croatica. Chim Acta.,** 73(2000): 23.
45. S. Harisha, J. Keshavayya, B.E.K. Swamy and C.C. Viswanath; ***Dyes and Pigments***, 136(2017): 742-753.
46. A.M. Jreo; Biochem. Anal. Biochem., 4(2015): 1-5.
47. A.H. Al-Khafagy; ***J. Chem. Pharm. Res.***, 8(2016): 296-302.
48. K.J. Al-Adille and S. Adnan; ***Orien. J. Chem.***, 33(2017): 1815-1827.

49. A.J. Jarad, I.Y. Majeed and A.O. Hussein; ***J. Physcis: Conf. Series***, 1003(2018): 1-13.
50. J. Savic and V. Vasic; ***Acta. Chem. Slov.***, 53(2006): 36-42.
51. A.J. Jarad, K.F. Suhail and A.L. Hussien; ***Al-Mustansiriya. J. Sci.***, 21(2010): 251-257.
52. H.H. Alshamsi, K.J. Al-Adille and S.A. Jaber; ***Orien. J. Chem.***, 31(2015): 809-818.
53. K.J. Al-Adille, K.A. Abdelrazaq and Z.M. Al-Hamdiny; ***Asian J. Chem.***, 25(2013): 10475-10481.
54. A.K .Abbas and R.S. Kadhim; ***Orien. J. Chem.***, 33(2017): 402-417.
55. H.M. Farhan; ***World. J. Med. Sci. Res.***, 2(2014): 026-034.
56. J.C. Knight, M. Wuest, F.A. Saad, M. Wang, D.W. Chapman, H.S. Jans, S.E. Lapi, B.M. Kariuki, A.J. Amoroso and F. Wuest; ***Dalton Trans***, 42(2013): 12005-12014.
57. S. Al-Ashqer, K.S. Abou-Melha, G.A.A. Al-Hazmi, F.A. Saad and N.M. El-Metwaly; ***Spectrochim. Acta A***, 132(2014): 751-761.
58. M. Saha, R. Nasani, M. Das, A. Mahata, B. Pathak, S.M. Mobin, L.M. Carrella, E. Rentschler and S. Mukhopadhyay; ***Dalton Trans***, 43(2014): 8083-8093.
59. S.A. Dhahir, N.M. Aziz and S.R. Bakir; ***Int. J. Basic. Appl. Sci.***, 12(212): 58-67.
60. A.M. Hassan, B.H. Heakal, T.M. Kehela, O.A. Fouad and A.M. Eldin; ***J. Chem. Pharm.Res.***, 8(2016): 771-782.
61. D.A. Kennedy, V. Vembu, F.R. Fronczek and M. Devocelle; ***J. Org. Chem.***, 76(2011): 9641-9647.
62. A.A. Syhood and H.J. Mohammed; ***Int. J. Sci. Res.***, 4(2015): 504-508.

63. V. Marvaniya, H. Marvaniya, D.N. Tiwari, S. Patel and R. Kaur; ***Int. J. Allied Med. Sci. Clini. Res.***, 5(2017): 625-631.
64. T. Chukwu and K. Desai; ***IOSR J. Appl. Chem.***, 8(2015): 1500-158.
65. A.S. Thakar, H.B. Friedrich, K.T. Joshi and G.E. Maguire; **South African J. Chem.**, 68(2015): 39-44.
66. H.F. Rizk, M.A. El-Badawi, S.A. Ibrahim and M.A. El-Borai; ***Arabian J. Chem.***, 4(2011): 37-44.
67. M.N. Al-Jibouri; ***Eur. Chem. Bull.***, 3(2014): 447-451.
68. S.N. Chaulia; ***Der. Pharm. Chem.***, 8(2016): 254-272.
69. A.J. Jarad; ***Baghdad J. Sci.***, 13(2016): 838-845.
70. G. Hussain, N. Abass, G. Shabir, M. Athar, A. Saeed, R. Saleem, F. Ali and M.A. Khan; J. Appl. Res. Techn., xxx(2017): xxx-xxx.
71. M. Shafeeulla, G. Krishnamurthy, H.S. Bhojynaik and T. Manjuraj; ***Turk. Chem. Soc.***, 4(2017): 787-810
72. A.H. Al-Khafagy; J. Bio. Innov., 7(2018): 286-296.
73. G. Giambastiani and J. Camproa; ***"Olfen ungrading catalysis by nitrogen-based metal complexes"***, Spriger Science, 36(2011): 29.
74. F.A. Saad and A.M. Khedr; ***Bulgarian Chem. Comm.***, 47(2015): 654-663.
75. D.S. Wankhede; ***Der Chem. Sinica***, 6(2015): 52-58.
76. A.Z. El-Sonbati, M.A. Diab, A.A. El-Bindary, M.I. Abou-Dobara and H.A. Seyam; ***Spectrochim. Acta A:Mol. Biomol. Spectroscopy***, 104(2013): 213-221.
77. R.C. Maurya, J. Chourasia and P. Sharma; ***Indian J. Chem.***, 46A(2007): 1595-1604.
78. N. Raman, R. Jeyamurugan, A. Sakthivel and R. Antony; ***J. Iran. Chem. Res.***, 2(2009): 277-291.
79. B. Kirkan and R. Gup; ***Turk. J. Chem.***, 32(2008): 9-17.

80. M. Singh and S. Anant; ***Int. J. Inorg. Chem.***, Article ID767080(2012): 1-6.
81. M. Usharani, E. Akila and R. Rajavel; ***Int. J. Pharm. Techn. Res.***, 5(2013): 311-319.
82. I.M.I. Moustafa and M.H. Abdellattif; ***Modern Chem. Appl.***, 5(2017): 1-7.
83. R. Adiguzel, N. Turan, K. Buldurun and H. Korkoca; ***Int. J. Pharm.***, 14(2018): 9-19.
84. A. Gheath, N. Elsharif and E. Alabiedy; Libyan ***J. Sci. Techn.***, 7(2018): 32-35.
85. C.T.K. Kumar, J. Keshavayya, T. Rajesh and S.K. Peethambar; ***Int. J. Pharm. Pharm. Sci.***, 5(2013): 296-301.
86. M.B. Halli, K. Mallikarjum and S. Suryakant; ***J. Chem. Pharm. Res.***, 7(2015): 797-1804.
87. K.J. Al-Adille, A.K. Abass and A.M. Taher; ***J. Mol. Struct.***, 1108(2015): 378-397.
88. M.L.H. Nair and A. Sheela; ***Indian. J. Chem.***, 47A(2008): 1787-1792.
89. S. Pal and C. Sinho; Proc. ***Ind. Acad. Sci.***, 113(2001): 173-182.
90. R. Carballo; ***Polyhedron***, 20(2001): 2415-2420.
91. Y. SI, Q. Hu, Z. Huang, G. Yang and J. Yin; ***Turk. J. Chem.***; 29(2005): 135-140.
92. R.H. Fayadh, A.A. Ali and F.M. Al-Jabri; ***Int. J. Engin. Techn. Res.***, 3(2015): 24-28.
93. S. Wang, S. Shen, H.Hu, D. Gu, J. Yin and X. Dong; ***Mater. Sci. Eng. B-Solid***, 79(2001): 45-48.
94. G.B. Vadher and R.V. Zala; ***Int. J. Chem. Sci.***, 9(2011): 87-94.

95. M.H. Abdul-Latif, M.A.K. Alsouz, I.J. Dawood and A.J. Jarad; ***Chem. Proc. Engin. Res.***, 19(2014): 1-14.
96. T.N. Chhowala and K.R. Desai; ***Int. J. Sci. Res.***, 4(2013): 901-905.
97. J.O. Otutu; ***IJRRAS***, 15(2013): 292-296.
98. K.R. Raghavendra and K.A. Kumar; ***Int. J. Chem. Tech. Res.***, 5(2013): 1756-1760.
99. A.A.S. Al-Hamdani, A.M. Balkhf, A. Falah and S.A. Shaker; ***J. Chil. Chem. Soc.***, 60(2015): 2774-2785.
100. A.A.S. Al-Hamdani; Dirasat; 39(2013): 61-72.
101. A.A.S. Al-Hamdani and S.A. Shaker; ***Orint. J. Chem.***, 27(2011): 835-845.
102. M. Al-Sheikh, H.Y. Medrasi, K.U. Sadek and R.A. Mekheimer; ***Molecules***, 19(2014): 2993-3003.
103. S. Karthikeyan, N.S. Kumar, R. Ebenezer, S.C. Mohan and P. Balasubramanian; ***Der Chemica Sinica***, 6(2015): 1-6.
104. M.S. Suresh and V. Parakash; ***Int. J. Phys.Sci.***, 5(2010): 2203-2211.
105. J.R. Anacona and J.Estacio; ***Trans. Met. Chem.***, 31(2006): 227-231.
106. K. Nakamoto; "***Inrared and Raman Spectral of Inorganic and Coordination Compounds***", John Wiley and Sons, 5th Ed, New York, (1998).
107. V. Reddy, N. Patil and S.D. Angadi; ***E. J. Chem.***, 5(2008): 577-583.
108. J.R. Anacona and I.J. Rodriguez; ***J. Coord. Chem.***, 57(2004): 1263-1269.
109. H.R. Marady and N.S.Patel; ***J. Baraz. Chem. Soc.***, 12(2001): 1-6.
110. A.A. Oswole; ***E. J. Chem.***, 5(2008): 130-135.
111. A. Saxena and R. Saxena; ***Orien. J. Chem.***, 29(2013): 89-595.
112. R.C. Sharma, P.P. Giri, D. Kumar and Neelam; ***J. Chem. Pharm. Res.***, 4(2012): 1969-1973.

113. V.H. Patel, M.P. Patel and R.G. Patel; ***J. Serb. Chem. Soc.***, 67(2002): 727-734.
114. A. Ghames, T. Doudi, M. Allain and G.M. Bouet; ***Polyhedron***, 25(2005): 3201-3208.
115. H.R. Maradiya; ***Turk. J. Chem.***, 25(2001): 441-450.
116. Z. Zhu, M. Kojima and K. Nakajima; ***Inorg. Chim. Acta.***, 2(2008): 83-90.
117. K.O. Ogunniran, K.O. Ajanaku, O.O. James, O.O. Ajani, J.A. Adekoya and O.C. Nwinyi; ***African. J. Pure. Appl. Chem.***, 2(2008): 69-74.
118. N. Kumer and P. Mishra; ***Arch-Appl. Sci. Res.***, 5(2013): 191-197.
119. V.V. Raju, K.P. Balsubrhamania, C. Balkirshaman and V. Chinnusamy; ***Int. J. Appl. Bio.***, 2(2012): 76-87.
120. K.J. Al-Adille; ***Res. J. Pharm. Bio. Chem. Sci.***, 5(2015): 1297-1308.
121. M.S. Masoud, A.A. Soayed, A.E. Ali and O.K. Sharsherh; ***J. Coord. Chem.***, 56(2003): 725-742.
122. N. Turan, R. Adiguzel, K. Buldurun and E. Bursal; ***Int. J. Pharm.***, 12(2016): 92-100.
123. S. Gaur and B. Sharma; ***J. Indian. Chem. Soc.***, 82(2003): 841-842.
124. V.S. Shivankar, R.B. Vaidya, S.R. Dharwadkar and N.V. Thakkar; ***Syn. Reac. Inorg. Metal-Org. Chem.***, 33(2003): 1597-1622.
125. D. Maiti, H. Paul, N. Chanda, S. Chakraborty, B. Mondal, V.G. Puranik and G.K. Lahiri; ***Polyhedron***; 46(2004): 831-840.
126. Y. Li, B.O. Patrick and D. Dolphin; ***J. Org. Chem.***, 74(2009): 5237-5243.
127. K.J. Al-Adilee; ***Asian. J. Chem.***, 24(2012): 5597-5243.

128. S.S. Pandit, S.S. Pardhe and Y.B. Pandit; ***J. Iran. Chem. Comm.***, 35(2017): 227-236.
129. R. Karvembu and K. Natarajan; ***Polyhedron***; 21(2002): 219-223.
130. A. Sharma, T. Mehta and K.S. Manish; ***Der. Chem. Sci.***, 4(2013): 141-146.
131. G.G. Mohamed, M.M. Omar and A.N. Hindy; ***Turk. J. Chem.***, 30(2006): 61-382.
132. M. Sanmez and M. Sekerci; ***J. Am. Chem.***; 67(2002): 121-126.
133. Rajavel, M. Senthil and C. Anitha, ***E-J. Chem.***, 2008, **5**, 620-626.
134. J. H. Yoe and A. L. Jones; ***Ind. Eng. Chem. Anal. Ed.,*** 16(1944): 111-115.
135. V. G. Vosburgh and G. R. Copper; ***J. Amer. Chem. Soc.***, 63(1941): 437-442.
136. H.W. Cao and J.F. Zhao; ***Cro. Chem. Acta.***, 76(2003): 1-6.
137. G. Wtter, N. Ludwig and S. Horst; ***"Thermodynamics and statistical mechanics"***, Springer- Verlag, (1996): 101.
138. W.J. Geary; ***Coord. Chem. Rev.***, 7(1971): 81-122.
139. D. Gatteschi, O. Kahn, J. Miler and F. Palacio; ***Eds. Molecular magnetic materials.,*** NATO ASI Series., Kuwer: Dordrecht, the Netherlands., (1991): .
140. I.A. Mustafa and S.E. Al-Mukhtar; ***"Inorganic and Coordination Chemistry"***; Libray for printing and publishing, Mosul, Iraqi (1988): 611-670.
141. A.J. Jarad and Z.S. Kadhim; ***Int. J. Human. Arts. Med. Sci.***, 3(10): 197-210.
142. A. Saxena and R. Saxena; ***Orient. J. Chem.***, 29(2013): 589-595.
143. A.J. Jarad, M.T. Tawfiq and S. Shakir; ***Int. J. Engin. Sci. Res. Techn.***, 3(2014): 401-406.

144. S.H. Quiasim; ***M.Sc., Thesis, University of Baghdad***, (2018).
145. M.M.H. Khalil, E.H. Ismail, G.G. Mohamed, E.M. Zayed and A. Badr; ***Open. J. Inorg. Chem.***, 2(2012): 31-21.
146. S. Guney, V.T. Yilmaz and W.T.A. Harrison; ***J. Coord. Chem.***, 59(2006): 1123-1130.
147. K.R. Anitha, V. Reddy and K.S.V. Rao; J. Chem. Pharm. Res., 3(2011): 511-519.
148. H. Esener, A. Adiguzel, Z. Ergin, E. Aktan, N. Turan and M. Sekerci; ***Adv. Sci. Lett.***, 4(2011): 3669-3675.
149. K.S. Patel, J.C. Patel, H.R. Dholariya, V.K. Patel and K.D. Patel; ***Open. J. Met.***, 2(2012): 49-59.
150. W.H. Mahmoud, G.G. Mohamed and M.M.I. El-Dessouky; ***Spectrachim. Acta A***, 122(2014): 598-608.
151. R. Pallikavil, M.B. Umnathur and K. Krishnankuty; ***Arch. Appl. Sci. Res.***, 4(2012): 223-2227.
152. A.M. Khedr and F.A. Saad; ***Turk. J. Chem.***, 39(2015): 267-280
153. S. Joshi, V. Pawar and V. Uma; ***Res. J. Pharm. Biol. Chem. Sci.***, 2(2011): 61-70.
154. I. Waziri, N.P. Ndahi, G.A. Mala and M.B. Fugu; ***Der. Pharm. Chem.***, 6(2014): 118-122.
155. P. Subbaraj, A. Ramu, N. Raman and J. Dharmaraja; ***Int. J. Emer. Sc. Engin.***, 1(2013): 79-84.
156. J. Anacona, Y. Pineda, A. Bravo and J. Camus; ***Med. Chem.***, 6(2016): 467-473.
157. A. Yahyazzdeh and V. Azimi; ***Eur. Chem. Bull.***, 2(2013): 453-455.
158. F.A. Alsaif; ***Int. J. Electrochem. Sci.***, 9(2013): 398-417.
159. R. Pallikavil, M.B. Umnathur and K. Krishnankuty; ***Arch. Appl. Sci. Res.***, 4(2012): 223-2227.

160. A.J. Jarad; ***Eur. Chem. Bull.***, 2(2013): 383-388.
161. A.J. Jarad and Z.S. Kadhim; ***Int. J. Sci. Res.***, 7(2018): 1291-1301.
162. H. Esener, R. Adiguzel, Z. Ergin, E. Aktan, N. Turan and M. Sekerci; ***Adv. Sci. Lett.***, 4(2011): 3669-3675.
163. A.Z. El-Sonbati, R.M. Issa and A.M. Abo El-Gawad; ***Spectochim. Acta A: Mol. Spectrosc.***, 68(2007): 134-138.
164. A.M.A. Hamil, M.M. El-Ajaily and H.A.A. Bogdadi; ***Int. J. Pharm. Tech. Res.***, 1(2009): 1714-1717.
165. M.M. Al-Rufaie; ***Modern Chem. Appl.***, 4(2016): 1-5.
166. B.K. Patel and S.D. Patel; ***J. Pharm. Sci. Bio. Res.***, 7(2017): 148-152.
167. Z.A. Al-Mousway, B.W. Khmmas and A.J. Jarad; ***Int. J. Engin. Sci. Res. Tech.***, 2(2013): 959-967.
168. T.H. Al-Noor, A.J. Jarad and S.B. Abo; ***Int. J. Curr. Res.***, 7(2015): 15605-15609.
169. T.H. Al-Noor, A.J. Jarad and A.O. Hussein; ***Chem. Mater. Res.***, 6(2014): 20-30.
170. M.H. Jebur, R.T. Mahdi and A.M. Ali; ***Asian. J. Res. Chem.***, 6(2013): 1156-1159.
171. N.K. Fayad, T.H. Al-Noor and F.H. Ghanim; ***J. Adv. Phys. Theories Appl.***, 9(2013): 1-13.
172. S.M.H. Al-Naimi, A.S. Kindeel, A.J. Jarad and T.H. Al-Noor; ***Trans. Engin. Sci.***, 4(2016): 42-47.
173. R.N. Pandey and K. Shahi; ***J. Ultra Chem.***, 10(2014): 25-30.
174. A. Yahyazzdeh and V. Azimi; ***Eur. Chem. Bull.***, 2(2013): 453-455.
175. L. Mangsup, S. Siripasisarnpipat and N. Chaichit; ***Anal. Sci.***, 19(2003): 1345-1351.

176. M. Ravanasiddappa, T. Sureshg, K. Syed, S.C. Radhavendray, C. Basavaraja and S.D. Angadi; ***E-J. Chem.***, 5(2008): 395-403.
177. S.A. Shaker, F. Yang and A.A.S. Al-Hamdani; ***Eur. J. Sci. Res.***, 33(2009): 702-709.
178. M.R. Manrao, K. Balbir. K.K. Matharu, V. Gill, K. Kaul and J.R. Sharma; ***J. Indian. Chem. Soc.***, 86(2009): 531-534.
179. A.K. Mapari and K.V. Mangaonkar; ***Int. J. Chem. Tech. Res.***, 3(2011): 477-482.
180. M. Ravanasiddappa, T. Sureshg, K. Syed, S.C. Radhavendray, C. Basavaraja, C. and S.D. Angadi; ***E-J. Chem.,*** 5(2008): 395-403.
181. S.G. Shirodkar, P.S. Mane and T.K. Chondhekar; ***Indian. J. Chem.***, 40A(2001): 1114-1117.
182. G.G. Mohamed and M.M. Omar; ***Turk. J. Chem.***, 30(2006): 361-382
183. S.A. Shaker, Y. Fanina, S. Mahmmod and M. Eskender; ARPN J. Eng. Appl. Sci., 4(2009): 29-33.
184. S. Naskar, S. Biswas, D. Mishra, B. Adhikary, L.R. Falvello, T. Soler, C.H. Schwalbe and S.K. Chattopadhyay, ***Inorg. Chim. Acta.***, 357(2004): 4257-4264.
185. R. Gup and B. Kirkan; ***Spectrochim Acta A***, 62(2005): 1188-1195.
186. T.H. Al-Noor, R.A. Manhel and A.T. Al-Jeboori; ***J. Chem. Mater. Res.***, 3(2013): 114-124.
187. M.S. Suresh and V. Prakash; ***Int. J. Phys. Sc.***, 5(2010): 1443-1449.
188. N. Raman, R. Jeyamurugan, S. Sudharsan, K. Karuppasamy and L. Mitu; ***Arabian. J. Chem.***, 6(2013): 235-247.
189. K.P. Srivastava, A. Singh and S.K. Singh; ***IOSR-J. Appl. Chem.***, 7(2014): 16-23.

190. T.H. Al-Noor, K.F. Ali, A.J. Jarad and A.S. Kindel; ***Chem. Mater. Res.***, 3(2013): 126-133.
191. M.M. Omar and G.G. Mohamed; ***Spectrocheim Acta A***, 6(2005): 929-936
192. G. Pandey and K.K. Narang; ***Synt. React. Inorg. Met-Org. Chem.***, 34(2004): 291-311.
193. G.G. Mohamed, M.A. Zayed and N.E.A. El-Gamel; ***Spectrochim Acta A***, 15(2002): 3167-3178.
194. S. Naskar, S. Biswas, D. Mishra, B. Adhikary, I.R. Falvello, T. Soler, C.H. Schwalbe and S.K. Chattopadhyay; ***Inorg. Chim. Acta.***., 357(2004): 4257-4264.
195. M. Sebastian, V. Arum, P.P. Robinson, P. Leeju, G. Varsha, D. Varghese and K.K.M. Yusuff; ***J. Coord. Chem.***, 64(2011): 525-533.
196. F.S. Alassbaly, M.M. El-Ajaily, S.F. Ben-Gweirif and A. Maihub; ***J. Chem. Soc. Pak., 36***(2014): 10341042.
197. M.M. El-Ajaily, F.S. Alassbaly, A.M. Etorki and A.A. Maihub; ***Int. Res. J. Pure Appl. Chem.***, 5(2015): 229-237.
198. F.S. Alassbaly, A.A. Maihub, S.F. Ben-Gweirif, M.M. El-Ajaily and T.H. Al-Noor; ***Saudi J. Pathol. Microbiol.***, 1(2016): 29-35.
199. A.A. Maihub, M.M. El-Ajaily and N.A. El-Hassy; ***Int. J. Chem. Techn. Res.***, 4(2012): 631-633.
200. R.L. Prasad, A. Kushwaha, B.S. Gautam; ***J. Coord. Chem.***, 62(2009): 2983-2994.
201. M.B. Halli and R.S. Malipatil; ***Der*** Pharm***. Chem.***, 3(2011): 146-157.
202. R. Pallikkavill, M.B. Ummathur and Krishnannair; ***Arch. Appl. Sc. Res.***, 4(2012): 2223-2227.

203. G.E. Iniama, E.N. Nfor, E.D. Okon and I.T. Iorkpiligh; ***Int. J. Sci. Techn. Res.***, 3(2014): 73-77.
204. H.E. Gafer and R.R. Zaky; ***Egypt. J. Chem.***, 53(2010): 719-730.
205. F. Karci, I. Sener and H. Deligoz; ***Dyes and Pigments***, 62(2004): 133-141.
206. R. Hrdina, D. Lustine, P. Stolin, L. Burgert, S.L. Jr and M. Holcapek; ***Adv. Colour. Sci. Techn.***, 7(2004): 6-17.
207. T.N. Chhowala and K.R. Desai; ***Int. J. Sci. Res.***, 4(2015): 901-905.
208. N.A. El-Wakiel, H.F. Rizk and S.A. Ibrahim; ***Appl. Organometallic Chem.***, DOI 10.1002/aoc. 3723(2017): 1-10.
209. H. Yousef, A. Yahyazadeh, M.R. Yazdanbakhsh, M.R. Enayatollah and M. Rufchahi; ***J. Mol. Struct.***, 5(2012): 27-32.
210. P. Deshmukh, P.K. Soni, A. Kankoriya, A.K. Halve and R. Dixit; ***Int. J. Pharm. Sci. Res.***, 34(2015): 162-170.

الخلاصـــــــــة

تتضمن هذة الدراسة تحضير ليكاندات آزو جديدة ($L_{١}$–$L_{٤}$) إرتكزت جميعها على ٤–امينو انتيبيرين و٢–امينو بنزوثيلزول، تمتلك الصيغ التركيبية الآتية:

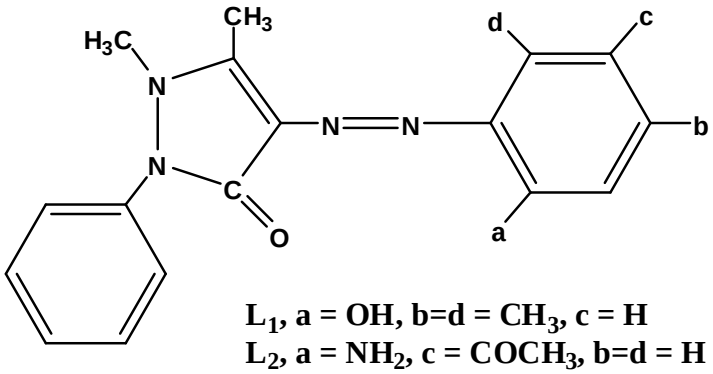

L_1, a = OH, b=d = CH_3, c = H
L_2, a = NH_2, c = $COCH_3$, b=d = H

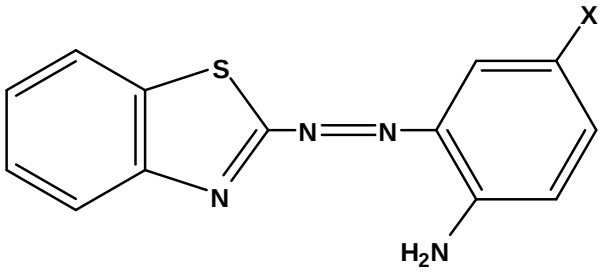

L_3 , X = $COCH_3$, L_4 , X = NO_2

شخصت الليكاندات المحضرة بأستخدام (FT-IR,UV-Vis,^{١}H,^{١٣}C-NMR,TGA وLC–Mass) والتحليل الكمي الـدقيق للعناصـر(C.H.N.S.O)، فضـلاً عـن درجـات الأنصهار. حضـرت مجمـوعـة مـن المعقدات للأيـونـات الفـلزيـة (Cu^{II}, Co^{II}, Ni^{II} وZn^{II}) مع الليكاندات ($L_{١}$-$L_{٤}$). بعد تثبيت الظروف المثلى من دالـة حامضـية وتركيز مولاري من خلال دراسة أطياف الأشعة فـوق البنفسجية– المرئية لمحاليـل مـزج الأيونات الفلزية مع محاليل الليكاندات أعلاه ولمدى واسع من الدالـة الحامضـية والتراكيـز المولارية الخاضعة لقانون لامبرت– بير، وقد إختلفت ظروف التحضير بـإختلاف الأيونـات الفلزية المستخدمة.

استخدمت طريقتي النسب المولية وطريقة جوب للتعرف علـــى تراكيـــب المعقـــدات المحضرة ووجد أن نسبة الفلز: الليكاند هي (٢:١). أما معقدات مزيج الليكانـــد فقـــد كانـــت النسبة (١:١:١) (فلز: L:L).

شخصت المعقدات المحضرة بوساطة أطياف UV-Vis وFT-IR والتحليـــل الكمـــي الدقيق للعناصر(C.H.N.S.O)، وقيست النسبة المئوية للفلز بإســـتخدام طيـــف الإمتصـــاص الذري اللهبي والتحاليل الفيزياوية وعينت درجة المغناطيسية للمعقدات المحضرة وموصـــليتها الكهربائية، فضلاً عن قياس درجات الإنصهار. أما دراسة ثابت التكوين للمعقـــدات ودراســـة التحليل الحراري (T.G.A) فقد أظهرت أن معظم المعقدات تتمتع بإستقرارية عالية. اســـتنادا الى النتائج المستحصلة للدراسات المذكورة فقد تم أقتراح الشكل ثماني الســـطوح للمعقـــدات المحضرة.

لقد تم الإفادة من الليكاندات والمعقدات قيد الدراسة في إمكانية إســـتخدامها كأصـــباغ لصباغة الأنسجة القطنية نظراً لما يتميز به من ألوان زاهية، وقد تبين أن ألوانها ثابتـــة وذات مقاومة عالية للغسل والمنظفات ولضوء الشمس. وأخيرا تمت دراسة الفاعلية الحيويـــة علـــى انواع مختلفة من البكتريا مثـــل المكـــورات العنقوديـــة الذهبيـــة (Staphylococcus Aureus)

و البكتريا القولونية (E . Coli) وأنواع من الفطريات مثل فطريات المبيضة (Candida albicans) و الفطريات المبيضة المدارية (Candida tropicalis) .

جمهورية العراق
وزارة التعليم العالي والبحث العلمي
جامعة بغداد
كلية التربية للعلوم الصرفة/ ابن الهيثم
قسم الكيمياء

تحضير، تشخيص ودراسة الفعالية البايولوجية لمعقدات اصباغ ألآزو مع أيونات بعض العناصر الفلزية

اطروحة مقدمة الى
مجلس كلية التربية للعلوم الصرفة- ابن الهيثم - جامعة بغداد
وهي كجزء من متطلبات نيل درجة دكتوراه فلسفة في الكيمياء

من قبل
جنان محمد محمود
بكالوريوس علوم كيمياء- 1999- جامعة بغداد
ماجستير علوم كيمياء- 2002- جامعة بغداد

باشراف
أ.د. عامر جبار جراد

1440هـ 2019م